CHEMICALLY DERIVED CERAMIC COMPOSITES

By

BURTRAND INSUNG LEE

A DISSERTATION PRESENTED TO THE GRADUATE SCHOOL
OF THE UNIVERSITY OF FLORIDA IN
PARTIAL FULFILLMENT OF THE REQUIREMENTS
FOR THE DEGREE OF DOCTOR OF PHILOSOPHY

UNIVERSITY OF FLORIDA
1986

ACKNOWLEDGEMENTS

It is difficult for me to acknowledge everyone who gave helping hands during the tenure of my research as a graduate student at the University of Florida.

It is hardly necessary to mention my advisor Professor Larry L. Hench for his inspiring support and stimulating thoughts. His sense of humor maintained a relaxed research atmosphere. He helped me to mature as an independent scientist. I am especially grateful for the freedom and independence he has given me throughout this research. It was indeed a privilege and pleasure to work with him.

Dr. Robin Sinclair at 3M Co. not only provided the facility to synthesize some of polysilanes but also taught me the techniques in polymer chemistry. The analytical services of 3M Co. which provided analytical data of the polysilanes are acknowledged with gratitude. Dr. Curt Schilling at Union Carbide is also acknowledged for his support by providing some of their experimental polysilanes.

My thanks are extended to D. Dunnagan and D. Folz for thermal analyses, E. Jenkins for SEM, W. Acree for XRD, Dr. J. Newkirk and C. Turner for TEM, Dr. A. Gupta for GC, S. Yoon and S. Kong for proton NMR, Lester at the Engineering Machine Shop of the University of Florida, G. LaTorre for FT-IR, S. Kang for density and microhardness measurements, and Professor Batich and Dr. S. Kurinec for help in XPS.

The financial support of the U.S. Air Force Office of Scientific Research through contract no. F49620-83C 0072 was certainly an essential part of my life at the University of Florida and is especially acknowledged as is the encouragement of Dr. D. R. Ulrich, contract monitor.

I am also grateful to the members of my supervisory committee, Professors C. Batich, M. D. Sacks, L. Malvern, D. Clark, and E. D. Whitney, for their advice and reading of the entire manuscript of this dissertation.

On the nontechnical side, special personal thanks goes to my family. Instead of complaining about not spending much time with them, they rather were truly the Gatorade, "a thirst quencher." My mother-in-law, in particular, played too great a role to describe.

TABLE OF CONTENTS

Table of Contents (continued)

LIST OF ABBREVIATIONS, ACRONYMS, INITIALISMS, AND SYMBOLS

Ac	Acetate ion or group
AIBN	Azobisisobutyronitrile
A-PSS	Allylic polysilastyrene
B.E.	Binding energy in eV
BPO	Benzoyl peroxide
-C=C or	Vinyl group
-C-C=C or 	Allyl group
$CDCl_3$	Deuterochloroform
D_6D_6	Deuterobenzene
CFRI	Chemical free radical initiator
DCCA	Drying control chemical additive
DCP	Dicumyl peroxide
DMDCS	Demethyldichlorosilane; Me_2SiCl_2
DSC	Differential scanning calorimetry
DTGA	Derivative thermogravimetric analysis
EDS	Energy dispersive x-ray spectroscopy
en	Ethylenediamine
EtOH	Ethanol
FID	Flame ionization detector
FT-IR	Fourier transform infrared
GC	Gas chromatography
GPC	Gel permeation chromatography
IR	Infrared
J-PSS	PSS prepared by Shinnisso Kako Co., Japan

Me	Methyl group, $-CH_3$
$\overline{M}n$	Number average molecular weight
$MeCl_2$	Methylene chloride
MPDCS	Methylphenyl dichlorosilane, $MeSiPhCl_2$
Mrad	Mega rad
M.W.	Molecular weight
PC	Polycarbosilane
PDMS	Polydimethyl silane
PDS	Polydimethyl silane
Ph	Phenyl group, $-C_6H_5$
PrOH	Isopropyl alcohol
PS	Polysilane
PSS	Polysilastyrene
PSS-O	Oligomer fraction of polysilastyrene
P-PSS	Petrarch's polysilastyrene
R	Reflectance, or diameter to length ratio of a fiber
RT	Room temperature
T	Temperature, or transmittance
TEOS	Tetraethylorthosilicate: tetraethoxysilane
TMOS	Tetramethoxysilane
TMS	Tetramethylsilane
SEM	Scanning electron microscopy
SS	Silastyrene, oligomer fraction of polysilastyrene
STEM	Scanning transmission electron microscopy
TEM	Transmission electron microscopy

TGA	Thermogravimetric analysis
TMA	Thermomechanical analysis
UV	Ultraviolet
v/o	Volume percent
ViSO	Vinylic silane oligomer
ViSP	Vinylic silane polymer
w/o	Weight percent
w/v	Weight percent volume
XPS	X-ray photoelectron spectroscopy
XRD	X-ray diffraction

Greek Symbols

α	Linear coefficient of thermal expansion
γ	Uncharged high energy electromagnetic quanta
ρ	Density, g/cc
λ	Wavelength
ν	Frequency
$\bar{\nu}$	Wavenumber
Δ	Differential value
σ	Stress, strength

Subscripts

x	Crystalline
g	Glass
c	Carbide

Abstract of Dissertation Presented to the Graduate School
of the University of Florida in Partial Fulfillment of the
Requirements for the degree of Doctor of Philosophy

CHEMICALLY DERIVED CERAMIC COMPOSITES

By

BURTRAND INSUNG LEE

May 1986

Chairman: Dr. Larry L. Hench
Major Department: Materials Science and Engineering

Silicon carbide was made from various organosilane precursors by crosslinking and pyrolyzing them in an inert atmosphere. Crosslinking of these silane precursors was studied by various means. The most successful means of crosslinking was found to be via a chemical free radical initiator, dicumyl peroxide. The mechanism of crosslinking for the precursors was determined.

Pyrolyses of the silane precursors were carried out and increased ceramic yields after crosslinking were shown as compared with uncrosslinked precursors. The ceramic yields determined by TGA ranged from 10-70% depending on the precursors and the crosslinking treatments.

Partially densified sol-gel derived silica monoliths were impregnated with the silane precursors while the silica monoliths were still

highly porous. Diamond microhardness values increased 2-3 times from unimpregnated gel derived silica monolith. A moderate increase in fracture toughness, K_{IC}, and flexural strengths was achieved. Optical and mechanical properties, and porosity data are presented.

Using sol-gel silica precursors and the processing techniques of polysilanes to obtain β-SiC, molecular composites of SiC with SiO_2, with TiO_2 and with Al_2O_3 were made in monoliths and powder forms. Monolithic composites with a molecularly dispersed SiC phase in the SiO_2 gel matrix showed a hardening effect by the SiC phase.

The molecular composite powders of SiC/Al_2O_3 showed no or little crystallization of either phase after heating to 1400°C.

Monolithic silicon carbide/silica composites were made using commercially available fibrous silicon carbides and a tetralkoxysilane precursor. Modest to low flexural strengths were obtained after heat treating to 900-1400°C, because of the high porosity in the composite. Cold pressing of the SiC and silica sol slurry improved the density and flexural strengths. Notched 3-point fracture toughness values, K_{IC}, was as high as 7 $MPa \cdot m^{1/2}$. Excellent thermal shock resistance and oxidation resistance of these composites are shown.

CHAPTER I
OVERVIEW OF CHEMICALLY DERIVED CERAMICS

Ceramic materials are of critical importance in high technology (high-tech) areas where unique combination of properties, such as high strength, strength retention at high temperature, low thermal and electrical conductivity, high hardness and wear resistance, and high chemical stability are required. However, because of their brittle nature, ceramic materials produce problems in design reliability in high performance structural applications resulting in catastrophic failures under stress. This inherent problem combined with poor cost effectiveness in fabrication of complex shapes severely limits wider applicability of current ceramic materials.

Ceramic materials derived from chemical reagents have the potential to overcome these problems by

1) Low temperature processing compared with traditional ceramic processing,
2) Starting chemical compounds that can easily be purified to increase the purity of the ceramic materials,
3) Having versatility in forming complex shapes and precise control of each step in the processing,
4) Rendering homogeneous mixing; uniformity and, thus, reliability of the formed bodies can be improved, and
5) A unique combination of microstructure and phase assemblages not obtainable by traditional ceramic processes may be obtained.

Ceramic materials obtained by chemical processing are a rather recent development, despite the fact that the science behind the processing existed long before the ceramic applications were realized. Traditional ceramic science has been based more on physics and has been developed by optimizing the physical behavior with the microstructure of the materials.

The term "ultrastructure processing" of ceramics has been introduced[1] to represent the chemical manipulation and control of surfaces and interfaces during the earliest stages of formation in atomic or molecular scales. The so called "high-tech" ceramics are largely based on "ultrastructure processing" as this is one way in which engineering ceramics can potentially yield properties approaching the theoretical limit.

Organic chemistry, once an anathema to ceramists, is recognized as a major source of new ceramic materials. By using ordinary chemicals as precursors to ceramic materials, one can study and control the chemical process in every step during the evolution of ceramics, from the starting chemical to the final product. Greater versatility in fabrication with more precise control of the process leading to an extremely homogeneous composite with superior properties is the goal and advantage of this approach.

Ceramic fibers, optical glasses, ultrapure and ultrafine powders, and ceramic monolithic parts are some of the demonstrated materials derived chemically.[1,2] Figure I-1 summarizes some of the chemical processes.

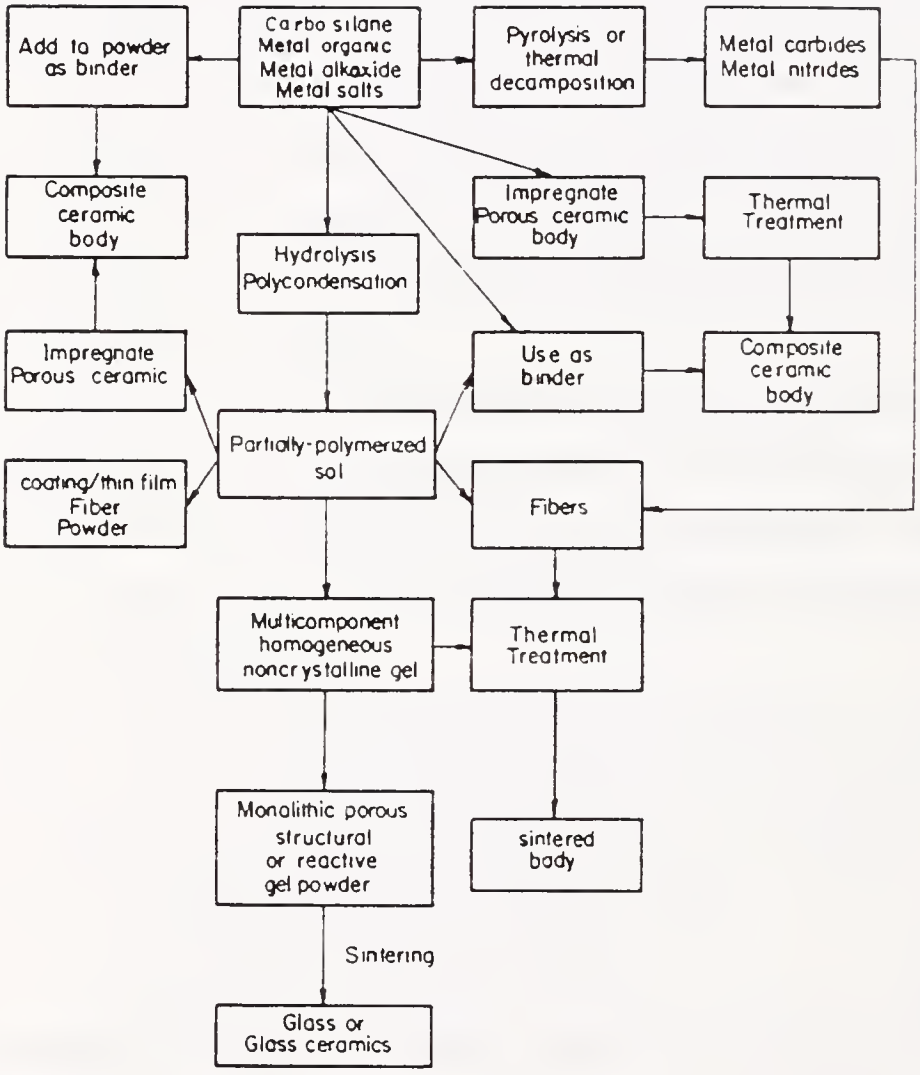

Fig. I-1. Flow Diagram of Some of Chemically Derived Ceramics and Composites

The sol-gel method, as shown in Fig. I-1, is a notable example of obtaining oxide ceramics from metal-organic precursors. Pure monolithic parts, thin coatings, matrices for reinforced composites, etc. have been produced with controlled properties. Uranium oxide fuels were fabricated by the sol-gel method at Oak Ridge National Laboratory in the 1970's.[3] Active research is underway to understand the fundamental chemistry in the reaction steps, as well as in the applications.[2,4] All facets of chemistry are involved. For example, a nuclear magnetic resonance technique has been found helpful in understanding the reaction mechanism of the sol-gel process.[2]

It has been shown[2] that certain chemical additives change the physical-chemical state during sol-gel transformation. The mechanism of how these additives function chemically is not fully understood. Various dopants may be added to the sol as a chemical reagent by forming a molecularly homogeneous solution.

The most understood sol-gel process is in the production of silica glass. Silica sol-gel reactions involve hydrolysis and polycondensation steps of a metal-organic precursor, as shown in eqs. I-1 and I-2.

$$\equiv Si(OR)_4 + n\ H_2O \rightarrow \equiv Si\text{-}OH + 4\ ROH$$

$$2 \equiv Si\text{-}OH \rightarrow \equiv Si\text{-}O\text{-}Si \equiv + H_2O \qquad (I\text{-}2)$$

The hydrolysis and polycondensation reactions initiate at numerous sites within the $Si(OR)_4$ precursor + H_2O solution as mixing occurs. They eventually form a three dimensional linkage of Si-O-Si in a submicron scale and are called sol particles. The sol particles come in contact to form a gel network. As the gel network is aged at an elevated temperature, the monolithic body is strengthened and becomes more like a ceramic body.

Some other oxide ceramic materials derived chemically may be given below, 1) alumina from $Al(OR)_3$ by Yoldas,[5,6] 2) lead titanate by Gurkovich and Blum,[7] 3) indium tin oxide films by Arfsten et al.,[8] 4) monosized SiO_2 and TiO_2 powders by Barringer et al.,[9] and 5) single and mixed phase oxide powders by Mazdiyasni.[10]

Similar to the sol-gel process of obtaining metal oxides, pyrolysis of organometallic precursors results in nonoxide ceramic materials of the constituent elements. Thus far, successful examples are silicon carbide (SiC) and silicon nitride (Si_3N_4) from polymers containing silicon-carbon and silicon-nitrogen bonds in the backbone.[4] Boron nitride and boron carbide can also be made from organometallic precursors.[4] Titanium carbide, titanium nitride, titanium boride, silicon boride, and aluminum nitride may be possible from organometallic precursors.[4] Table I-1 lists ceramic materials that can be made from chemical processing of organometallic compounds.[4]

It is difficult to make complex shapes of dense refractory ceramics such as SiC or Si_3N_4 using conventional high temperature sintering, hot pressing, or hot isostatic pressing methods without a sintering aid. Grain boundary phases are often introduced in materials, degrading high temperature performance and oxidation resistance. Refractory carbide and nitride fibers are nearly impossible to make using traditional processing methods.

In making fibers from pyrolysis of an organometallic precursor, densification accompanies pyrolysis, which eliminates a separate sintering process. By analogy to a carbon fiber made from a carbon polymer,

Table I-1.
Ceramic Products That Can Be Made From Organometallic Precursors.‡

Products Available	Theoretical Density, g/cc	Products Under Development	Theoretical Density, g/cc
Silicon Carbide (SiC)	3.2	Aluminum Boride (AlB_{12})	2.6
Silicon Nitride (Si_3N_4)	3.2	Calcium Boride (CaB_6)	2.5
Boron Nitride (BN)	2.2	Silicon Boride (SiB_6)	2.4
Boron Carbide (B_4C)	2.5	Titanium Boride (TiB_2)	4.4
		Titanium Carbide (TiC)	4.9
		Aluminum Nitride (AlN)	3.3
		Titanium Nitride (TiN)	5.2
		Boron Phosphide (BP, B_6P)	3.0, 2.6
		Titanium Silicide (TiSi, $TiSi_2$)	4.2, 4.0

‡ Based on Ref. 11.

organometallic precursors offer a means to make refractory carbides and nitrides at potentially lower temperatures with the easy forming operations of traditional polymers.

One of the primary thrusts in applications of these materials is in gas turbine engines because these materials are strong and stable at temperatures no metal can withstand, and they also have high thermal shock resistance, which is necessary for heat engine components. Ceramic materials derived from polymer precursors in the form of foam may also be used for thermal insulation, filtration, and packing. Thin films may be applied in electronic devices and metal-ceramic joints. Extremely homogeneously doped high temperature semiconductors may be made this way as well. Boron nitride fiber made from organometallic precursors can be used as a dielectric material where alumina and silica fibers are less desirable. These organometallic precursor materials can also be used as binders in powder forming processes. There is also a high probability of obtaining infrared transmitting films of sulfides and selenides, superconductive fibers of NbN, NbC, silicides, sulfides, and borides via polymer precursor pyrolysis.

Intrinsic flaw sensitivity and brittleness continue to impede the broader applications of monolithic ceramic components. These instrinsic weaknesses can be overcome by incorporating a high modulus, small diameter ceramic reinforcing phase in a ceramic matrix to change the failure mechanisms to tough, noncatastrophic modes.

Composite materials on the ultrastructural level can be achieved by mixing polymer precursors containing constituent elements, e.g., a

polysilane mixed with polyphenylborazole yields a composite of SiC/BN.[3] Polymers containing Si, C, and N can be used to obtain a SiC/Si_3N_4 composite.[4]

A reaction of polycarbosilane and $Ti(OR)_4$ can yield a composite of SiC/TiC.[12] In this composite process $Ti(OR)_4$ not only provides the TiC phase, but also crosslinks the polycarbosilane, hence maintaining the shape of the green body during the subsequent heat treatments and increasing the ceramic yield. The structural scale of these precursor based composites is in the 1-10 nm range, as compared with the 1 to 100 μm or larger range of composites made by traditional processes.[13]

Composites are leading a new era in structural engineering. The development of high performance materials and advances in fabrication technology are laying the groundwork for revolutionary changes in structural design. In order to go forward with high speed in ceramic composite technology, it is necessary for engineers to break away from engineering thought processes that have been developed over decades of working with conventional materials.

Active research on ceramic matrix composites began no earlier than 1982, according to Persh.[14] Even then, the ceramic matrix composites were based more on applied physics using the traditional processing methods, such as hot pressing matrix phase powder with a reinforcing phase.

The objectives of this dissertation are thus based on an exploratory study and development of new methods to obtain ceramic materials derived by chemical means. Processing and properties of SiC/SiO_2

composites utilizing techniques of sol-gel derived SiO_2 and SiC via organosilanes are the main topics of this work. Other ceramic composites from chemical origins are also part of this dissertation. The primary motivation and objectives for the work presented in this dissertation are an interest in the development of new processing methods based on chemical processes and an understanding of these processes. For ceramic and composite materials in this work, the emphasis is more on concepts rather than the final products with exciting quantitative data in part because concepts are felt to be of greatest use to those developing ceramic composites.

The more elaborate and topical introductions are given in the beginning of each chapter.

CHAPTER II
SILICON CARBIDE FROM ORGANOSILANE PRECURSORS

Introduction

Many ceramic materials have specific properties that make them ideal for energy related systems. Silicon carbide (SiC) is one of the leading candidates for high temperature structural applications because of its low density, high-temperature strength, chemical stability, refractoriness, high thermal shock resistance, and creep resistance. To achieve these desirable properties of silicon carbide, it is necessary to develop a reproducible and reliable method for producing the material in complex shapes and with a controlled ultrastructure.

In the conventional process for producing SiC material, silica in the form of sand and carbon in the form of a coke are reacted together at 2400°C in an electric furnace. The SiC produced is in relatively large grains which are subsequently ground to the desired size.[15]

The Cutler process[16] was developed to produce SiC material with superior properties and cost effectiveness by using rice hulls. From this process, the commercially known α-SiC whisker Silar™ by ARCO is obtained. The major advantage of it is that it has a much lower processing temperature, ~1600°C, than the more traditional process.

The increasing search for new types of high-strength materials, and for performance improvement in the existing ceramics, has pushed several nonconventional approaches to ceramic synthesis.

As presented in Chapter I, obtaining nonoxide ceramics via pyrolysis of organometallic precursors has potential advantages over the conventional methods of producing materials in low temperature process, higher purity, fabrication of complex shapes, greater homogeneity, new fabrication procedures leading to continuous fiber, coatings, and impregnated porous structures. At a more fundamental level, polymer routes can allow control over the microstructure of the intended ceramic product with a unique combination of microstructure and phase assemblages and important consequences for both physical and chemical properties.[4] Some of the more important applications of nonoxide ceramic materials obtained via polymer routes are listed in Table II-1.

The first use of organic polymers to produce an inorganic refractory material was probably the development of graphite fiber from polyacrylonitrile in late 1950.[17] Other ceramic materials from organometallic polymers were first noted by Chantrell and Popper.[19] A partial history of the development of nonoxide ceramics from organometallic precursors is given in Table II-2.[4]

However, early workers[50-52] in organosilanes (OS) genuinely believed that polysilanes were worthless and regarded them as undesirable by-products of a faulty synthesis. This all changed in 1975 when Yajima and his coworkers[22-30,53-55] demonstrated that the polydimethylsilane that was regarded as an undesirable by-product by previous investigators[50-52] is indeed a precursor to β-SiC. The reaction scheme, as shown in Fig. II-1, is the polymerization of dimethyldichlorosilane $[(CH_3)_2SiCl_2]$ by dechlorination to yield polydimethylsilane (PDMS). The

Table II-1.
Some of the Demonstrated Applications of
Nonoxide Ceramics Derived from Organometallic Precursors

Form	Applications
Fiber	Reinforcement for composites weaves, wovens, mattes
Monolith	Monolithic bodies for high temperature parts
Foam	Filters, packing, insulation, heat exchanger
Powder	Press to bulk body, Filler material
Thin Film	High temperature electronic devices
Thermosetting polymer	Metal-ceramic, ceramic-ceramic joints, binder in powder forming

Table II-2
A Partial History of Nonoxide Ceramics Via Polymer Routes

Year	Precursor Polymers	Ceramic Products	Investigators	Ref.
1960	phosphonitric chlorides	P-N	Ainger, Herbert	18
1965	unknown	BN, AlN, Si_3N_4, SiC	Chantrell, Popper	19
1974-75	polysilanes	Si-C-N	Verbeek and Winter et al.	20, 21
1976-81	polycarbosilanes	SiC	Yajima et al.	22-30
1976	polyphenylborazole	BN	Taniguchi, Harada Maeda	31
1978	carboranesiloxane	SiC-B_4C	Rice et al.	32, 33
1979-80	polycarbosilanes	SiC	Schilling, Williams, Wesson	34-39
1980-81	polysilastyrene polycarbosilanes	SiC SiC, Si-C-N	West et al. Baney and Gaul	40 41-46
1981	polytitanocarbosilane	Si-Ti-C	Yajima et al.	12
1982	polysilazanes	Si-C-N	Penn et al.	47
1982	polysilazanes	Si_3N_4	Seyferth, Wiseman	48, 49
1984	vinylic polysilane	SiC	Schilling and Williams	39

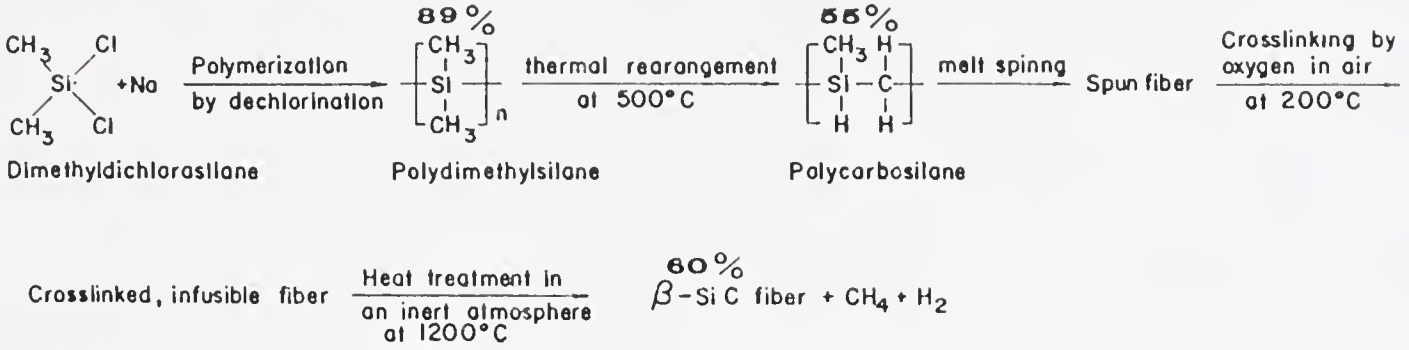

Fig. II-1. Reaction Steps for the Yajima Process to Produce β-SiC via Polycarbosilane and Oxygen Crosslinking, % Yield Shown above the Intermediates and the Product.

polymer chain then is rearranged to make it more reactive for a thermosetting condition. The rearranged polymer called polycarbosilane has alternating silicon and carbon atoms. The thermosetting or crosslinking carried out in air is a necessary step in the Yajima SiC fiber synthesis to maintain the fiber shape during the subsequent heat treatments. During the heat treatment, hydrocarbon products are eliminated to yield a ceramic char of SiC.

Since Yajima and coworkers[22-30,53-55] developed a β-SiC fiber with excellent mechanical properties from the polycarbosilane, there have been several other precursors potentially superior to the Yajima process.[34-40] These are vinylic silanes developed by Wesson and Williams[34-36] and Schilling et al.[38,39] and polydimethyl phenylmethylsilane, better known as polysilastyrene (PSS) developed by West et al.[40]

The vinylic silanes are reactive under a thermal crosslinking condition but, because of their low viscosity (liquid at room temperature), control of viscosity to draw fibers may require extra steps. On the other hand, PSS is a solid with good solubility in common solvents and possesses excellent tractability with good melt viscosity. However, it possesses no reactive functional groups for crosslinking. It was noted by West et al.[40] that the polymer strongly absorbs UV light at ~330 nm. Irradiation of UV with $\lambda \approx 330$ nm on PSS was shown to crosslink the polymer on the surface.[40] However, the practicality of UV crosslinking of PSS for larger structural ceramics is in question. An alternate way to achieve bulk crosslinking is needed.

It is important to note that vinylic silanes and PSS are potentially superior to polycarbosilane because they can be processed without

the separate thermal rearrangement and oxygen crosslinking (Fig. II-1), as required in the Yajima process. Oxygen crosslinking undoubtedly introduces Si-O-Si in the network and ends up as silica in the final product β-SiC. In order for the potential advantages of vinylic silanes and PSS to be realized, it is essential that crosslinking methods be developed which will avoid oxygen in the SiC lattice following pyrolysis.

The term polymer used here is defined as any organic or organometallic compound that is not a monomer. However, in some specific cases, oligomers are distinguished from polymers.

It is the objective of this work to investigate crosslinking methods and some applications of vinylic silanes and PSS precursors to SiC. In this chapter the following topics are investigated and discussed: 1) synthesis and characterization of the polymers, 2) modification of the polymers for crosslinking, and 3) crosslinking and pyrolysis to obtain SiC.

Experimental

Preparation of equimolar dimethyl phenylmethyl copolymer

Reagent grade toluene for a solvent was dried with sodium metal in ~1 g sodium per 1 l toluene by refluxing for 24 hours followed by distillation through a one way air sealed glass apparatus using mineral oil bubbler.

A starting monomer dimethyldichlorosilane (Me_2SiCl_2) from Aldrich Chemical Co. was purified by distillation using a trap-vacuum technique with liquid nitrogen. Methylphenyl dichlorosilane ($PhMeSiCl_2$) monomer

also from Aldrich Chemical Co. was vacuum distilled in a Yamato model rotary evaporator at 80°C.

A reagent grade sodium metal bar was cut to 47.5 g and placed in a dry 2 liter 3-necked round bottom flask. These operations were carried out in a glove box with N_2 atmosphere. The dried and distilled toluene (850 ml) was added to the flask and the polymerization reaction apparatus was set up, as shown in Fig. II-2.

Sodium and toluene were mixed by stirring and heating to obtain a molten mixture of sodium dispersed in the solvent. Heating was discontinued to add dichlorosilane monomers. A premixed solution of 61 ml of Me_2SiCl_2, 81 ml of $PhMeSiCl_2$, and 50 ml of dry toluene was added slowly through the air sealed side arm, while stirring was continued and N_2 gas was continuously flowing through the apparatus.

The rate of addition of the premixed dichlorosilane monomers was adjusted to maintain the gentle refluxing temperature of ~98°C, since the initial dechlorination reaction is highly exothermic. A typical duration of the monomer addition was ~30 min. Upon completion of the monomer addition, external heating was restored to achieve a gentle reflux. The reaction flask was kept dark by wrapping it with aluminum foil. The reflux continued for 1.5 hours before cooling the reaction mixture to room temperature and then poured into an isopropyl alcohol bath (PrOH) with stirring.

Fractionation of the reaction products was carried out by first separating them in PrOH. The polymer fraction was precipitated out while the oligomer fraction remained in the solution. The oligomer

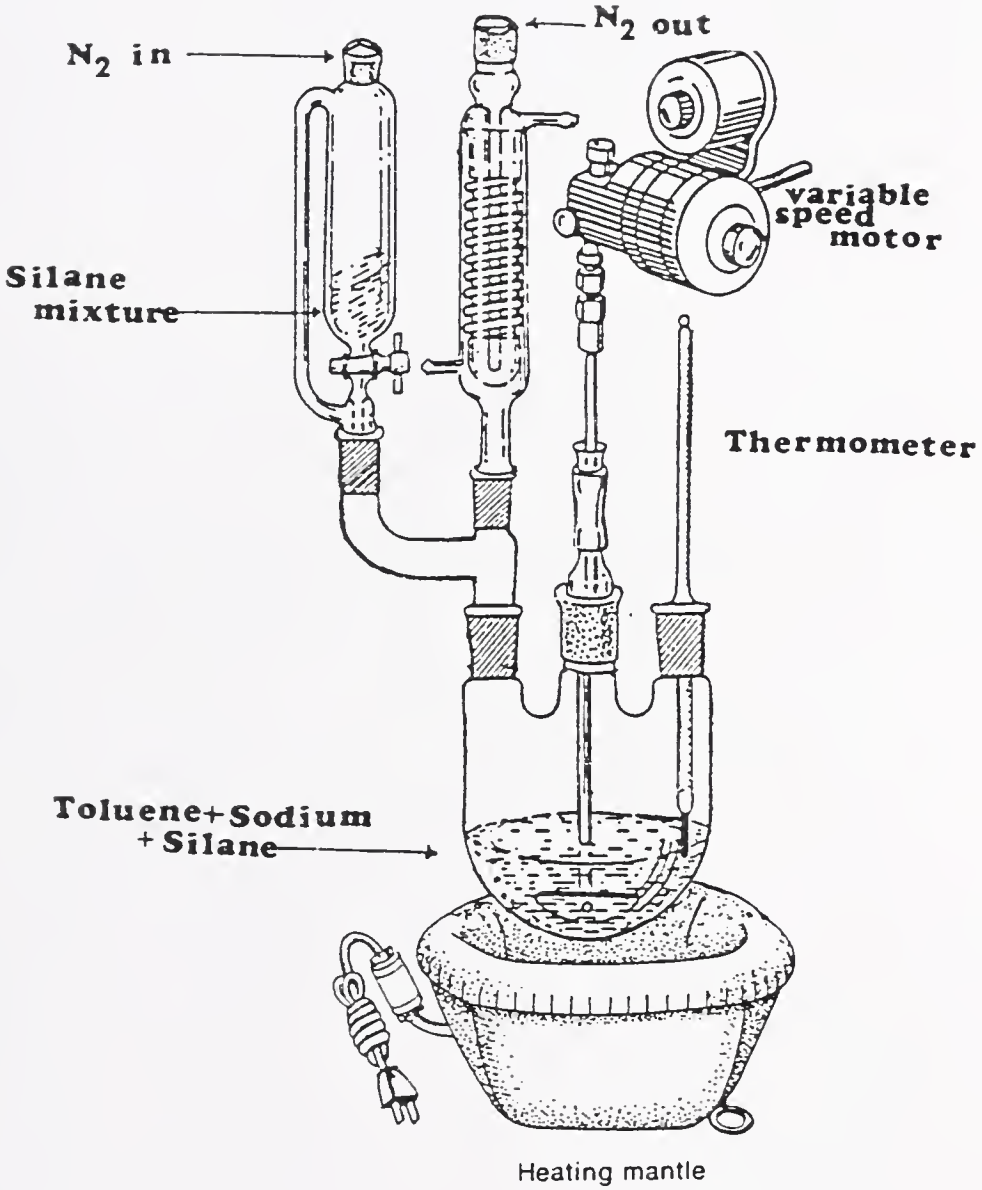

Fig. II-2. Apparatus for Polymerization Reactions for Synthesizing Polysilastyrene

fraction in PrOH was collected by distilling off the solvent by a rotary evaporator. The excess sodium residue was decomposed in PrOH. The oligomer fraction collected was redissolved in toluene and washed with distilled water three times in a 200 ml separatory funnel to extract any residual salt product. Then the toluene solution of the oligomer was rotoevaporated to obtain a viscous oligomer fraction of PSS (PSS-O) which was kept in a brown bottle after vacuum drying and weighing.

The PrOH insoluble fraction was washed with 200 ml PrOH and with 200 ml EtOH twice after draining the PrOH by filtering. After the solid polymer fraction was dried in a vacuum oven for five hours at 55°C, it was redissolved in warm toluene and the toluene insoluble fraction was separated out. The toluene insoluble fraction was thought to be a highly crosslinked polydimethylsilane. This fraction was washed with water five times in a separatory funnel and dried in a vacuum oven at 80°C for ten hours.

The toluene soluble fraction (PSS-P) in toluene solution was washed with water five times to insure that all unreacted Si-Cl is hydrolyzed out. This was done by titrating the effluent with $AgNO_3$ solution. Then PSS-P in toluene was reprecipitated in 7 liters of PrOH. The bright white precipitate was collected by filtration and dried in a vacuum oven at ~50°C for ten hours. A pure PSS-P should appear as a white powder or a clear, colorless solid.

The variations in reaction conditions for the subsequent runs are given in Table II-3.

Table II-3. Summary of Reaction Conditions for Preparation of Polysilastyrene and Product Designation.

Product I.D.	Mole Dichlorosilanes Mole Na Volume Toluene	Addition Time, min.	Reaction Time, hr.	Reaction Temp., °C
PSS-10 PSS-1P	0.5 mole each 2.05 mole 1 l	40	1.5	105
PSS-20 PSS-2P	0.5 mole each 2.09 mole 1 l	30	2	108
A-PSS-P A-PSS-O	0.5 mole $MePhSiCl_2$ 0.4 mole Me_2SiCl_2 0.1 mole Allyl $MeSiCl_2$ 2.04 mole Na 1 l toluene	17	2	108

Infrared spectra for the polymerization products were taken by using a Perkin-Elmer IR Spectrophotometer Model 283 with KBr Pellet in transmission mode and also by a Nicolet MX-1 FT-IR Spectrophotometer in diffuse reflectance mode. Proton NMR spectra were obtained by using a Varian XL-100 with $CDCl_3$ or C_6D_6 as solvents without the TMS reference. Molecular weight distributions of the products were determined by gel permeation chromatography (GPC) using polystyrene as a reference in THF solvent and using a refractive index detector.

Other PSS samples were provided by Shinnisso Kako Co. of Japan through the 3M Co. (J-PSS1 and J-PSS2), courtesy of Dr. R. Sinclair and also by Petrarch Systems, Inc. (P-PSS), courtesy of Dr. B. Arkles. Vinylic silanes were provided by Union Carbide, courtesy of Dr. C. Schilling. They are oligomer and polymer fractions of

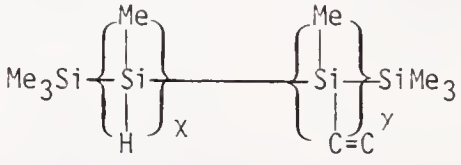

Two kinds of siloxane substituted PDMS containing a hydride functional group or phenyl group were provided by Petrarch System, Inc., courtesy of Dr. B. Arkles.

The structure of each polymer unit and physical state of all the polysilanes used in this study are given in Table II-4.

Crosslinking and pyrolysis

For crosslinking via γ-ray irradiation, PSS was melt-coated on thin stainless steel plates in glass test tubes with vacuum, Ar, N_2, He, air,

Table II-4. Structure Formulas of Polysilane Unit and Physical State of the Organosilanes at Room Temperature

Organosilane	Structure Formula	Physical State At Room Temperature
PSS-P	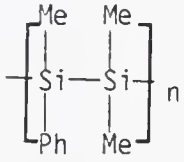	White to dull yellow solid
PSS-O	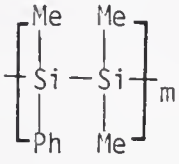 (where m < n)	Yellow to brownish viscous liquid
Allylic PSS	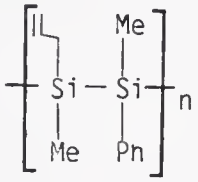	
A-PSS-P		Light yellow solid
A-PSS-O		Brownish viscous liquid
Vinylic Silanes	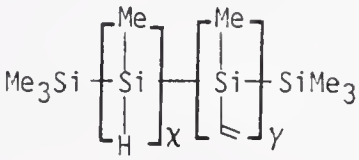	
ViSP		Colorless clear viscous liquid
ViSO		Colorless clear low viscosity liquid
Siloxane PDMS Hydride	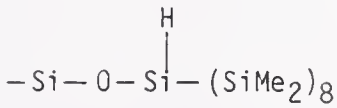	Yellowish viscous clear liquid
Phenyl	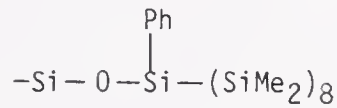	Yellowish viscous cloudy liquid

or N_2O atmospheres. Some portions of the silane precursors were dissolved in benzene in glass test tubes and sealed for irradiation. The vinylic silanes were placed in evacuated borosilicate test tubes. The glass tubes containing silane samples were irradiated with γ-radiation from a ^{60}Co source at 1" distance for various lengths of time up to 29 days at room temperature.

Chemical free radical initiators (CFRI), benzoyl peroxide (BPO), aszobisisobutyronitrile (AIBN), and dicumyl peroxide (DCP) obtained from Polyscience Co. were recrystallized from methanol before use. A few grams of silane were dissolved in 5-10 ml of benzene in a test tube or in a 3-neck round bottom flask and then the silane solution was degassed with an inert gas. After 30-60 min., a CFRI in the range of 3-10 wt% was added under an inert atmosphere and the crosslinking reaction was carried out with heating on a hot plate or by a heating mantle, as shown in Fig. II-3. The crosslinking reaction in the 3-neck flask was allowed to reflux for twelve hours with continuous stirring before cooling to room temperature. The crosslinked product was extracted and washed with methanol.

Crosslinking via DCP was carried out also in a sealed Teflon container for ViSP, ViSO, and PSS. About 1-2 g of vinylic silanes were well mixed with 0.05-0.07 g DCP by a spatula under N_2. Polysilastyrene was also mixed with DCP after the polymer was made into a thick solution in toluene. The silane + DCP mixtures were cured in an oven at 110-150°C after the containers were tightly sealed. Other portions of polysilanes were cured without DCP under the same condition.

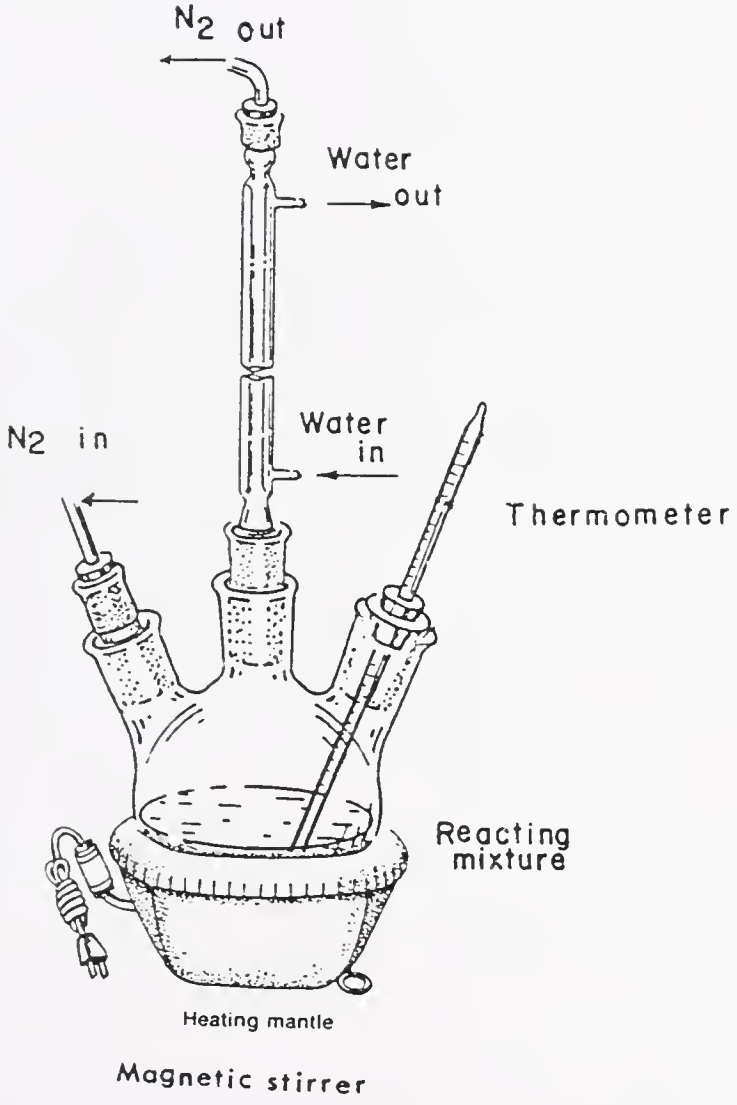

Fig. II-3. Apparatus for Crosslinking of Polysilastyrene

For crosslinking via Pt^{4+}, a 1.2 x 10^{-4} M solution of Pt^{4+} was prepared by dissolving 3.1 mg of $H_2PtCl_6 \cdot 6H_2O$ in 50 ml of a mixed solvent of acetone (20 ml), ethyl ether (16 ml), toluene (10 ml), and EtOH (4 ml). Crosslinking via Pt^{4+} was tried for A-PSS, ViSP, and ViSO precursors by adding 10^{-6}-10^{-12} moles of Pt^{4+} to 0.05-0.4 g of the silanes.

Crosslinkings of Petrarch's siloxane PDMS were carried out by adding drops of concentrated THF/H_2O solution of $Zn(Ac)_2$, $SnCl_4$, $[Co(en)_3]_2(SO_4)_3$, $SnCl_2$, triethanolamine, $ZrCl_4$, DCP, BPO, AIBN, Pt^{4+}, and ethanolic NaOH followed by heating and curing in an air sealed glass vial up to 150°C or heating in N_2 gas up to 300°C.

Detection and confirmation of crosslinking of the polymers were tested by using FT-IR, solubility in a solvent (benzene or THF), and fusion at ~200°C. Pyrolysis of the polymers was carried out in a high temperature furnace with an inert gas flowing at a rate of ~100 ml/min. and also in a DuPont TGA 951 Thermogravimetric Analyzer with N_2 or Ar continuous flowing with a heating rate of 10°C/min. Differential scanning calorimetry (DSC) using the same DuPont Model 951 was carried out in continuous Ar flowing with a heating rate of 5°C/min.

Crosslinking reaction products of PSS via DCP were identified by GC's in order to elucidate the reaction mechanism. The product gasses were introduced into a Tracor GC 550 and an HP 5880A GC. The detailed experimental conditions and sample preparation are as follows:

Approximately 0.1 g of PSS-1P was dissolved in 1.5 ml of degassed benzene, and then ~0.01 g DCP added and mixed in a 20 ml glass vial. The thick solution was vacuum dried to evaporate benzene at room temperature

for two hours. The dried sample (PSS/DCP) was placed in a glass vial with a rubber septum or in a Pyrex glass loop directly attached to the Tracor GC injection port. The samples in the glass containers were heated to ~300°C by a Bunsen burner for 0.5-1 min. The product gasses were either directly introduced to the silica gel column of a Tracor 550 through a valve or drawn by a syringe through the septum. The gas drawn by a syringe was dissolved in a methylene chloride ($MeCl_2$) solvent; a few microliters of this solution was injected into the capillary column of an HP 5880A GC.

The GC parameters used are given below.

Instrument:	Tracor 550 and HP 5880A interfaced to an HP 85 computer
Column:	Silica gel 2.7 m 60-200 mesh and glass capillary
Detector:	Flame ionization
Column T:	45°C and programmed from 80°C to 250°C at 20°/min.
Injector T:	180°C
Detector T:	180°C
Carrier Gas:	N_2

The overall experimental conditions for crosslinking of various OS precursors are summarized in Table II-5.

Infrared spectra, SEM micrographs, and EDS spectra were obtained by using a Nicolet MX-1 FT-IR Spectrophotometer and a JEOL model JSM-35C electron microscope, respectively. The assignments of IR bands are based on reference number 56 and are given in Table II-6.

Table II-5. Summary of Experimental Conditions for Crosslinking of Various Polysilanes.

Silane	Means	Solvent or Atmosphere	Crosslinking T, °C	Length of Crosslinking Treatment
PSS-P	γ-ray 1-2.5 cm distance	air Ar He N_2O vac. benzene	RT	1-29 days
	DCP BPO AIBN	N_2 vac. benzene toluene	100-250	10 min-20 hrs
	DCP/γ-ray	benzene	RT	1 hr-5 days
	thermal	benzene/N_2 vac.	85-300	10 min-4 days
	oxygen	air	80	3 weeks
PSS-O	γ-ray	air Ar vac. benzene	RT	1-20 days

Table II-5 (continued).

	DCP BPO AIBN	benzene THF N_2 air	20-250	10 min-20 hrs
	thermal	N_2	150-300	10 min-2 days
	oxygen	air	80°	3 weeks
A-PSS	thermal	toluene N_2 air sealed	100-300	20 min-24 hrs
	DCP	air sealed	70-170	1-24 hrs
	Pt^{4+}	air sealed	70	0.15-12 hrs
ViSP	thermal		70-300	1-24 hrs
	DCP	air sealed	120	1-10 hrs
	Pt^{4+}		65-150	1-48 hrs
ViSO	thermal	vac.	70-300	1-24 hrs
	γ-ray	vac.	RT	18 hrs-10 days
	DCP BPO AIBN	air sealed	110 75	0.5-3 hrs 1-12 hrs
	Pt^{4+}	vac.	70-150°C	1-48 hrs

Table II-5 (continued).

Siloxane PDMS	$ZnCl_4$ $SnCl_4 \cdot 5H_2O$ $SnCl_2$ $Zn(Ac)_2$ $[Co(en)_3]_2(SO_4)_3$ ethanolic NaOH DCP BPO AIBN Pt^{4+}	N_2 air sealed	60-300°C	0-5 days

Table II-6. Infrared Absorption Bands of Polysilanes

$\bar{\nu}$, cm^{-1}	Mode	Shape, Intensity
300	Si-Si bending	weak
420	H-Ph rocking	weak
400-480	Si-Si stretching	
700-800	Si-C stretching	broad
800-850	Si-CH_3 rocking	
850-1000	Phenyl C-H bending	
1020	Si-CH_2-Si wagging	shoulder
1100	Si-O-Si stretching	sharp
	Si-Ph	medium
1250	Si-CH_3 bending	strong
1400	-CH_3 deformation	broad, strong
1480-1580	Aromatic C=C	weak, sharp
1620	OH bending of adsorbed water	
1600-1680	C=C aliphatic	
1710	C=O	medium
1800	-Ph	broad
2100	Si-H	sharp, medium
2900	C-H stretching in Si-CH_3	strong
3050	C-H stretching in atomatic	narrow
3450	OH stretching	broad
3630	Si-OH stretching	broad

Results

Characterizations of the precursor silanes

Some of typical IR, EDS, and NMR spectra are given in Figs. II-4 through II-19. The M. W. distributions, % yield of each fraction, and $MePhSi/Me_2Si$ ratio for PSS are given in Table II-7. The $MePhSi/Me_2Si$ ratios were estimated by integrating the area under the peaks and normalized by the number of protons in each group of the peak.

The oligomer fraction of PSS-1 in Fig. II-4 shows some C-OH and Si-OH (~3300 cm^{-1} and 3600 cm^{-1}), Si-H (~2100 cm^{-1}), possibly some unsaturated carbon, i.e. C=C (~1600-1900 cm^{-1}), strong and sharp Si-Me stretch (~1250 cm^{-1}), the strong and broad band for Si-O-Si, and Si-Ph overlapped with Si-O-Si (~1100 cm^{-1}), -Ph (~700 cm^{-1}), and an Si-Si stretching band at ~450 cm^{-1}. In PSS-1P, there is not as much Si-OH and little C-OH, less Si-H, and a small but sharp peak for Si-Ph at ~1100 cm^{-1} is shown (Fig. II-5).

Figure II-6 suggests that the oligomer fraction of PSS-1 has a more complex structure, indicated by multplets of the CH_3 region (~1-2 ppm δ scale) and the Ph-H region (8-9 ppm), than the corresponding structure of the polymer fraction. It also shows a possible C=C band at ~4.9 ppm which is absent in the polymer fraction (Fig. II-7). The peak at ~2.6 ppm may be ascribed to to $-CH_2-$ or to Si-H.

Figure II-8 for PSS-20 shows that a larger proportion of Si-H is present in the oligomer, but less Si-OH and C-OH is present than in PSS-10 (Fig. II-6). Although PSS-10 and PSS-20 are both oligomer fractions of PSS, the IR spectra show that they are not exactly the same

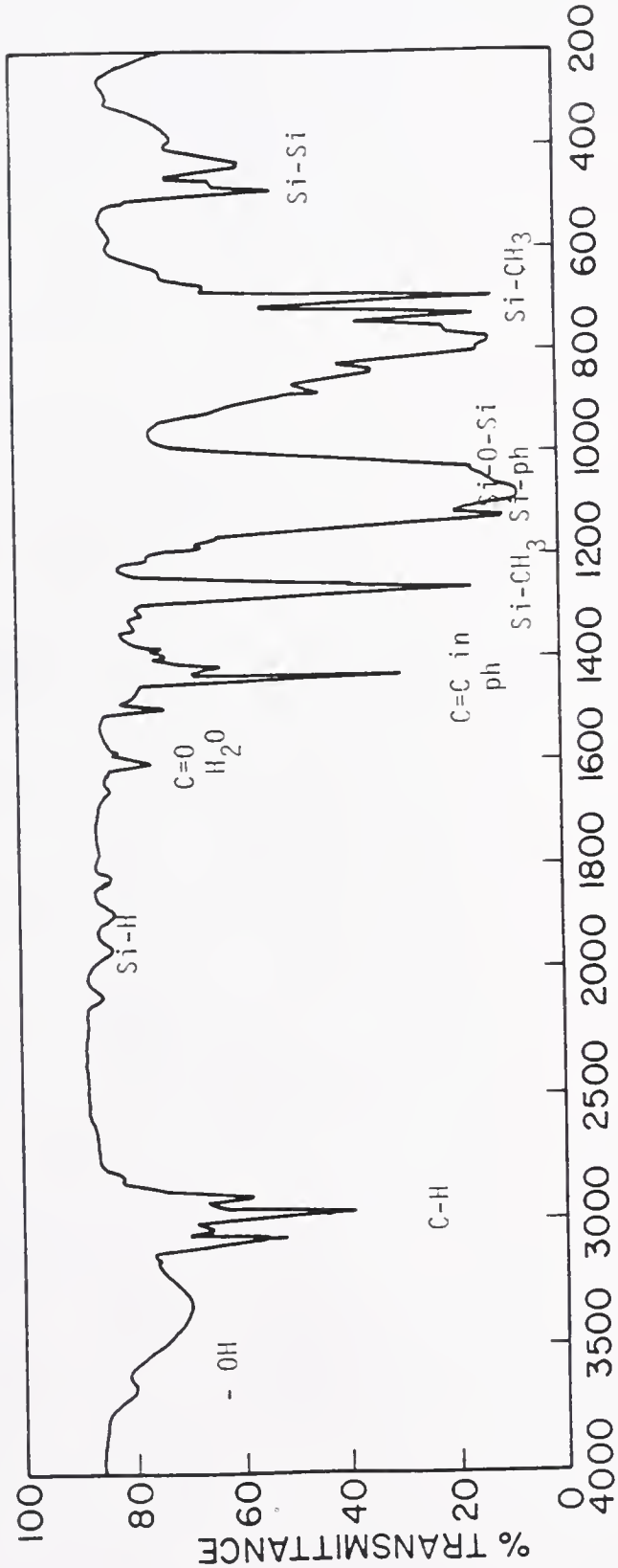

Fig. II-4. Infrared Spectrum of a Oligomer Fraction of Polysilastyrene (PSS-10)

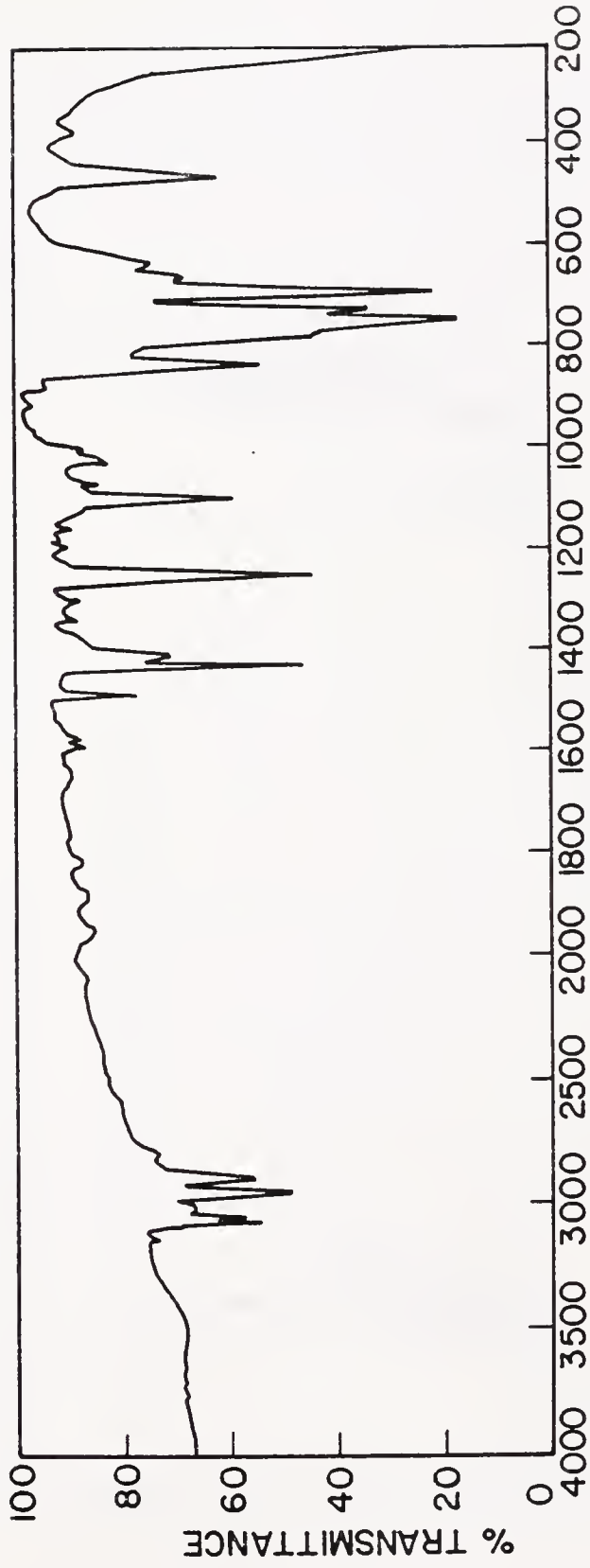

Fig. II-5. Infrared Spectrum of Polymer Fraction of Polysilastyrene (PSS-1P)

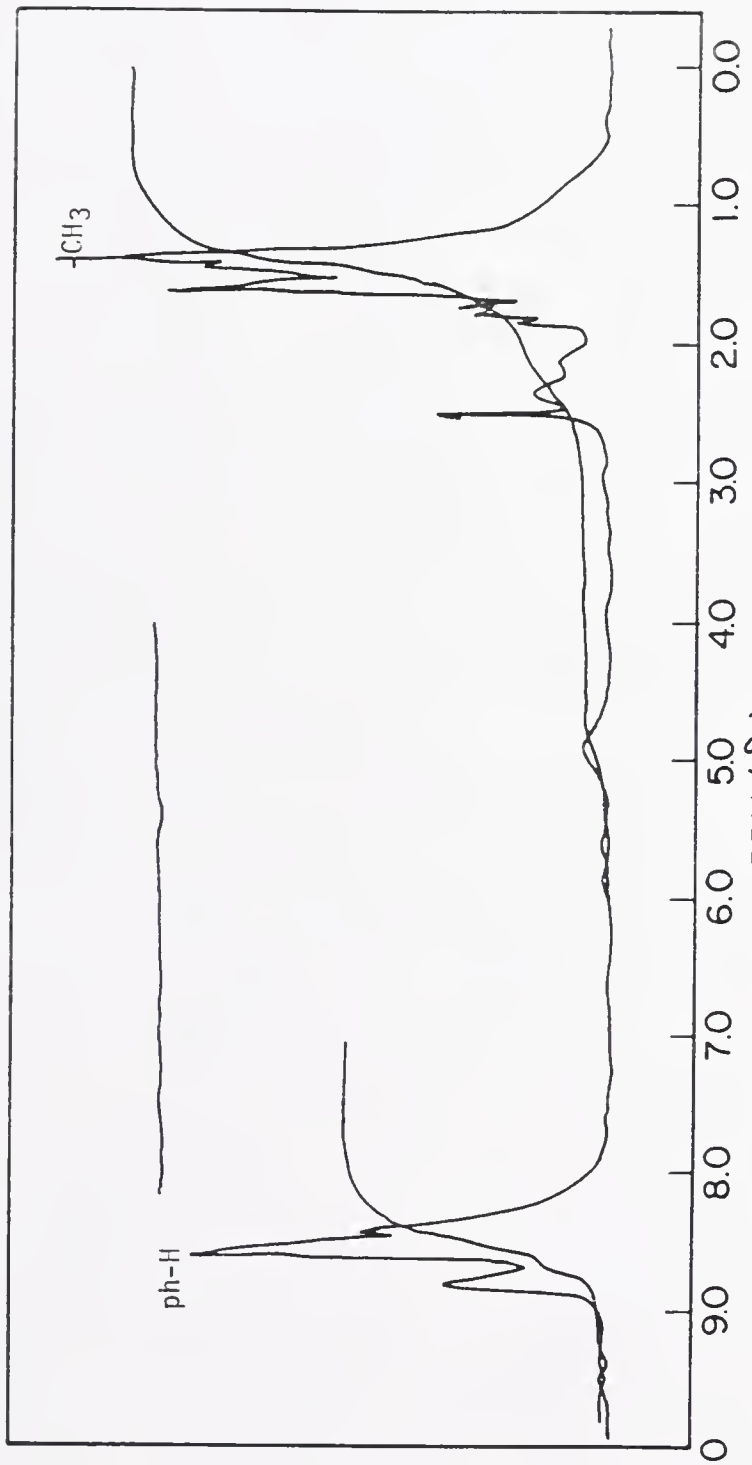

Fig. II-6. Proton Nuclear Magnetic Resonance Spectrum of PSS-10

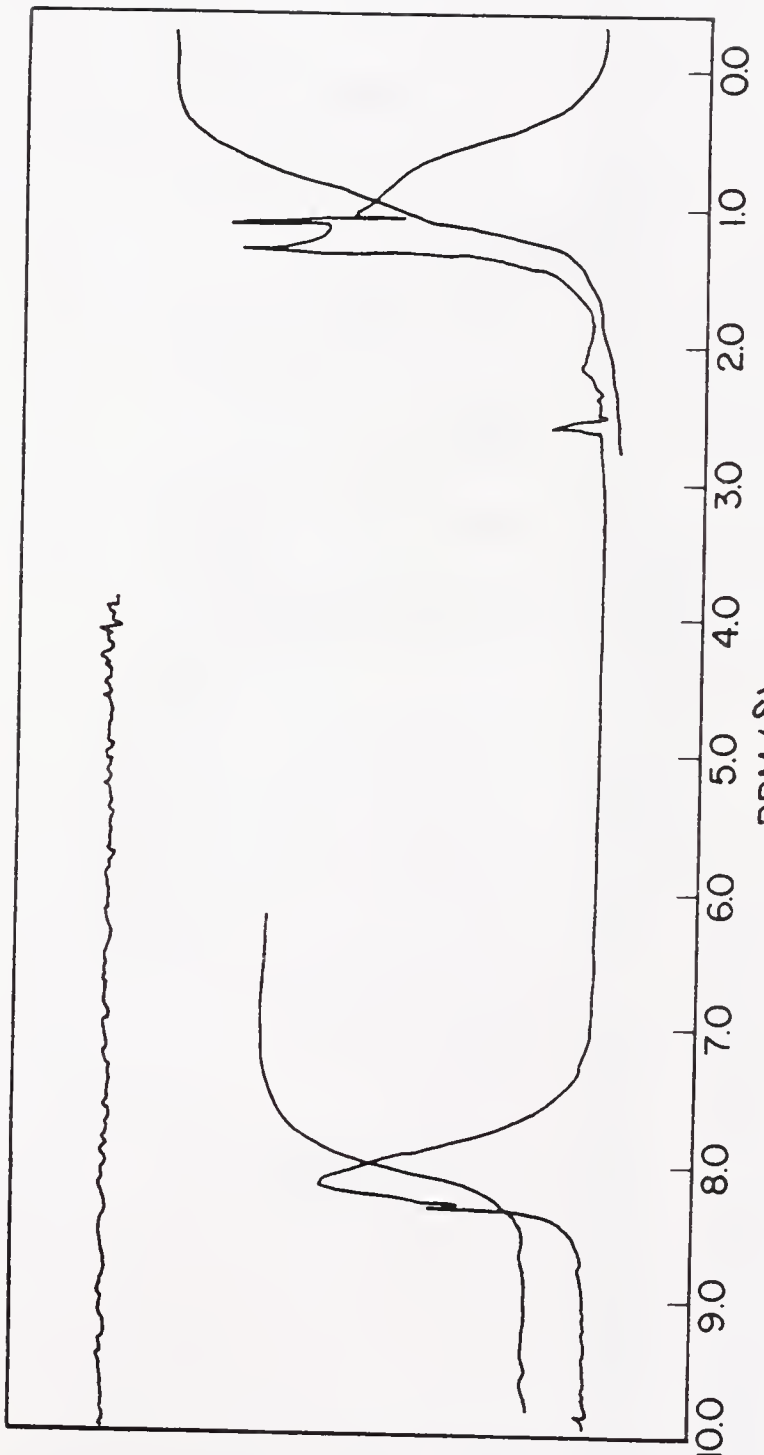

Fig. II-7. Proton Nuclear Magnetic Resonance Spetrum of PSS-1P

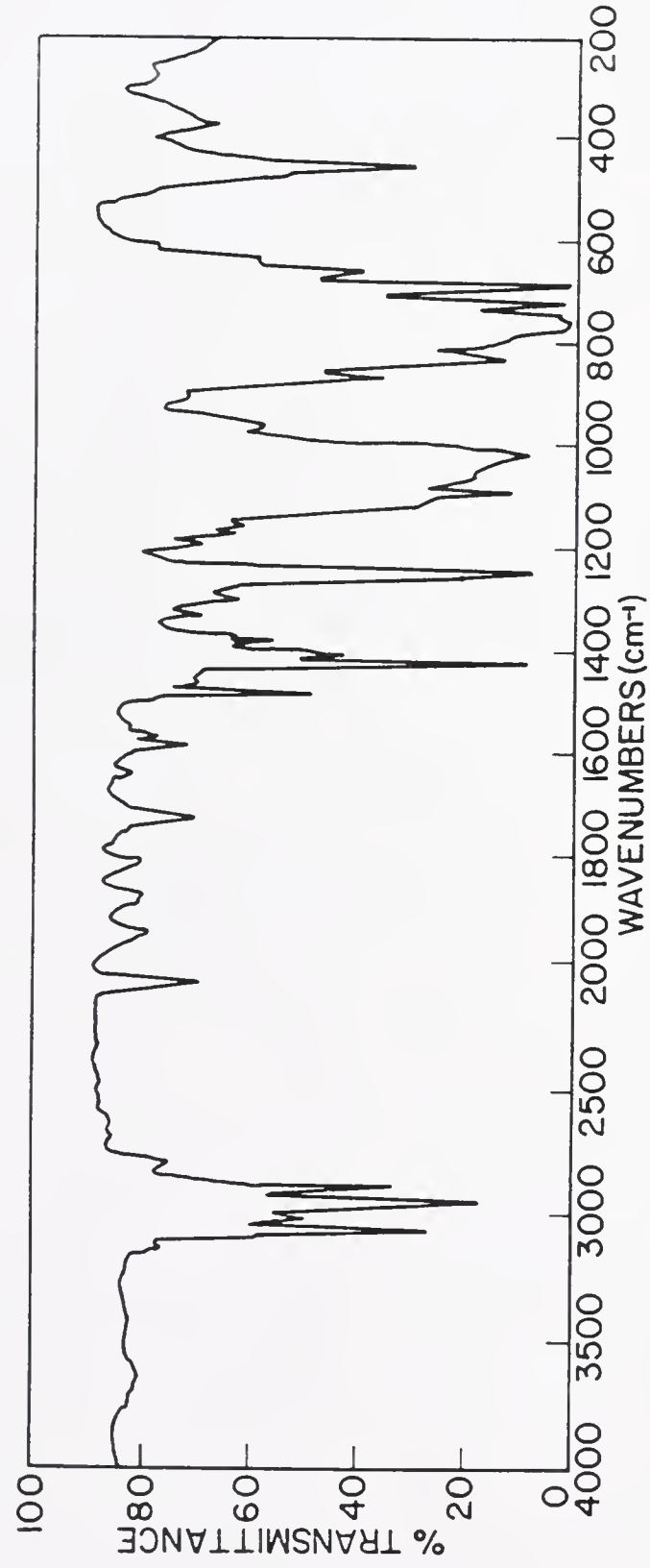

Fig. II-8. Infrared Spectrum of PSS-20

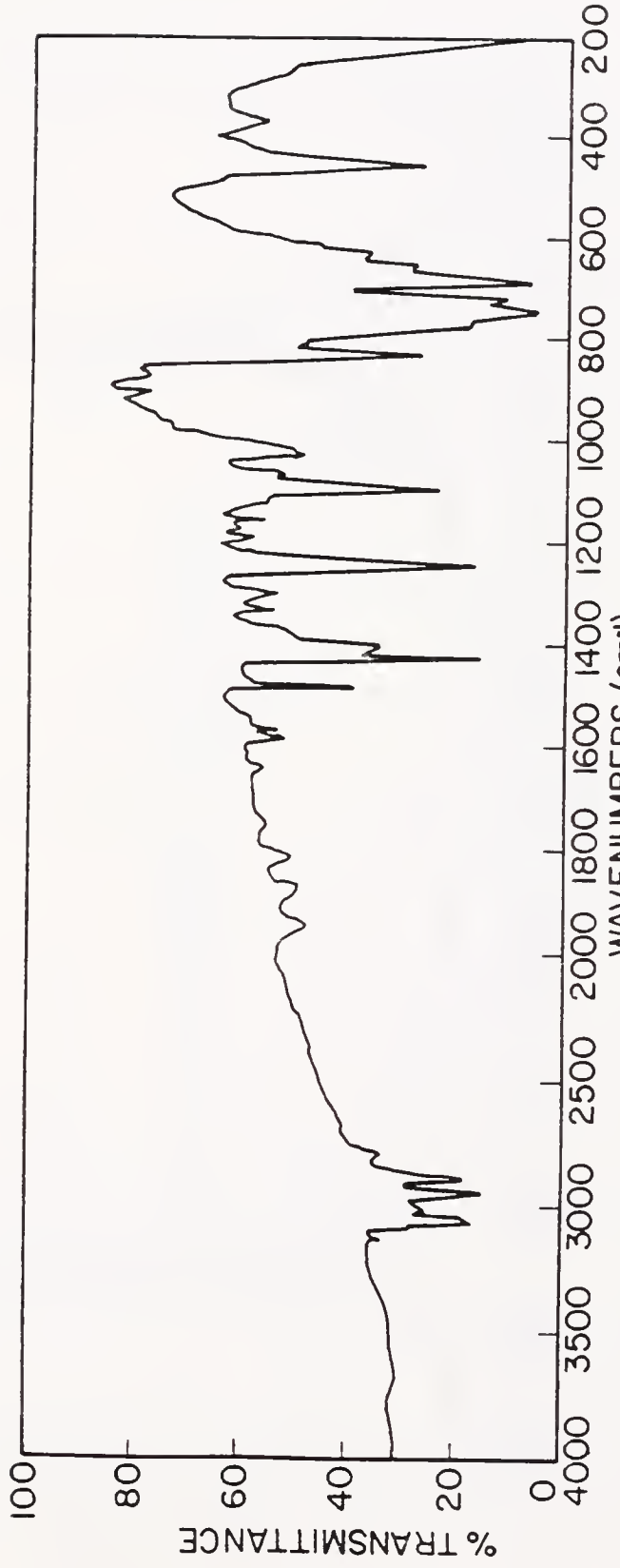

Fig. II-9. Infrared Spectrum of Allylic PSS Oligomer

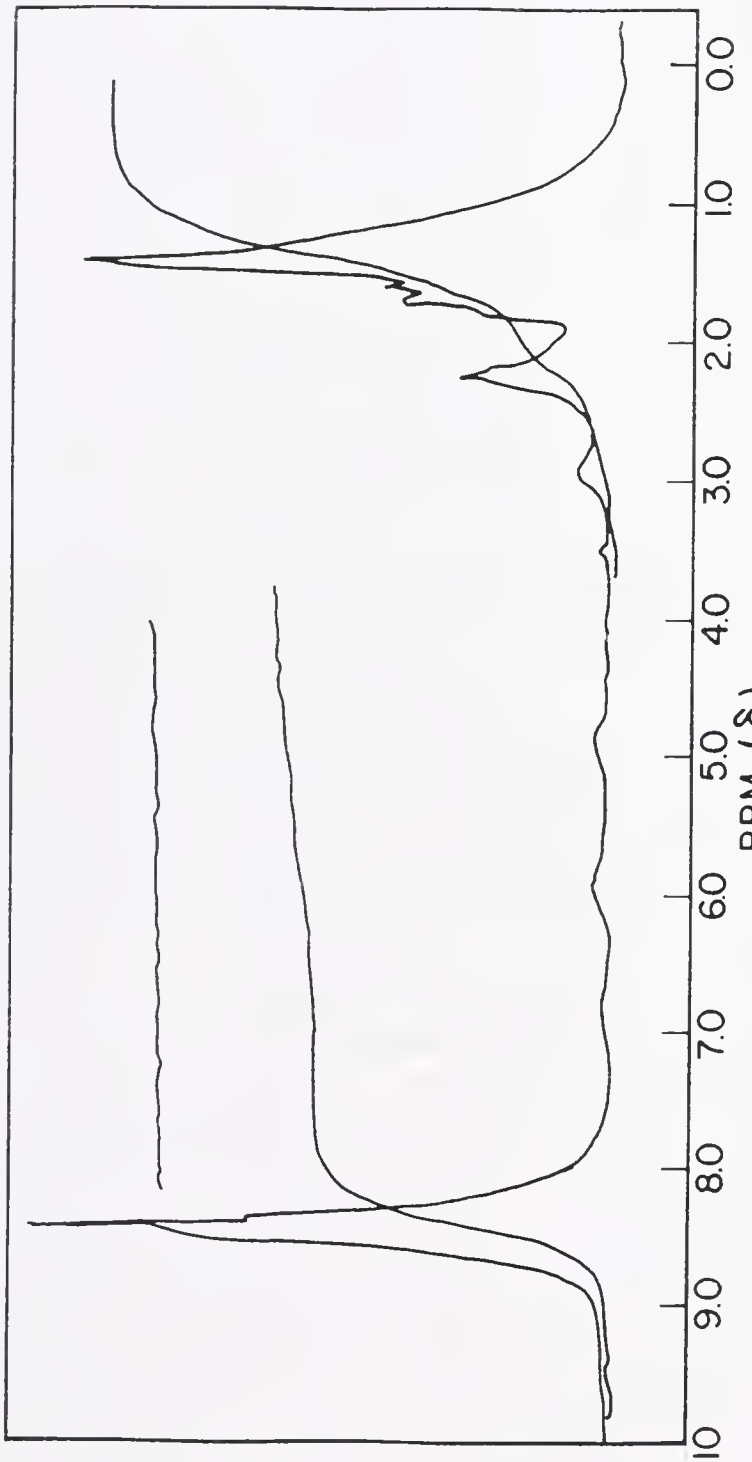

Fig. II-10. Proton Nuclear Magnetic Resonance Spectrum of Allylic PSS Oligomer

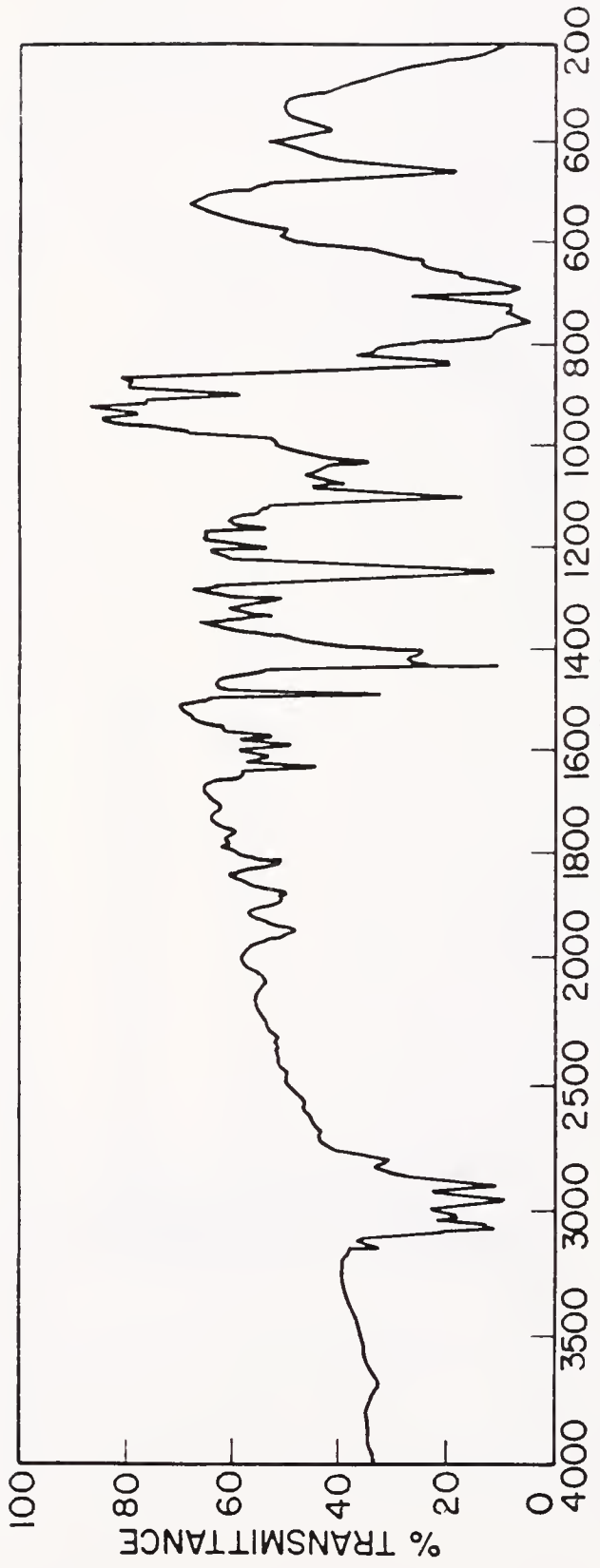

Fig. II-11. Infrared Spectrum of Allylic PSS Polymer

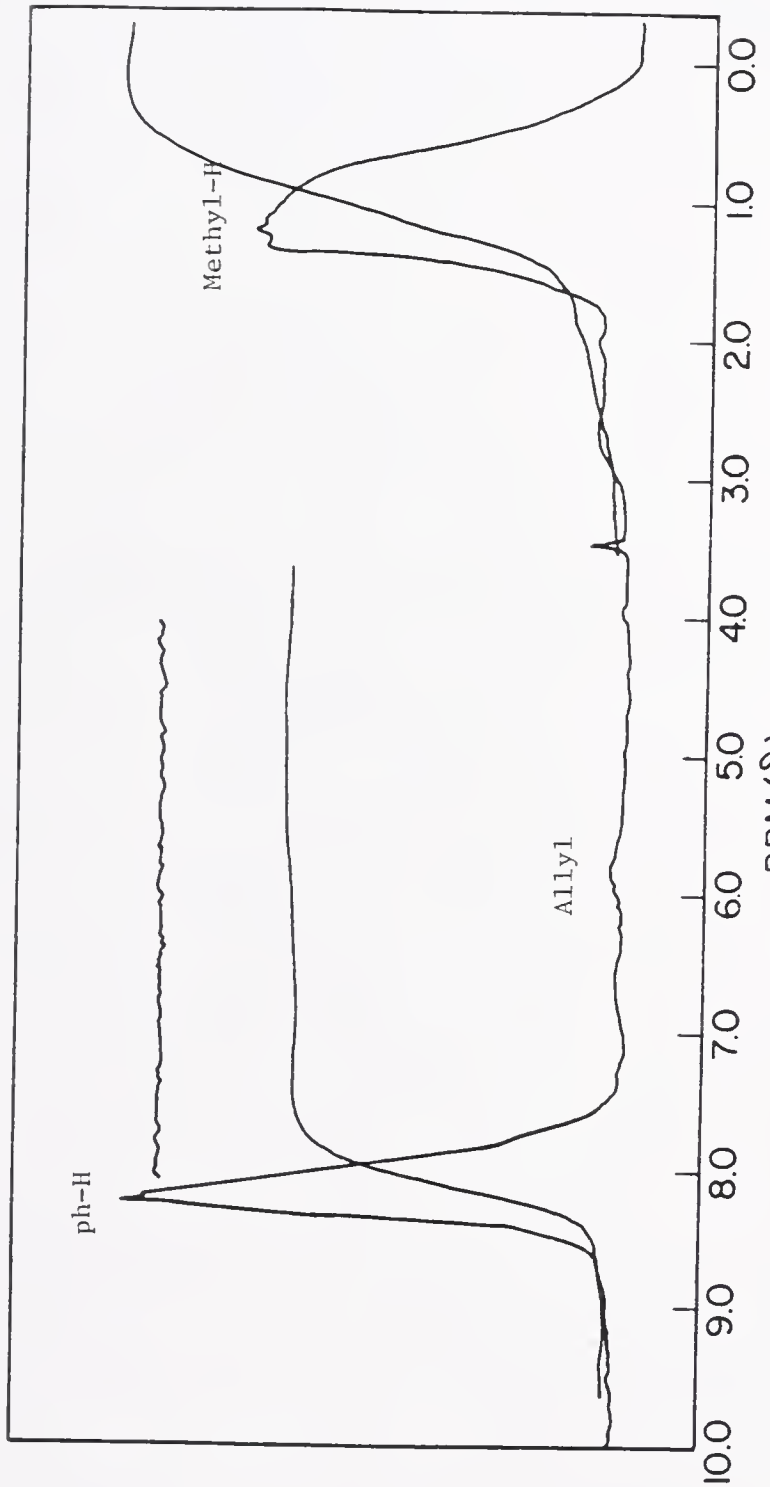

Fig. II-12. Proton NMR Spectrum of Allylic PSS Polymer

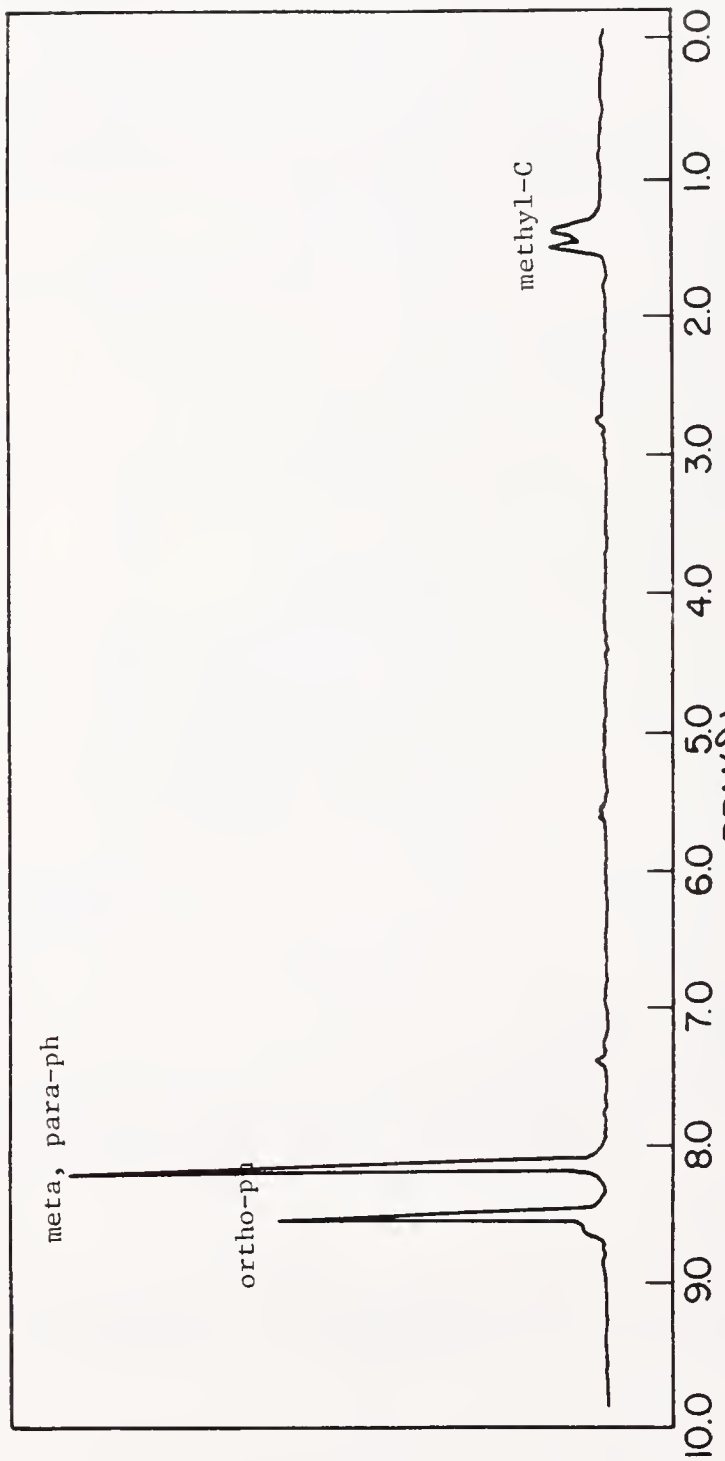

Fig. II-13. Carbon-13 NMR Spectrum of Allylic PSS Polymer

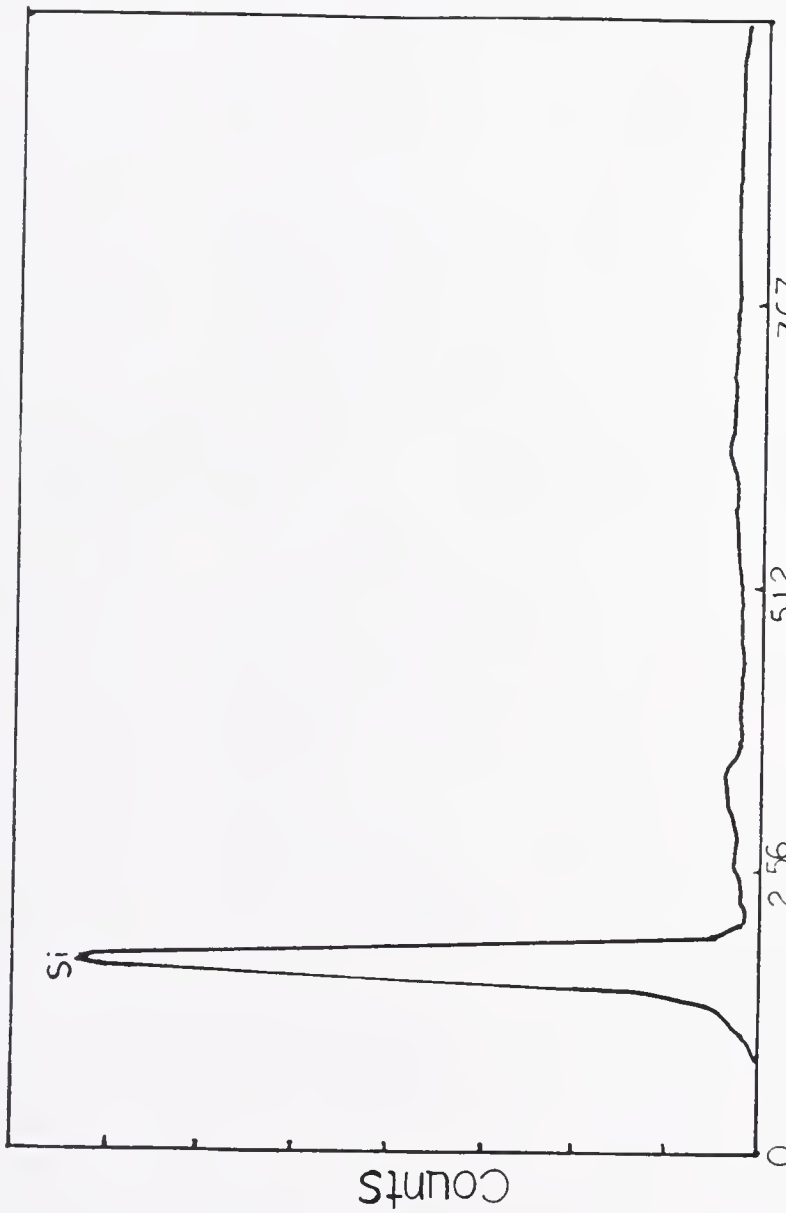

Fig. II-14. Energy Dispersive Spectrum of PSS

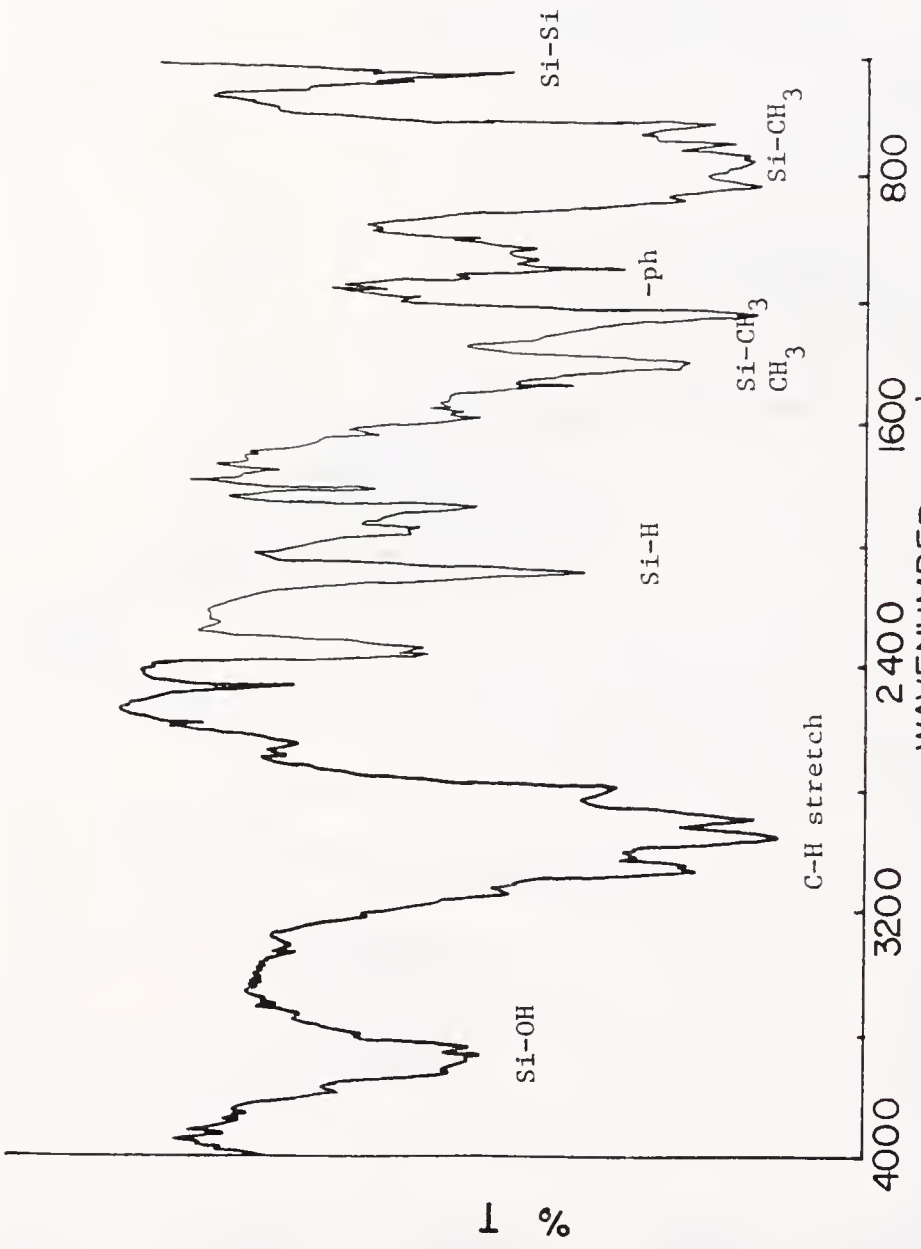

Fig. II-15. FT-IR Spectrum of Solvent Insoluble Fraction of PSS-1

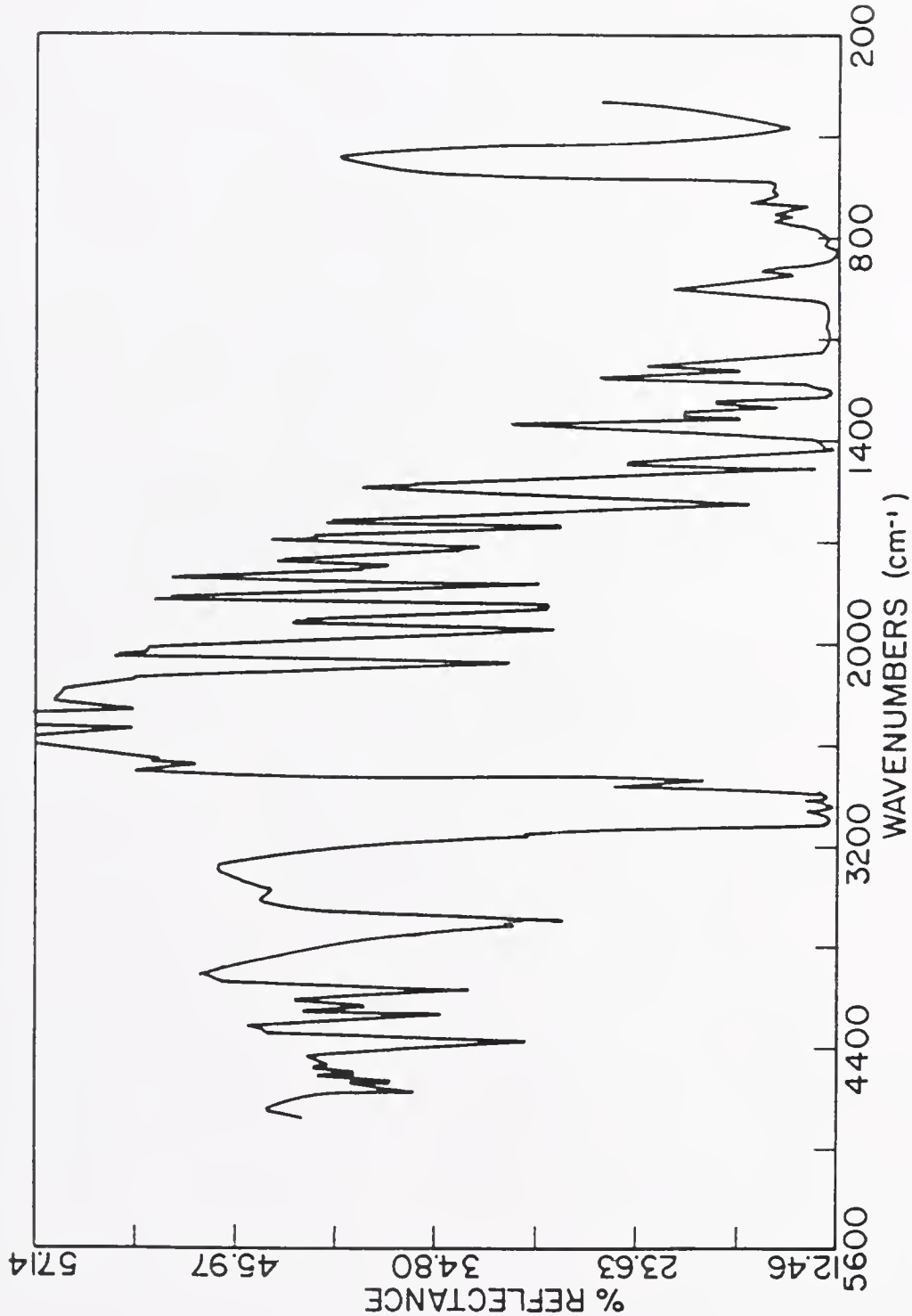

Fig. II-16. FT-IR Spectrum of J-PSSI

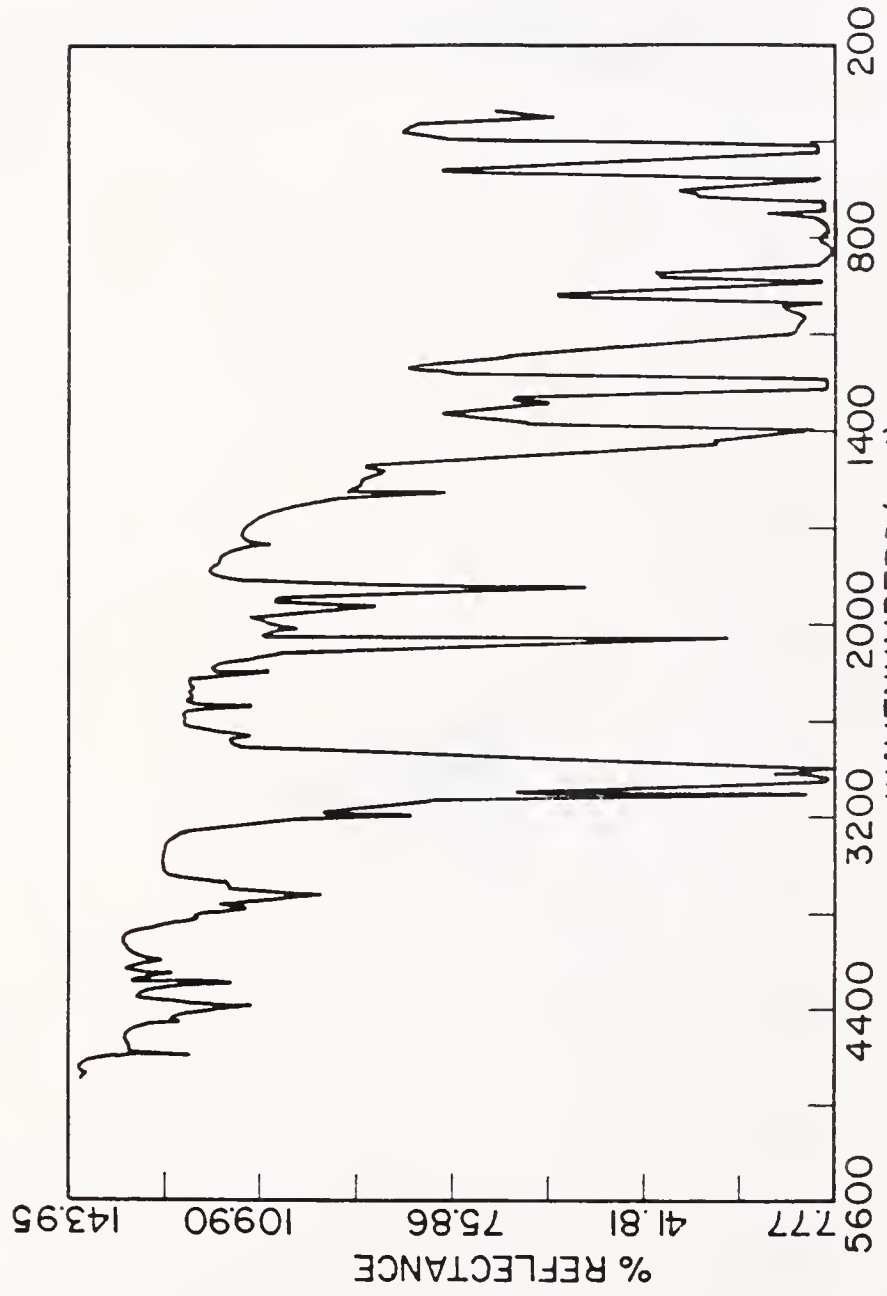

Fig. II-17. FT-IR Spectrum of Oligomer Fraction of Vinylic Silane (ViSO)

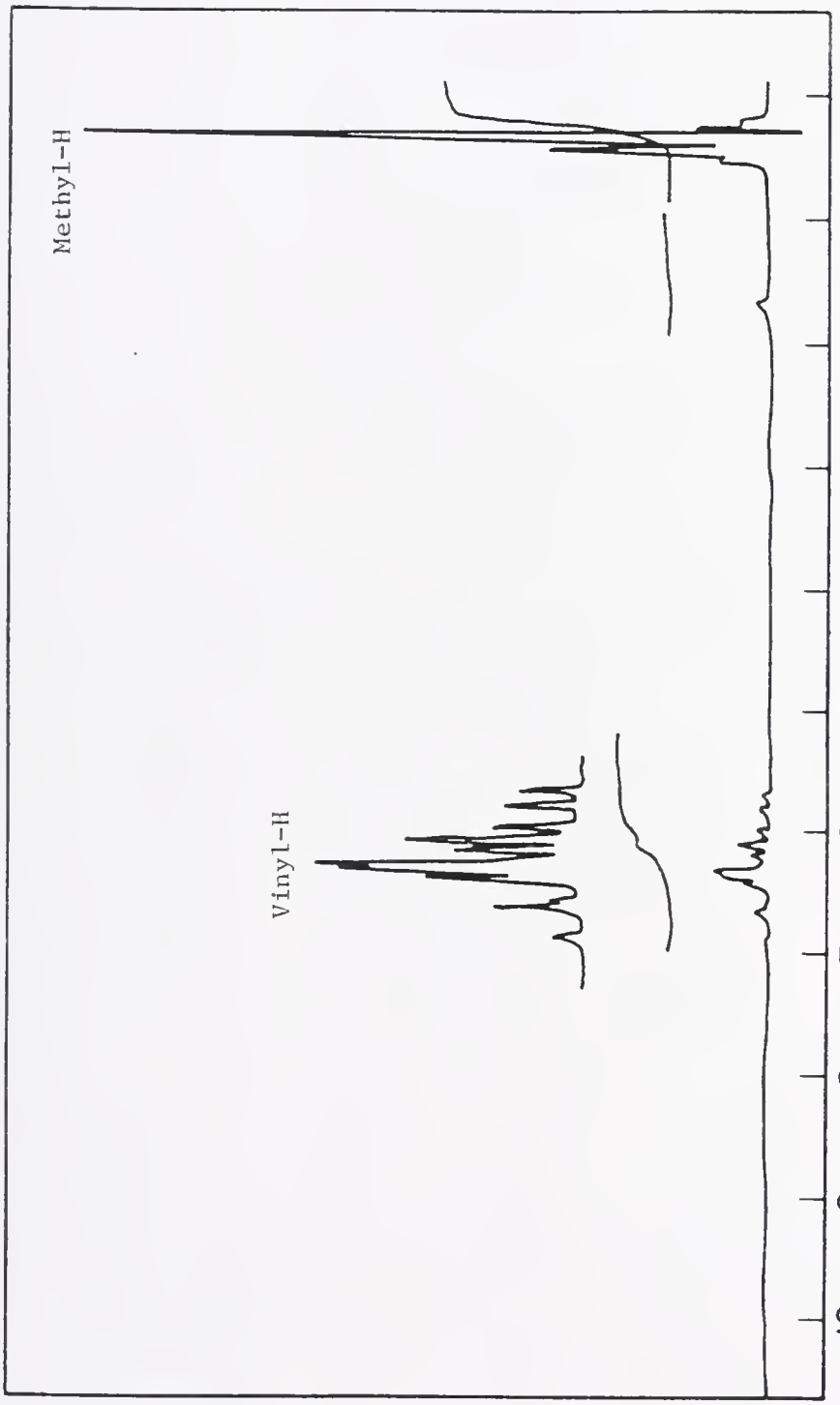

Fig. II-18. Proton NMR Spectrum of Vinylic Silane Oligomer

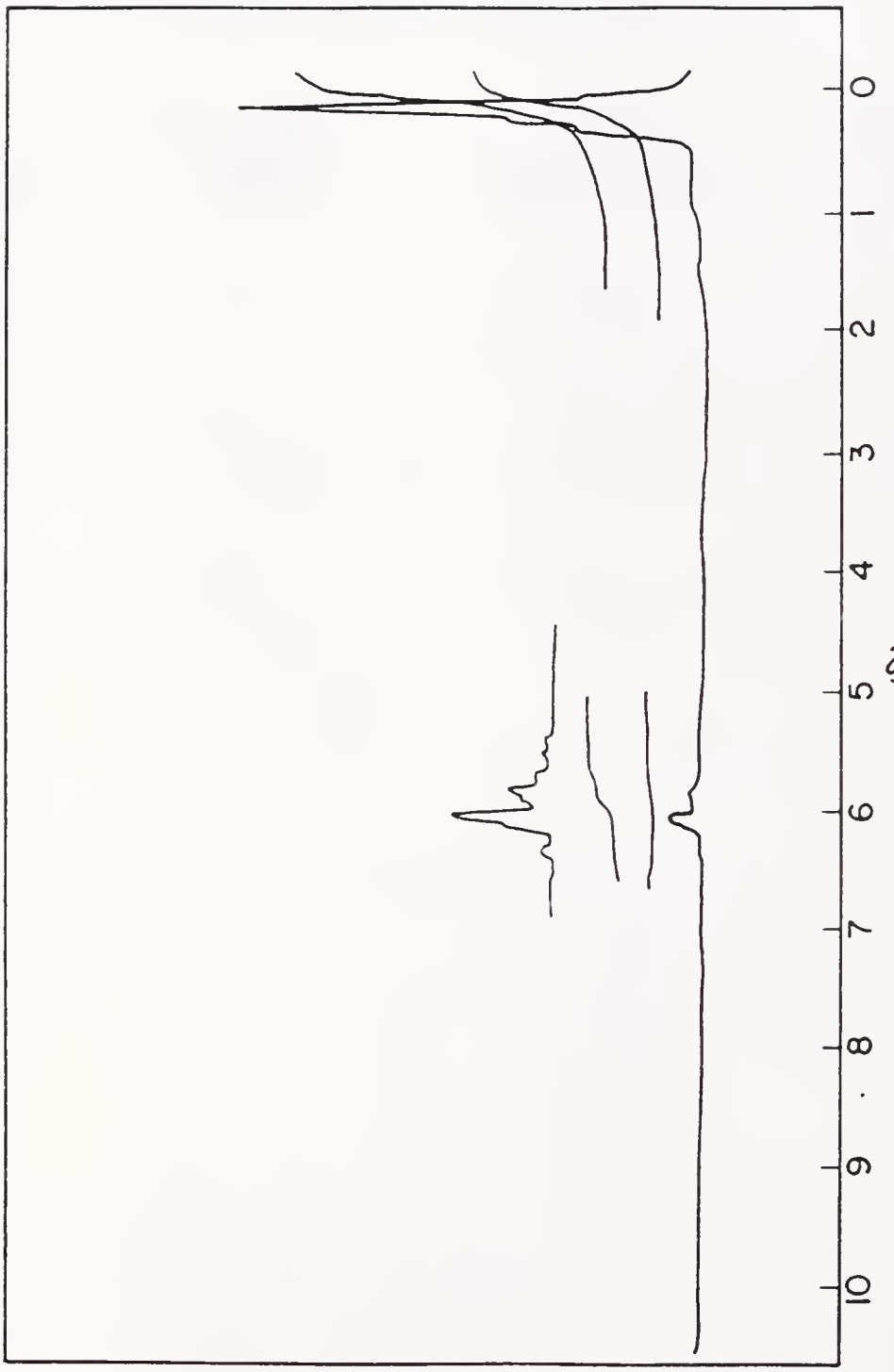

Fig. II-19. Proton NMR Spectrum of Vinylic Silane Polymer

Table II-7. M. W. Distribution, % Yield, and the Ratio of $MePhSi/Me_2Si$ for PSS

Silane	M. W. ($\overline{Mn}$) Oligomer Polymer	% Yield Oligomer Polymer Insol. Polymer	Ratio $MePhSi/Me_2Si$ Oligomer Polymer
PSS-10	390	72	1.05
		19	1.1
PSS-1P	10×10^3	8	
PSS-20	344	72	1.20
		15	1.35
PSS-2P	11×10^3	11	
A-PSS-P	331	75	1.1
		12	1.2
A-PSS-O	11×10^3	11	
J-PSS1	6.8×10^4		

compound; see qualitative differences at ~1720 cm^{-1}, ~1580 cm^{-1}, ~1250 cm^{-1}, and ~450 cm^{-1}.

Figures II-9 and II-10 show that the allylic PSS oligomer has a greater unsaturated carbon group, as indicated by the broader band at ~1600 cm^{-1}; this is supported by the NMR data which show small humps around 3-7 ppm. However, this cannot be conclusive because the bending mode of water is also at ~1600 cm^{-1}. The band shape at ~1450 cm^{-1} is different from the nonallylic PSS. A significant amount of Si-O-Si may be present in A-PSS-0. Groups including possibly Si-H and an allyl group represent ~4% of the total protons based on the NMR data. Allylic PSS polymer represented by Figs. II-11 and II-12 contains a smaller proportion of Si-H relative to C=C. Carbon-13 NMR (Fig. II-13) does not reveal any additional information.

Figure II-14 shows that only Si as a metallic element is present in PSS-1P under EDS analysis.

Figure II-15 for the solvent insoluble fraction of PSS-1 presumably due to the crosslinked network indicates that the polymer may be mainly composed of

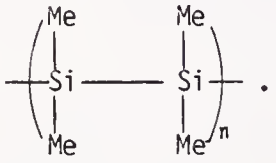

An infrared spectrum of J-PSS1 (Fig. II-16) obtained from the diffuse reflectance mode of FT-IR indicates that Si-H is present, as well as -OH, but not as much Si-O-Si is shown. An IR spectrum for ViSO (Fig. II-17) obtained by the same way as for J-PSS1 shows a larger proportion of Si-H. A small but sharp band at ~1600 cm^{-1} may be that of C=C. The

NMR spectrum of ViSO in Fig. II-18 shows the presence of a vinyl group at 6.2 ppm. It is difficult to see the presence of Si-H, although small humps between 1-4 ppm are shown. The NMR spectrum for ViSP (Fig. II-19) indicates that the polymer has essentially the same structure as the oligomer ViSO.

Crosslinking and pyrolysis

Silanes exposed to a γ-ray dose greater than 200 Mrad (~30 days at 1" distance from the source at 0.3 Mrad/hr) were infusible at temperatures above 200°C and were insoluble in THF or in benzene, indicative of crosslinking. Additions of CFRI prior to γ-ray irradiation made no difference in the crosslinking reaction rate.

Fourier Transform IR spectra of PSS samples before and after 29 days of γ-ray irradiation are shown in Fig. II-20. The polymer film on a stainless steel plate after 29 days of irradiation in vacuum showed insolubility in THF and infusibility upon heating up to 250°C.

Gamma-ray irradiation of the vinyl silane oligomer in vacuum showed an increase in viscosity within twelve days from a watery fluid to a semisolid form. The vinyl silane upon heating at ~200°C for 10 min in N_2 was transformed into a light yellow translucent solid which was insoluble in toluene.

Gamma-ray irradiation of PSS in a N_2O atmosphere for >11 days changed the color of PSS from translucent yellow-green to bright red-brown. The viscosity of PSS decreased sharply, indicating the degradation of the polymer.

Among the CFRI's investigated (BPO, AIBN, and DCP), only DCP in the range of 2-15 wt% in PSS/benzene solution showed a positive crosslinking

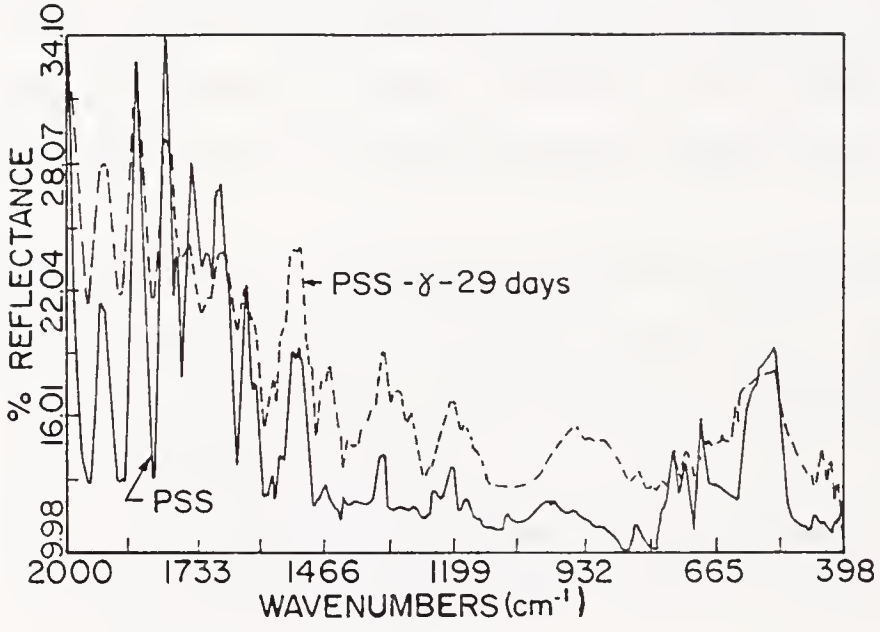

Fig.II-20. Reflectance FT-IR Spectra of PSS Before and After 29 Days of γ-ray Irradiation in Vacuum

reaction. The CFRI DCP has the highest decomposition temperature of ~150°C of all other CFRIs. The FT-IR spectrum of DCP crosslinked PSS at 250°C compared with that of the as-synthesized PSS is shown in Fig. II-21. The DCP reacted polymers were insoluble in benzene and infusible at temperatures above 200°C. The density of PSS crosslinked by DCP measured by mercury volume displacement was 0.77 g/ml. Fourier Transform IR spectra of A-PSS samples after they were treated at different crosslinking conditions are compared in Figs. II-22 and II-23. Oxygen crosslinking by heating in the air at 25-80°C came out negative for all PSS precursors.

In the crosslinking of ViSP without DCP under the same conditions as with DCP, no solidification was observed within 20 hrs. However, curing at 30°C higher temperature 140°C resulted in solidification of the liquid ViSP, signifying crosslinking.

The difference in the chemical structure of the ViSP samples crosslinked thermally compared with ViSP samples crosslinked with DCP is shown by FT-IR spectra in Fig. II-24.

Chromatograms of the gaseous products from a crosslinking reaction of PSS with DCP after being separated by a GC is given in Figs. II-25 and II-26. Approximately 100 times more methane is produced as compared with ethane, as shown in Fig. II-25.

Differential scanning calorimetry thermograms are given in Figs. II-27 and II-28 to compare the crosslinking mechanisms. In Fig. II-29, DSCs of oligomer and polymer PSS are compared. Scanning electron micrographs of the surface of DCP crosslinked and pyrolyzed PSS and ViSP are shown in Figs. II-30 and II-31.

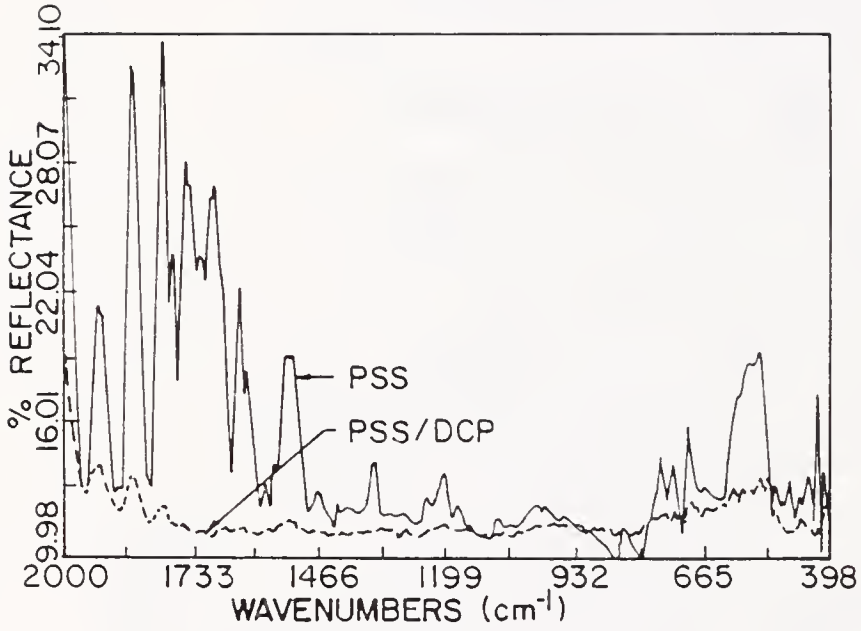

Fig. II-21. FT-IR Spectra of PSS-1 and PSS-1 Crosslinked With 8% DCP

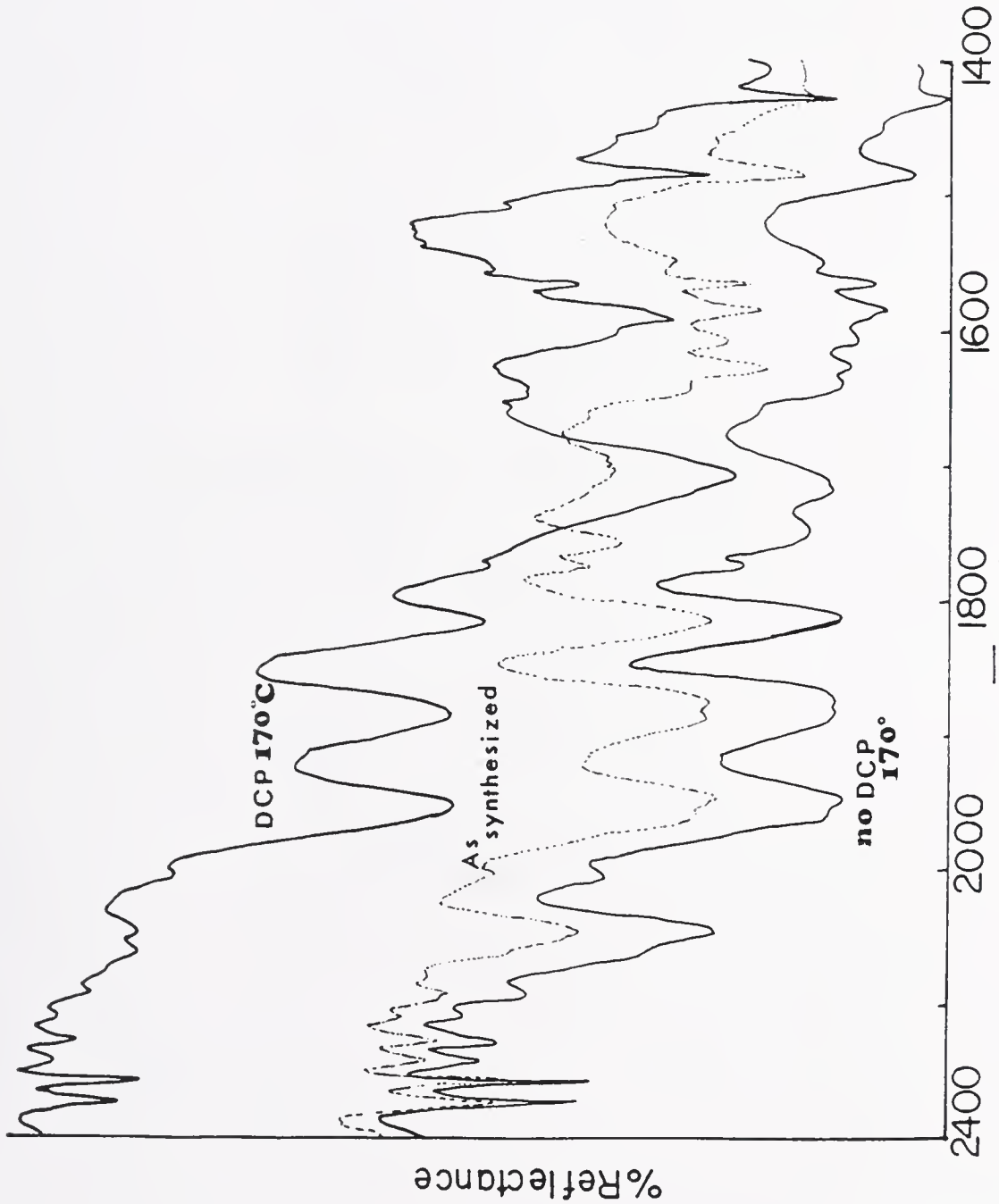

Fig. II-22. FT-IR Spectra of Allylic PSS Before and After Crosslinking

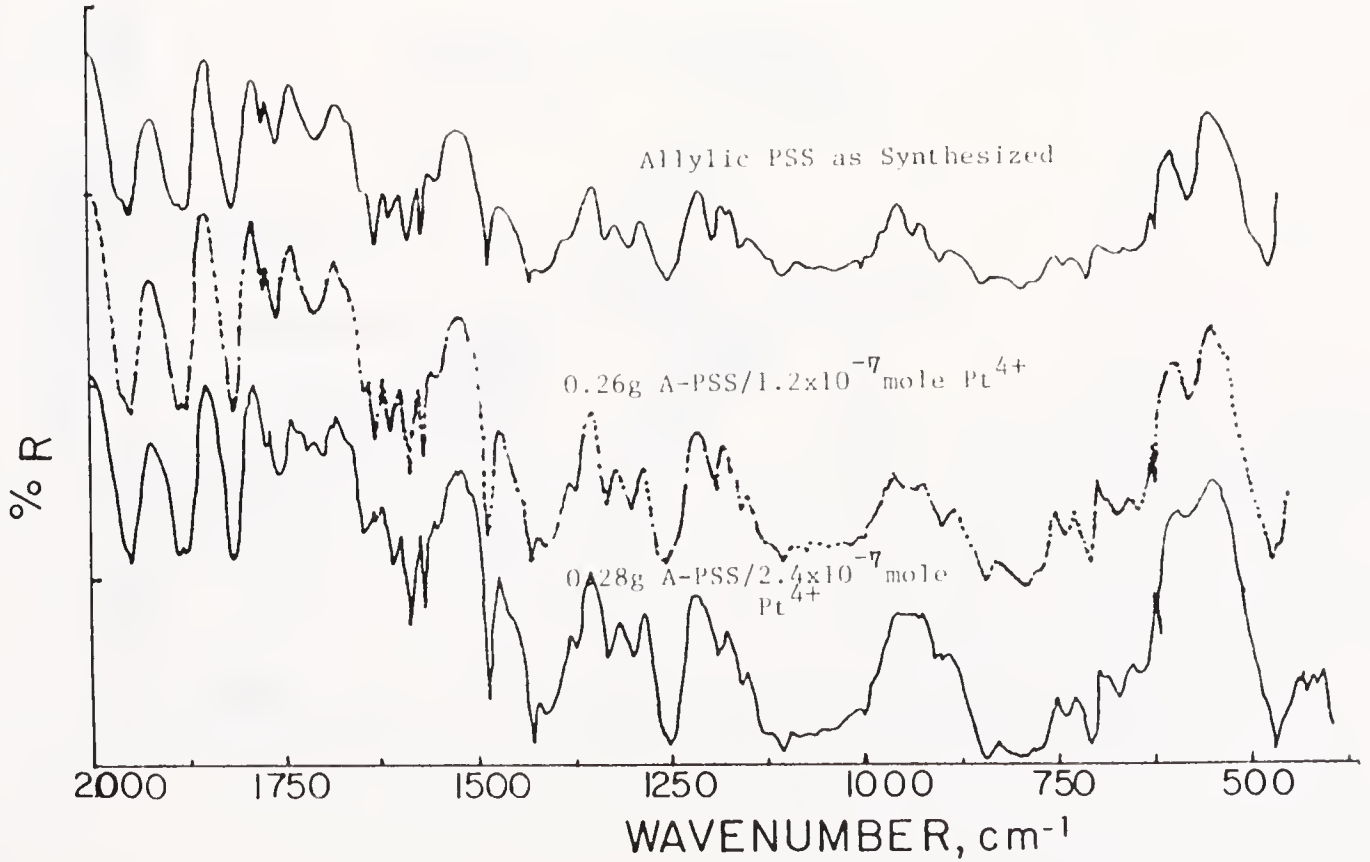

Fig. II-23. FT-IR Spectra Showing the Crosslinking Effect of Pt^{4+} Catalyst on Allylic PSS

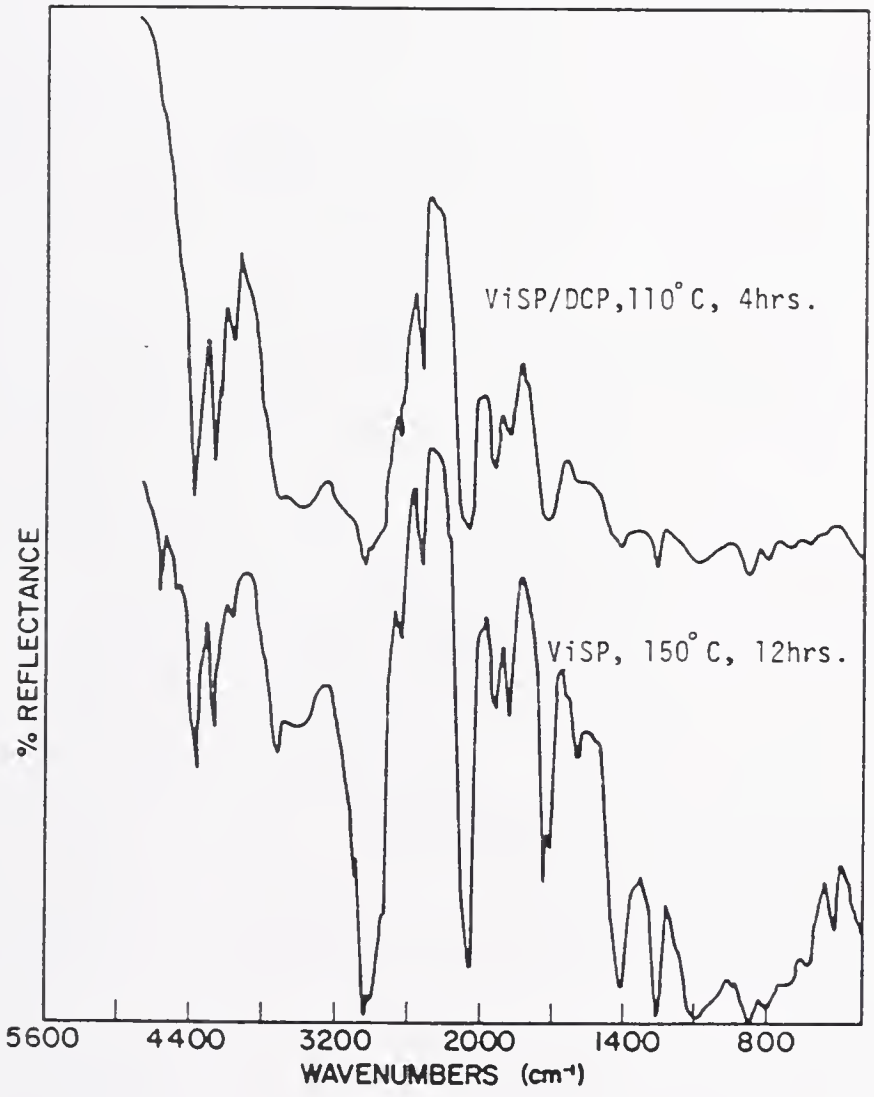

Fig. II-24. FT-IR Spectra of Crosslinked Vinylic Silane Showing the Effect of DCP, Temp., and Time.

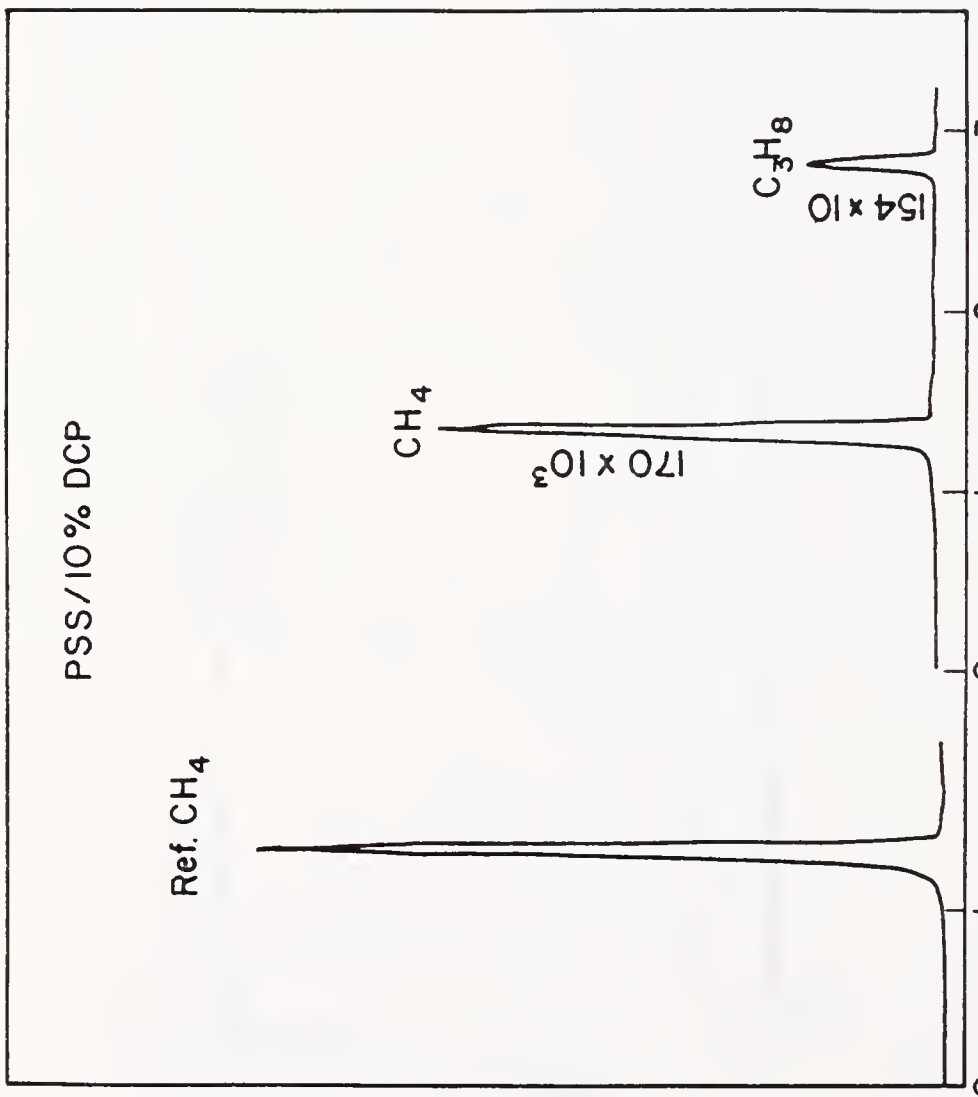

Fig. II-25. Gas Chromatograms of the Gaseous Products From PSS/DCP Crosslinking Reaction Showing Methane as a Major Product

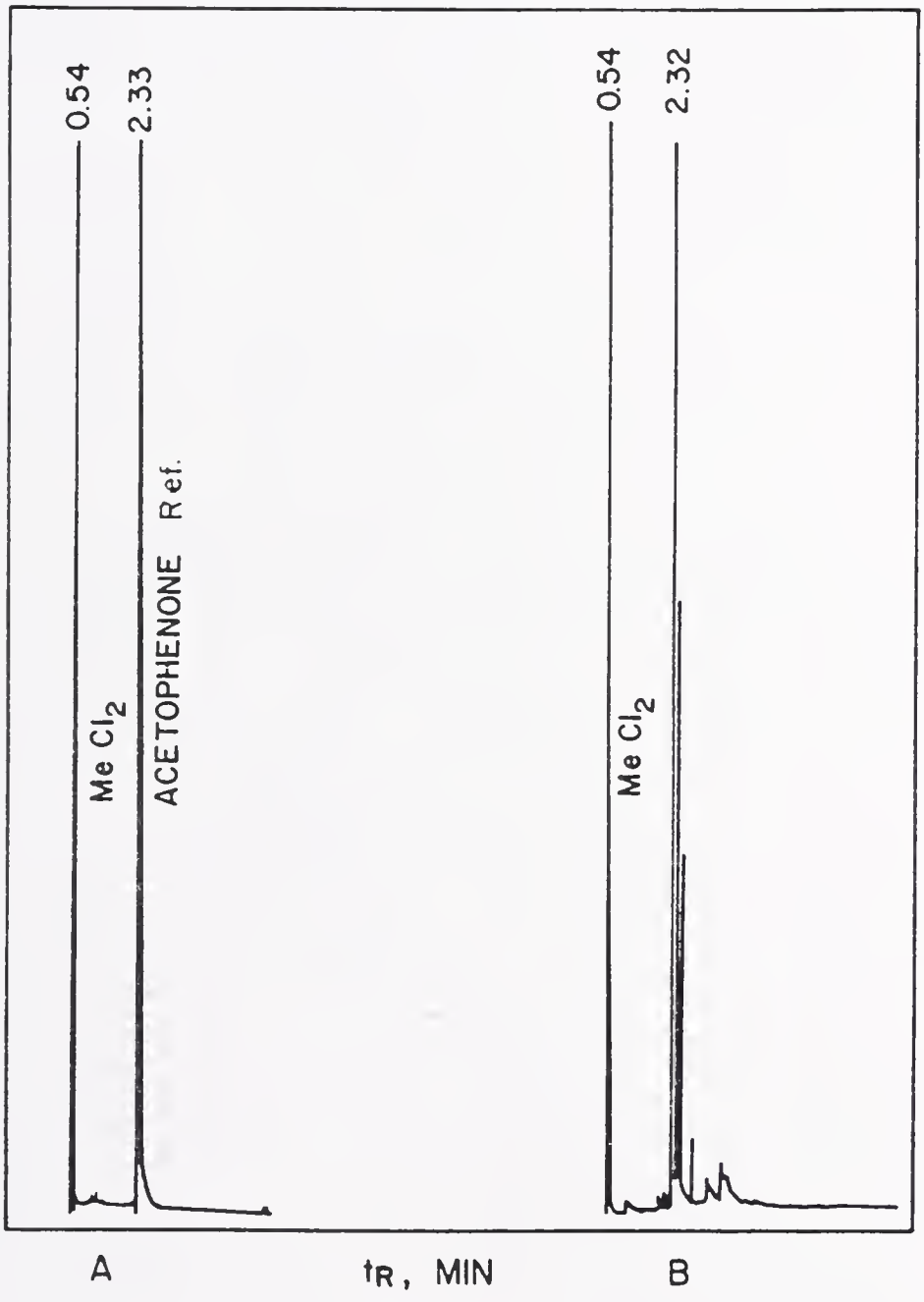

Fig. II-26. Gas Chromatograms of the Reference and the Reaction Product From PSS/DCP Crosslinking Reaction Dissolved in Methylene Chloride ($MeCl_2$). The Numbers on the Peaks Are the Retention Times in Minute.

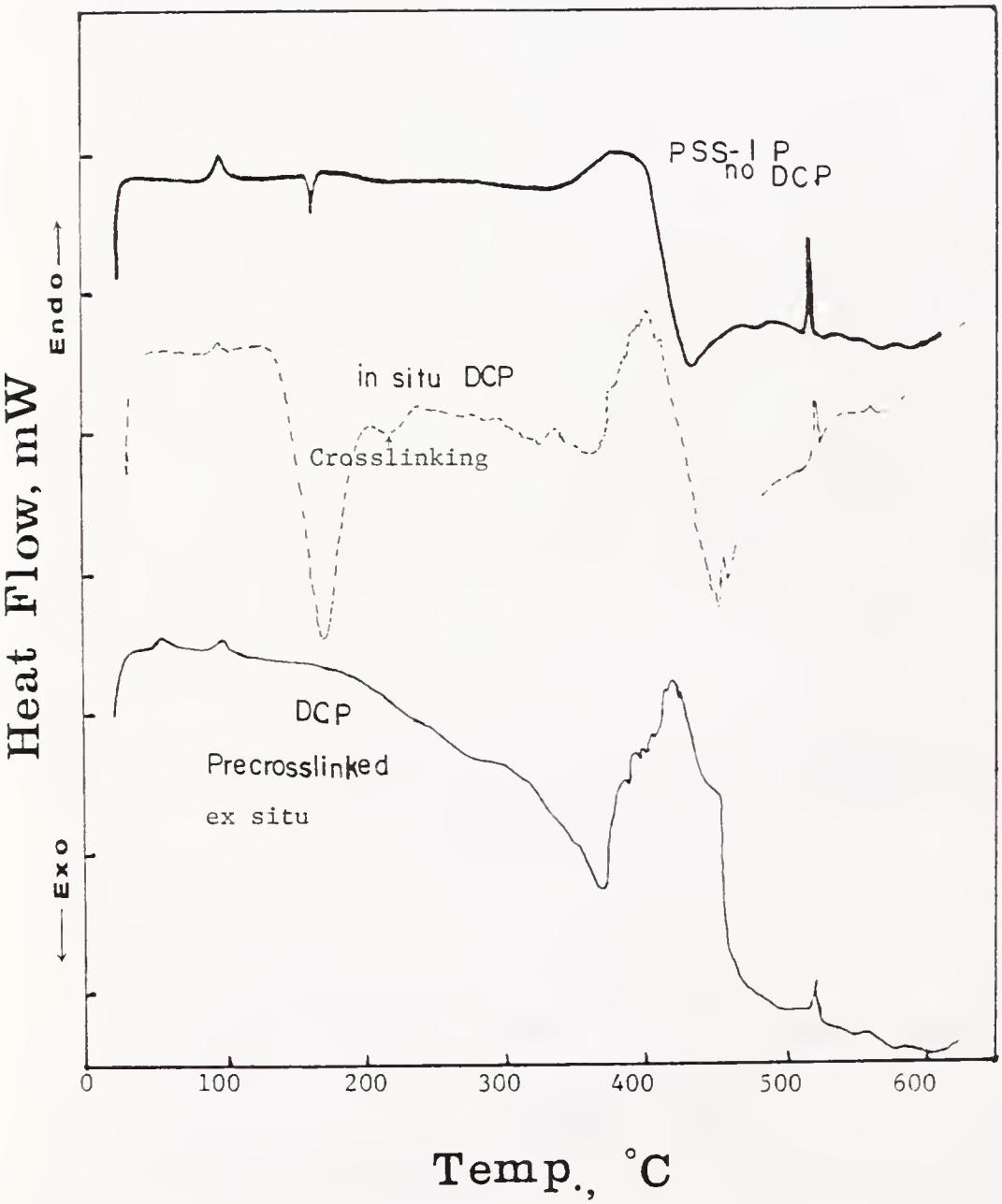

Fig. II-27. DSC Thermograms of PSS1 and PSS1/DCP Before and After the Crosslinking Reaction

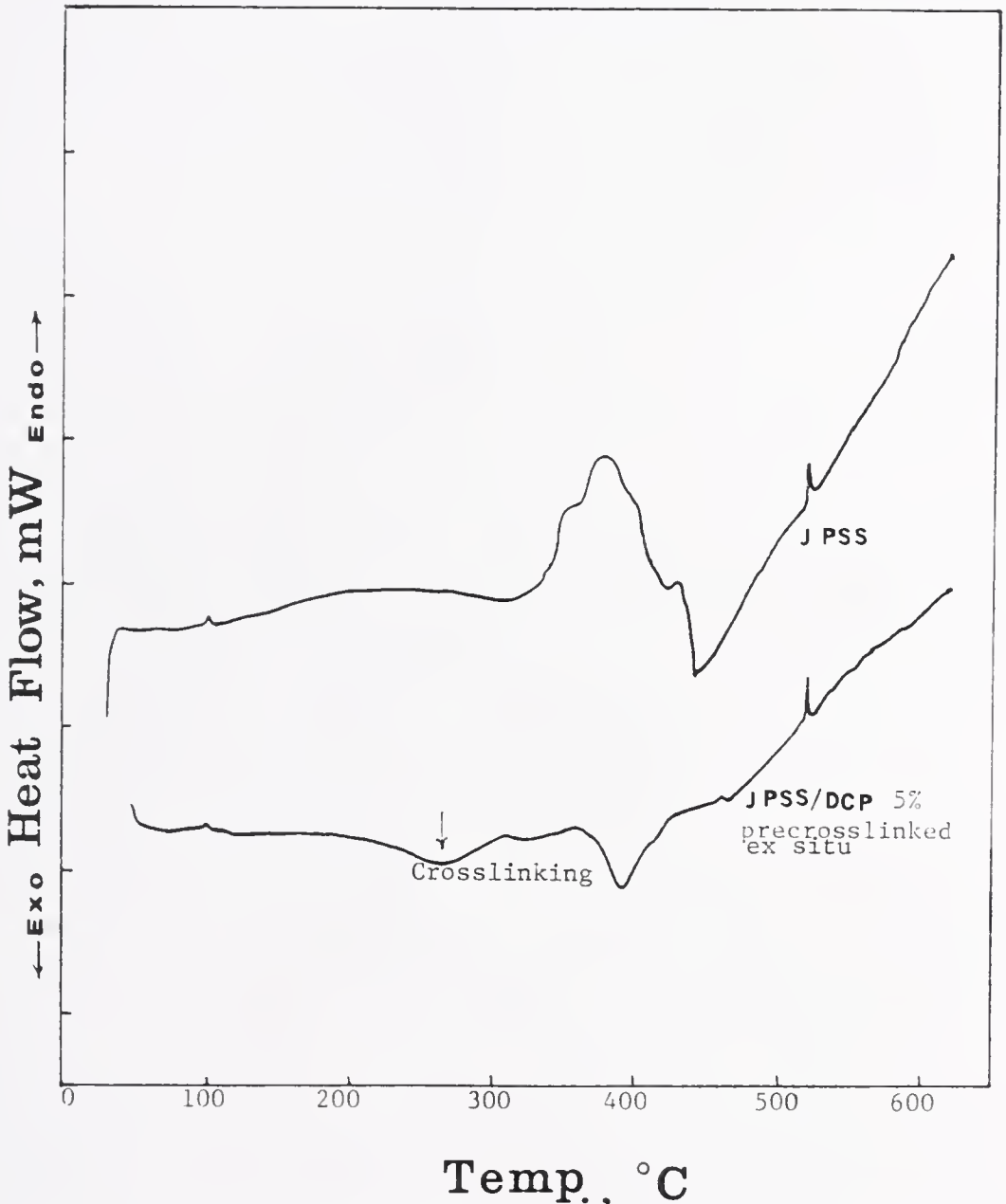

Fig. II-28. DSC Thermograms of J-PSS2 and J-PSS2/DCP After the Croslinking Reaction

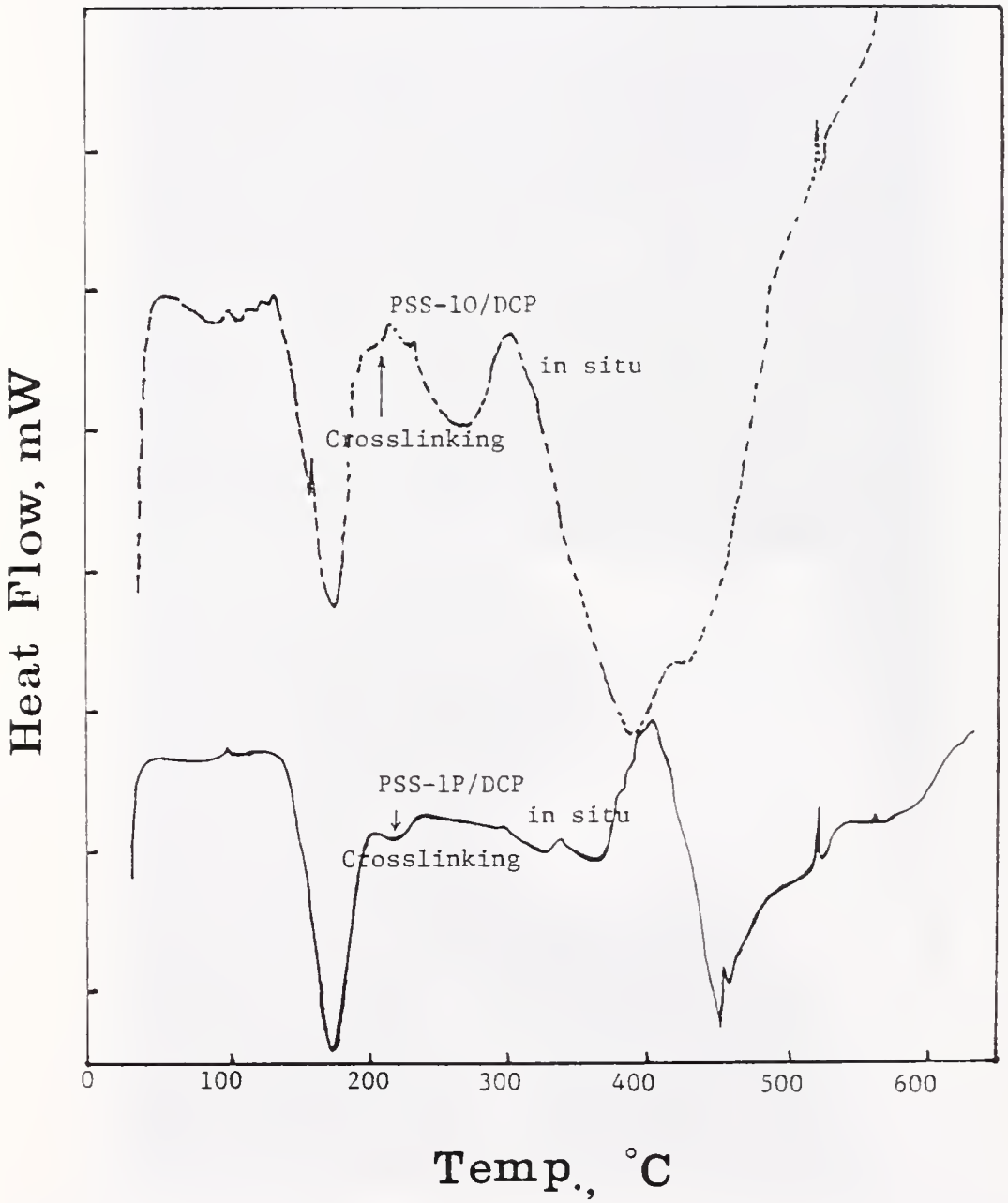

Fig. II-29. DSC Thermograms of PSS-1 Oligomer and PSS-1 Polymer Reacting in situ With DCP

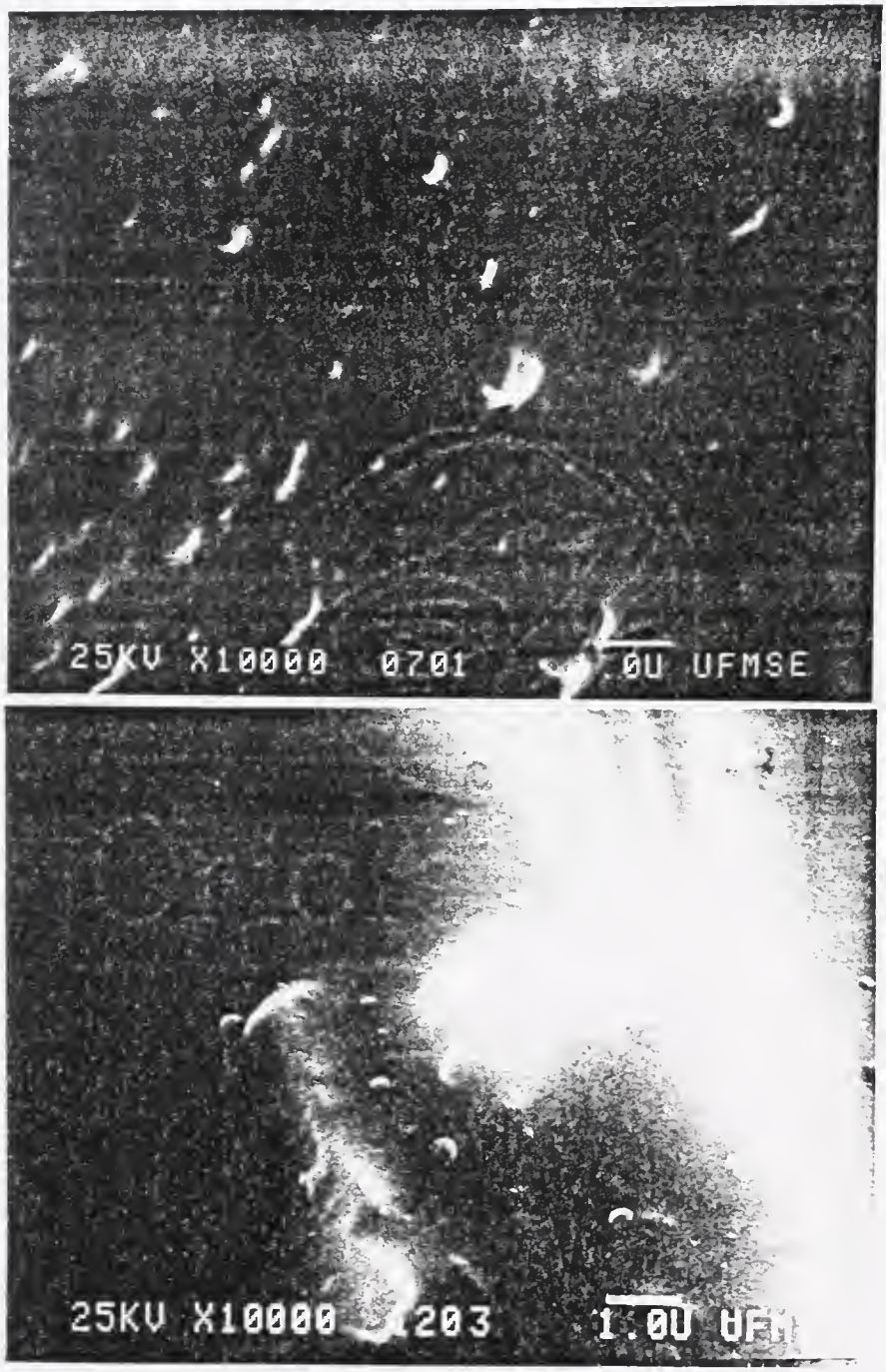

Fig.II-30. SEM Micrographs of PSS/DCP Showinx Blisters and Pores Generated by Gas Evolution. Top: After Crosslinking and Pyrolysis at 400°C in Vacuum, Bottom: After Crosslinking and Pyrolysis at 900°C in Nitrogen

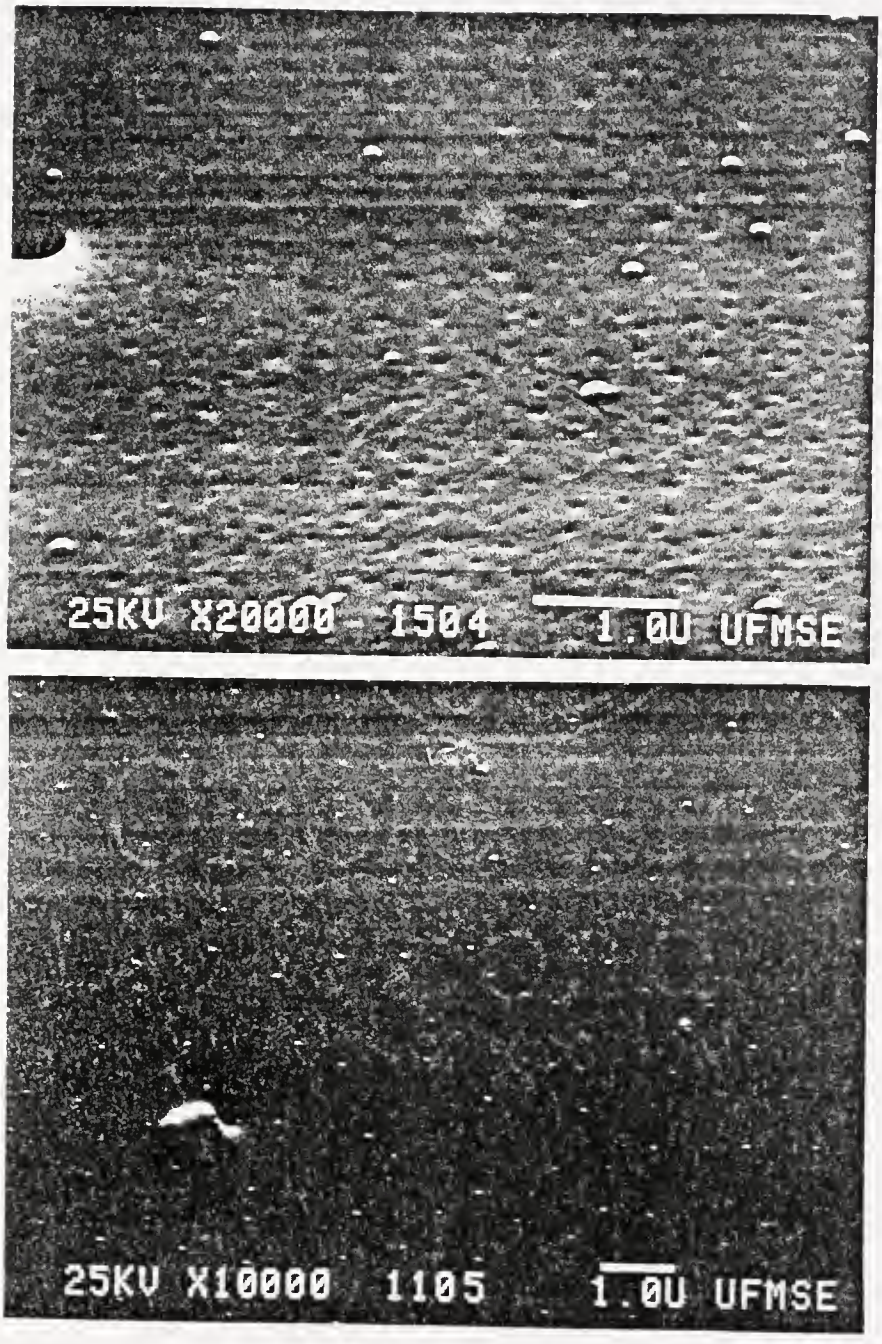

Fig.II-31. SEM Micrographs of ViSP/DCP Showing Pores and Surface Texture. Top: After ViSP Crosslinked With DCP at 110°C, Bottom: After Crosslinking and Pyrolysis at 900°C in N_2

The more effective crosslinking conditions among the techniques tested on the various silanes are summarized in Table II-8.

TGA thermograms of the precursor silanes are given in Figs. II-32 through II-37 to show the char yield of SiC. Fourier Transform IR spectra of the pyrolyzed products are given in Figs. II-38 through II-42. In Fig. II-39, the SiC product from PSS/DCP is compared with the commercial β-SiC Nicalon®. The spectra show the characteristic absorption band of Si-C stretching at 793 cm^{-1} along with a small SiO_2 band at ~1040 cm^{-1}. An XRD powder pattern of PSS showed that the pyrolyzed product is amorphous which is identical with Nicalon®.

The char yield of PSS without crosslinking was less than 20 wt%, which is close to the char yield of ViSO, while the char yield of the PSS/DCP systems show 52-61 wt% SiC. The char yields of pyrolyzed products of SiC from various silane precursors are listed in Table II-9. An XPS spectrum for Si2P of SiC derived from ViSP in Fig. II-43 shows ~20 atom% oxide silicon on the surface of SiC indicated by an overlapped peak at ~107 eV B.E.

Discussion

Based on IR and NMR data, PSS-1P contains a low level of Si-OH (~3400 cm^{-1}) and Si-H (~2100 cm^{-1}) bonds. Unsaturated carbon components (~1600 cm^{-1}) may also be present at a low level. In PSS-10, significant amounts of Si-O-Si overlapped with Si-Ph, as shown by the broad absorption band at ~1100 cm^{-1}. The formation of Si-O-Si may be caused by water used to hydrolyze the residual Si-Cl in the polymer and the alcohol solvent used for fractionation.

Table II-8. Summary of Effective Crosslinking Conditions Found for Different Silane Systems

Silane	Means	Effective Conditions
PSS-P	γ-ray	vac. 29 days at 2.56 cm RT
	CFRI	DCP 110-200°C in 10 min-10 hrs absence of oxygen
PSS-O	CFRI	DCP, 140-250°C in 20 min-12 hrs absence of oxygen
A-PSS	Thermal	300°C in 20 min or 170°C in 14 hrs absence of oxygen
	CFRI	150°C, 20 hrs absence of oxygen
	Pt^{4+}	80°C, 12 hrs
ViSP	Thermal	150°C, 24 hrs absence of oxygen
	CFRI	DCP, 120°C, 4 hrs absence of oxygen
ViSO	Thermal	> 200°C, 72 hrs
	γ-ray	10 days, polymerization not a crosslinking
	CFRI	DCP/110°C, ~3 hrs or 75°C, ~12 hrs no oxygen
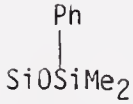	CFRI	DCP/N_2, 300°C 20 min

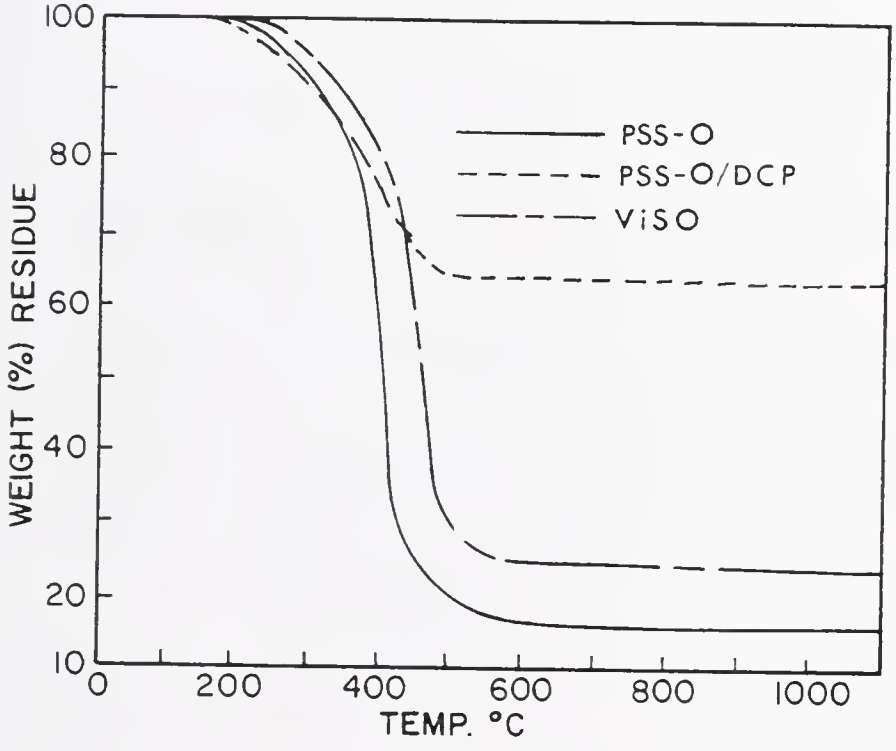

Fig. II-32. TGA Char Yields of PSS-10, PSS-10 After DCP Crosslinking, and ViSO

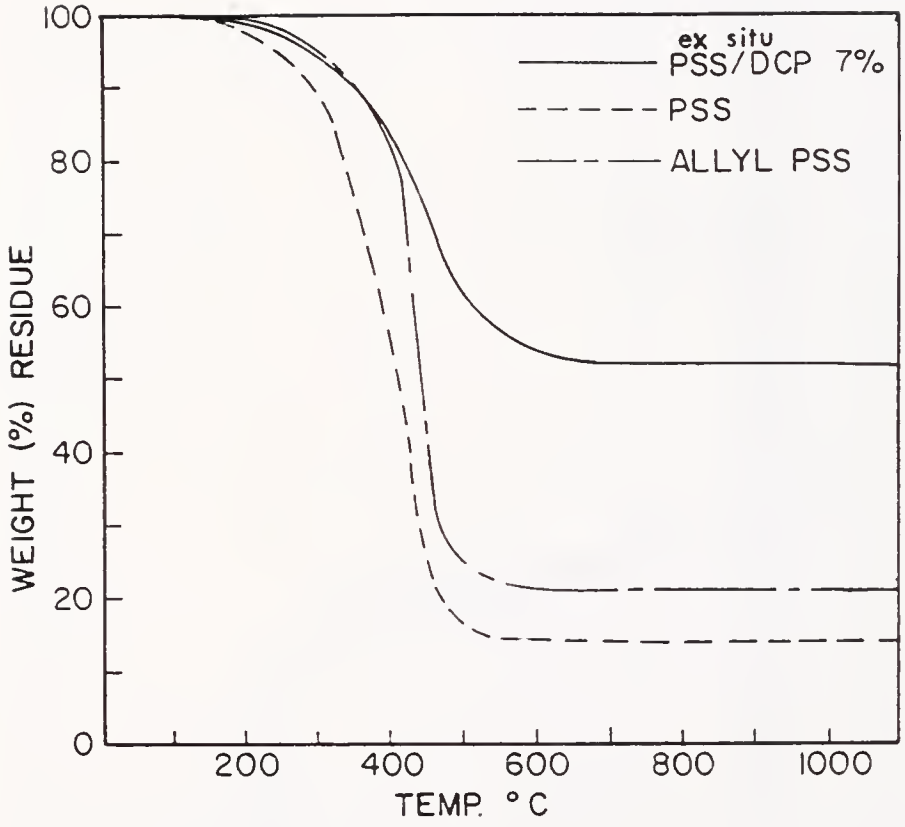

Fig.II-33. TGA Char Yields of SiC From PSS-1P, PSS-1P After DCP Crosslinking, and Allylic PSS

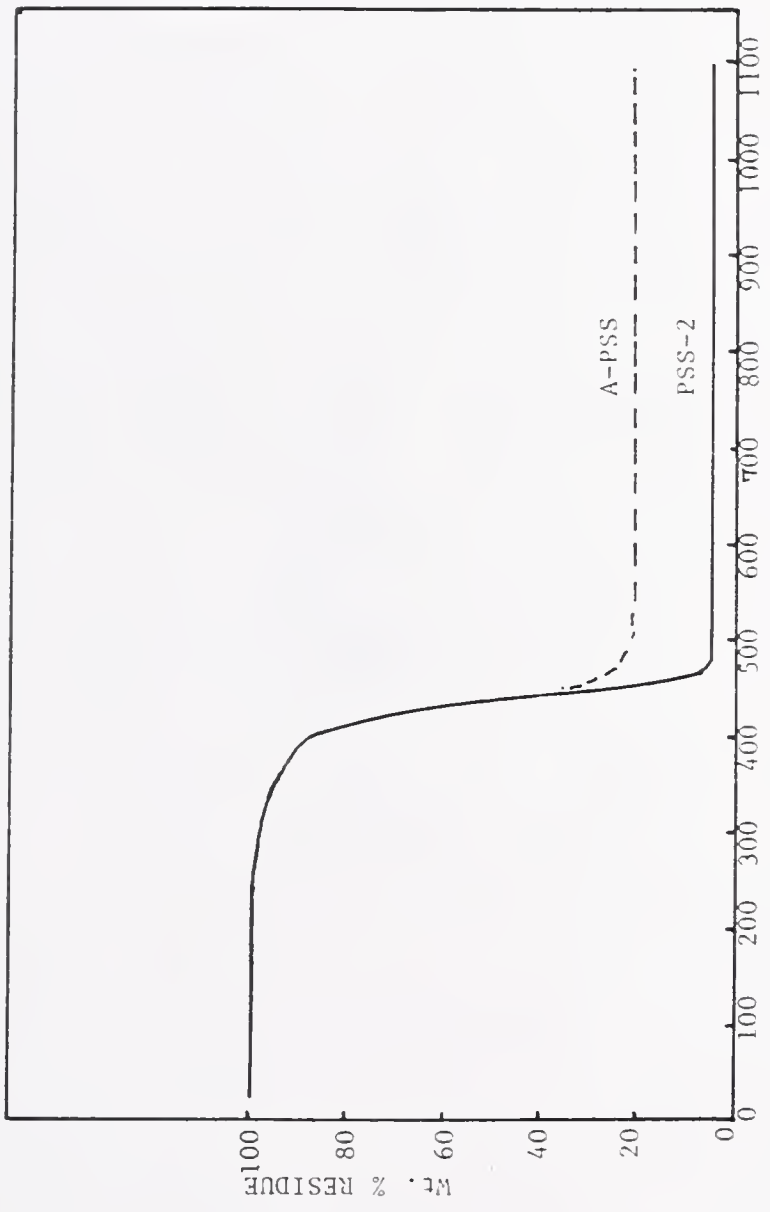

Fig. II-34. Solvent Insoluble Fraction of PSS Showing Low Char Yields

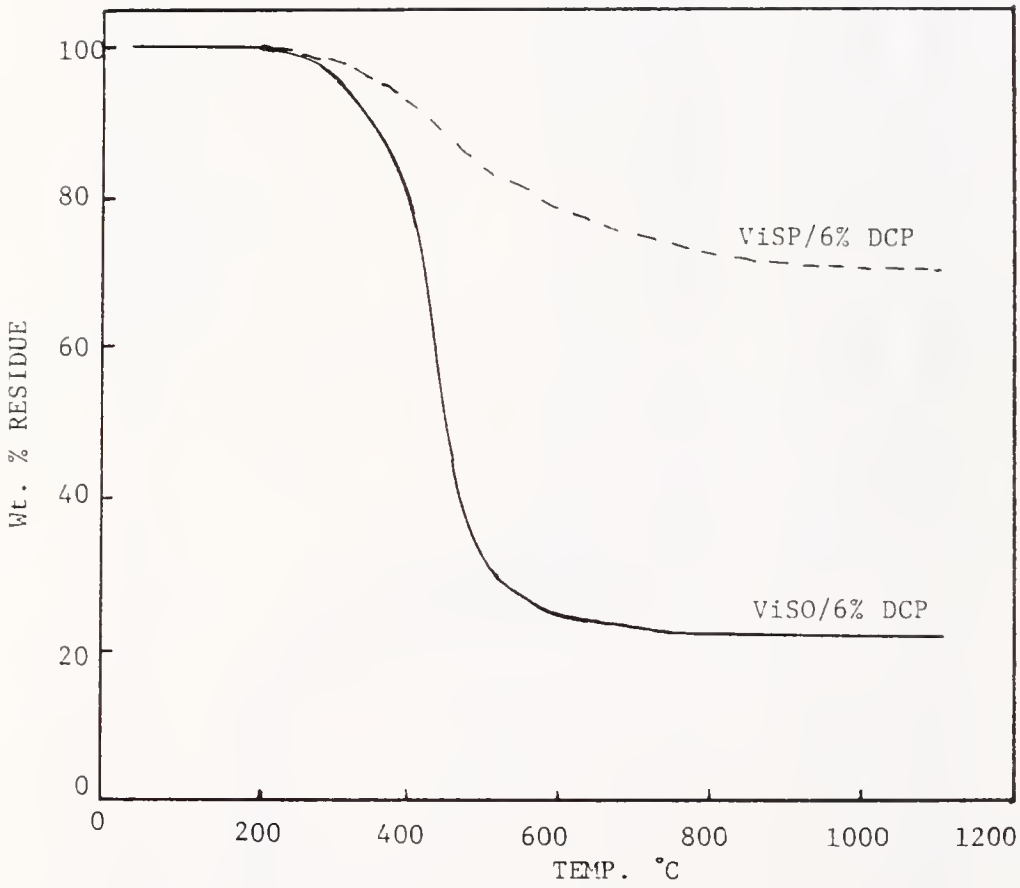

Fig. II-35. TGA Char Yields of SiC for ViSP and ViSO After Crosslinked With DCP

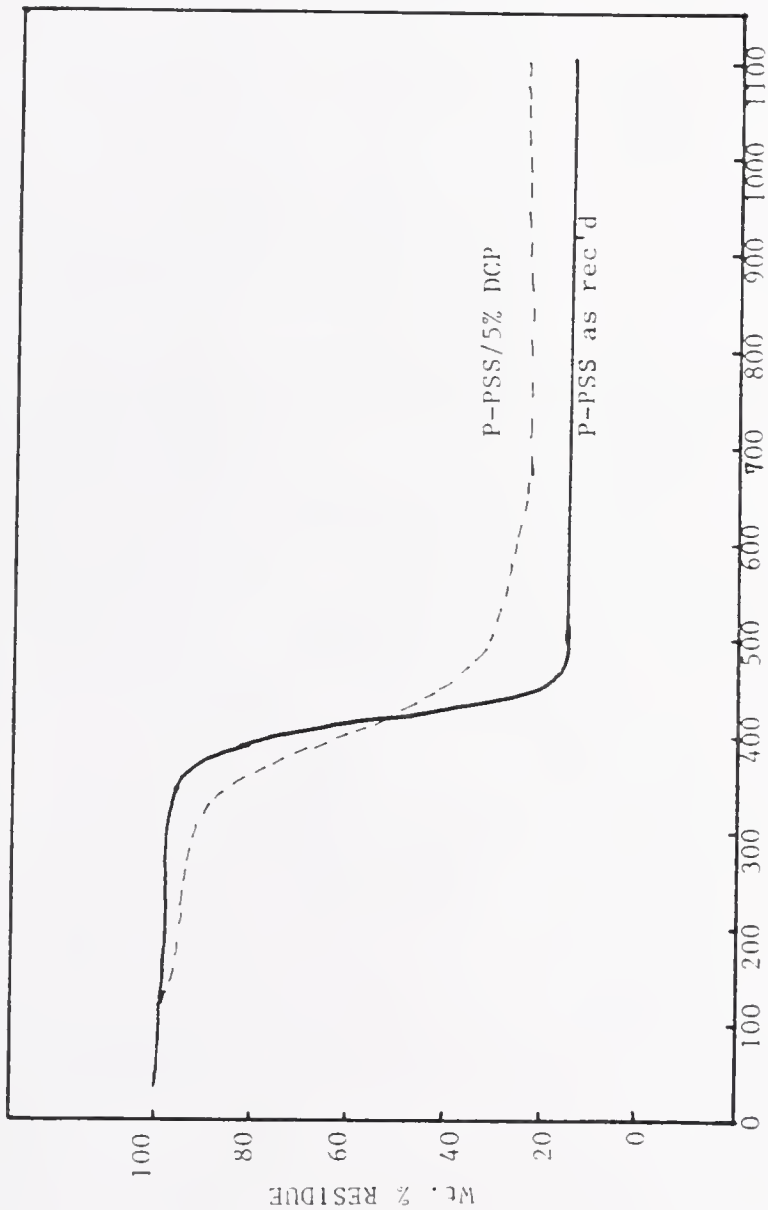

Fig. II-36. TGA Char Yields of SiC for P-PSS Before and After Crosslinking With DCP

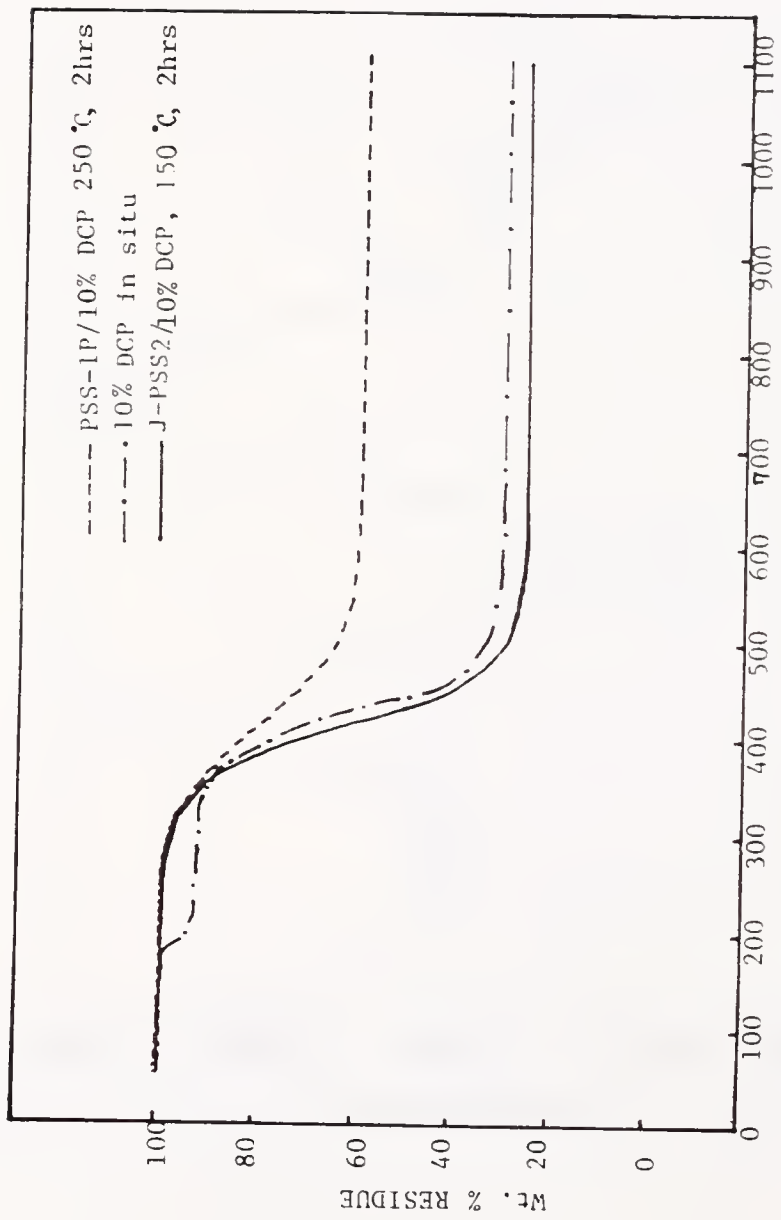

Fig. II-37. TGA Char Yields of SiC for PSS' Showing the Effect of Time and Temperature of the Crosslinking Reaction

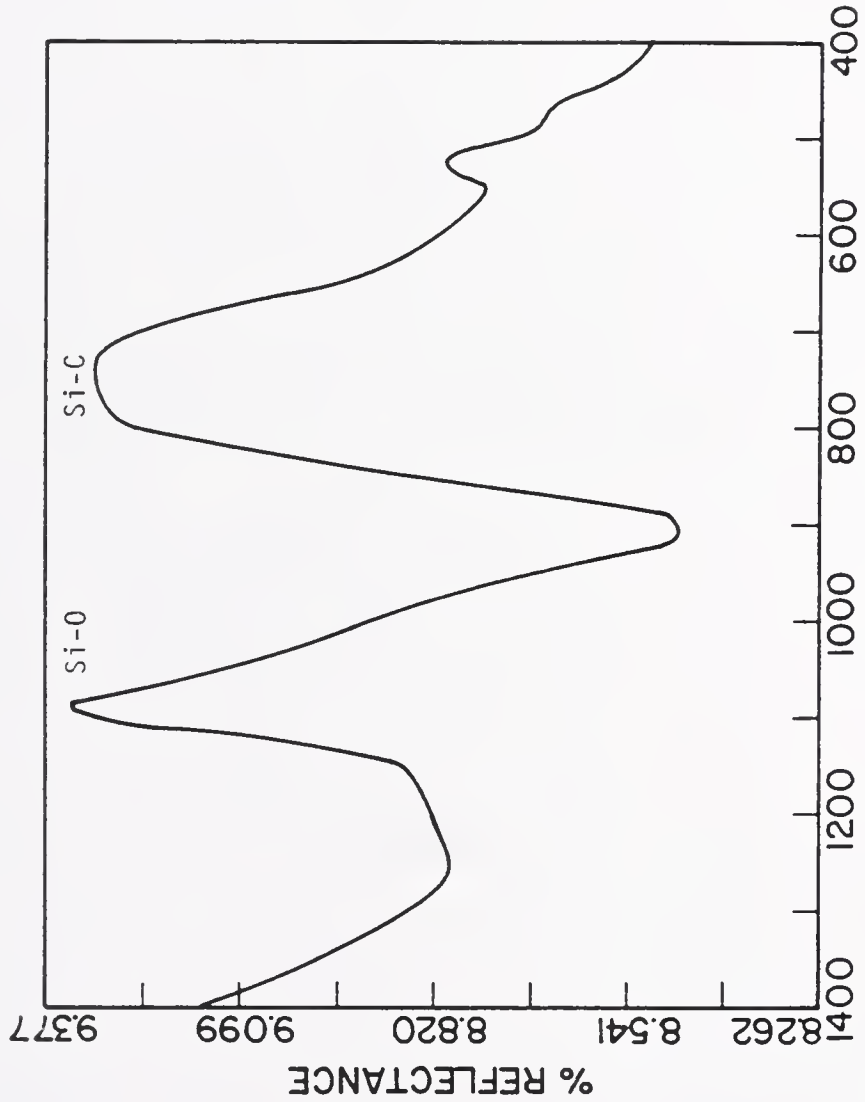

Fig.II-38. FT-IR Spectrum of DCP Crosslinked PSS-1P After Pyrolysis at 960 °C in Nitrogen Atmosphere

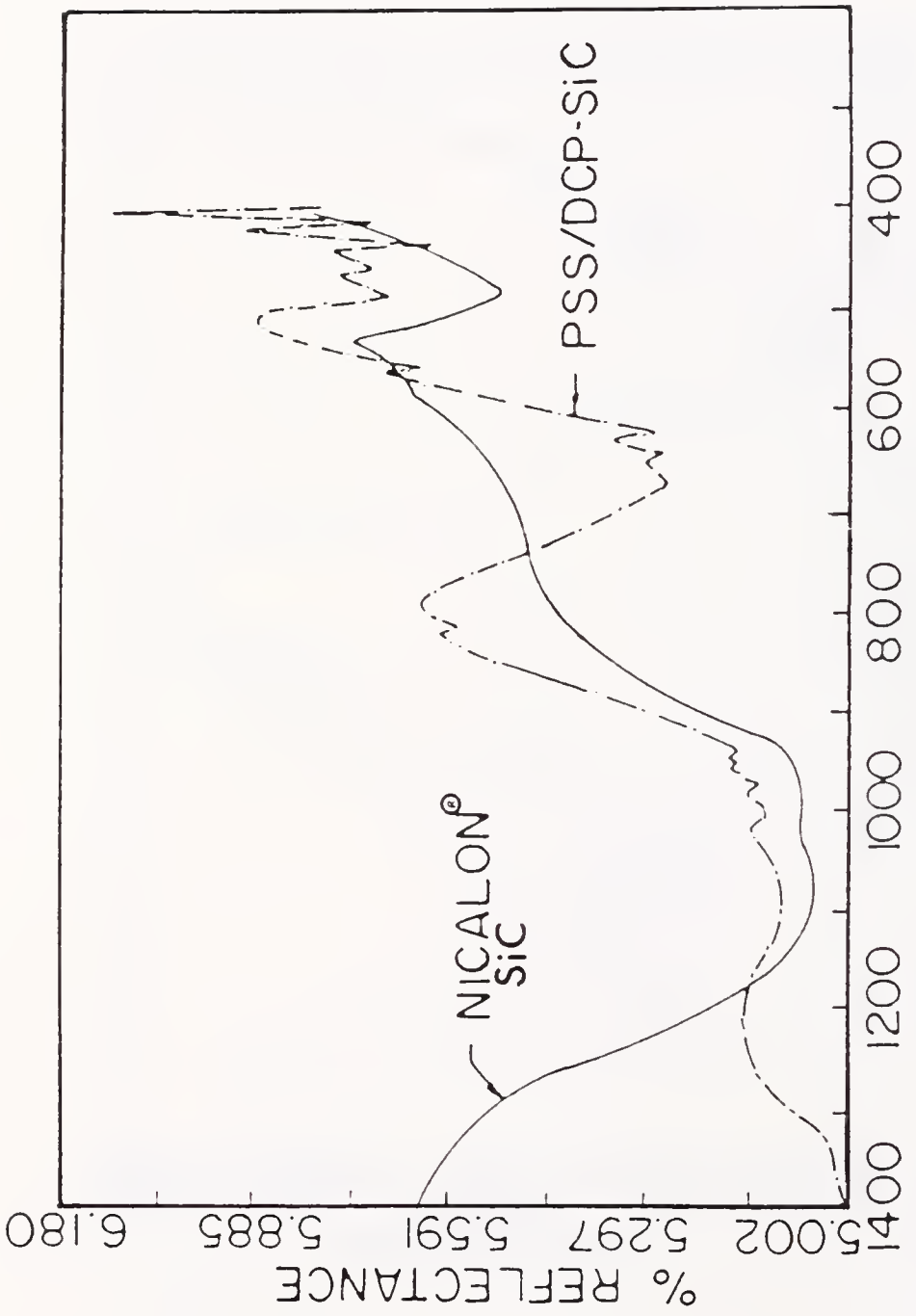

Fig.II-39. FT-IR Spectra of Nicalon® SiC and SiC from DCP Crosslinked PSS

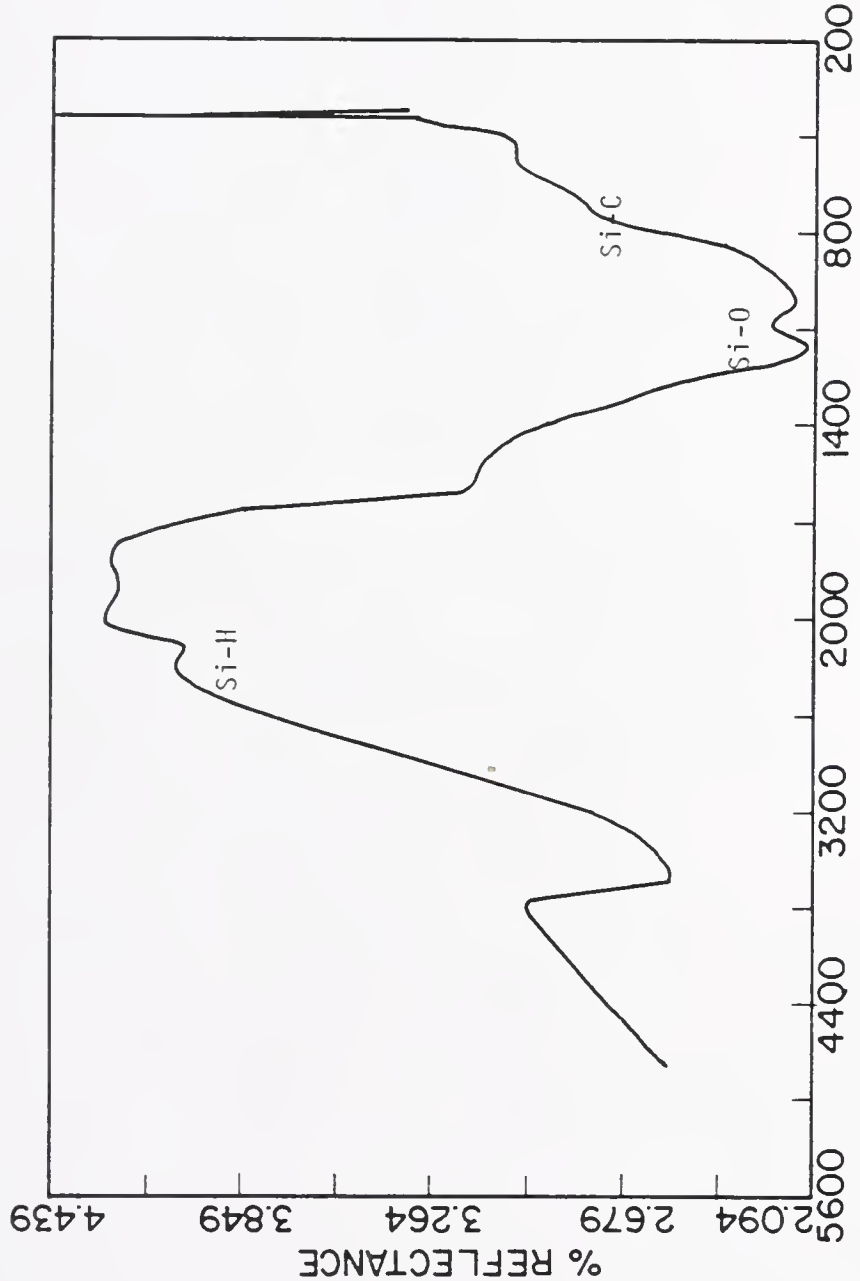

Fig.II-40. FT-IR Spectrum of J-PSS2/DCP After Pyrolysis at 1000°C

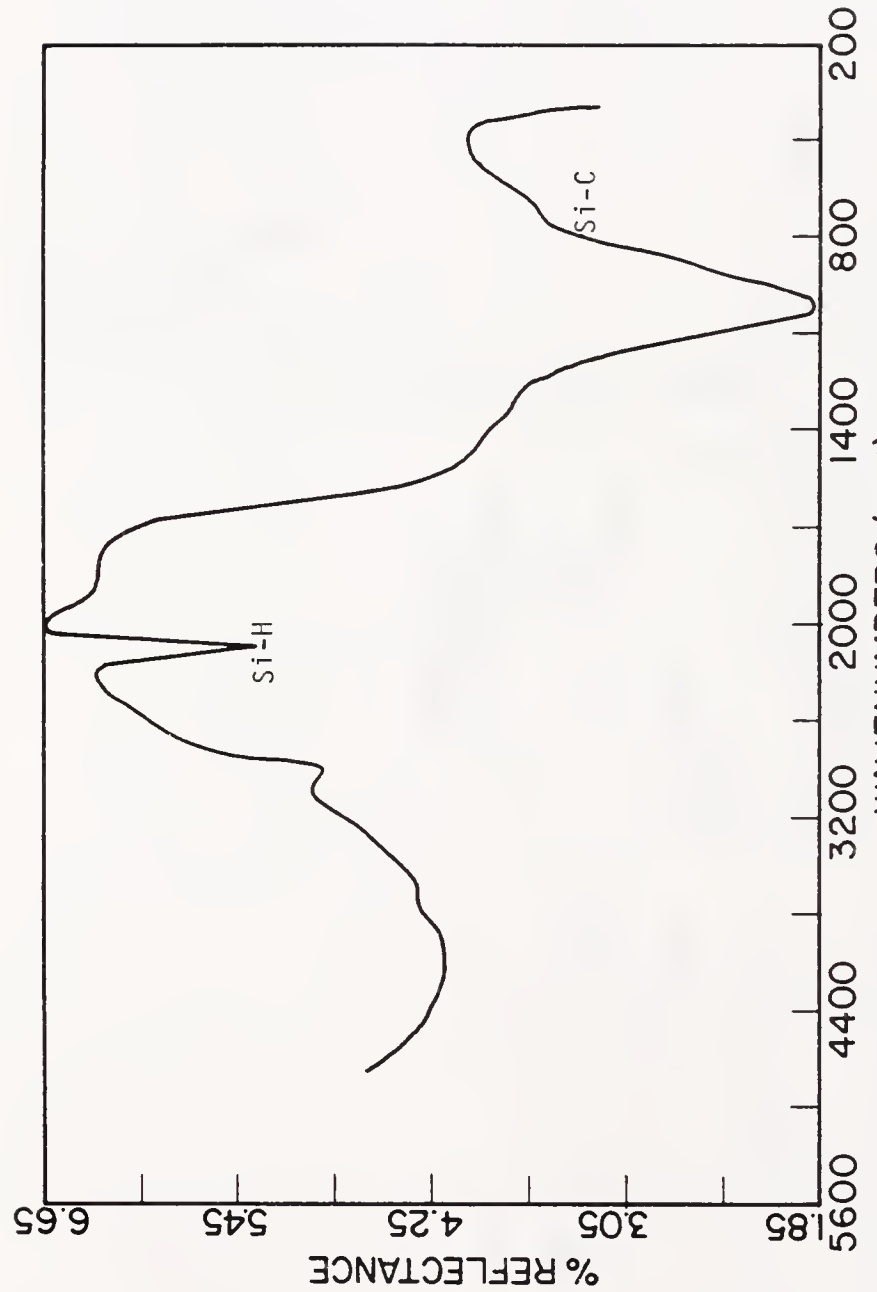

Fig.II-41. FT-IR Spectrum of ViSP/DCP after Pyrolysis at 900°C

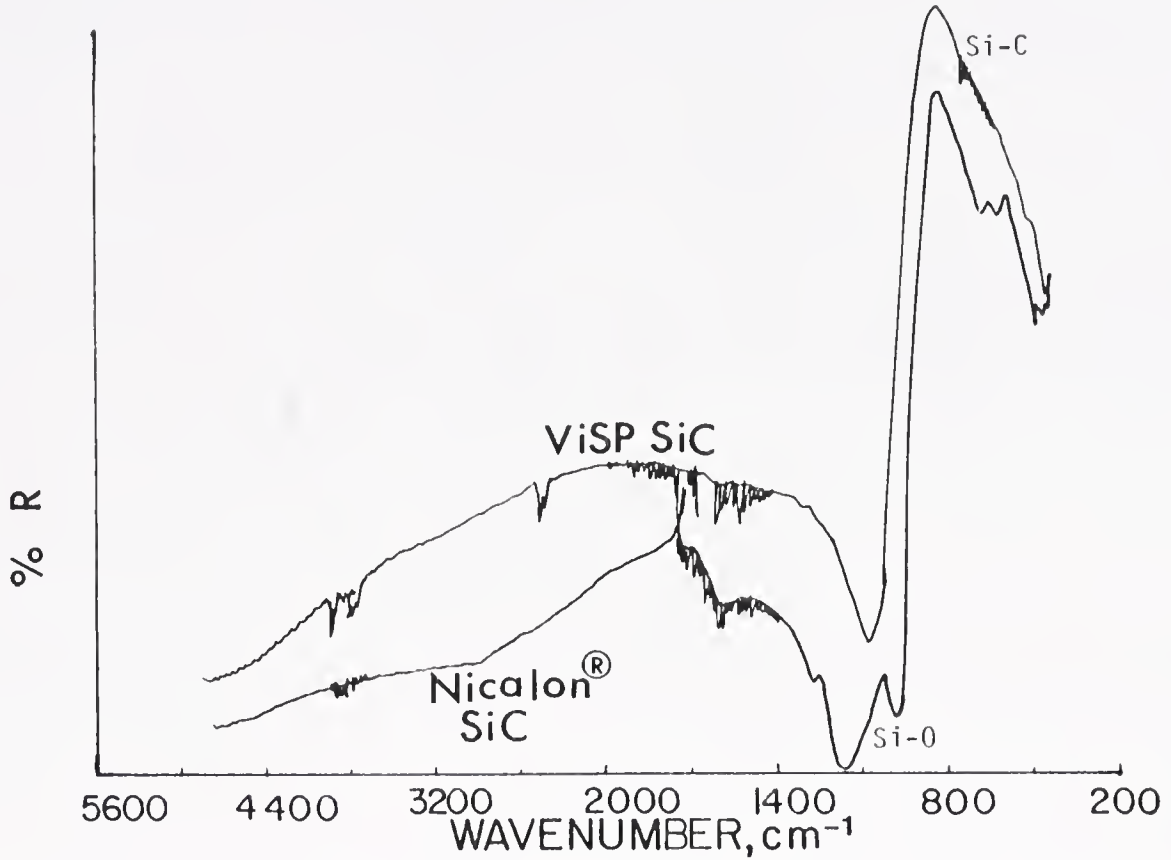

Fig.II-42. FT-IR Spectrum of SiC Obtained from ViSP/DCP Compared With the Spectrum of Nicalon. Note the Absence of Si-O band in ViSP/SiC

Table II-9. Char Yield of Pyrolyzed Products SiC from Various Silane Precursors

Silane	Crosslinking method and Conditions	Pyrolysis Method	Char Yield %
PSS-1P	10% DCP in situ	TGA	30
	10% DCP, 250°C 20 min, vacuum	TGA	61
	7% DCP, 250°C 10 min, N_2	TGA	52
	5% DCP, 110°C 10 hrs, air sealed	TGA	23
PSS-2P	8% DCP, 250°C 20 min, N_2	TGA	52
	----------	TGA	12
J-PSS1	----------	800°C, 1 hr, N_2	2
J-PSS2	5% DCP, 150°C, 12 hrs air sealed	TGA	25
P-PSS	5% DCP, 130°C, 12 hrs air sealed	TGA	20
	----------	TGA	15
A-PSS-P	----------	TGA	21
	Pt^{4+}, 80°C, 12 hrs	TGA	35
	5% DCP, 170°C	900°C, 1 hr.	22
ViSO	----------	TGA	25
	4% DCP, 110°C, 6 hrs, air sealed	TGA	25
PSS-10	8% DCP, 150°C, 12 hrs, air sealed	TGA	16

Table II-9 (continued).

Silane	Crosslinking method and Conditions	Pyrolysis Method	Char Yield %
PSS-20	7% DCP, 300°C 20 min, N_2	TGA	67
Insol. PSS	----------	TGA	5
Insol. A-PSS	----------	TGA	18
ViSP	thermal, 150°C, 24 hrs	920°C, 1 hr, N_2	55
	3% DCP, 120°C, 3 hrs	920°C, 1 hr, N_2	54
	6% DCP, 130°C, 4 hrs	TGA	72
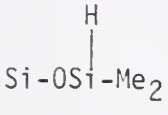	----------	TGA	<4
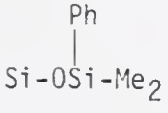	8% DCP, 250°C	TGA	27

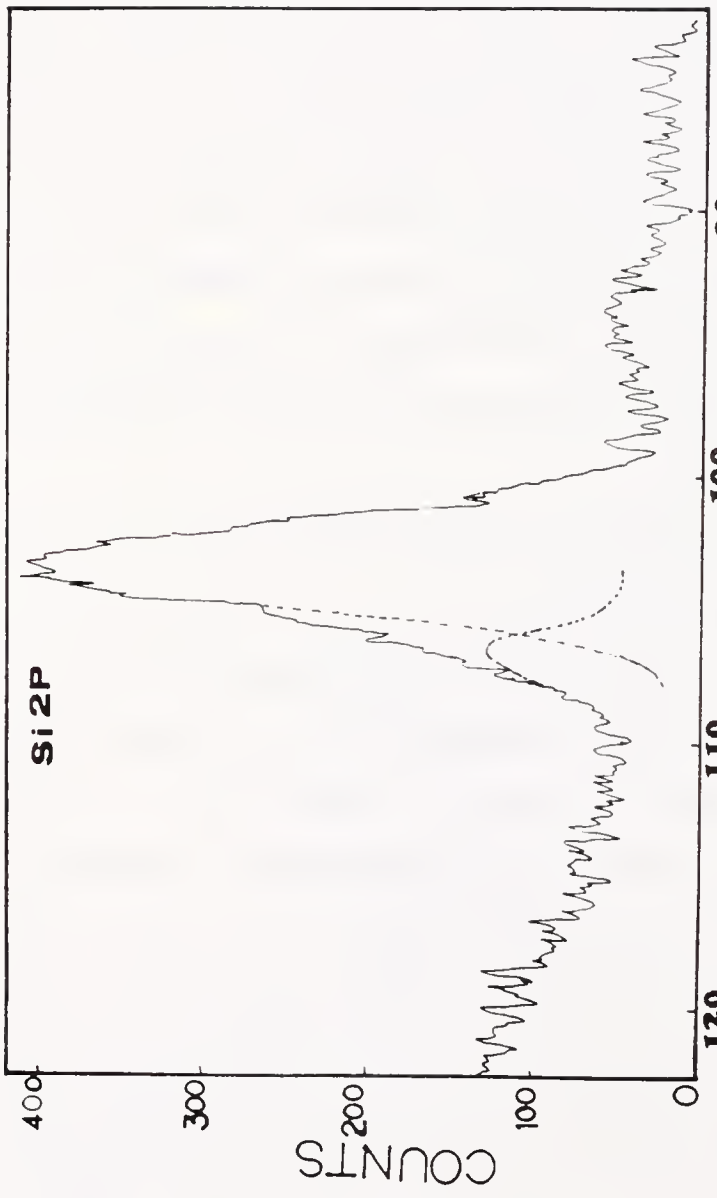

Fig.II-43. XPS Spectrum of ViSP/SiC Showing ~20 atomic % Oxide Silicon as a Contaminant

All of NMR spectra show slight excess of the PhSiMe unit in the PSS copolymer chain over the MeSiMe unit, despite the intention to form an equimolar copolymer. This must mean that the PhSiMe monomer unit is more reactive than the MeSiMe unit during the polymerization reaction. This means that in order to achieve an exactly equimolar copolymer of PSS, one would have to use a slight excess of Me_2SiCl_2 monomer.

Hydrogen directly bonded to silicon in PSS comes from the fact that the polysilane chain ends are probably anionic in the sodium/toluene milieu and abstract hydrogen from the alcohol that was added to quench excess sodium. Since the Si-H is hydrolyzable to give Si-OH, when the Si-H ends find Si-OH ends, they form a Si-O-Si linkage by a condensation reaction.

Although early workers of polysilane[50-52] considered that $\left(\begin{smallmatrix} Me \\ | \\ -Si- \\ | \\ Me \end{smallmatrix}\right)_n$ from $MeSiCl_2$ was useless because of its insolubility, introduction of a phenyl group improves its solubility and tractability.

As given in Table II-6, all polymerization reactions carried out produced ~3 times larger oligomer fractions than polymer fractions. Although it is generally thought that polymer fractions are the desired product in these reactions, the oligomer was successfully repolymerized and crosslinked by using a DCP as a CFRI. This is an especially important finding since the oligomer fraction in a liquid state at room temperature is more convenient to impregnate porous ceramic bodies in order to strengthen them. David,[56] who pioneered PSS, has unsuccessfully tried to repolymerize the oligomer fraction by restarting the polymerization reaction with sodium in toluene, sodium chloride, lithium metal, lithium t-butoxide, potassium t-butoxide, or sodium with biphenyl as an

electron transfer agent. David[56] clearly concluded that "all one can do is to fractionate them out of a polysilastyrene product and discard them, . . ." Petrarch System, Inc., the only company that makes PSS commercially in the U.S., follows this practice.[57]

Oligomers of PSS are believed to be in cyclic form so that the crosslinking mechanism is expected to be different from the polymer fraction by opening up the six membered ring. This is partly evidenced by a higher TGA yield (67%) than that of a polymer (Figs. II-32 and II-33). The DSC data (Fig. II-29) show that oligomers require a higher temperature for crosslinking than polymers and the decomposition begins at ~50°C lower temperature than polymers. The high char yield of the oligomers, however, was partly caused by the loss of volatiles through the vacuum line during the ex situ crosslinking reaction with DCP.

The longer reaction time of PSS polymerization, e.g. 10 hrs, was believed to degrade the formed polymer by excess hot sodium. However, it appears that a longer reaction time than ~2 hours could have been used to increase the polymer fraction of PSS. It is not yet completely clear to what extent the longer reaction time improves the yield of the polymer fraction. A systematic study of the effect of reaction time on the M. W. of the silane products must be continued.

In the allylic PSS polymer, small amounts of Si-O-Si and Si-H are shown (Fig. II-11). The unsaturated carbon component, probably from the allyl group, is shown at ~1600 cm^{-1}. The mole ratio of MeSiPh to MeSiMe is 1.2:1. The ^{13}C NMR (Fig. II-13) did not reveal any more evidence of the presence of an allyl group in A-PSS-P. Some indications of allyl groups in A-PSS-O are also shown in Fig. II-9. The group representing

Si-H and the allyl is shown as ~4% of the total protons in A-PSS-P (Fig. II-12). Apparently, not all the allyl methyldichlorosilane ended up in the products. A further study to account for this is needed.

The low solubility of J-PSS1, J-PSS2, and P-PSS in the solvents must be a result of incomplete fractionation of the insoluble high M. W. fraction. This variation in the M. W. distribution in a polymer is most likely affected by the fractionation procedures. The consequence of this was observed in the different behavior of PSS under the same cross-linking conditions used in this study.

The average number M. W. ($\overline{M}n$) for different PSS precursors are in close agreement, except that of J-PSS1. The GPC chromatograms show that the PSS polymer is bimodal with a ~4 times larger lower M. W. portion ($\overline{M}n$ 9 x 10^3) than the higher M. W. ($\overline{M}n$ 3 x10^5).

The very high M. W. fraction that is insoluble in common solvents and infusible upon heating, appears to be polydimethylsilane with some Si-H, Si-Ph, and Si-O-Si, as shown by the IR spectrum in Fig. II-15. The linear

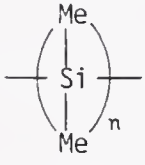

linkage apparently has been crosslinked via bridging oxygens of Si-O-Si type. The TGA char yield of this fraction was <10% (Fig. II-34), which agrees with the result of Yajima et al.[54]

In vinylic silanes, a large and sharp Si-H band at ~2080 cm^{-1} is shown for ViSO in Fig. II-16. The vinyl double bond appeared at ~1650 cm^{-1}. However, the hydride proton is not apparent in NMR (Fig. II-18).

This should be due to the relatively low concentration of the hydride, but this obviously disagrees with the IR data. This point will be discussed further in the latter part of this section.

An energy equivalent to 200 Mrad or greater γ-ray irradiation required to crosslink PSS is not unusual because of the phenyl group[58] on the chain and the absence of an Si-H functional group.

In Fig. II-20 the effect of γ-ray irradiation on the PSS structure after 29 days is shown and the sharp bands at ~700 cm^{-1} representing the methyl group are lost. The DCP reacted PSS lost most of its IR bands for $Si-CH_3$, and Si-H (Fig. II-21).

The enhanced crosslinking of carbon polymers in N_2O under γ-irradiation, as shown by Okada,[59] did not occur with silanes but rather the opposite was observed.

Among the several CFRI studied, only DCP yielded an insoluble and infusible solid of polysilanes. This is probably due to the active methyl radical, which was not present in any other CFRI used. In the crosslinking reaction, DCP has to be decomposed to give the methyl radicals. This occurs at ~150-200°C.

Allylic PSS is observed to be more reactive under crosslinking conditions than PSS. As shown in Fig. II-22, A-PSS can be crosslinked thermally or via use of the CFRI DCP. For thermal crosslinking, a temperature >170°C is required for complete reaction. Allylic PSS is also shown to be crosslinkable by Pt^{4+} catalyst. At least 2.4×10^{-7} mole Pt^{4+} per ~0.3 g A-PSS was required for an effective crosslinking of A-PSS, as shown by IR spectra (Fig. II-23).

The crosslinking reaction of A-PSS must be between Si-H and C = C, as shown in equation II-1.

$$\equiv SiH + C{=}C \xrightarrow{\text{catalyst}} \equiv Si\text{-}C\text{-}C\text{-}H \qquad \text{(II-1)}$$

The coupling reaction is catalyzed by Pt^{4+}.[60] The TGA yield of A-PSS without a precrosslinking treatment (21%) is still greater than that of PSS-P (12%). After being crosslinked with Pt^{4+}, the yield increased to 35%. Differential scanning calorimetry (Fig. II-44) shows that the crosslinking between Si-H and  occurs at ~240°C. The CFRI DCP requires temperatures >170°C for complete crosslinking, but Pt^{4+} catalyzed the reaction at a temperature of ~80°C. This crosslinking reaction by Pt^{4+} is unique to A-PSS and demonstrates the advantage of incorporating an allyl group into polysilane synthesis.

Although a monomer with an Si-H functional group was not added in the A-PSS synthesis, the small amount of Si-H at the chain ends was still shown to be effective in the coupling reaction. However, intentional small amounts of a monomer with a Si-H functional group, e.g. 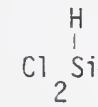 should improve the crosslinkability even further.

Vinylic silanes can be crosslinked both thermally and via the CFRI DCP. With DCP, the crosslinking is achieved faster and required a lower temperature: 110°C for ~4 hours as compared to 150°C for 12 hours without DCP. Without DCP, 150°C for 12 hours treatment still did not produce complete crosslinking, as shown by the large Si-H IR peak in Fig. II-24. This is also shown in Fig. II-45 with an expanded scale.

The vinylic silanes (ViSP and ViSO) received from Union Carbide were reported[61] to have both functional groups Si-H and  .

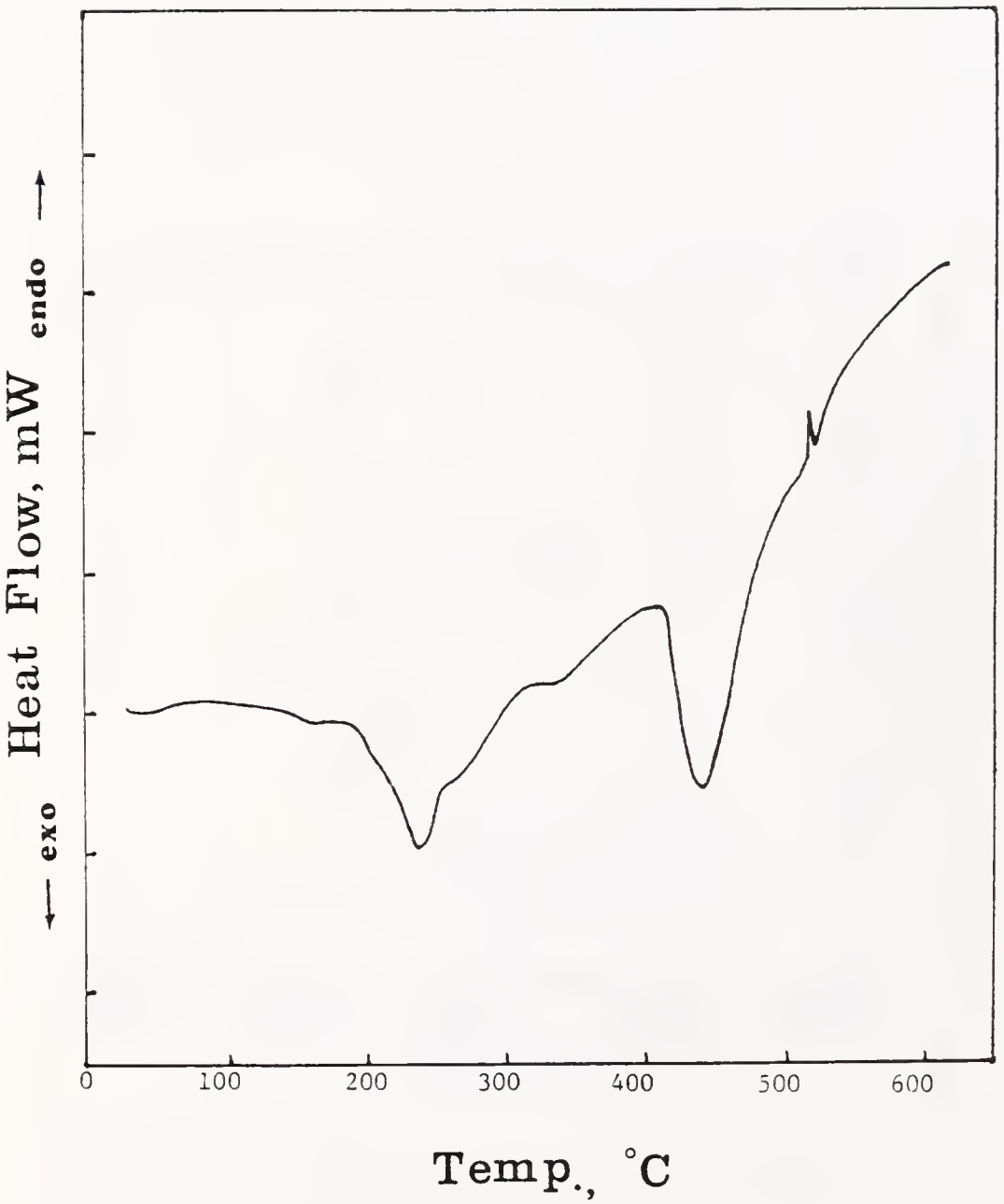

Fig.II-44. DSC Thermogram of A-PSS-P Showing that the Thermal Crosslinking Occurs at ~240°C

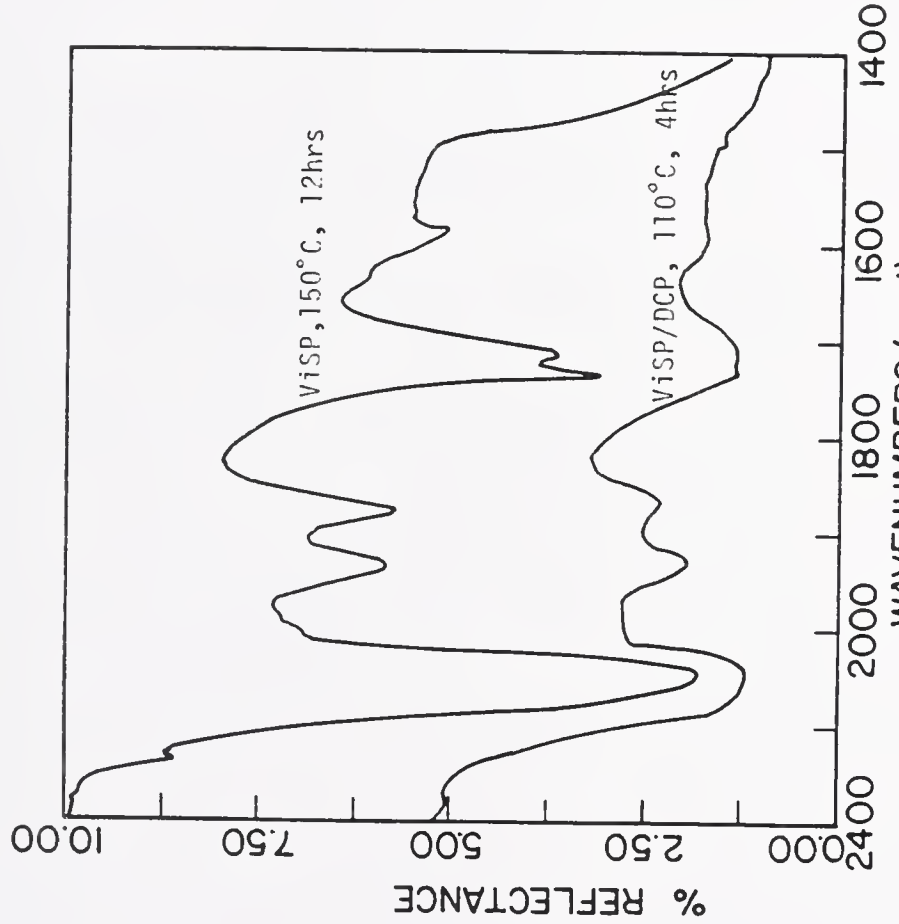

Fig.II-45. FT-IR Spectrum of ViSP Showing the Effect of DCP on Si-H Band Intensity and on Crosslinking

Although NMR confirmed the presence of —\\ , the presence of Si-H is not certain. If ViSP and ViSO contain Si-H and —\\ functional groups, they should be crosslinkable via Pt^{4+} even more readily than allylic PSS because —\\ is more reactive than —\= . However, this was not observed. The vinylic silanes with a Pt^{4+} concentration greater than 9×10^{-7} mole per 1 g silane and T > 80°C for several hours did not solidify the liquid silanes. This is a question which cannot be answered unless further work is performed.

The size of the Si-H peak in the IR spectra cannot directly be used to estimate the degree of crosslinking because of the high bond energy (~314 KJ/mole).[54] This is shown by the Si-H IR band at ~2080 cm^{-1} in SiC after pyrolysis at both 1000°C (Fig. II-40), and 900°C (Fig. II-41).

Morterra and Low[62] also observed the growth of the Si-H absorption peak when methoxylated aerosil was heated in a vacuum up to 750°C, while the absorption peak for the $-CH_3$ stretching band at ~3000 cm^{-1} decreased as the length of heat treatment at 750°C in vacuum increased.

Nevertheless, it is shown in Figs. II-22, II-24, II-45, and II-46 that the degree of crosslinking appears to be a function of the Si-H peak size. This is another area that needs to be further investigated.

A difference between vinylic and allylic silanes under crosslinking conditions is in the reactivity of the functional groups. Vinyl groups are more reactive than allyl groups by vinyls forming more stable radical intermediates. This was shown by the lower temperatures needed to crosslink vinylic silanes. This advantage is somewhat curtailed by a greater tendency of vinylic silane to be oxidized. Thus, one should

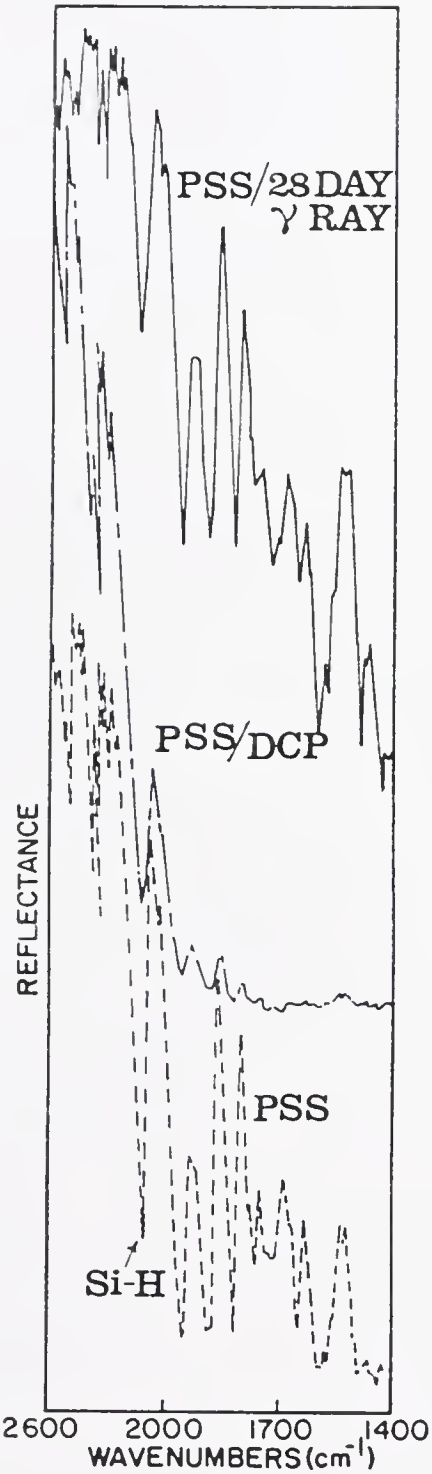

Fig.II-46. FT-IR Spectrum of a Region Showing the Effect of Crosslinking on Si-H Band Intensities at ~2080 cm^{-1}

expect that in synthesizing more reactive silane precursors for crosslinking there is the danger of introducing more oxygen contaminant in the polymer and, thus, in the pyrolyzed product.

In Fig. II-46, the as-received PSS shows a sharp and strong absorption band for Si-H at ~2100 cm^{-1}, a medium sized band for γ-ray irradiated PSS, and a small band for 10 wt% DCP treated PSS. This means that PSS crosslinking can occur between Si-H's (Fig. II-27), as well as by methyl free radicals from DCP at higher temperatures. The bond energy of ≡ C-CH_2-H is 418.4 KJ/mole[63] and the bond energy of ≡ Si-CH_2-H should be a little less than that of ≡ C-CH_2-H because of a greater electropositivity of a Si atom than that of C atom. Still, the bond energy of Si-H (314 KJ/mole)[54] is much smaller than that of ≡ Si-CH_2-H, hence the crosslinking of PSS by DCP proceeds with Si-H bonds breaking at ~150°C followed by formation of Si-C-C-Si linkages via methyl radicals at ~250°C. In Fig. II-27, as-synthesized PSS shows a small exothermic peak at ~160°C, which probably corresponds to the crosslinking reaction via Si-H. The DSC for J-PSS2 in Fig. II-28 before the DCP treatment shows negligible crosslinking via Si-H coupling during the heating schedule of the DSC. Rearrangement of the polymer chain is thought to occur at ~400°C. The small spikes at 100°C correspond to water evaporation. The reason for sharp endothermic peaks at ~520°C is not known, but it is thought to be the evaporation of a fraction of low volatility. After the endothermic rearrangement, decomposition to eliminate H_2, CH_4, C_6H_6, etc. actually begins to occur at ~420°C.

The minimum at ~200°C for PSS with in situ DCP crosslinking (Fig. II-27) must be due to the decomposition of DCP. Under the heating rate

of DSC (5°C/min), the DCP crosslinking reaction may not be able to keep up with tne heating rate. The exothermic reaction was incomplete until the temperature was ~220°C. This supports the previous observation of incomplete crosslinking with DCP at temperatures below ~200°C and the low TGA char yield of the in situ DCP crosslinked PSS (Fig. II-37).

In the DCP precrosslinked J-PSS (Fig. II-28) no chain rearrangement is evident. Instead of rearrangement, the decomposition begins at a slightly lower temperature, ~400°C. Tnis may mean that the molecular rearrangements have occurred during the preceding DCP crosslinking reaction. The primary chain rearrangement is probably a Kumada type,[64] as shown in equation II-2.

$$\equiv \overset{\overset{Me}{|}}{Si}\text{-}Si \equiv \rightarrow \quad \rightarrow \overset{\overset{H}{/}}{Si}\text{-}CH_2\text{-}Si \equiv \qquad \text{(II-2)}$$

A pyrolysis GC study of PSS (Figs. II-25 and II-26) with DCP showed a large amount of methane and acetophenone, which are some of the products from the proposed crosslinking reaction given in Fig. II-47. The amount of methane is too much to come from the Si-H coupling alone. Thus, the methane must be formed by the methyl radicals of DCP after abstracting methyl hydrogen from $Si\text{-}CH_3$. The possibility of crosslinkage via Si-Ph-Ph-Si is doubtful because of the greater bond energy for  (112 Kcal/mol) than for $-CH_2-H$ (104 Kcal/mol).[65]

During crosslinking and pyrolysis, a precursor polymer is decomposed and fragmented, preferably with free radical modes to achieve a high ceramic yield. However, pyrolysis conditions strongly affect the density of the pyrolyzed product. Density is increased during

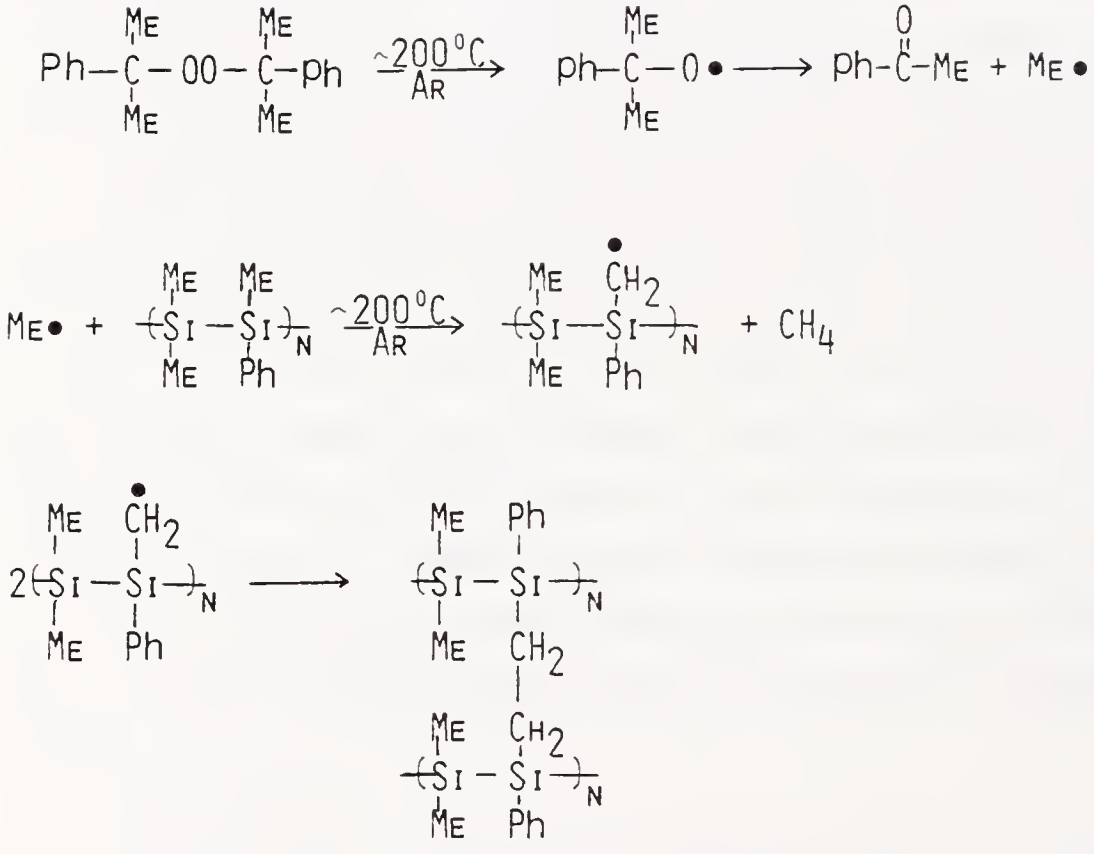

Fig.II-47. The Crosslinking Mechanism of PSS by DCP

pyrolysis but not usually to the theoretical value due to the porosity generated by evolved gasses during the process. Figures II-30 and II-31 show the uneven surfaces and pores formed on PSS and ViSP after crosslinking and pyrolysis at 900°C in vacuum or in N_2. The blisters formed on a sintered mass of SiC that are created during the crosslinking process are in submicron sizes and remain after pyrolyzing up to 900°C.

Although the SiC formed from organosilanes and pyrolyzed at ~1000°C is known to be the beta phase, the x-ray diffraction pattern of the powder is amorphous because of its extremely fine grain size (~3 nm).[24]

Most TGA data for char yield are for samples after being ex situ precrosslinked in either N_2 or in a vacuum. The 67% char yield of PSS-O suggests that some of the most volatile fractions escape during the crosslinking reaction. However, the char yields of crosslinked PSS-O with respect to the PSS-O starting weight are in the range of 35-45%, which is close to the theoretical yield of 45%, according to equation II-3.[40]

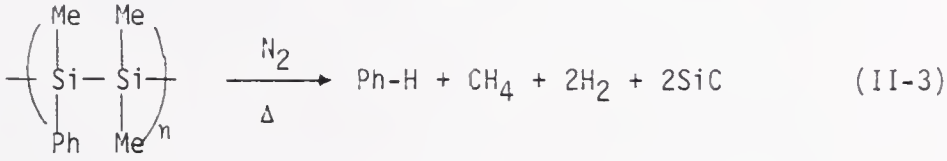

$$\xrightarrow[\Delta]{N_2} \text{Ph-H} + CH_4 + 2H_2 + 2SiC \qquad \text{(II-3)}$$

This demonstrates the potential usefulness of PSS oligomers as a filler phase for porous ceramic bodies by infiltrating the pores as small molecules followed by crosslinking and pyrolysis in the pores of the ceramic body.

A higher char yield of A-PSS than that of PSS without precrosslinking treatments is thought to be a result of crosslinking between Si-H

and ⁀⁀ during the pyrolysis, as discussed previously in this chapter. This in situ thermal crosslinking also applies to ViSO and ViSP.

In the case of the more reactive ViSP, temperatures above 110°C with DCP and above 150°C without DCP are required for crosslinking (Table II-9). The Petrarch's H—Si-Si-O substituted PDMS was difficult to crosslink by all methods tried. This raises a doubt that the polymer has a Si-H functional group, or that a Si-O group may somehow effectively inhibit the functionality. No characterization to determine the structure was carried out on the Si-O linked polysilanes. Other evidence to increase doubt of the presence of a Si-H group is in the essentially nil TGA yield of the polymer upon pyrolysis. It may be the Si-O which makes the crosslinking very difficult.

The Petrarch's phenyl substituted Si-Si-O PDMS was crosslinked with difficulty by DCP which increased the TGA yield to 27%. The crosslinking mechanism of this polymer by DCP is presumed to be similar to the PSS/DCP system, but a Si-O group must be suppressing the free radical crosslinking. The usefulness of this polymer in ceramic applications is presently unknown, i.e. the effect of Si-O substitution needs to be investigated further.

The TGA yield of in situ DCP crosslinked PSS-1P is ~30%, which is lower than the theoretical yield of 45%. This low yield is due to the constant rapid heating rate (10°C/min) in the TGA operation so that the crosslinking temperature in the ~200°C region is passed in a few minutes, which is not enough time for complete crosslinking.

A pyrolysis study of PSS was carried out by Sinclair[66] at 400°C in vacuum. Each fraction he obtained is shown quantitatively below. This

distribution of PSS fractions suggests that the crosslinking of PSS via DCP allows recovery of fractions up to some of medium volatility (54.2%) as SiC product. The char yield of ~50% is in fact the maximum theoretical yield. However, without crosslinking, only the nonvolatile solid and maybe some of the low volatile solid fraction (~10%) is recovered as SiC upon pyrolysis.

Fraction	Wt%	
Highest volatility lost through vacuum line	12.4	
High volatile liquid	31.7	
Medium volatile liquid	17.7	
Low volatile solid	28.6	54.2
Nonvolatile solid	7.9	

As the organosilanes were heated in a quartz tube furnace in N_2, yellow gas was generated and condensed on the colder region of the tube wall. This same gas corroded the DSC metallic sample chamber, TGA sample boat made of platinum, Nicalon® continuous SiC fiber in SiC/SiC composites, and the thermocouple of a furnace. The yellow corrosive gas was first suspected as a chlorine compound, e.g. Cl_2, HCl, HOCl, etc., formed by the residual chlorine from the starting dichlorosilane monomers. The residual chlorine was tested by dissolving PSS in benzene and hydrolyzing any Si-Cl with water by shaking the benzene phase and water phase in a separatory funnel, then the aqueous phase was titrated with $AgNO_3$ solution. No precipitate was observed. Based on this test, the possibility of the yellow gas as a chlorine compound was ruled out.

Silicon and/or SiC, at low oxygen partial pressure, can form silicon monoxide at elevated temperatures.[15,67] It is then possible that the yellow gas is SiO, but the chemical reactivity of SiO with respect to metals, SiC, and SiO_2 is not known. If it were SiO, the low partial pressure oxygen source must be in the inert gas, e.g. a commercial research grade N_2 gas contains ~1 ppm O_2 and ~1 ppm H_2O, and also in the organosilane itself.

Figure II-38 shows a large absorption peak for SiO_2 at ~1078 cm^{-1}. This large absorption band of SiO_2 is caused by a SiO_2 film on the surface of a monolithic PSS/SiC sample after crosslinking and pyrolysis at 960°C. This surface oxidation must be caused by oxygen in the inert gas and/or during handling in air prior to pyrolysis. An FT-IR spectrum of the same PSS/SiC sample after the monolith was crushed into fine powder was taken again. This is shown in Fig. II-39, along with commercial β-SiC Nicalon®, which is made from polycarbosilane. The large SiO_2 absorption band previously shown is diminished to a small hump at ~1050 cm^{-1}, while the bands corresponding to Si-C at ~800 cm^{-1} remained the same.

In Figs. II-40 and II-42 for J-PSS/SiC and ViSP/SiC pyrolyzed at 900-1000°C, it can be seen that some type of organic residue still remains, as well as Si-H groups. This may be either from an incomplete transformation of the organosilanes to β-SiC or from contaminants from external sources during handling prior to pyrolysis. This means that temperatures above 900°C are required to convert an organosilane completely to β-SiC. However, an FT-IR spectrum of a ViSP/SiC monolith

pyrolyzed at 950°C and surface polished with SiC grit followed by washing with acetone shows an essentially identical spectrum as Nicalon® (Fig. II-43). Therefore the organic residue must be concentrated on the surface.

Conclusions

It has been shown that these various organosilanes as polymers and oligomers can be successfully converted to β-SiC after crosslinking treatments and nearly reach the theoretical yield upon pyrolysis. The process of SiC production from silane monomers and PSS is summarized in Fig. II-48. The applications of these materials and techniques for making ceramic composites are the subjects of the following chapters.

The exploratory organosilane (OS) precursors used in this work have the potential to be formed into desired shapes using conventional low temperature plastic processing, then pyrolyzed to obtain SiC material with a yield that is nearly the theoretical limit. These precursors can also be used to impregnate porous ceramic bodies.

The highest char yield is given by the polymer fraction of vinylic silane (72%). The allyl group on the polysilane chain improved crosslinkability. A complete crosslinking of OS precursors increased the char yield of SiC. For complete crosslinking, DCP with temperatures greater than 250°C for PSS and greater than 130°C for vinylic silanes are required. Other combinations of the functional groups such as Si-H, ,  ,  , etc. should further improve crosslinkability and ceramic yield.

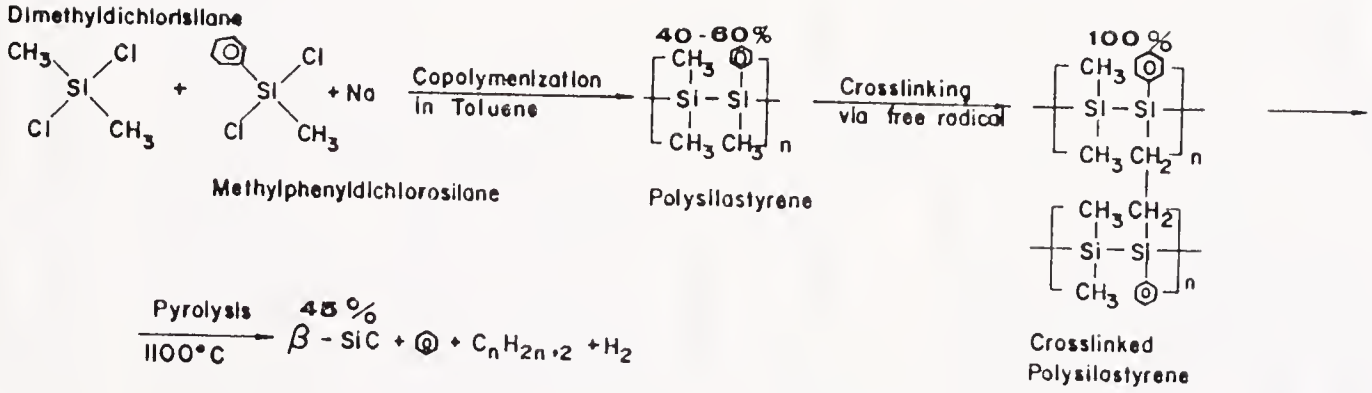

Fig.II-48. Polymerization, Crosslinking, and Pyrolysis Reactions of Polysilastyrene to Obtain Silicon Carbide

Char yield of SiC is roughly shown to be a function of concentration of the crosslinking agent DCP, and a function of temperature and time. However, temperature has a much greater effect on the degree of crosslinking than time. The possible oxygen contamination from the crosslinking agent, DCP was not observed.

These OS precursors are prone to oxidation during handling, crosslinking and pyrolysis to include oxygen contaminant in the final SiC product. For a complete freedom from oxygen contamination, there must be more convenient ways to process the OS precursors, e.g. a glove box fully equipped to avoid oxygen.

In order to increase the polymer fraction of PSS, a longer reaction time than two hours would be desired in the synthesis.

Variables that may have significant effects on the PSS polymer yield and quality are 1) rate of chlorosilane monomer addition, 2) amount and kind of solvent relative to the reactant, 3) state of dispersion and the amount of sodium, 4) reaction temperature, 5) reaction time, 6) reactant's molar ratio, and 7) environmental factors such as oxygen, ultraviolet light, etc.

To improve the lot-to-lot reproducibility of the processing of OS precursors to obtain SiC, more work on the polymerization procedure and an understanding of all the process variables is necessary to establish standard procedures.

Although γ-ray irradiation can crosslink OS, there needs to be a source with a higher dose rate than ^{60}Co to be practical for PSS. A source such as ^{137}Cs may hasten the crosslinking of OS.

To produce a large dense monolithic SiC body directly from OS, foaming and gas generation should be controlled during crosslinking and pyrolysis. In order to control these phenomena, a chemical additive as an antifoaming agent needs to be found and/or a new polymer with no foaming properties needs to be synthesized.

CHAPTER III
SILICON CARBIDE/SILICA COMPOSITES FROM CARBOSILANES AND ALKOXYSILANES

Introduction

The significance and advantages of the sol-gel route to produce glasses and ceramic materials have been given in Chapter I of this dissertation. Although the production of silica glass monoliths via the sol-gel method is highly significant by itself, the problem of intrinsic brittleness of glass may be modified by forming a composite.

If the strength of a glass were determined solely by its lattice cohesive energy, one would predict the glass to be very strong. In all cases, glasses are weaker than otherwise expected because flaws concentrate applied stresses. The problem is flaw sensitivity, causing catastrophic failure under applied stresses, and susceptibility to thermal shock. Because of these problems, glasses have acquired a reputation for mechanical unreliability.

Many ways to strengthen glasses have been studied,[68] including the following:

- annealing
- compressive stresses on the surface via tempering or ion exchange
- dispersion hardening
- fiber reinforcement
- reduction of flaws

The strengthening mechanisms and effects at room temperature for glasses may not be the same as the effects at high temperature. In metals, conventional precipitation-hardened metal alloys are not thermally stable and the precipitation may coarsen at elevated temperatures well below the softening temperature of the alloy, resulting in a reduction of mechanical strength.[69] In contrast, many ceramics and glasses maintain strength and exhibit stability at high temperatures with low density and chemical inertness.

In an effort to increase strength and toughness, barriers to crack propagation in the form of discrete particles or fibers have shown some success,[69] similar to the fine dispersion of second-phase particles long used for metallic systems.[70] The strengthening effect in the case of metals is attributed to various dislocation impedement mechanisms.[70] However, since dislocations do not exist in glasses, particle dispersion strengthening of glasses must rely on a different mechanism. Hasselman and Fulrath[71] observed dispersion hardening effects in certain systems of ceramics by dispersion limiting the size of Griffith flaws, thereby raising the stress required to initiate or propagate cracks. Lange[72] has proposed a mechanism that strengthening may occur as a result of a line-tension effect due to particles initially pinning a propagating crack front and causing a detour similar to that observed for dislocations.

Another aspect of dispersion hardening may be the strengthening effect of the dispersed particles with a higher elastic modulus than the matrix. A fine particle dispersion may also inhibit grain growth or

crystallization of glass at high temperatures and hence lead to an apparent increase in strength. Therefore a distribution of dispersed particles on a molecular scale should yield a large improvement in the mechanical properties of a glass.

Using the techniques described in Chapter II, organosilanes may be introduced directly into the monolithic body of a sol-gel derived silica glass matrix to obtain a strengthened silica body after appropriate heat treatments. The organosilane precursors to SiC are thereby dispersed homogeneously in the matrix of silica gel. Upon pyrolysis, the SiO_2 matrix is reinforced by molecularly dispersed SiC particles, thereby yielding a molecular composite. Developing procedures and understanding the process are the objectives of this work.

In this chapter, results of the expected hardening of SiO_2 glass by SiC molecular dispersion are presented, as well as the fabrication techniques used to produce such a body.

Experimental

Infiltration of silica gel matrix with carbosilanes

Silica gel matrices to be impregnated were prepared by hydrolyzing tetramethoxysilane (TMOS) at ~90°C with water in TMOS/H_2O molar ratio of 1 mole of TMOS per 4-17 moles of water and adding 0.5-2 w/o of acids or 1:10 molar ratio of the acid to TMOS. This liquid mixture called a sol, was cast in plastic molds and aged at 60-80°C for 24 hours after the molds were tightly sealed to prevent liquid evaporation. At the end of 24 hours some gel monoliths were allowed to age for an additional 24 hours in the original molds and some gels were transferred to a water

bath for further aging. At the end of approximately three days from the beginning, the seals were broken for slow drying in an oven with a steady increase in temperature from 80°C to 150°C in 12 hours. The typical size of a dried gel was ~20cc.

The dried gels were decarburized in monolithic forms by heating them in air to 500-600°C with a heating rate of ~65°C/hour and held at 500°C for two hours. At this temperature, partial dehydroxylation and nearly complete decarburation is expected to occur. Tne decarburized and partially dehydroxylized gels were stored in a desiccator, after cooling to room temperature with ~80°C/hour rate, until the time for silane impregnation.

The organosilanes or carbosilanes used to infiltrate the silica gels were polysilastyrene (J-PSS2), vinylic silane oligomer (ViSO), and vinylic silane polymer (ViSP). The structures and physical states of these silanes have been described in Chapter II. The solid silane J-PSS2 was dissolved in toluene or THF to make up ~20 w/o solution. The high viscosity liquid ViSP was diluted with THF in 1 g silane/2 ml THF for impregnation.

The impregnation of silanes into the silica gels was carried out by placing a monolithic piece of the gel in a silane solution containing 1 vol% of 3-aminopropyl triethoxysilane as a wetting agent and 5 wt% of DCP and soaking it for 2 to 12 hours. For deeper penetration of silanes into the gel body, vacuum impregnation for 30 min-6 hours was used. At the end of infiltration, the infiltration chamber was brought to atmospheric pressure and left for 30 min. before transferring it into a pyrolysis tube. The processing map is shown in Fig. III-1.

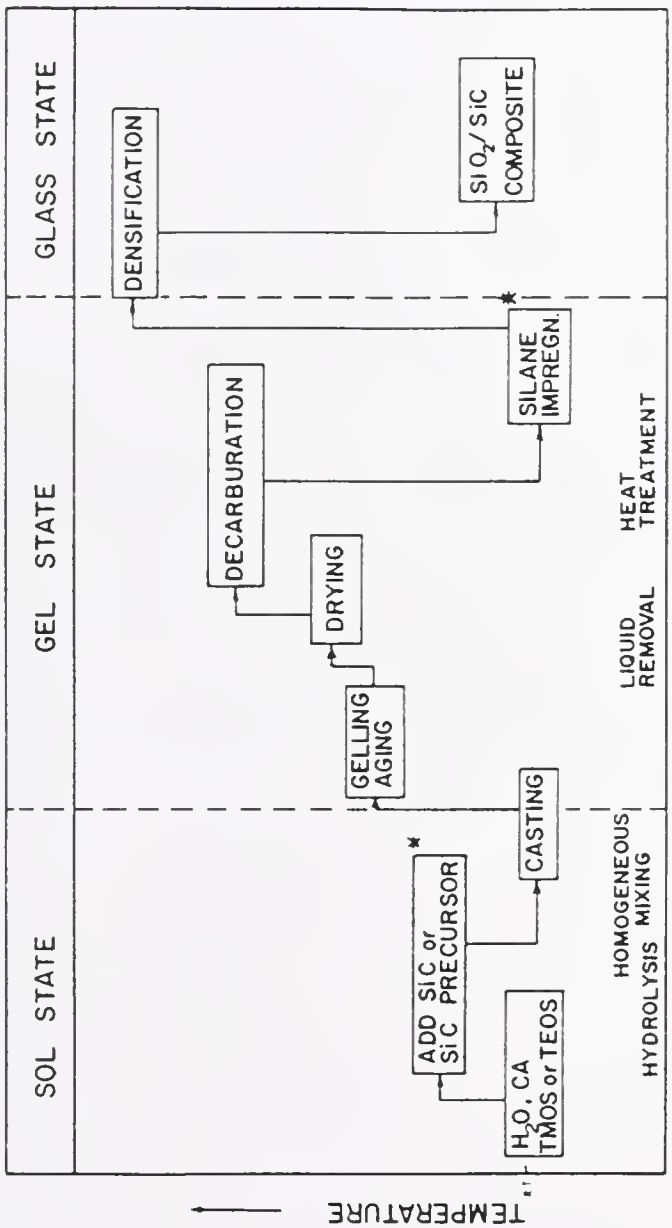

Fig. III-1. Processing Map of SiC/SiO_2 Composites, * May be Mutually Exclusive

The impregnated gels were pyrolyzed in N_2 or in Ar at various temperatures with the heating rate typically 50°C/hr. The pyrolyzed SiC/SiO_2 composite monoliths were stored in a desiccator, after they were cooled to room temperature from the pyrolysis temperature, until microhardness, porosity, surface area, densities, etc. were measured. Microhardness values were measured by using a Kentron Tester or a Leco Model DM-100 with 0.5-2 kg load and a 136°C diamond pyramid indenter. Both diagonals of the indentation were measured and the average values were used to compute the Diamond Pyramid Number (DPN). Porosity and surface areas were determined by using Quantachrome's Autosorb-6. Densities were measured by mercury, water or propylene glycol volume displacement.

In situ molecular composites of Bulk SiC/SiO_2 Monoliths.

For a silica gel matrix, TMOS was hydrolyzed using acidified water in 1:4 molar ratio of TMOS/H_2O and organic solvents. The water used here was previously degassed by inert gas purging to improve the action of CFRI DCP. The acids used in ~2 vol% were lactic acid and formic acid. These are strong organic acids and are expected to catalyze the hydrolysis of TMOS readily and possibly improve the compatibility of the TMOS with organosilanes. Solvents used were isopropyl alcohol, THF, toluene, n-butanol, and amyl alcohol in 100-150 v/o of TMOS. Approximately 1 v/o of 3-amino propyl triethoxysilane was added as a wetting agent to promote the retention of polysilanes in the matrix.

After the hydrolysis was complete (~20 min. stirring by a magnetic stirrer at room temperature), 0.4-4 w/o of an organosilane (OS) dissolved in THF (~1/5 volume of TMOS) with 4-5 wt% DCP (wt% with respect to

OS) was mixed with the hydrolyzed sol for 20 min. at 30-40°C in a closed container.

The OS/SiO_2 sol mixture was cast in Teflon molds. They were sealed tightly to prevent any evaporation of solvents and water, followed by gellation and aging at ~60°C for 12 hours. Curing was followed with the temperature gradually raised to ~150°C in 6 hours. The gels containing OS were cured at ~150°C for 6 hours. The temperature was brought down to 60°C at the end of 6 hours of curing and the seals were broken for slow drying in an inert atmosphere. Drying was continued for two days at 60°C in N_2 or Ar with a gradual increase of solvent evaporation by opening the lids. The typical size of a dried gel was ~20cc.

Pyrolysis and densification were carried out by placing the dried composite green bodies in a tube furnace with N_2 gas flowing at ~5 ml/min rate and a heating rate of ~20°C/hour up to 150°C and held at 150°C for three hours. The temperature was raised to the range of 150-850°C with a rate of ~100°C/hour and held at 850°C for two hours. The cooling rate was also controlled; 200°/hour to 650°C, held at 650°C for one hour, 200°C/hour to 300°C, held at 300°C for one hour, then 100°C/hour to room temperature.

Microhardness, pore volume, surface area, and density were measured the same way as for the infiltrated SiC/SiO_2 composites described in the previous section. The processing map for this process is also given in Fig. III-1.

SiC/SiO_2 molecular composite powder

A powder form of a SiC/SiO_2 composite was prepared by mixing 0.6-6.3 g PSS, 8-10 ml TMOS in 10-15 ml benzene or toluene, and 0.05-0.8 g

DCP, in an apparatus shown in Fig. II-3 with N_2 gas flushing over the solution for two hours before heating began. After two hours of degasing with N_2, the solution was heated to a gentle reflux for 12 hours with continuous N_2 flowing. At the end of 12 hours, the solution color changed from dull gray to brownish yellow.

The reaction mixture was precipitated in 80/20 by volume MeOH/H_2O solvent and washed with the solvent three times before drying in a vacuum oven at 70°C for five hours. After reprecipitation in MeOH, an 80-90% yield was achieved.

Characterization of products.

Fourier-transform IR spectra were taken by using a Nicolet MX-1 FT-IR Spectrophotometer, SEM micrographs and EDS spectra by a JEOL Model JSM-35C, NMR by a Varian XL-100 Nuclear Magnetic Resonance Spectrometer, and by Nicolet's High Resolution FT-NMR, BET surface area and pore size distributions by Quantachrome's Autosorb-6, UV-Vis transmittance by Perkin-Elmer's 552 UV-Vis Spectrophotometer, IR transmittance by Perkin-Elmer's 283B IR Spectrophotometer, reflectance of visible light by a custom built optical microreflectometer. X-ray photoelectron spectra were taken by using a Kratos model 800. Hot-stage x-ray diffraction patterns in a helium atmosphere were obtained by using a Philips X-ray Powder Diffractometer as the sample powder was heated on a platinum substrate with HTK10 High Temperature Hot Stage by AP Parr Co. of Graz, Austria. Microhardness and fracture toughness of the monolithic composites were determined by using a Leco Microhardness Tester and according to Antis et al.[73] Flexural strengths were determined by using an Instron Testing machine.

Variations in experimental conditions, reactant amounts, and chemical additives are summarized in Table III-1 for the typical composites.

Results

A photograph of partially dried OA gel monoliths to be impregnated with silanes is shown in Fig. III-2. The pore size distribution of the OA gel is given in Fig. III-3. The BET surface areas, mean pore sizes, and total pore volumes of typical composites are summarized in Table III-2. The volume loading of SiC in the pyrolyzed composites are estimated from the TGA char yields given in Chapter II for each OS and the volume OS added to the sol. Approximately 3 vol% SiC was maintained.

Repeated attempts to produce edge-notched SiO_2 matrix monolithic specimens for fracture toughness were unsuccessful. Attempts to heat the composites higher than ~850°C in nitrogen also failed due to the foaming of the matrix.

A photograph of an SiO_2 monolith strengthened by in situ bulk decomposition of an organosilane along with a pure gel matrix and gel with OS before thermal treatment is shown in Fig. III-4.

Infrared transmittance curves of SiC/SiO_2 glasses with a fused silica glass as a control are shown in Fig. III-5. A reflectivity curve of a bulk SiC molecular composite glass is compared with a blank gel glass in Fig. III-6. Ultraviolet-Vis transmittance curves of the composites are compared with a blank FA gel glass in Fig. III-7. Figure III-8 shows IR reflectance curves of FA gel and ViSP/FA gel. An enlargement of the band at ~800 cm^{-1} is shown in Fig. III-9.

Fourier-transform IR spectra of PSS-10/104 composite powder before and after pyrolyzing at 900°C and at 1270°C for three hours are shown in

Table III-1.
Summary of Experimental Conditions, Reactant Amounts, and
Chemical Additives Used to Synthesize Some of SiC/SiO_2 Composites

Gel Composition	Silane Type	Method of Infiltration Amount of Silane	Composite I.D.
Silane Infiltrated SiO_2 Gel			
1 mole TMOS	ViSO	room temp., atm. pressure	OA-ViSO
15 mole H_2O	ViSP/THF	soaking	OA-ViSP
0.1 mol. oxalic acid or HCl			
5 w/o DCP			
0.01 mole APTES			
1 mole TMOS	ViSO	room temp., vacuum	FA-ViSO
9 mole H_2O	ViSP/THF	impregnation	FA-ViSP
0.1 mol formic acid	J-PSS		FA-JPSS
0.05 mol lactic acid			
4 w/o DCP			
0.01 mole APTES			

Table III-1 (continued).

In Situ SiC/SiO_2 Molecular Composites

1 mole TMOS 4 mole H_2O 0.1 mole formic acid 0.05 mole lactic acid 0.5 mole BuOH 0.1 mole THF 6 w/o DCP	ViSO ViSP J-PSS/THF	1 g/25 ml TMOS 0.5 g/25 ml TMOS 0.6 g/25 ml TMOS	ViSO/BuOH ViSP/BuOH J-PSS/BuOH
1 mole TMOS 4 mole H_2O 0.05 mole formic acid 0.1 mole lactic acid 0.4 mole amyl alcohol 0.1 mole THF 6 w/o DCP	ViSO/PrOH ViSP 25 w/o J-PSS2/ benzene	1 g/25 ml TMOS 0.5 g/25 ml TMOS 0.6 g/25 ml TMOS	ViSO/PenOH ViSP/PenOH J-PSS/PenOH

SiC/SiO_2 Molecular Composite Powders

10 ml TMOS/3 g PSS-10/11 ml benzene/0.5 g DCP	PSS-10/924
10 ml TMOS/6.3 g A-PSS-0/10 ml benzene/0.5 g DCP	A-PSS-0/927
10 ml TMOS/12 g PSS-10/0.34 g DCP	PSS-10/104
8 ml TMOS/15.1 g J-PSS1/0.75 g DCP	J-PSS1/1120

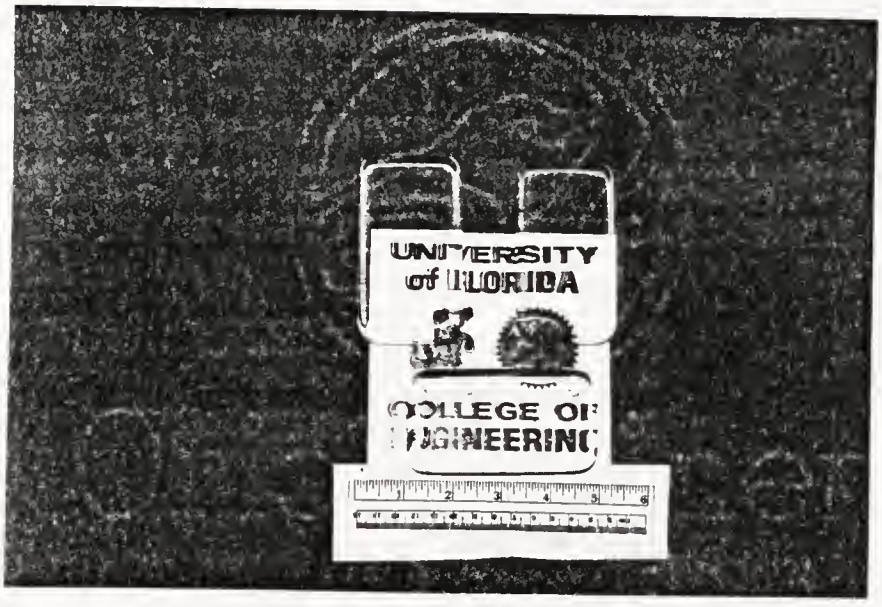

Fig.III-2. Silica Gel Matrices After Aging and Drying Prior to Decarburation and Impregnation.

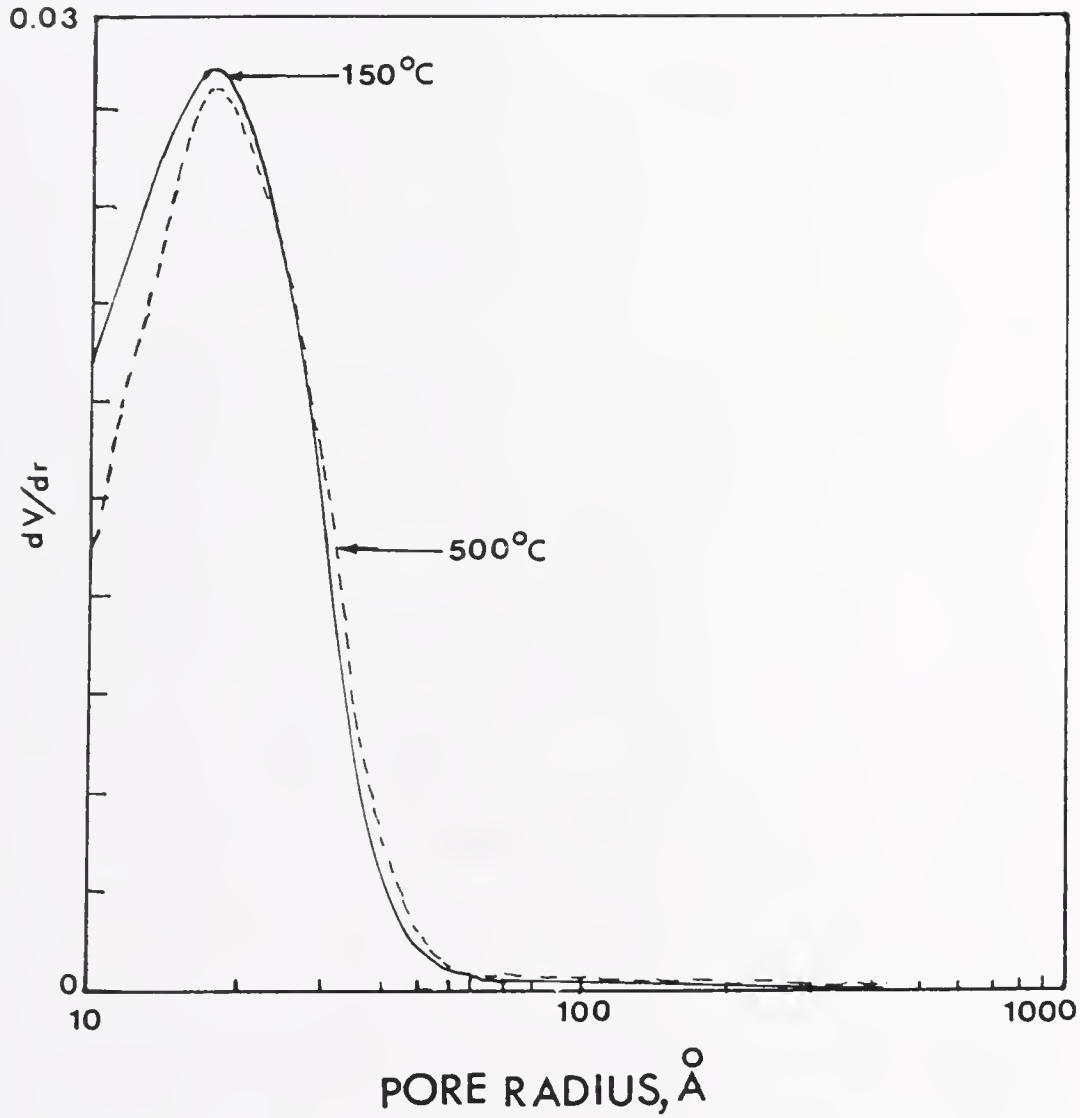

Fig. III-3. Pore Size Distribution OA Gel Showing no Change in Average Pore Sizes After 150°C and 500°C Heat Treatments

Table III-2. BET Surface Areas, Mean Pore Radii, Total Pore Volumes of SiC/SiO_2 Composites, and % True Density Calculated from the Pore Volume.

SiC/SiO_2 Composite	Treatment T, °C	BET, m^2/g	Mean Pore Radius, Å	Pore Volume, cc/g	% Theoretical Density
OA gel control	800	180	13.2	.12	74
OA-ViSO	600	455	14.0	.32	30
OA-ViSO	750	381	13.0	.25	45
OA-ViSO	800	165	12.7	.11	76
OA-ViSP	800	188	11.8	.11	76
FA-ViSP	850	448	15	.34	25
FA-JPSS	800	345	12	.21	34
ViSO/BuOH	800	258	40	.52	-14
ViSP/BuOH	800	13.4	17	.012	97
ViSP/PenOH	900	261	50	.656	-44
ViSP/BuOH	350	167	65	.546	-20
JPSS/PenOH	350	712	16	.58	28
	800	185	35	.32	30

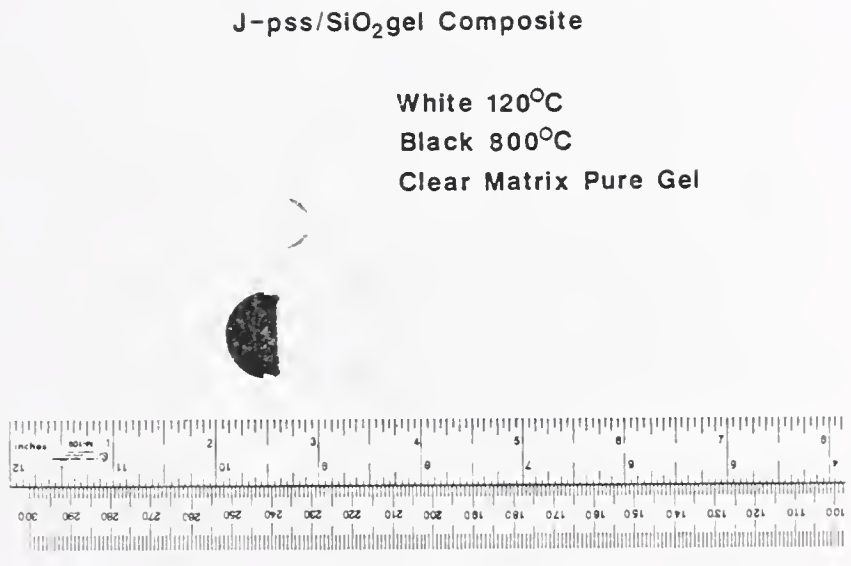

Fig.III-4. SiC/SiO_2 Molecular Composite from PSS/SiO_2 Gel Before and After Pyrolysis With a Pure Gel Matrix for a Comparison.

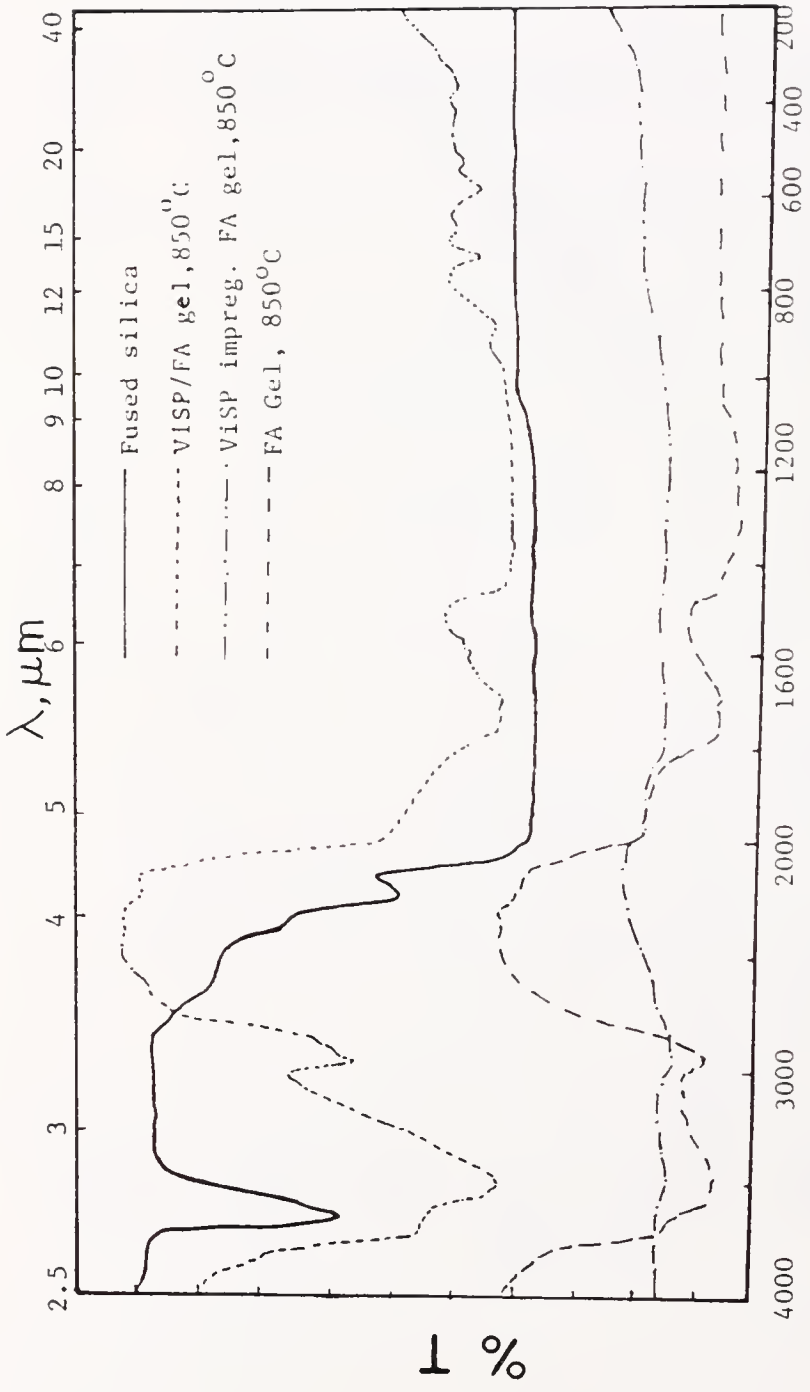

Fig.III-5. IR Transmittance Spectra of Fused Silica, FA Silica Gel, and FA Gel Impregnated With a Silane ViSP

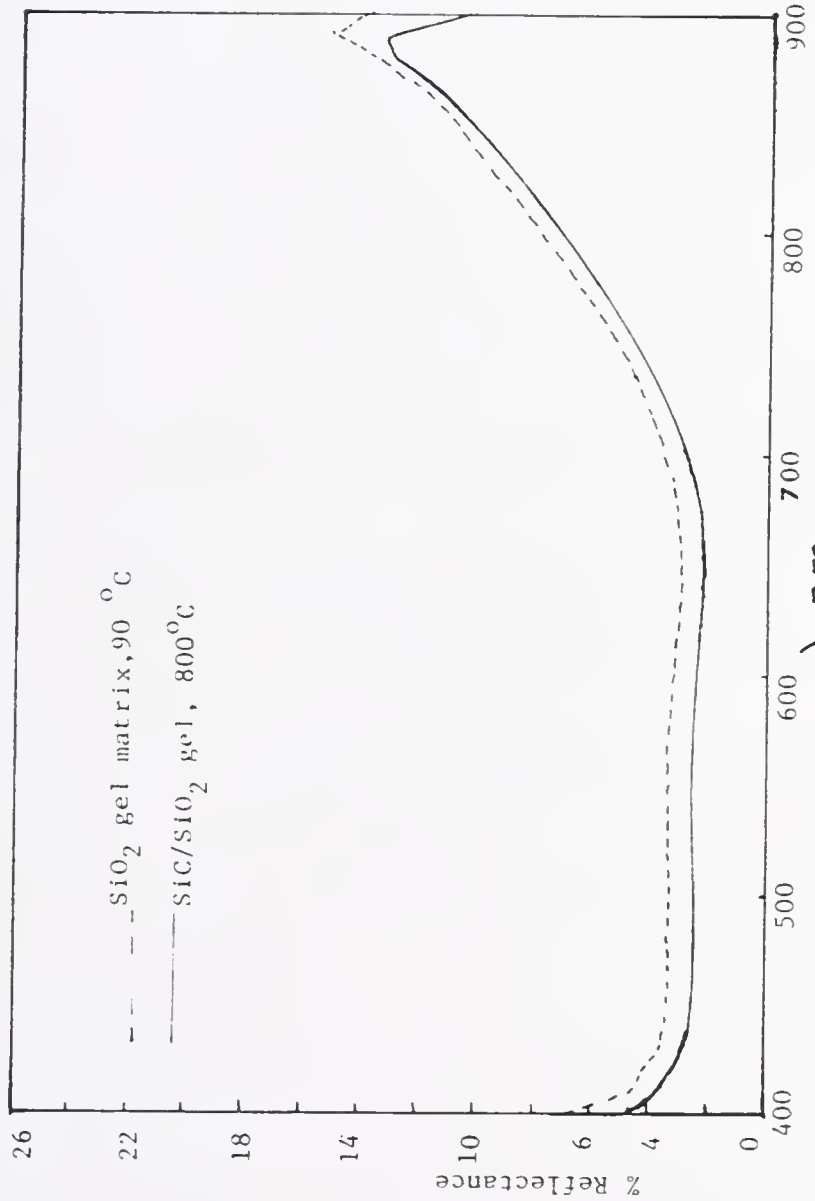

Fig.III-6. Rflectivities of Silica Gel and PSS Impregnated Gel After Pyrolyzed at 800 °C

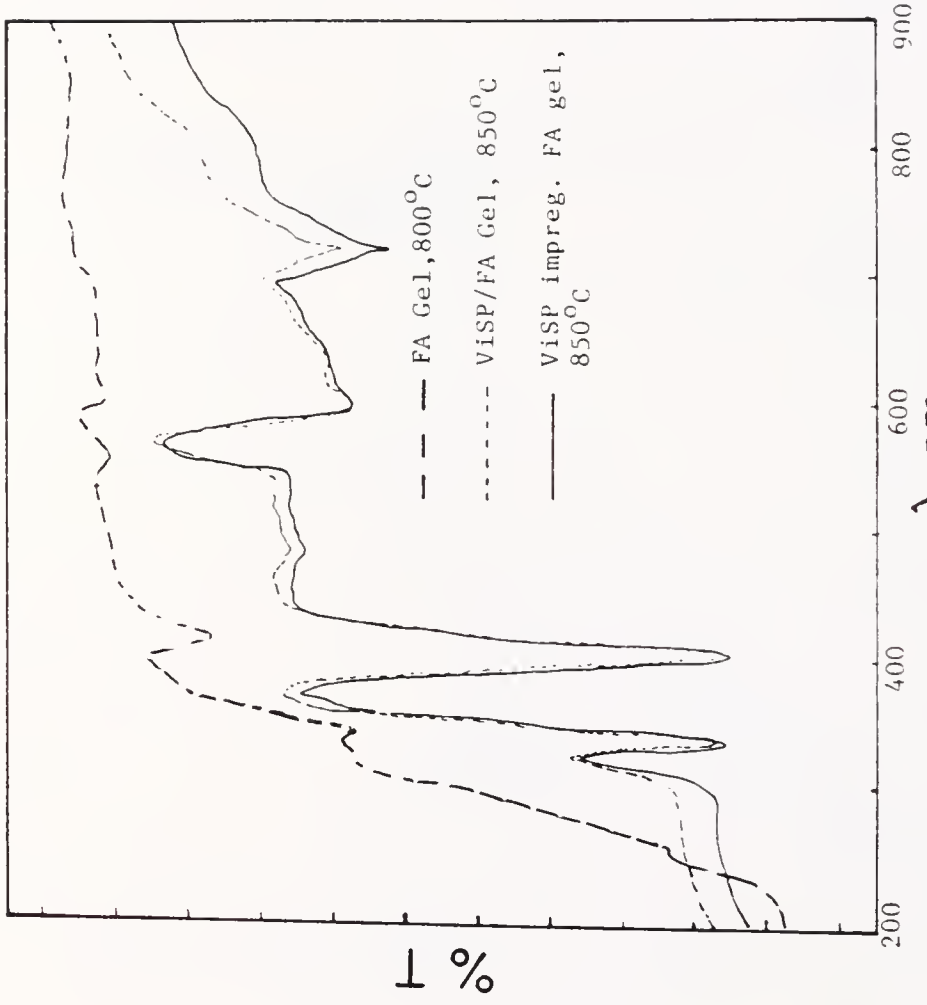

Fig.III-7. UV-Visible Spectra of FA Gel and FA Gel/SiC Composites

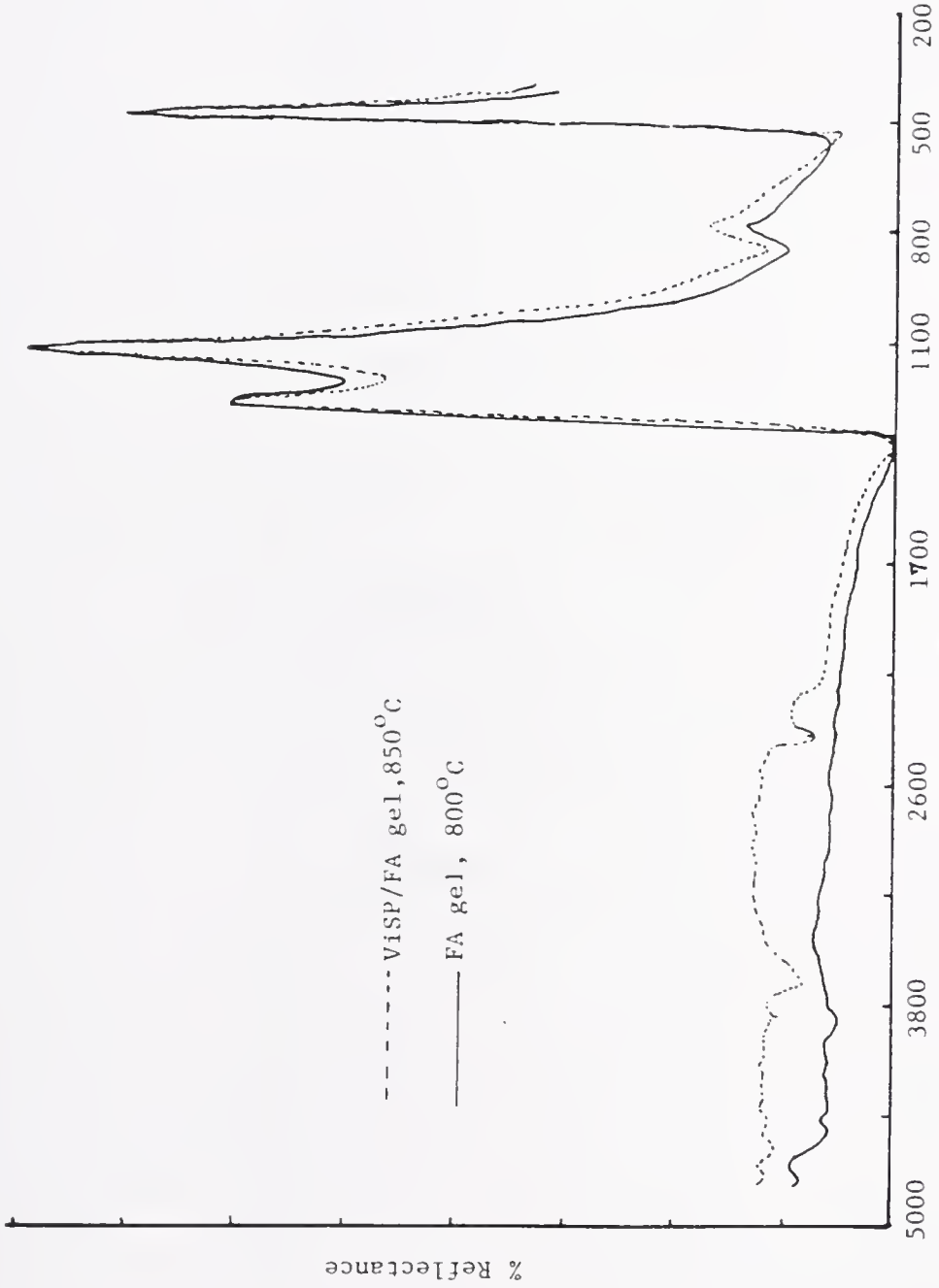

Fig.III-8. FT-IR Reflectance Spectra of FA Gel and SiC/FA Gel After Pyrolyses

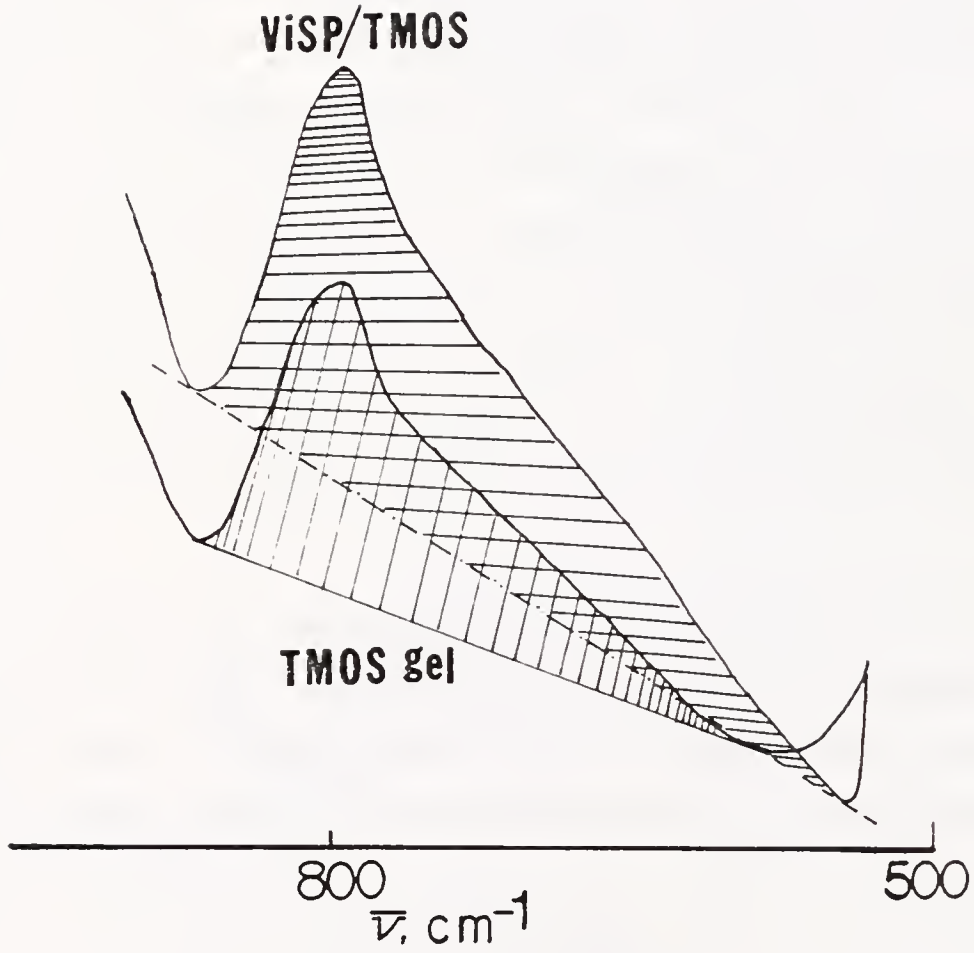

Fig.III-9. Enlarged Spectra of Fig.III-8 Showing Greater Peak Area at ~800 cm^{-1} For the SiC/SiO_2 Composite

Figs. III-10 and III-11. An expanded IR spectrum of J-PSS1/1120 with as received J-PSS1 for comparison is shown in Fig. III-12.

Proton NMR spectra of A-PSS-0/927, PSS-10/104, and J-PSS1/1120 are given in Figs. III-13, III-14, and III-15. The TGA char yields of the powder composites are shown in Fig. III-16. X-ray photoelectron spectra of PSS-10/924, A-PSS-0/927, and ViSP/BuOH composites for silicon after they have been pyrolyzed are shown in Figs. III-17, III-18, and III-19.

Scanning electron micrographs of fractured surfaces of ViSO/BuOH, ViSP/BuOH, and J-PSS/BuOH are given in Figs. III-20 and III-21.

The results of a diamond point microhardness test for SiO_2 gel impregnated with silanes are given in Table III-3 and Figs. III-22 and III-23 for DPN vs. pyrolysis temperature. An optical micrograph showing a diamond pyramid indentation on an impregnated composite is given in Fig. III-24. Results for the same test for bulk in situ SiC/SiO_2 molecular composites are given in Table III-4 and in Figs. III-25, III-26, and III-27.

The results of fracture toughness measurements directly from an indentation crack are given in Table III-5. Mean value of 5-10 measurements were used in the calculation of K_{IC}. The formula used to convert the crack lengths to K_{IC} described by Antis et al.[73] is given below in Eq. III-1.

$$K_{IC} = 0.016 \left(\frac{E}{H}\right)^{1/2} \frac{P}{(c/2)^{3/2}} \qquad \text{III-1}$$

where: E = Elastic modulus in pascals

H = Microhardness in pascals = $\frac{P}{2(a/2)^2}$

P = Indentation load in newtons

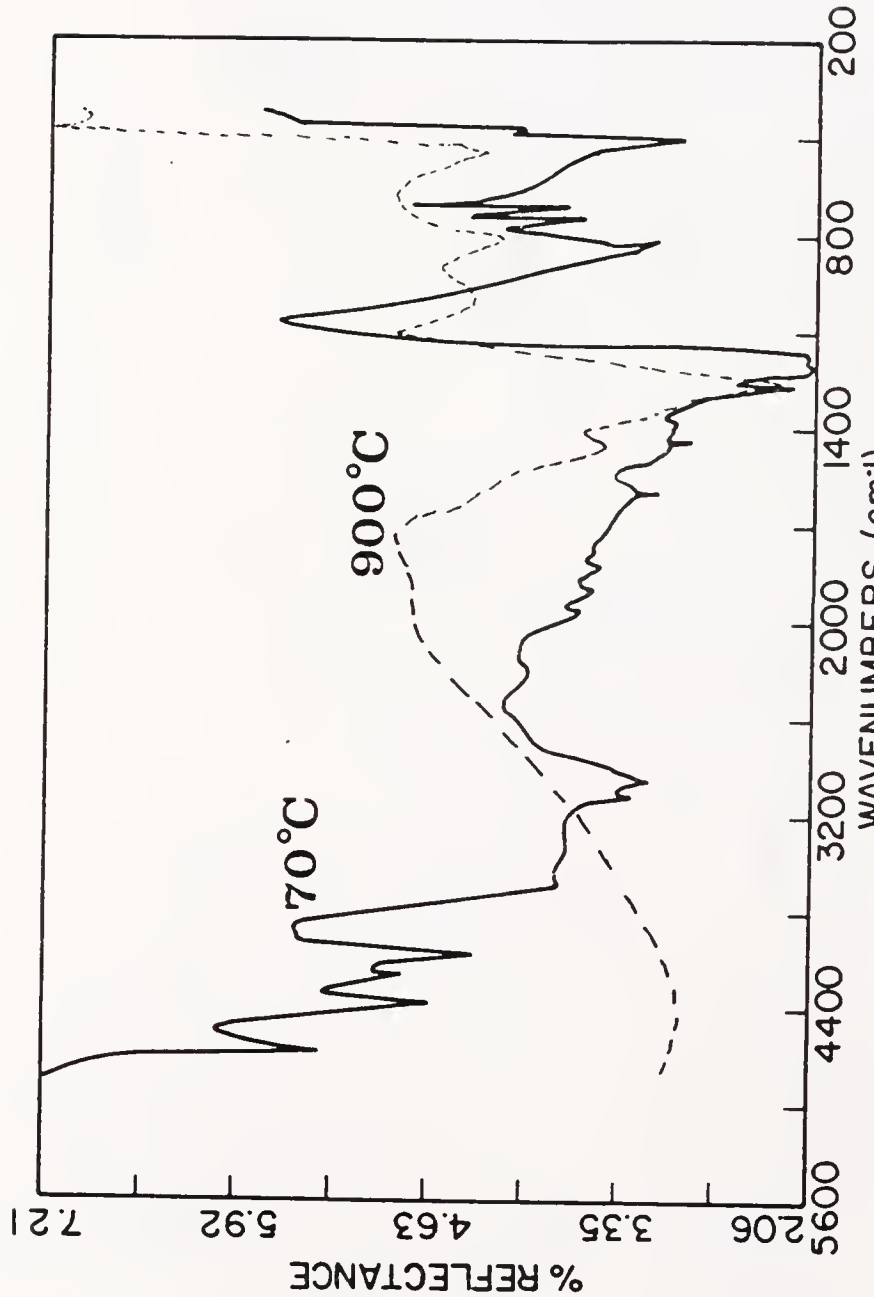

Fig.III-10. FT-IR Spectra of PSS-10/104 Before and After Pyrolysis

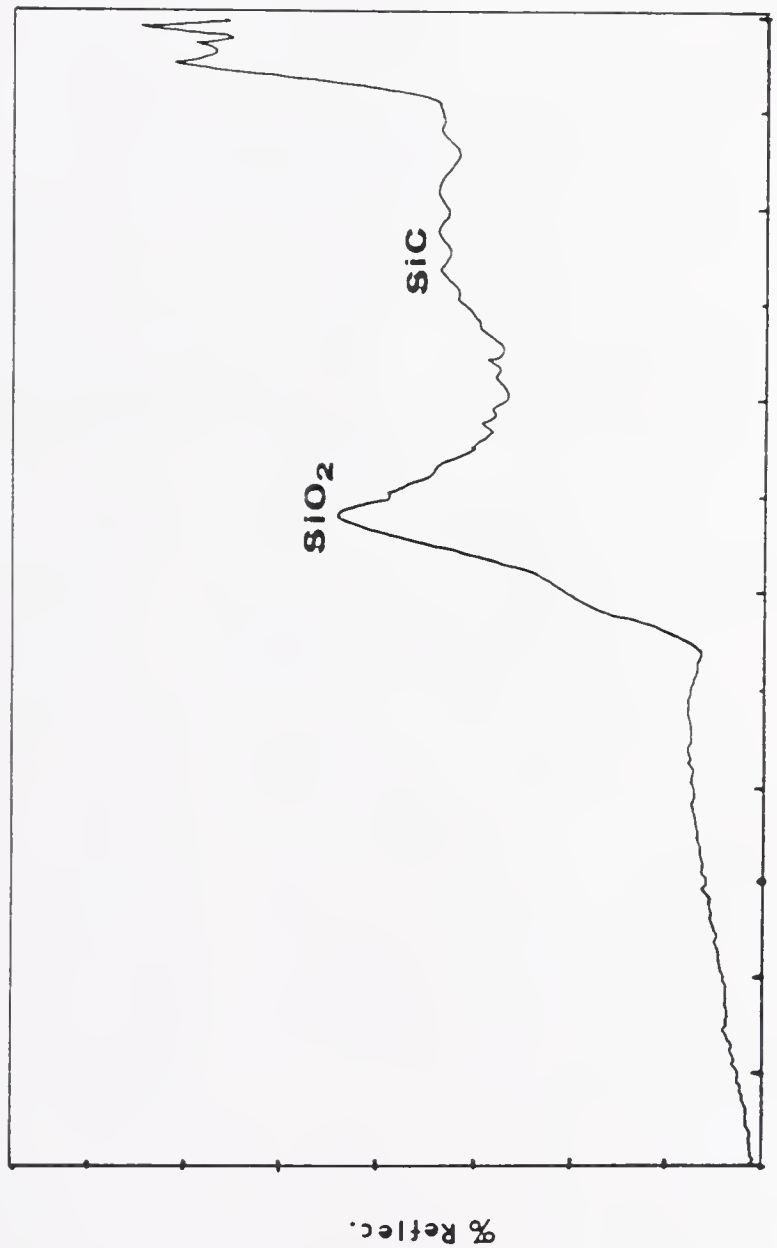

Fig.III-11. FT-IR Spectrum of PSS-10/104 After Pyrolysis at 1269°C

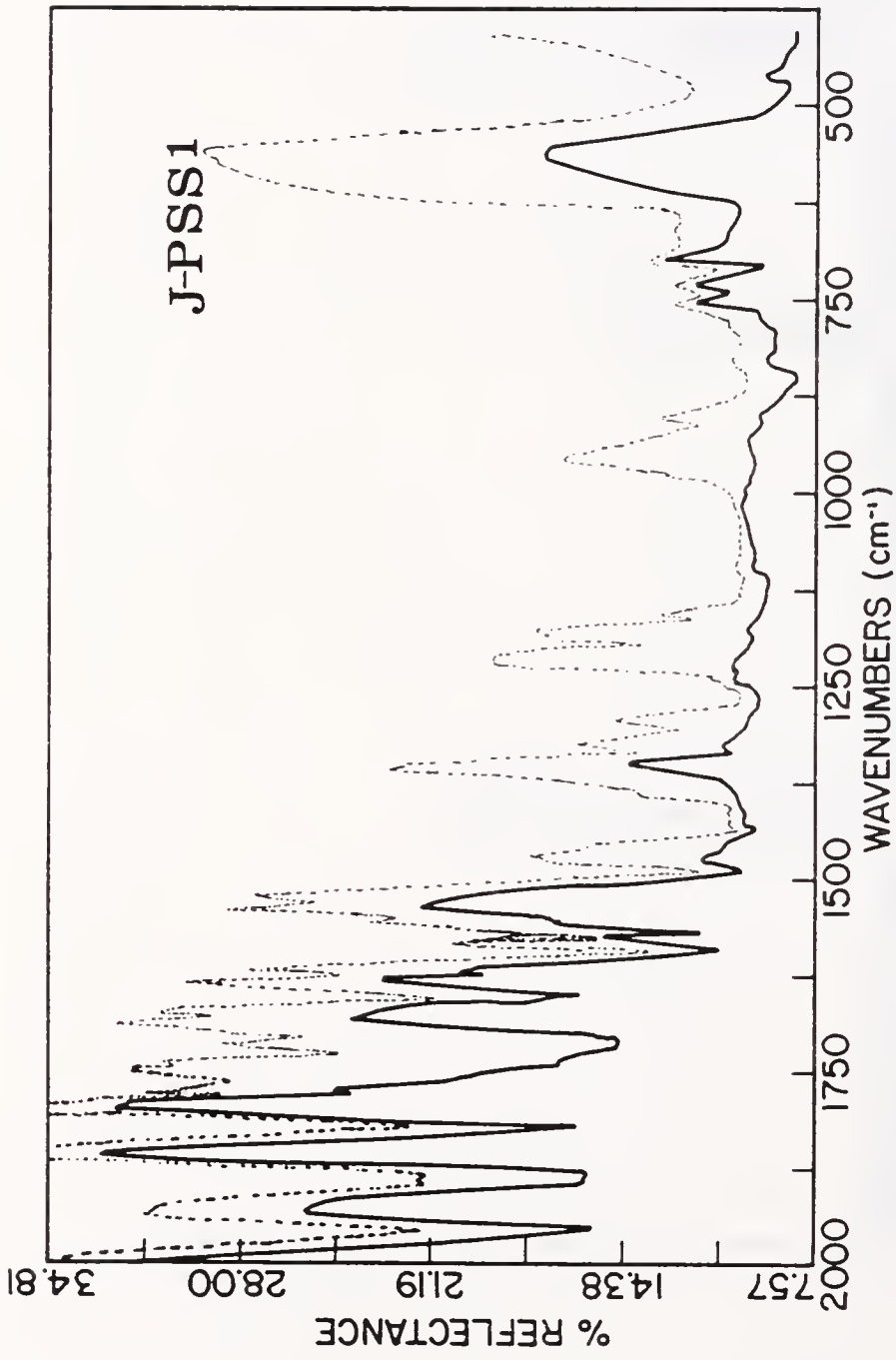

Fig.III-12. FT-IR Spectra of J-PSS1/1120 and J-PSS1

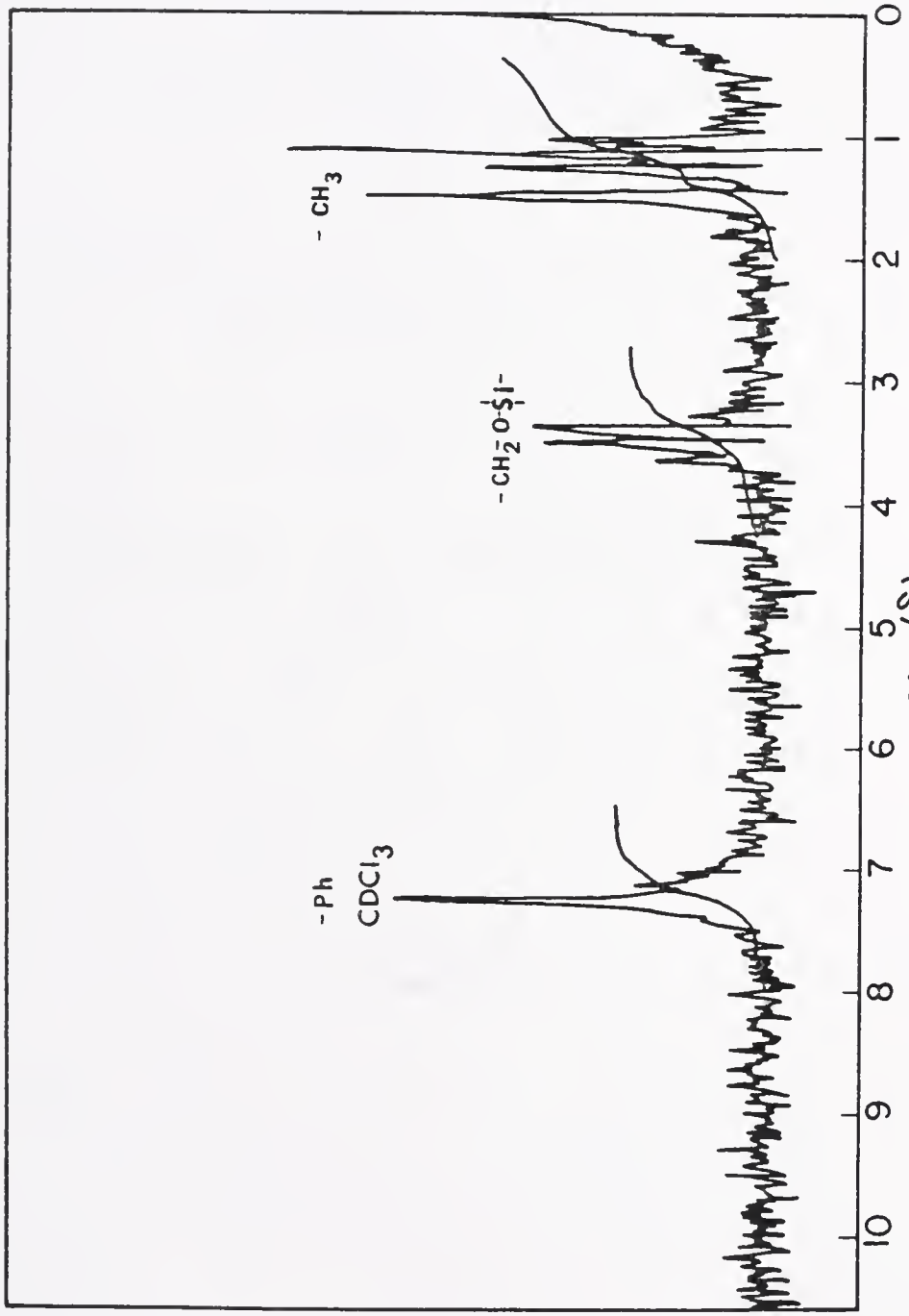

Fig.III-13. Proton NMR Spectrum of A-PSS-0/92 Showing C-O-Si Crosslinkage

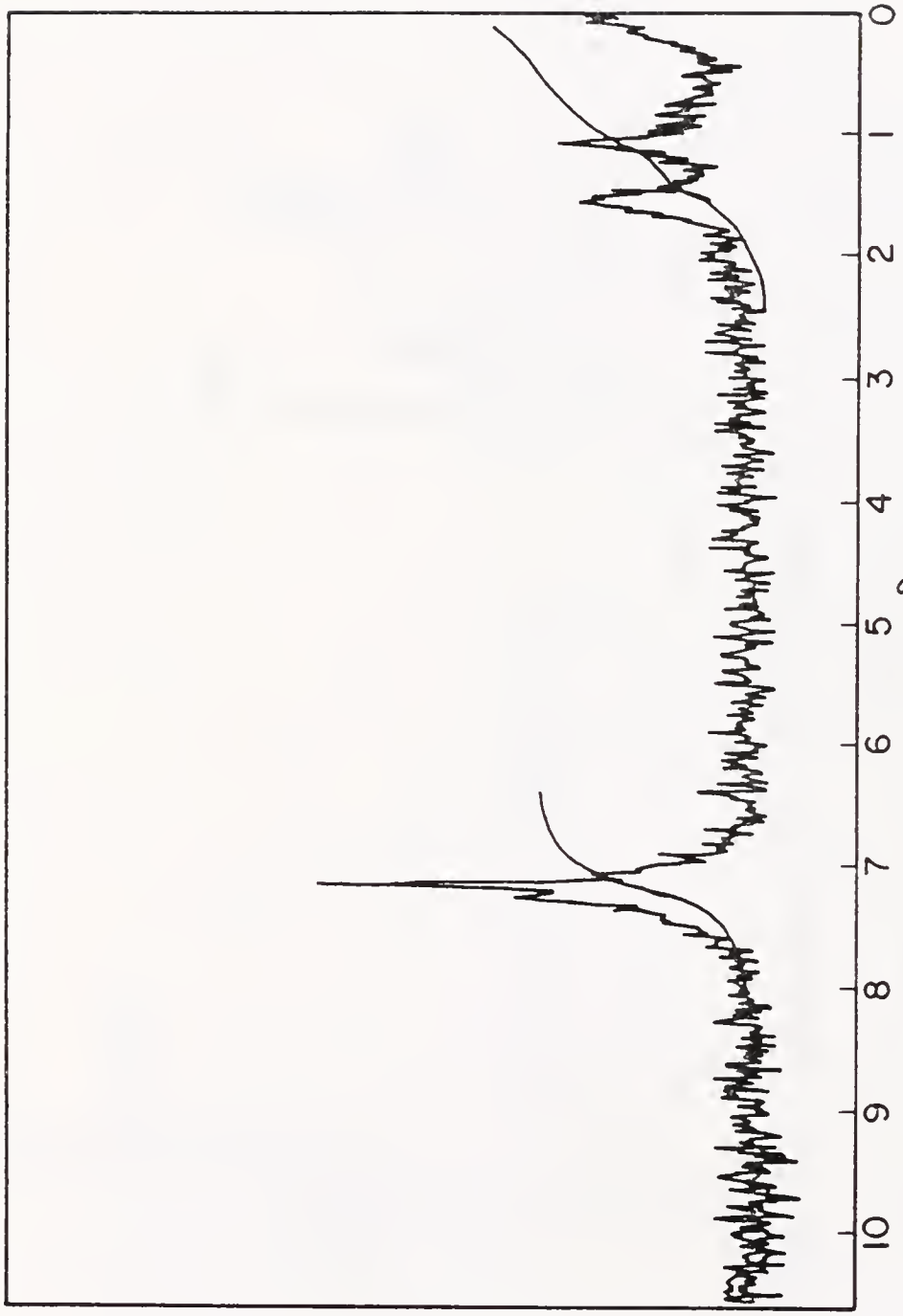

Fig.III-14. Proton NMR Spectrum of J-PSS1/1120 Showing no C-O-Si Crosslinkage

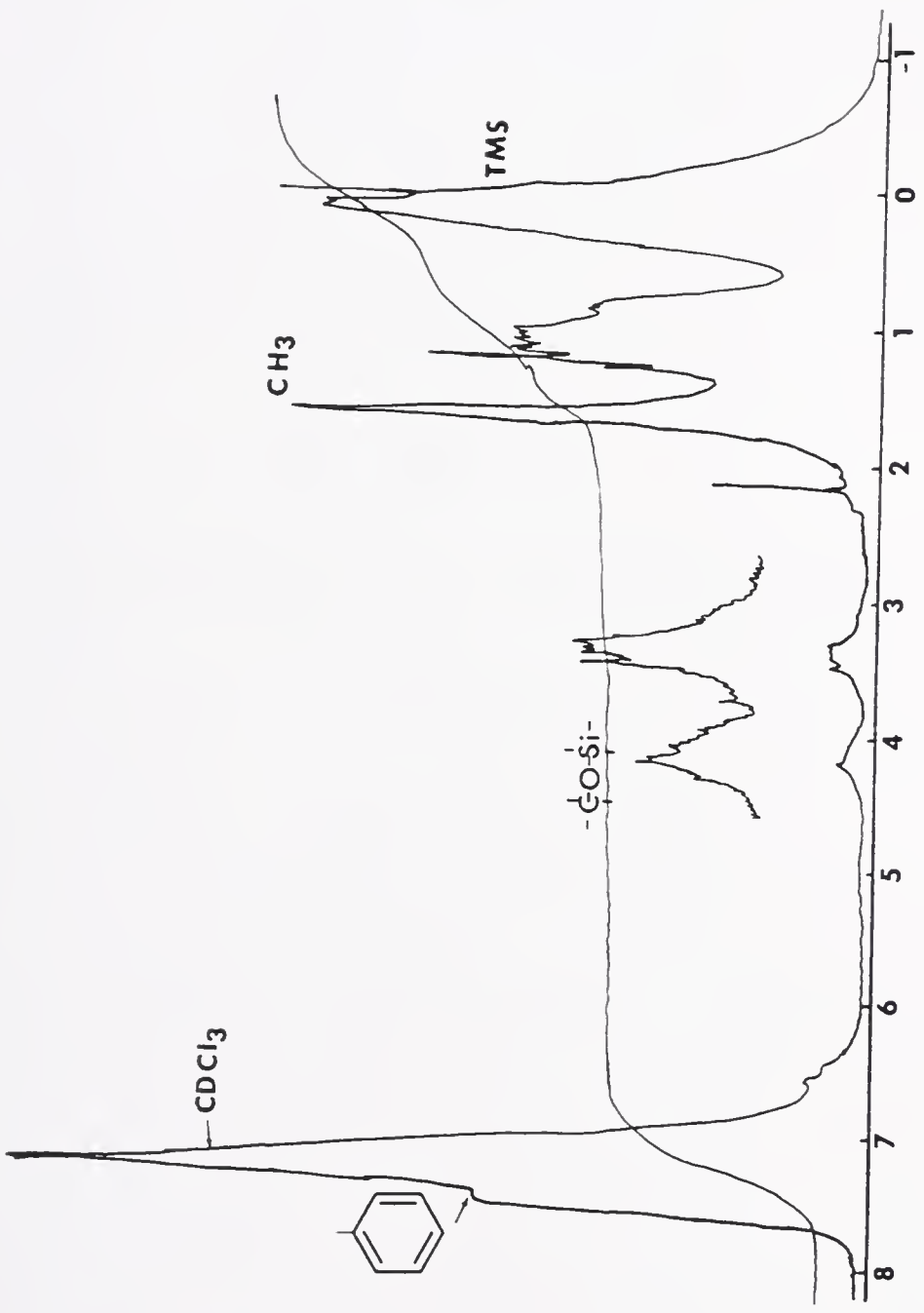

Fig.III-15. Proton NMR Spectrum of PSS-10/104 Showing $-CH_2-O-Si\equiv$ Crosslinkage

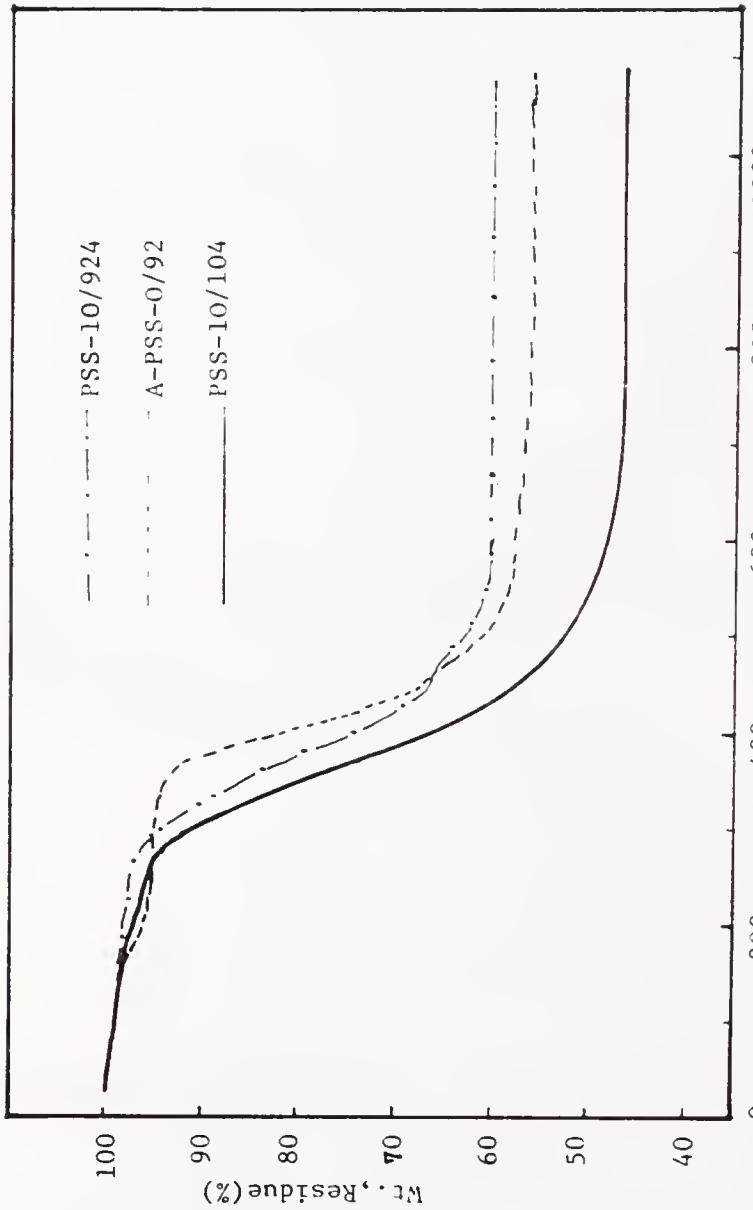

Fig.III-16. TGA Char Yields of SiC/SiO_2 Molecular Composite Powders

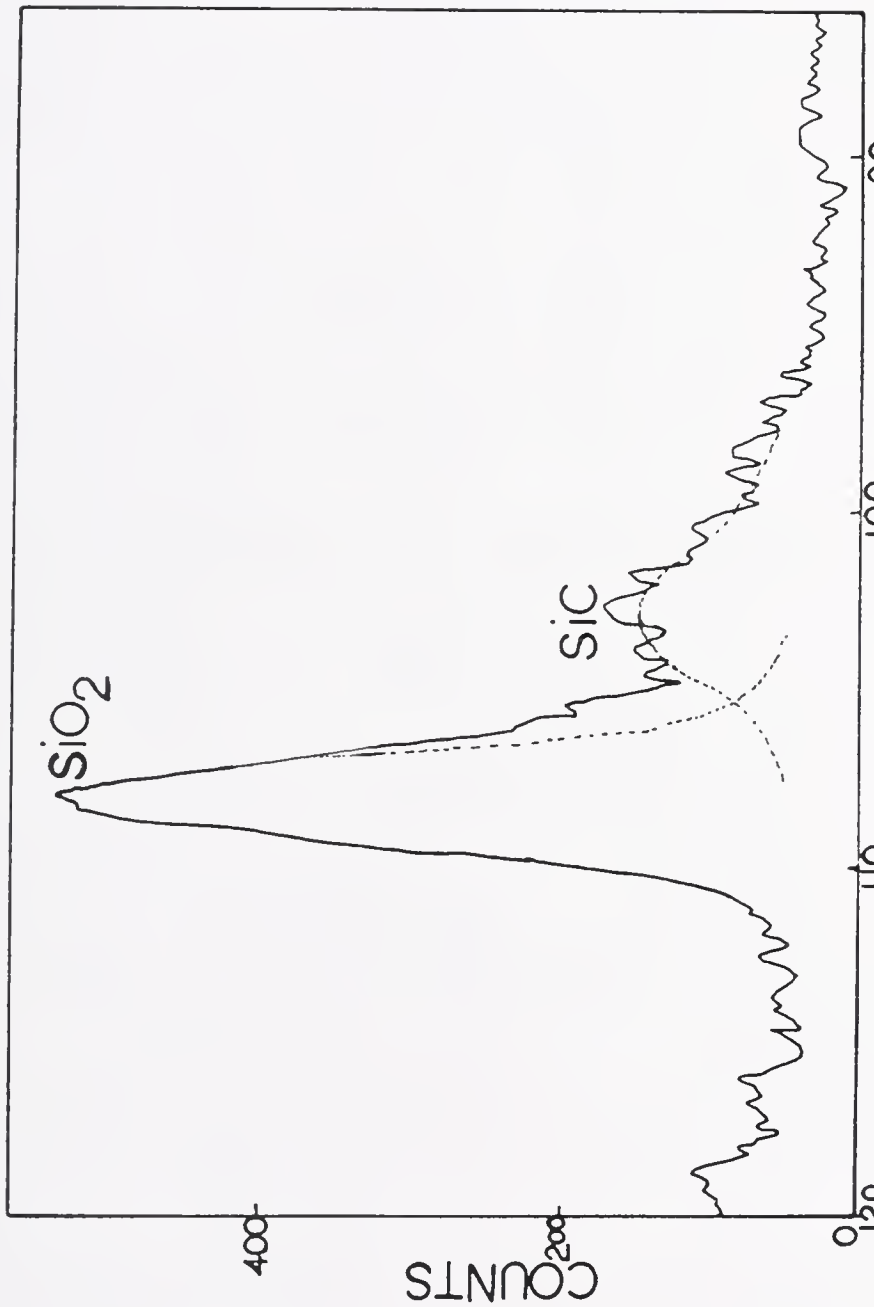

Fig.III-17. XPS Spectrum of SiC/SiO_2 Composite PSS-10/924 Showing Atomic Proportion of Silicon As Oxide and Carbide

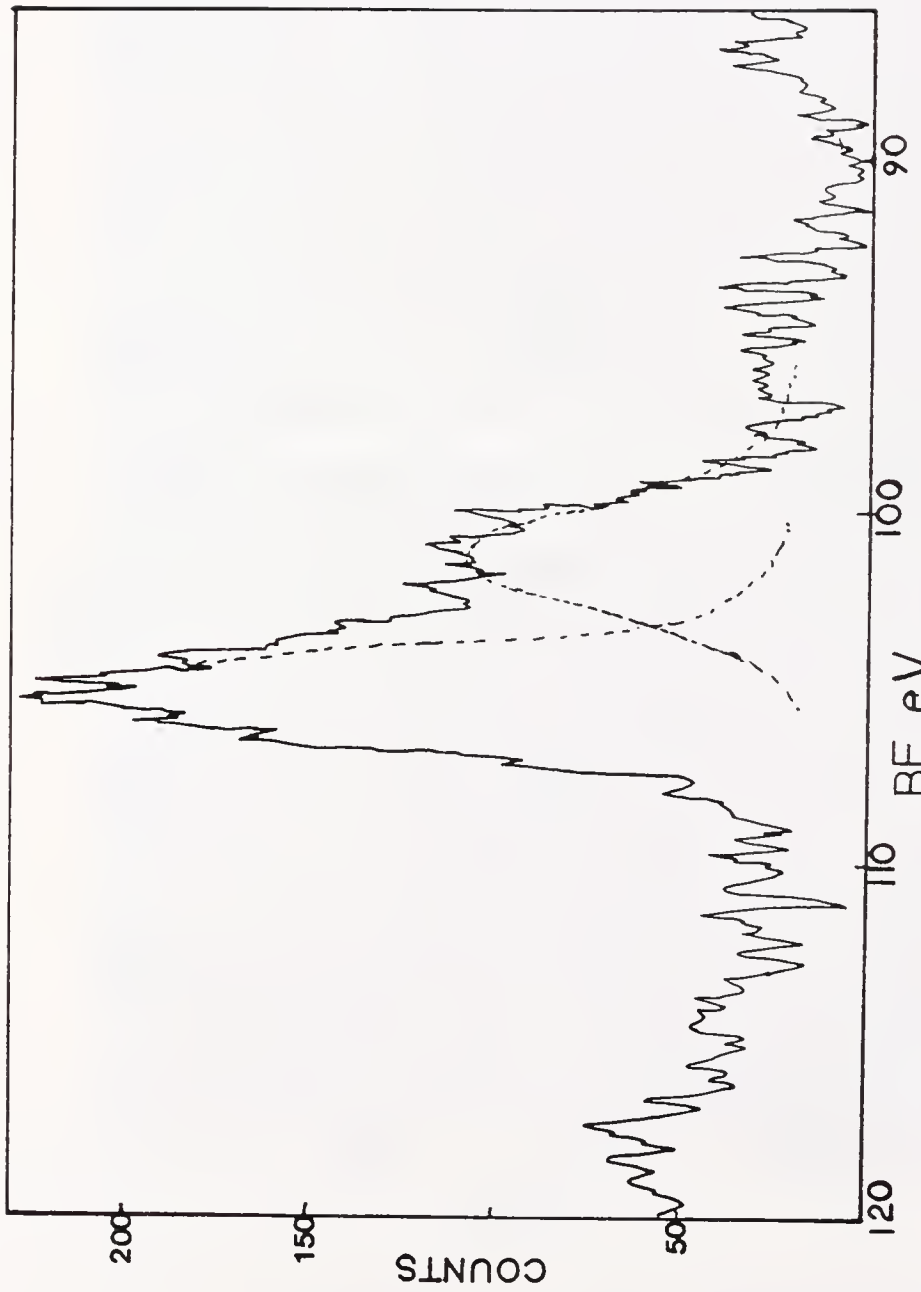

Fig.III-18. XPS Spectrum of SiC/SiO_2 Composite A-PSS-0/92 Showing the Atomic Proportion of Silicons As Oxide and Carbide

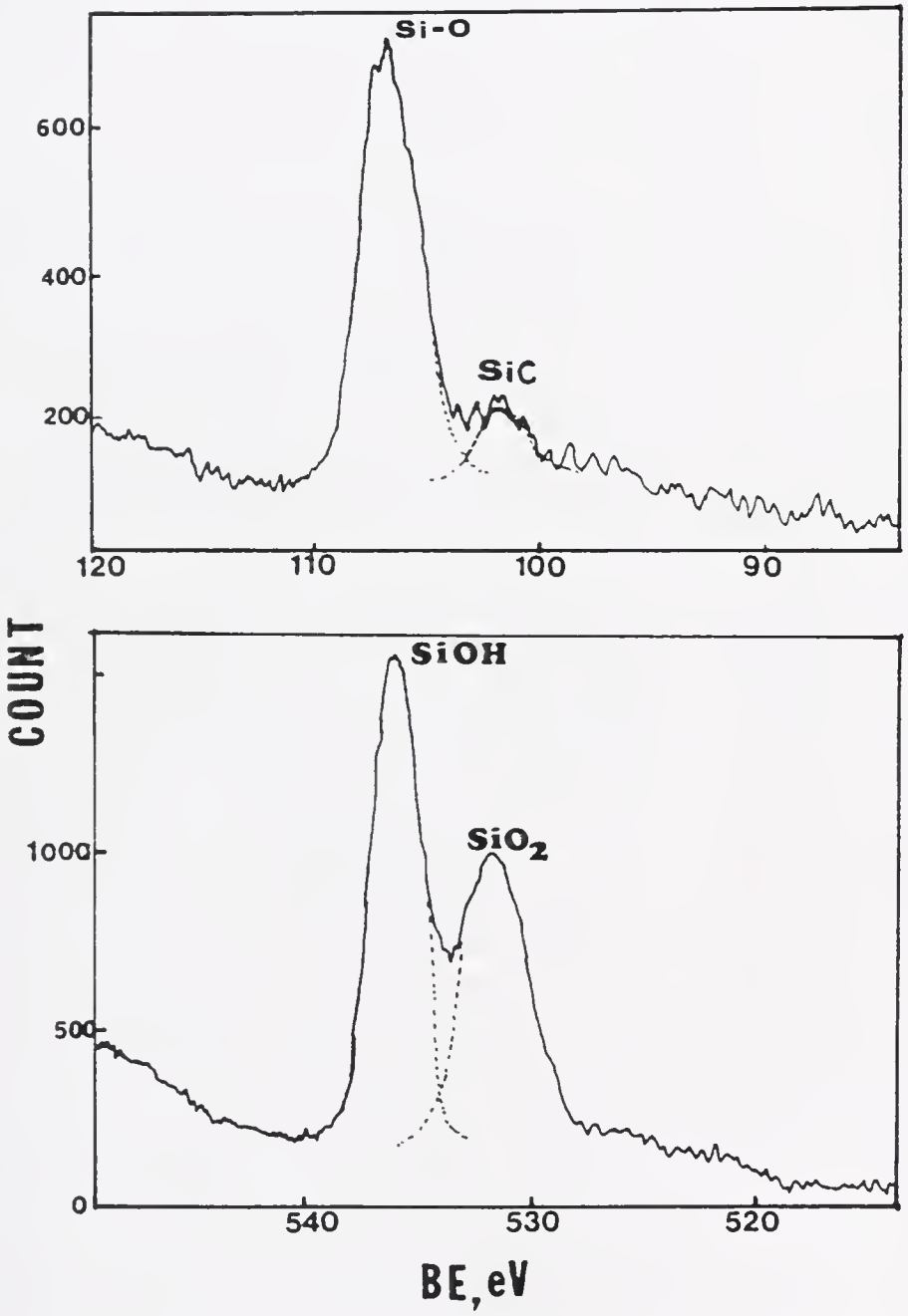

Fig.III-19. XPS Spectra of SiC/SiO_2 Composite ViSP/BuOH Proportions of Silicon and Oxygen As Oxide and Carbide (top), Oxide and Hydroxide on the Surface, Respectively

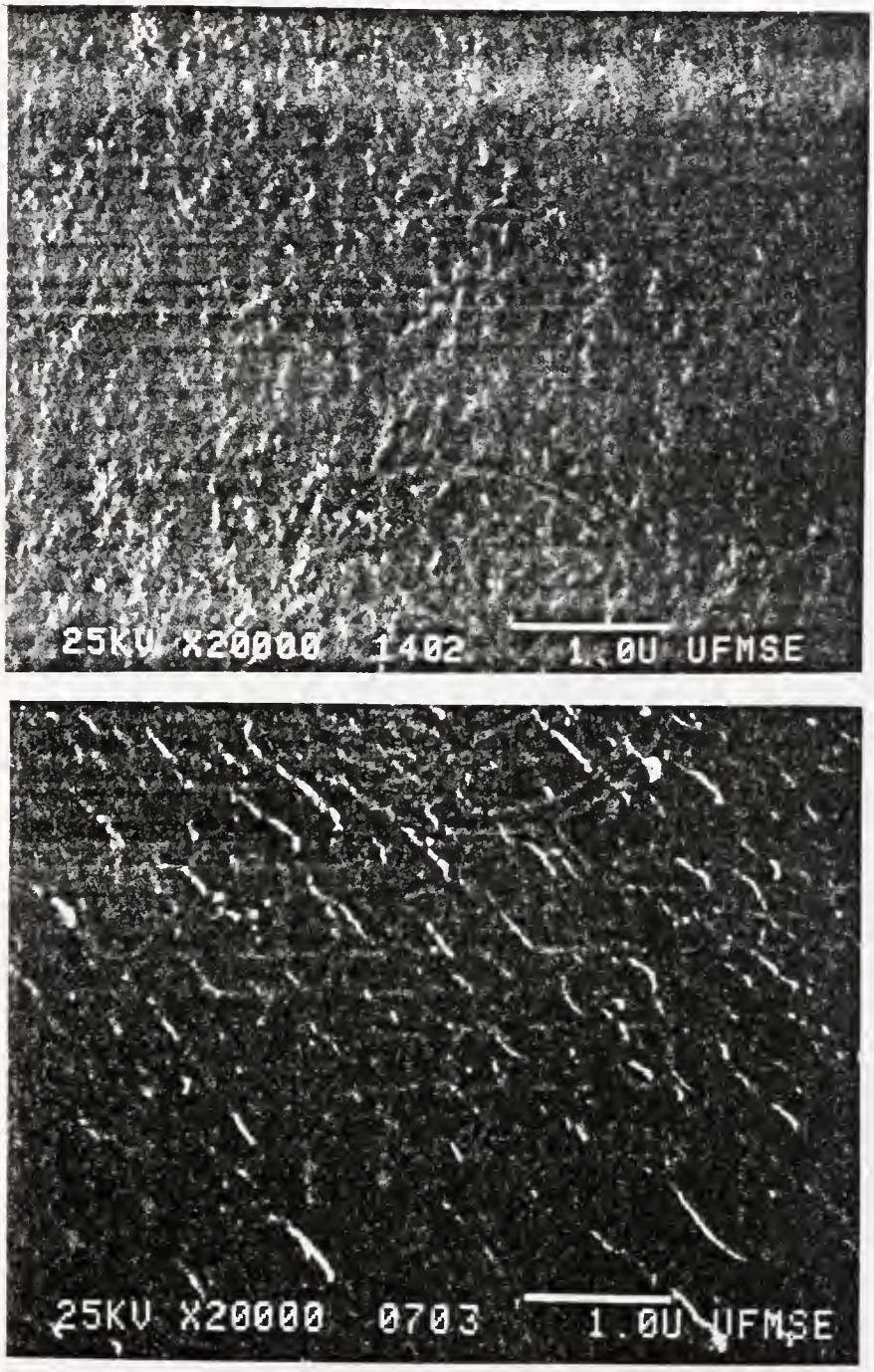

Fig.III-20. SEM Fratographs of Bulk in situ Molecular Composite.
Top: ViSO/SiO_2, Bottom: J-PSS/SiO_2

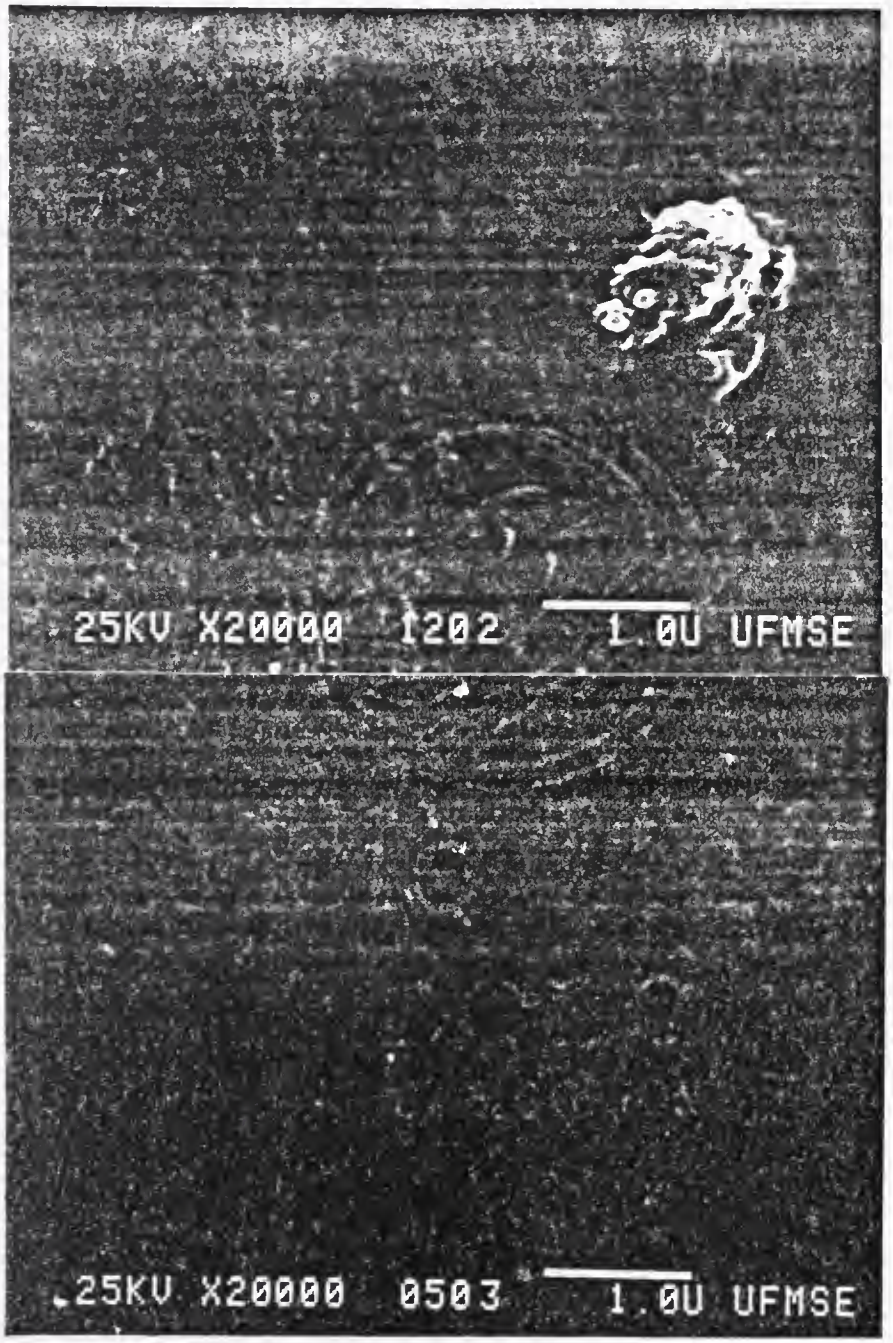

Fig.III-21. Fractured Surfaces of ViSP/SiO_2 Gel, a Bulk SiC/SiO_2 Molecular Composite Before(top) and After Pyrolysis at 830°C

Table III-3. Microhardness of Organosilane Infiltrated SiC/SiO_2 Composites as a Function of Pyrolysis Temperatures

Composites and Control	~~I~~ DPN	520°C	600°C	700°C	800°C	900°C
OA-ViSO		139±1	233±15	239±14	669±173	814±200
OA-gel		146±58	157±1	174±25	210±51	305±103
FA-ViSP		192±66	342±75	351±87	403±46	550±180
FA-gel		129±64		171±24	210±51	291±67

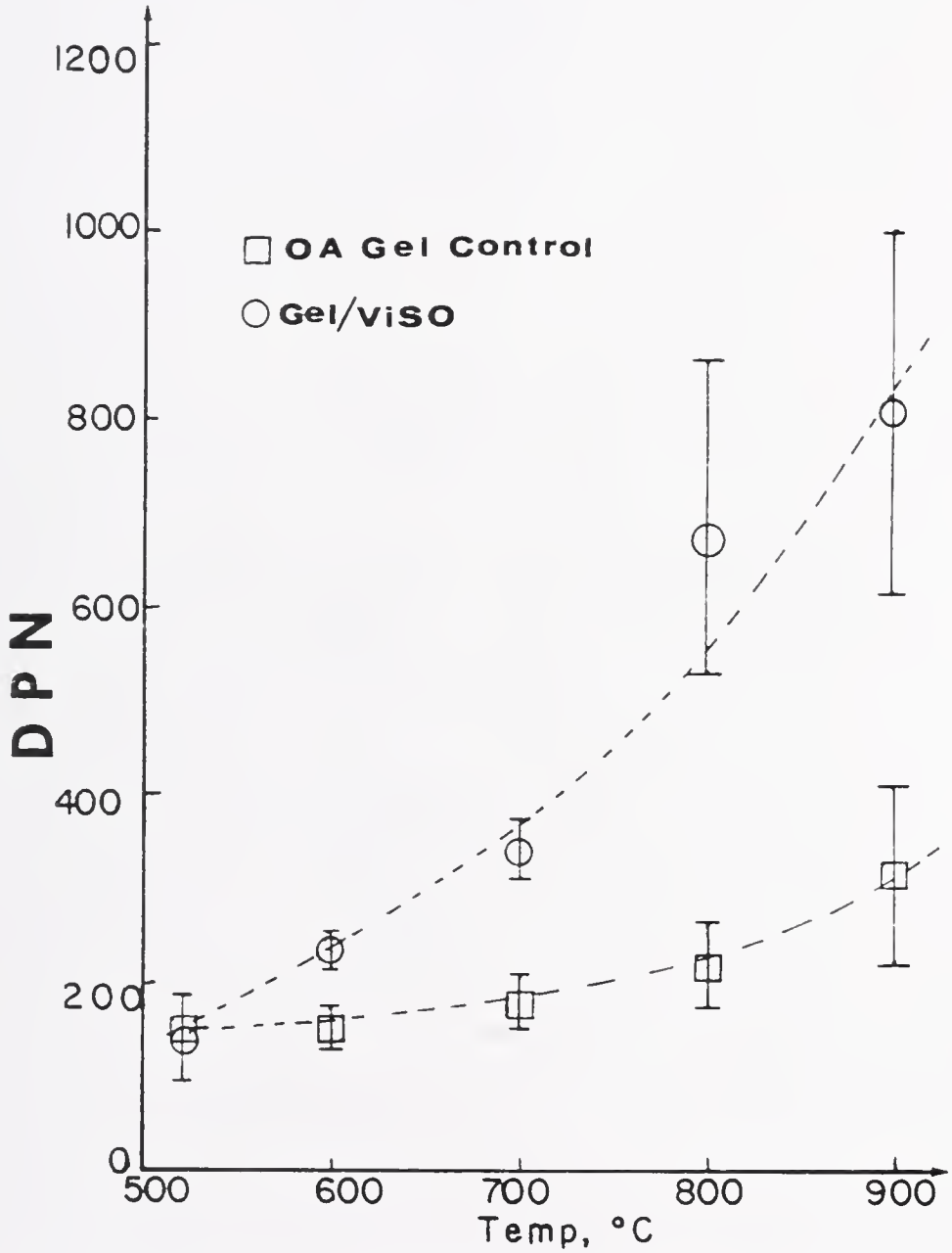

Fig.III-22. DPN As a Fuction of Pyrolysis Temperature for OA Gel and OA Gel Impregnated With ViSO

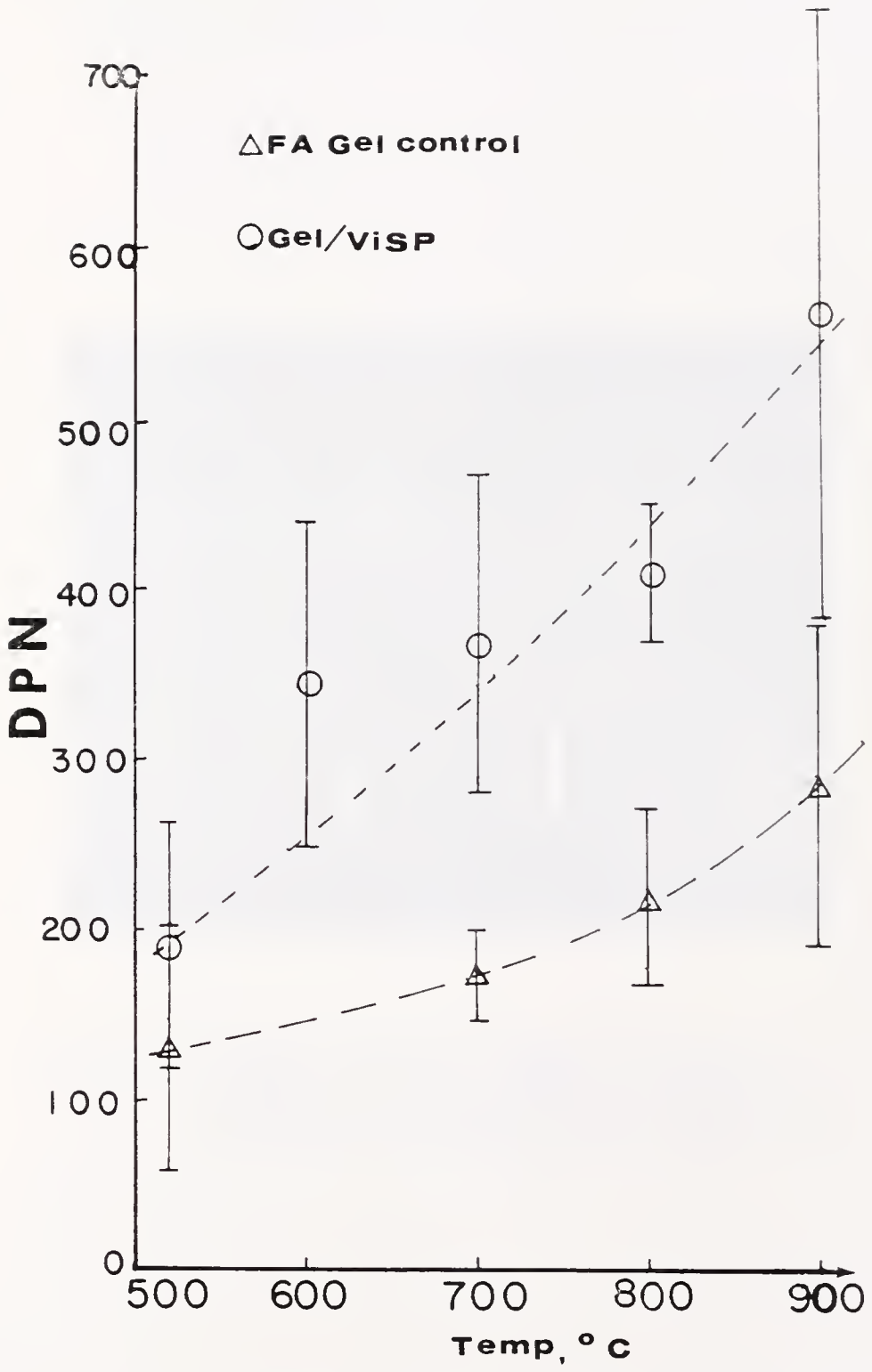

Fig.III-23. DPN As a Fuction of Pyrolysis Temperature for FA Gel and ViSP Impregnated FA Gel Composite

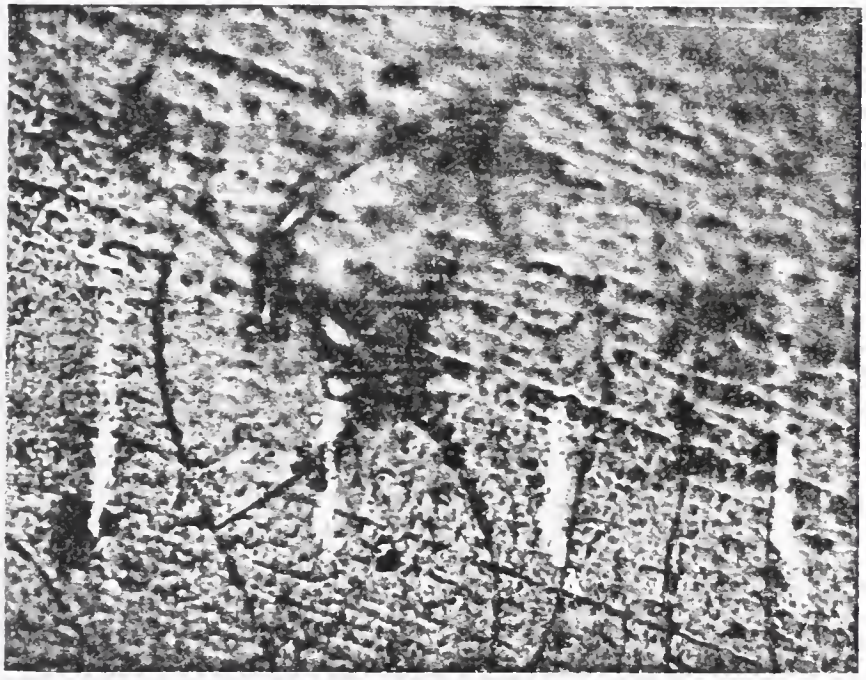

Fig.III-24. Indentation Cracks Formed by Loading of a Diamond Indenter at 1200 g on FA Gel/ViSP Impregnated and Pyrolyzed at 800°C, Mag.:200X Photo Taken After 3 weeks of Indentation

Table III-4. Microhardness and Density of ViSP/BuOH, a Bulk SiC/SiO_2 Composite as a Function of Pyrolysis Temperature.

Temperature (°C)	ρ, g/cc	DPN
600	0.8±0.1	250±50
700	0.95±0.1	350.8±134
800	1.20±0.1	500.0±100
850	1.45±0.1	551±169
900	1.75±0.1	366.3±250

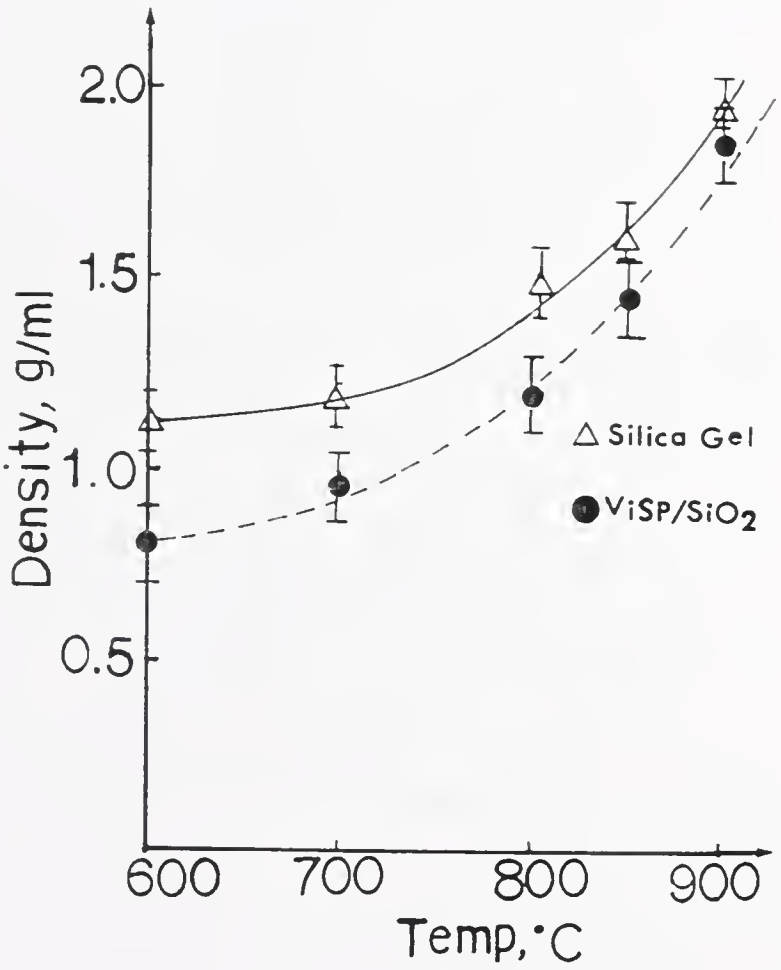

Fig.III-25. Density as a Function of Pyrolysis Temperature for Bulk ViSP SiC/SiO_2 Composite as Compared With Pure Silica Gel Matrix

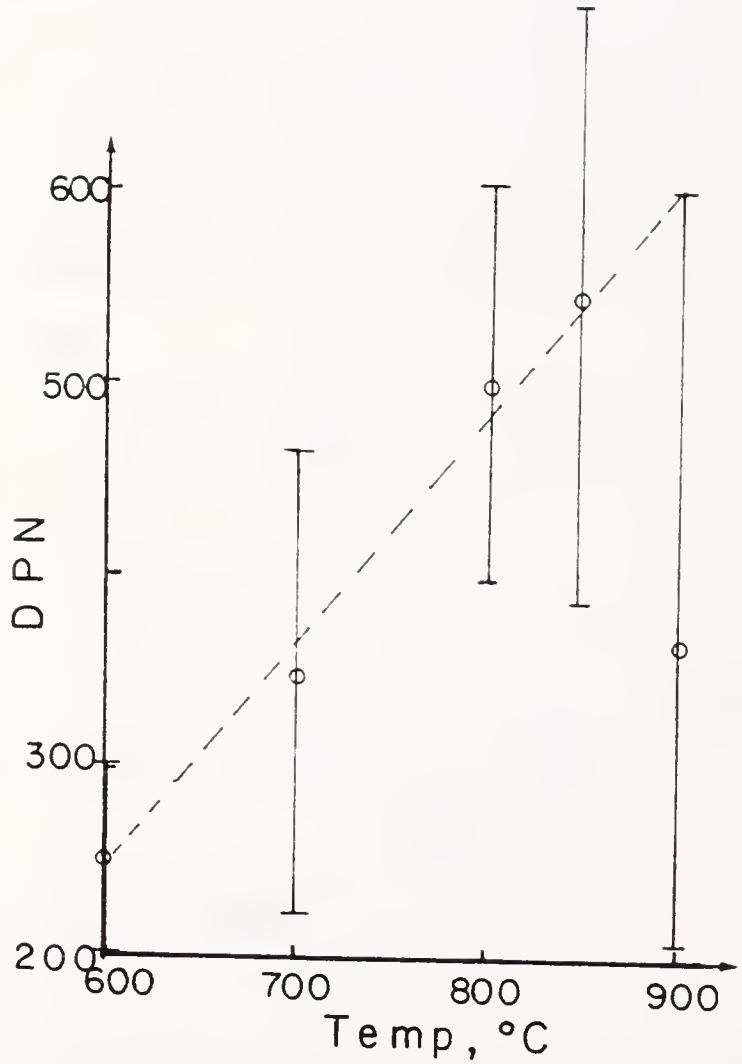

Fig.III-26. DPN as a Function of Pyrolysis Temperature for ViSP/BuOH Composite

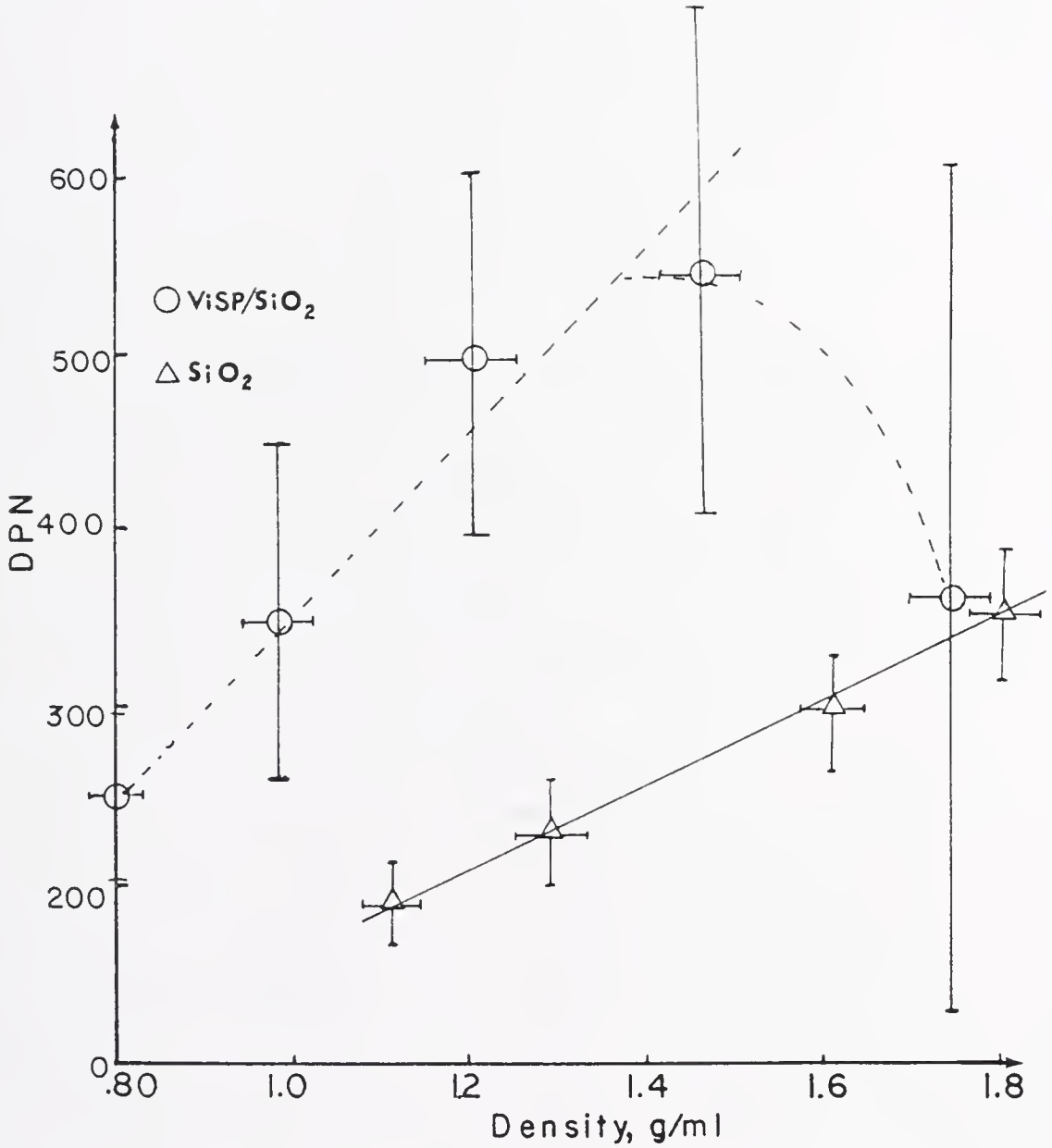

Fig.III-27. Relationship Between DPN and Density of ViSP Bulk SiC/SiO_2 Composite and SiO_2 Gel Matrix

Table III-5. Microhardness, Fracture Toughness (K_{IC}), and K_{IC}/ρ Ratio of SiC/SiO_2 Composites Obtained From Direct Diamond Indentation Cracks.

Sample	ρ, g/cc±0.1	E,[a] GPa	Load, kg	$\bar{a}$, μm	$\bar{c}$, μm	$\bar{H}$, GPa	K_{IC}, MPa·$m^{1/2}$	$\bar{K}_{IC}/\rho$
Fully dense[b] fused silica	2.19	65	1	41.1±5	94.4±25	12.3±3	1.1±0.2	0.46
			0.5	31.1±4	69.2±9	10.1±2	0.96±0.2	
OA gel 500°C	1.18	21	0.5	51±6	86±11	7.8±1	0.67±0.3	0.57
600°C	1.24	23	0.5	44±7	98±10	5.1±1	0.49±0.2	0.40
820°C	1.72	42	0.5	39±4	101±12	7.5±2	0.52±0.3	0.30
FA gel 800°C	1.91	50	1	29±5	74.3±9	20.8±2	1.1±0.5	0.58
			0.5	26±4	50.3±7	10.5±1	1.1±0.4	
ViSO infilt. FA gel, 820°C	1.94	63	1	46±6	70±8	9.3±2	1.97±0.4	1.0
ViSP soaked OA gel, 820°C	1.74	48	1	43±4	69±6	10.6±0.9	1.62±0.4	0.9
ViSO in situ bulk SiC/SiO_2 820°C	1.80	50	1	37±4	71±5	13.6±3	1.45±0.3	0.83
	1.82			33±5	48.4±5	16.9±4	2.3±0.4	1.26

a. Estimated by using $E = E_0 (1-1.9P + 0.9P^2)^{74}$ and the rule of mixture where P is porosity. The bar above a letter denotes mean value.

b. Corning Glass Works, Corning, NY, used as a reference.

a = Diamond point indentation diagonal length

c = Extended crack length

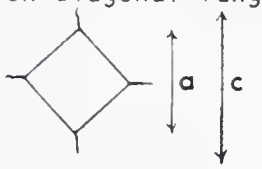

The results of flexural strengths of these composites obtained by using an Instron machine on 3-point bending are given in Table III-6. The detailed testing method will be given in the next chapter.

Hot-stage x-ray powder diffraction patterns for A-PSS-0/927 powder on a Pt substrate are shown in Fig. III-28.

Discussion

It has been demonstrated that incorporating an SiC phase into a pure SiO_2 glass matrix increases the strength of the composite material. However, the art of making large monolithic composites of SiC/SiO_2 via the sol-gel technique is in the successful fabrication of the SiO_2 glass matrix. In this work, it was found that the addition of organosilanes in a TMOS sol makes it more difficult to obtain a large monolithic glass. Despite the strengthening effect by the SiC phase, the increasing difficulty of monolithicity with increasing loading of SiC in the composite appears to be a combination of three factors:

1) the evolved gaseous products from pyrolysis of the organosilane creates flaws and pores (Fig. II-30),
2) the SiC phase strongly hinders viscous flow of the glass matrix, thus the necking is curtailed (Fig. III-25), and

Table III-6. Flexural Strengths of Organic Derived SiC/SiO_2 Composites.

Sample	ρ, g/cc	P, N	σ_{flex}, MPa*	σ_{flex}/ρ
12 hr soaked OA gel in ViSO 820°C	1.26 ± 0.1	31 ± 5	4.4 ± 1.5 (3)	3.5
Dried OA gel 150°C	1.17 ± 0.1	67 ± 6 71 ± 6 62 ± 4	25 ± 3 (3) 17 ± 3 15 ± 3	21
HCl gel 2 hr ViSO soaked 820°C	1.75 ± 0.1	533 ± 12	73 ± 6 (2)	42
HCl gel 820°C	1.76 ± 0.1	408 ± 17	60 ± 8 (2)	34
FA gel soaked in ViSO 10 hrs 800°C	1.34 ± 0.1	62 ± 9	9.2 ± 2 (3)	7
OA gel soaked in ViSP 6 hrs	1.59 ± 0.1	53 ± 8	25 ± 6 (3)	16
OA gel soaked in ViSO/ViSP 7 hrs	1.62 ± 0.1	67 ± 9	6 ± 2 (2)	6
ViSP bulk Molecular composite	0.91 ± 0.1	53 ± 10	5.8 ± 2 (3)	6.4

* The numbers in the parentheses denote the number of specimens tested.

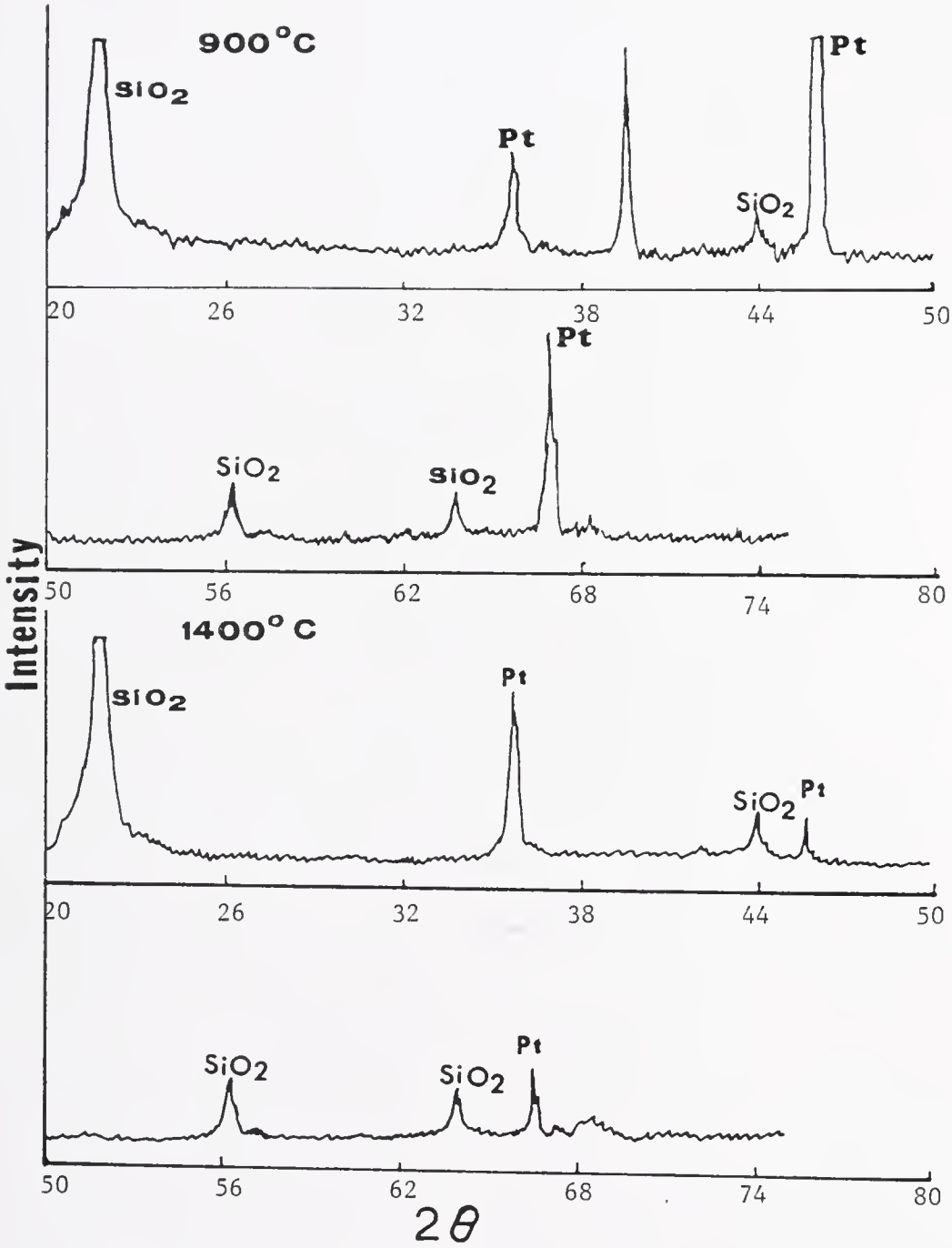

Fig.III-28. Hot-Stage XRD Powder Patterns of A-PSS-0/927 Composite

3) a mismatch of CTE between SiO_2 (0.5×10^{-6} in/in °C) and SiC (4.7×10^{-6} in/in °C)[75] increases residual stress (Fig. III-24).

Although these may all be related, the first factor has been discussed in Chapter 2 and it seems an inevitable phenomenon for this type of organosilane. The second factor was evidenced by densification behavior as a function of temperature (Fig. III-25). Gel derived silica without a SiC phase densified at a faster rate and at lower temperatures. The main reason for the sluggish densification behavior must be in the action of the SiC phase hindering the viscous flow of the glass matrix. However, the effect of atmosphere in densification behavior may have some effect on silica viscous flow, primarily due to water content in the atmosphere.

The third factor that was shown to be harmful to obtaining monoliths could give a positive effect on the strengthening and thermal properties of composites by introducing a compressive stress on the surface.[76]

An additional factor which has been repeatedly observed and mentioned previously is chemical reactions between the SiC precursor OS and the SiO_2 precursor gel during the pyrolysis process in a reducing atmosphere. This is an important phenomenon for fabrication of successful composites. Gels heavily impregnated with OS always came out like crackers: "cracker effect," after the OS/gel composite has been pyrolyzed in nitrogen atmosphere. Although the bodies, many times, generally remained monolithic, a severe spalling and/or pores were generated.

As a result, the flexural strengths and densities were significantly decreased.

The origin of the "cracker effect" may be thought to be from two sources. One is the anticipated outgasing by the decomposition of OS and elimination of any impurities during the pyrolysis. The other source is the actual chemical reactions between the reinforcing phase or the precursor of the reinforcing phase and the matrix phase as shown by Eq. III-2 for an example in the presence of impurities such as residual carbon, silicon, oxygen, etc.

$$2SiO_2(S) + SiC(S) \xrightarrow{\Delta} 3SiO(g) + CO(g) \quad \Delta G = -70Kcal/mol^{77} \qquad (III-2)$$

In this reaction, it can be seen that the glass network is destroyed as a result of the reaction. This reaction is further discussed in the next chapter with respect to oxidation of silicon carbide.

However, as shown in Figs. III-22, III-23, and III-27 and Tables III-3, III-4, and III-6, lightly (~2 hours soaking) impregnated composites exhibited a significant increase in microhardness, σ_{flex}, and K_{IC} with little increase in density.

The determination of K_{IC} by direct measurements of the crack length has not been universally established. The method is valid only for the test specimens which behave normally, i.e. give a well defined radial/median crack system.[73] Some brittle materials, e.g. glass, have shown to give lower K_{IC} values than values obtained by more standard methods, such as single-edged notch beam test.[73] These materials have shown slow crack growth well after the diamond point indenter is removed from the surface of the specimen. Moreover, the method[73] has not yet been proven

as a valid method for composite materials. This is reflected in the relatively large uncertainty in K_{IC} values (Table III-4).

The K_{IC} to ρ ratio of bulk ViSO reinforced SiO_2 gel (~1.3) is nearly as large as or larger than hot pressed 20 v/o SiC/borosilicate glass composites by Gac et al.[78] (K_{IC}/ρ = 1.6), by Samanta and Musikant[79] (K_{IC}/ρ = 1.2), and much larger than sintered chopped SiO_2 fiber/SiO_2 glass composites of Meyer et al.[80] (K_{IC}/ρ = 0.48). The ratio of ~1.4 for ViSO/ SiO_2 gel composites in this work is also superior to hot pressed 42 v/o SiC/Al_2O_3 composites by Cutler et al.[81] (K_{IC}/ρ = 0.80) and comparable with zirconia toughened alumina composite by Lange et al.[82] ($K_{IC}/\rho \approx 1.4$).

The flexural strength of lightly ViSO impregnated HCl catalyzed SiO_2 gel is increased (Table III-6) to 73 MPa from 60 MPa for the blank matrix. This is more than a 20% increase in strength. However, because of the statistical nature of strenyth, the significance of ~20% increase is in question and it needs further work. Optimization of the soaking time in relation to pore size and distribution is suggested for the maximum increase in σ_{flex} in future studies.

In order to improve the monolithicity of the composites, procedures in gel matrix preparation may need to be changed. Zarzycki et al.[83] suggested that larger pore sizes promote monolithicity of gel glasses. Yu et al.[84] supported the suggestion by experimental results. They showed that acid catalyzed gels always produce smaller pore sizes than base catalyzed gels. They successfully densified base catalyzed gels, but not the acid catalyzed ones. This suggests an advantage of the colloidal route to obtain a monolithic glass.

The acid catalyzed gels used in this work produced cracks and/or foaming at temperatures above ~850°C. As shown in Fig. III-3, the mean pore radius is in the range of 15 Å. This is very small for gases and hydroxyl groups to leave the gel structure before pore closure at the surface. In addition, larger pore sizes should increase SiC loading by OS infiltration. However, it is shown that larger loading of the SiC phase is not only unnecessary but also detrimental to the mechanical properties of the composite.

If a successful consolidation of the SiO_2 glass matrix monolithic composite can be obtained all the way up to full density, the hardness and strength of the composite body is expected to be much higher.

A J-PSS/SiO_2 bulk molecular composite, as shown in Fig. III-4 after pyrolyzing at 800°C for two hours, still maintained a low density of 1.32±0.1 g/cc. Heating above 800°C usually caused foaming. At this stage, to prevent foaming, use of a vacuum or a reactive gas atmosphere such as H_2 may be helpful. Composites made this way contain no more than 4 wt% SiC phase in the gel matrix.

An SiO_2 gel film heavily impregnated with a SiC precursor shows strong IR absorption in the range from 2.5 μm to 50 μm wavelength region (Fig. III-5). In the region of 3.8-4.6 μm, a bulk composite with a low level of SiC (~2 w/o) is more IR transmitting than a fully densified fused silica control. Above 5 μm, they both are IR absorbing.

The reflectivities of SiC/SiO_2 bulk composites from J-PSS2/TMOS in the visible range (Fig. III-6) are approximately the same. The curves above 820 nm are extrapolated by a computer and they may not necessarily

be accurate. The clear SiO_2 matrix shows ~2% higher reflectivity than the black SiC/SiO_2 composite. The low reflectivity of the gel matrix is caused by high transmittance and that of the black composite must be caused by strong absorption by the black color.

In the UV-Vis light range, the transmission characteristics of these chemically derived materials all absorb UV strongly and transmit visible light. The curves for the impregnated composite and the bulk SiC dispersed composite are essentially identical (Fig. III-7). The spikes at 720, 400, and 340 nm for the composites must be due to the SiC phase.

The infrared reflectance spectrum of a molecular composite ViSP/FA gel, as shown in Fig. III-8, is almost identical with pure FA gel, except for small absorptions at ~2500 cm^{-1} and ~3700 cm^{-1} for ViSP/FA gel caused by adsorbed CO or CO_2[85] and by adsorbed water, respectively (see also Fig. II-42). The absorption peak at ~800 cm^{-1} is mainly attributed to an SiO_2 tetrahedral response. However, the area under the peak for an SiC/SiO_2 composite is ~20% greater than a pure SiO_2 matrix, as shown in Fig. III-9. The unique absorption band for SiC is also in the region of ~800 cm^{-1}. Hence, the greater peak area for the composite must be due to the SiC phase in the composite.

Figures III-10 and III-11 show a somewhat larger proportion of the SiO_2 phase than the SiC phase in PSS-10/104. This agrees with the intended proportion, assuming a ~30% SiC yield from PSS-10. The proportion of SiC and SiO_2 phases are in the range of 40% SiC and 60% SiO_2 in the composite fired at 1270°C.

Figure III-12 shows the structural changes from J-PSS1 to J-PSS1/1120 by the reaction PSS, TMOS, and DCP. It is similar to the crosslinked PSS in Figs. II-20 and II-21. Proton NMR reveals that A-PSS-0/927 (Fig. III-13) is crosslinked via ≡Si-O-CH_2 by the action of $Si(OR)_4$. However, the NMR spectrum of J-PSS1/1120 does not show a C-O-Si≡ linkage (Fig. III-14). Instead, it appears that crosslinking has occurred via Si-C-C-Si, as shown for PSS in Fig. II-47. An NMR spectrum of PSS-10/104 shows, in Fig. III-15, a low level of H_2C-O-Si and -CH_2-OH. This means that $Si(OR)_4$ not only provides the SiO_2 phase for the composite, but also provides crosslinkages for the silane oligomers. The TGA char yields of these composites are given in Fig. III-16; all show higher yield than silane oligomers without $Si(OR)_4$ and DCP.

An XPS spectrum of PSS-10/924 for Si in Fig. III-17 shows that there is ~20% SiC with respect to Si species in the SiC/SiO_2 powder composite, as intended. The binding energies of peaks all shifted slightly towards the high B. E. side due to a differential charging effect. The B. E. at 102.75 eV should be for SiC and 108.25 eV should be for SiO_2 and/or $Si(OH)_4$. In A-PSS-0/927 (Fig. III-18), SiC is shown to be about one half the SiO_2 phase. In Fig. III-19, the ViSP/BuOH bulk SiC composite shows a small amount of SiC and a large amount of surface water or hydroxyl groups[86] of the composite, as represented by a peak at ~536 eV.

Fractured surfaces of SiC/SiO_2 bulk composites (Figs. III-20 and III-21) show rougher and coarser textures than a fracture surface of SiO_2 gel matrix. There are no differences in surface texture between 80°C dried and 850°C pyrolyzed surfaces of ViSP/BuOH. This is another

indication that the composite is still highly porous. The SEM micrograph suggests that there is a fracture pattern, as shown by wavy lines, in the composites seemingly indicating the direction of the fracture.

Microhardness values of SiC impregnated gel composites are much higher than the gel matrix controls, as shown in Table III-3 and Figs. III-22 and III-23. Unexpectedly, ViSO exhibits a greater hardening effect than ViSP which has the greater char yield. This may be caused by two factors: 1) ViSO infiltrated more because of the smaller size of the molecules, and 2) ViSO infiltrated more easily and stayed inside the pores because of its higher polarity and, hence, had a higher affinity to the polar gel matrix by maintaining greater wettability of the gel surface than the more nonpolar ViSP. As the hardness increased, the diamond indentation crack became more troublesome in measuring the indentation sizes, as shown by greater scattering in the DPN values. An indentation crack for a ViSP/FA gel composite is shown in Fig. III-24.

The strengthening effects of the bulk SiC composite ViSP/BuOH (as indicated by microhardness) are not as large as the infiltrated composites (Fig. III-25 and Table III-4). This must be the result of sluggish densification of the SiO_2 gel matrix in the presence of dispersed SiC. Moreover, the hardness value drops sharply with large scattering after heat treatment above ~800°C, although with little effect on the density (Figs. III-25, III-26, and III-27). This is attributed to the localized foaming of the matrix which begins at ~850°C for this type of gel. This foaming is thought to occur by entrapped gases in the pores.

In hot-stage XRD, an SiC/SiO_2 composite powder showed SiO_2 crystalline phases at 940°C, but no SiC phase at temperatures up to 1400°C.

This SiO_2 phase must come from the oxidation of SiC phase, not from the crystallization of the SiO_2 glass matrix.[87] More data on the oxidation of SiC will be given in the next chapter. The peaks for cristobalite matured slowly with time at 900°C and did not increase further up to 1400°C in a He atmosphere. This suggests that the SiC phase in the composite hinders the crystallization of SiO_2 glass; vice versa may well be true also since no SiC crystalline phase is shown at 1400°C in ~1 hour. These data are shown in Fig. III-28, along with peaks for the platinum substrate. A very intense peak at $2\theta = 39.4°$ (2.28 Å) may be that of tridymite, but it completely disappeared at 1400°C.

Conclusions

Sol-gel derived monolithic silica glasses can be reinforced by impregnating with SiC by way of an organosilane precursor. The reinforcing effect, measured by mircohardness, is nearly three times greater for the SiC infiltrated composite glass after a heat treatment to 900°C than for the matrix under the same condition. Approximately 100% increase in fracture toughness and a ~20% increase in flexural strength is achieved with the silane impregnation.

Incorporating a SiC phase on a bulk scale can be achieved by molecularly dispersing the SiC from an organosilane precursor in sol-gel derived silica. For monolithicity on a large scale, only 2-4 w/o SiC phase by way of an organosilane is allowed. However, it would be possible to increase the SiC loading by using a high vapor pressure solvent in a high temperature mold with an effective sealing capability. This

in situ bulk molecular composite gives a reinforcing effect as measured by an increase in microhardness values. The presumed transformation of the microstructure and physical properties of the SiC/SiO_2 composite as a function of temperature is shown schematically in Fig. III-29.

An obvious problem in all of these composites is in the densification procedure. Establishing improvements in the sol-gel processing of the silica glass matrix is necessary before high performance monolithic composites can be made routinely.

The experimentally observed "cracker effect" needs to be investigated further to improve composite properties and the fabrication procedure.

A SiC/SiO_2 molecular composite powder with varying amounts of SiC phase can be made by mixing an SiC precursor, e.g. an organosilane oligomer, and an SiO_2 precursor. The SiO_2 precursor $Si(OR)_4$ not only provides the SiO_2 phase in the composite, but also a crosslinking action as well. Crystallization of the SiC phase as well as the SiO_2 phase is suppressed in the composites.

Although the objectives of developing a procedure and an understanding of the process to produce SiC/SiO_2 molecular composites have been achieved, more work to improve properties is needed for actual applications.

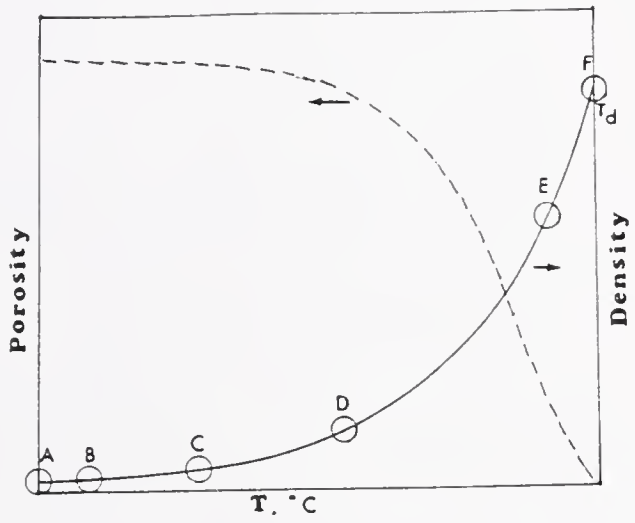

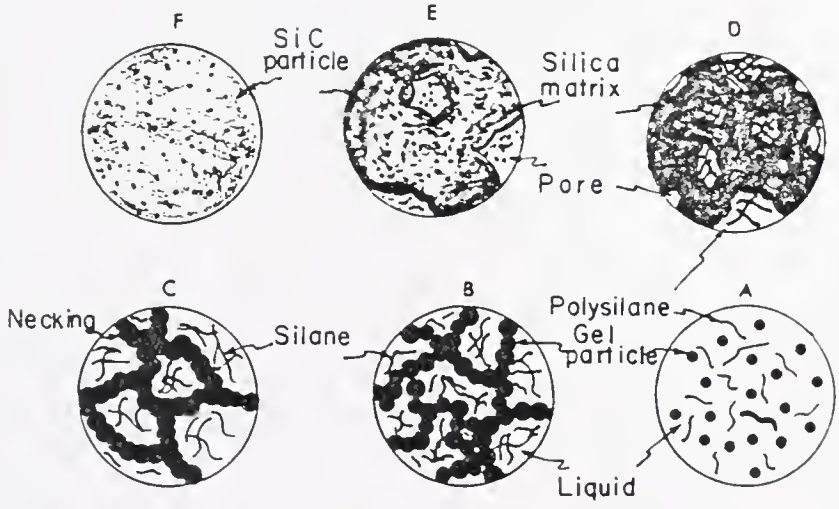

Fig. III-29. Conceptual Microstructure Transformation and Evolution of Physical Properties of Polysilane Dispersed Sol-Gel Silica Matrix

CHAPTER IV
SILICON CARBIDE/SILICA COMPOSITES FROM COMMERCIAL SILICON CARBIDE AND SILICON TETRALKOXIDE

Introduction

A keen interest in high performance materials in recent years has led to more attention to silicon carbide materials (SiC), as presented in the previous chapters. However, the excellent mechanical properties and chemical inertness of SiC have not been fully utilized because of difficulties in forming and sintering large complex shapes.

Incorporating SiC in a matrix which has desired properties and can easily be formed into desired shapes and sizes may be an answer to the problems of forming and sintering SiC. Fiber reinforced composites, particularly those incorporating SiC as reinforcement are being increasingly utilized for their excellent specific properties, i.e. for high strength to weight and rigidity to weight ratios.

The reinforcement of brittle materials with high strength fibers can yield composites of very high toughness. This was first demonstrated using carbon fibers in glass and glass-ceramics.[88-90] More recently the availability of continuous SiC fiber has led to tougher glass and glass-ceramic composites[91-94] which are more resistant to high temperature oxidation than the carbon fiber composites.

Despite its remarkable mechanical properties and chemical stability in ambient conditions, gradual oxidation at high temperature limits the

wider applications of SiC as a truly high performance/high temperature material.

There are several mechanisms known for the oxidation of SiC in the temperature range of 1000°-1500°C.[95-101] At low oxygen partial pressure (P_{O_2}), < ~3 x 10^{-4} atm at 1400°C, an "active" oxidation occurs due to the formation of gaseous products as shown by the Eqs. IV-1 and IV-2 below.[84]

$$SiC(S) + O_2(g) \rightleftarrows SiO(g) + CO(g) \qquad (IV\text{-}1)$$

$$SiC(S) + 3/2O_2(g) \rightleftarrows SiO(g) + CO_2(g) \qquad (IV\text{-}2)$$

At high P_{O_2}, "passive" oxidation due to a protective film of SiO_2 is operative according to the reaction Eqs. IV-3 and IV-4.[100]

$$2\ SiC(S) + 3O_2(g) \rightleftarrows 2SiO_2(S) + 2CO(g) \qquad (IV\text{-}3)$$

$$SiC(S) + 2O_2(g) \rightleftarrows SiO_2(S) + CO_2(g) \qquad (IV\text{-}4)$$

At any case, a gaseous product or products are formed.

If the latter mechanism of passive SiO_2 film formation is applicable for SiC oxidation, an intentional coating of the surface of SiC material with SiO_2 glass should help to prevent or passivate the further oxidation of SiC. Moreover, the SiO_2 glass matrix may be used to improve fabricability of SiC by viscous deformation at much lower temperatures. Thus the incorporation of SiO_2 glass into a SiC skeletal structure or vice versa by forming a composite has three potential advantages, 1) improving the fabricability of SiC, 2) reinforcing the matrix, and 3) minimizing the oxidation of SiC.

In spite of these obvious potential advantages, there have been only a few studies to investigate how a SiO_2 matrix can affect the oxidation kinetics of a SiC/SiO_2 composite at high temperatures.

The forming method used by the previous investigators[75-78] in making SiC/SiO_2 composites was the conventional hot pressing technique which has great limitations on sizes, shapes and complexities of the composite bodies. It is hypothesized that these limitations may be overcome by way of sol-gel processing. As discussed in the previous chapters, one of advantages of the sol-gel method is in the simplicity and ease of forming a green body. By casting the sol into inexpensive or disposable plastic molds followed by aging in an oven, a monolithic green body can be produced in almost any shape and size. The previous chapters describe methods for preparing a very low volume fraction of SiC in a SiO_2 matrix to form composites. In this chapter, however, a process is decribed to achieve a much greater SiC loading in the SiO_2 matrix derived from sol-gel technique and commercially available SiC fibers and whiskers.

A lengthy review on ceramic-matrix composites was reported by Donald and McMillan.[69] Factors in designing and making fiber-ceramic composites were given by Bialoskorski and Konsztowicz.[102] The factors include lengths of fibers, their contents, and types of fibers used for reinforcement. Wang and Sutula[103] showed that the detrimental effect due to the difference in thermal expansion between fiber and metal matrix in metal-matrix composites is minimized for short fibers. Lannutti and Clark[104-106] showed a potential usefulness of sol-gel derived alumina in SiC/Al_2O_3 composites using whiskers, mats, weaves, and short fibers of SiC. Rice et al.[107] showed the effect of interfacial bond strength between the fiber and the matrix on mechanical properties.

Some of important factors affecting mechanical properties of fiber reinforced ceramic composites are listed below.

1. Volume Fractions of Components
2. Porosity of the Composite

   Lower volume fraction of continuous phase often increases porosity
3. Ultimate Strength of Fiber and Matrix
4. Interfacial Bonding

   High bond strength between fiber and matrix

   Low bond strength between fiber and matrix
5. Thermal Expansion Coefficient Match

   Comparability of a thermal property at high temperature
6. Flaws, Defects, Impurities, etc.

The objectives of the work in this chapter are 1) developing a procedure to produce SiC/SiO_2 composites using the sol-gel process, and 2) understanding the variables affecting mechanical properties.

Experimental

Composites of β-SiC and α-SiC in a pure silica gel matrix were prepared using Nicalon®* and Silar™** as the reinforcing filler phase.

Chopped fibers of Nicalon were pretreated to remove a polyvinyl acetate coating by successive washing in ethyl acetate, benzene, and

---

* β-SiC by Nippon Carbon Co., distributed through Dow Corning, Midland, MI.

**α-SiC by ARCO, Greer, SC.

acetone followed by firing at 400°C in air for two hours. The cleaned Nicalon was further chopped in a polypropylene container with alumina balls on a vibratory mill for one hour. In addition, continous fibers and weaves of Nicalon were cut into the sizes of molds and the polymer coating was removed by burning it on a propane burner. Silar™ was used in its as-received form or after heating in air at 800°C for one hour. Scanning electron micrographs of Silar™ and the chopped Nicalon® are shown in Fig. IV-1.

Characteristics of the SiC used are listed in Table IV-1.

Silica sol was prepared by hydrolyzing tetraethyoxysilane (TEOS) with HCl in ethanol as the solvent in the mole ratio of 1:4:0.5 for TEOS:water:alcohol. Ten grams of SiC was mixed with 75 ml of the silica sol containing 1-5 ml of glycerol and/or 1-5 ml of formamide as drying control chemical additives (DCCA's) for 1-30 min followed by ultrasonication before casting in polystyrene molds of various shapes and sizes. The various configurations of the composites made in this manner are shown in Figs. IV-2 and IV-3.

The SiC/SiO_2 sol slurries, after being tightly sealed, were aged in an oven at 40-80°C for ~10 hours before slowly drying in air for 5 hours at 90°C. The dried green composite bodies were impregnated with SiO_2 sol up to four impregnation-drying cycles followed by a vacuum impregnation.

Cylindrical composite bodies for oxidation experiments were cut into thin wafers using a diamond rotating blade. The wafers were dipped into the silica sol twice after each drying in oven. The composite

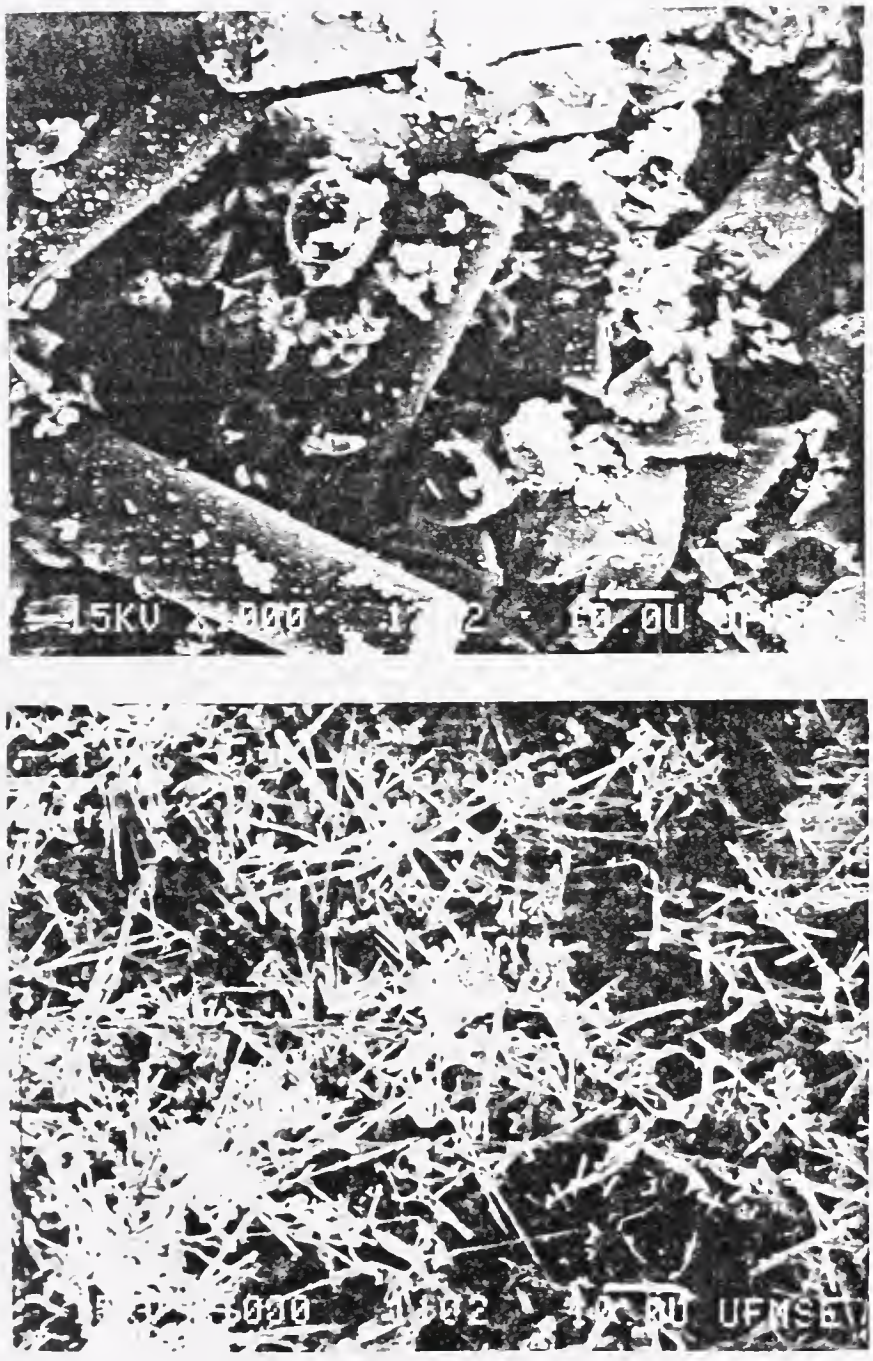

Fig.IV-1. SEM Micrographs of Chopped Nicalon® Fiber (top) and Silar™ Whisker (bottom)

Table IV-1. Properties of SiC Used in SiC/SiO_2 Composites, Data Provided by the Manufacturers

	NICALON®	SILAR SC9™
Tensile Strength - MPa	2000-2520	6890
Tensile Modulus - GPa	180-200	689
Elongation - %	1.5-2.0	--
Density - g/cc	2.55	3.17
Filament Diameter - μm	13-15	0.6
Length - μm	Infinite	10-80
Cross Section	Round	Hexagonal
Type of SiC	Beta	Alpha
Maximum Temperature	1200°C	1760°C
Form	Chopped or Continuous Fiber	Whisker Single Crystalline
Surface Area - m^2/g	--	3
Impurities - w/o	~20 Oxide ~15 Free Graphite	Trace of Metals and < 3% Oxide

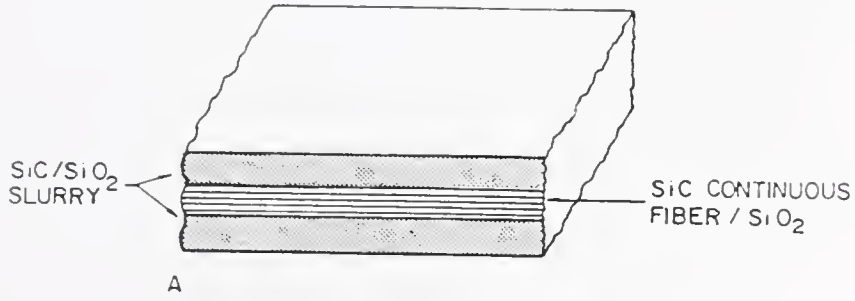

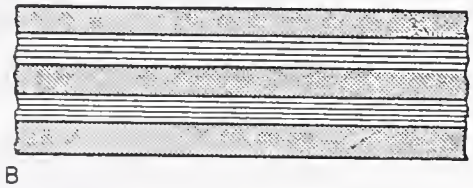

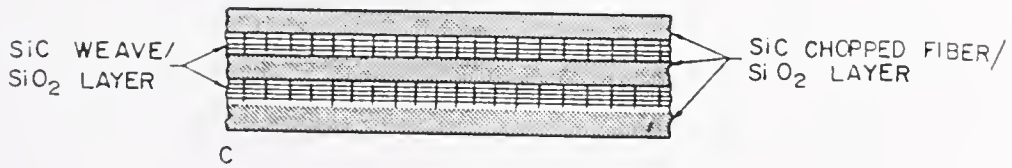

Fig.IV-2. Some of Layouts Used in Fabrication of Nicalon®/SiO_2 Gel Matrix Composite

Fig.IV-3. Cast Nicalon® /SiO_2 Gel and Silar™/SiO_2 Gel Composites of Various Shapes and Sizes.

wafers were exposed to 1100°C in a box furnace with dry static air and sequential oxidation of the wafers were carried out. The samples were heated to 1100°C beginning from room temperature each time at a rate of ~200°C/hr.

The wafers contained ~55% SiC, ~25% SiO_2, ~15% open pores, and ~5% closed pores by volume, on the average. The open porosity was measured by mercury porosimetry and the closed pores estimated by the theoretical density and a subtraction method. Excellent dimensional stability of the composite sample wafers was maintained. There was no warpage and the shrinkage was < 5 v/o. The mean density was 1.67 g/cm^3 which is ~70% of the theoretical density of the composite wafers. The density change was ± 0.2 g/cc during the oxidation.

After each oxidation exposure of the sample, FT-IR spectra were taken by using a Nicolet MX-1 FT-IR spectrophotometer in diffuse reflectance mode. Thermogravimetric analysis in P_{O_2} = 1 atm. was carried out in continuous flowing dry O_2 at 1000°C using a DuPont TGA model 1090.

Some of composites were made using ~ one-third the sol used in the cast composite above followed by cold pressing in a steel die (Carver Laboratory Press) at ~10,000 lbs load for 5 min at 25-80°C followed by oven drying and a vacuum impregnation of SiO_2 sol. The steel die was premachined to form notched sample bars for fracture toughness as shown in Fig. IV-4 as well as unnotched bars for a flexural strength test. Three point flexural strengths were determined by using an Instron Testing machine and the compressive modulus was measured with an MTS machine. A three-point instead of four-point test was used because of the specimen sizes. Microhardness was measured with a Kentron Tester using

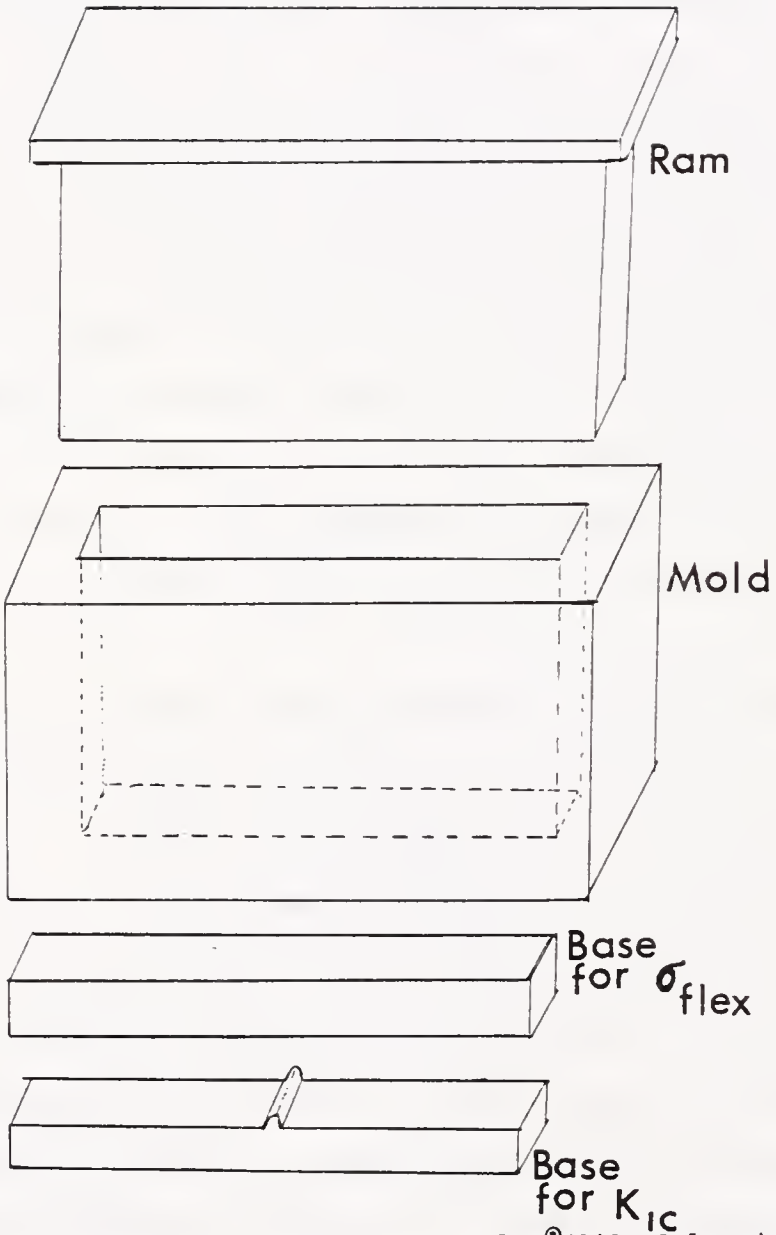

Fig.IV-4. Steel Mold Used to Cold Press Nicalon®/SiO_2 Gel and Silar™/SiO_2 Gel Composite Specimen for σ_{flex} and K_{IC}

1-2 kg loads. Porosity was measured using mercury porosimetry and an Autosorb-6. The composite bodies were measured by mercury volume displacement after each heat treatment. Measurements of fracture toughness (K_{IC}) were obtained by using the conventional 3-point bend tests on notched beams same way as for the 3-point flexural strengths. The indentation method[65] described in Chapter III was also used to determine K_{IC} and compared with the notched beam 3-point bending test.

A test for thermal shock resistance was carried out by heating cold pressed composite bar samples to 800°C in N_2 and quenching them in a silicone oil bath followed by flexural strength measurements. Effect of oxidation on strength of the composites was examined by heating the specimen in air at 900°C for four hours followed by flexural strength measurements.

Transmission electron microscopy (TEM) of Nicalon® and Silar™ composites was used to examine the interfacial region between the carbide and the oxide. To make the TEM specimen, thin disk composites were formed and cut into ~3 mm diameter disks, then reduced down to ~1 mm thickness by an ultrasonic saw. The disks were further polished down to ~150 μm with successive Carborundum polishing steps. The ~150 μm thick disks were dimpled by a VCR dimpler.* At this stage, the middle portion of the samples was ~30-50 μm. Further thinning until a perforation in the middle was obtained by using an Ar ion beam of 100 μA current and 6 KV potential. It typically took ~15-20 hours for the ion milling. Transmission electron micrographs were taken using a JEOL, JEM-200CX

* VCR Group, San Francisco, CA.

Analytical Electron Microscope with a 20 nm beam size and ~100 sec counting times. Thermomechanical analysis (TMA) and differential scanning calorimetry (DSC) analyses were obtained with a DuPont 1090 Thermal Analyzer.

The effect of OS impregnation into the porous NC and SC was examined by soaking the dried specimens into benzene or THF solution (~2 g OS/10 ml solvent) for 2-5 hours followed by pyrolysis at 900°C for 2-4 hours in N_2 and σ_{flex} measurements with an Instron Testing machine and K_{IC} measurements with a Leco Microhardness Tester.

Results

The SEM micrographs of Nicalon® and Silar™ in Fig. IV-1 show a ~10 μm diameter for Nicalon®, and ~1 μm for Silar™, and a mean length of 30 μm for both types of fibers. This gives $R \approx 3$ and $R \approx 30$ for Nicalon® and Silar™, respectively.

Differential scanning calorimetry of the as-received Nicalon® is shown in Fig. IV-5. The exothermic peak at ~320°C at the first heating in air is a result of the oxidation of the polyvinyl acetate coating on the fiber used for sizing. The peak for oxidation of the coating is absent in the second heating. The TGA in Fig. IV-6 agrees well with the DSC. A significant weight gain by the oxidation of SiC Nicalon® at temperatures above ~750°C is shown in Fig. IV-6. Thermomechanical analyses (TMA) of a Nicalon composite (NC) and a Silar composite (SC) after various heat treatments are shown in Figs. IV-7 and IV-8. Negative expansions caused by sintering are shown for all cases.

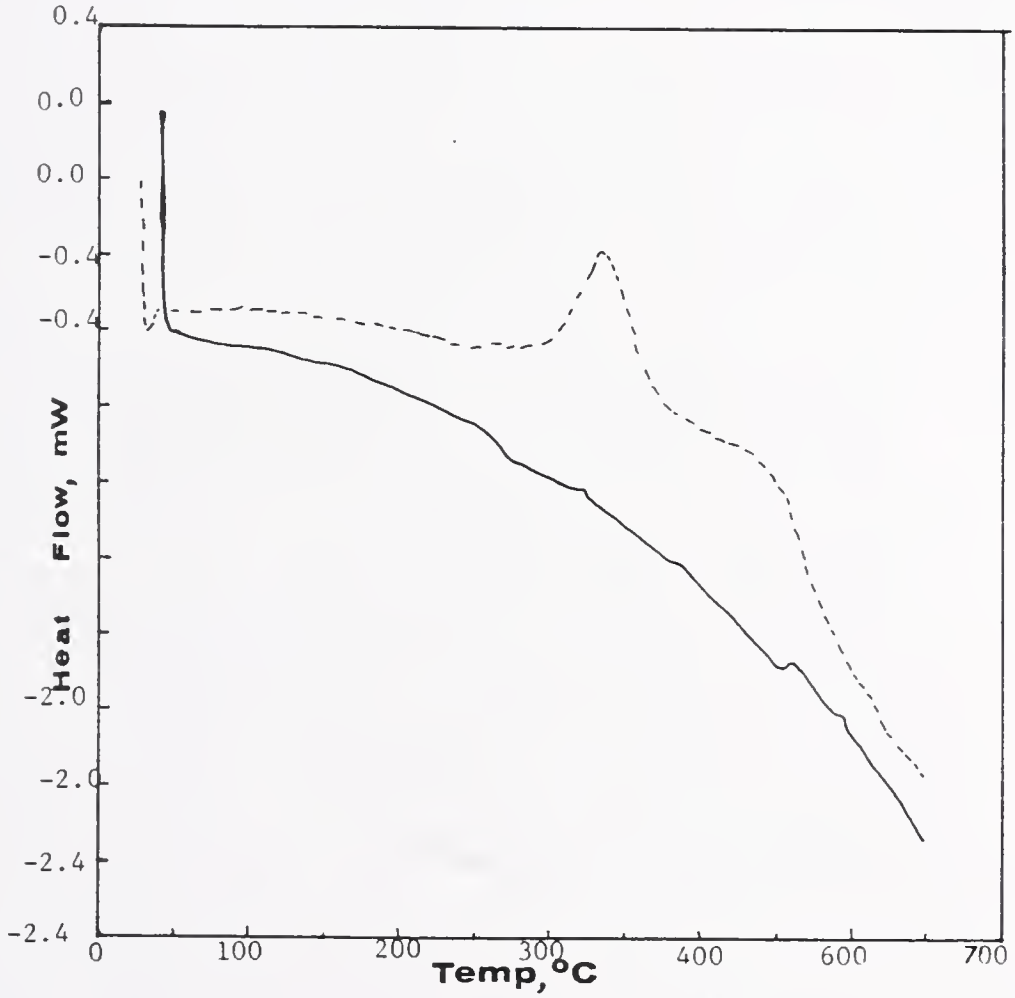

Fig.IV-5. DSC Thermograms of as-received Nicalon® Heating in Air Twice, The First Heating ----- and second ——— Showing the Removal of the Sizing Polyvinylacetate at ~320°C

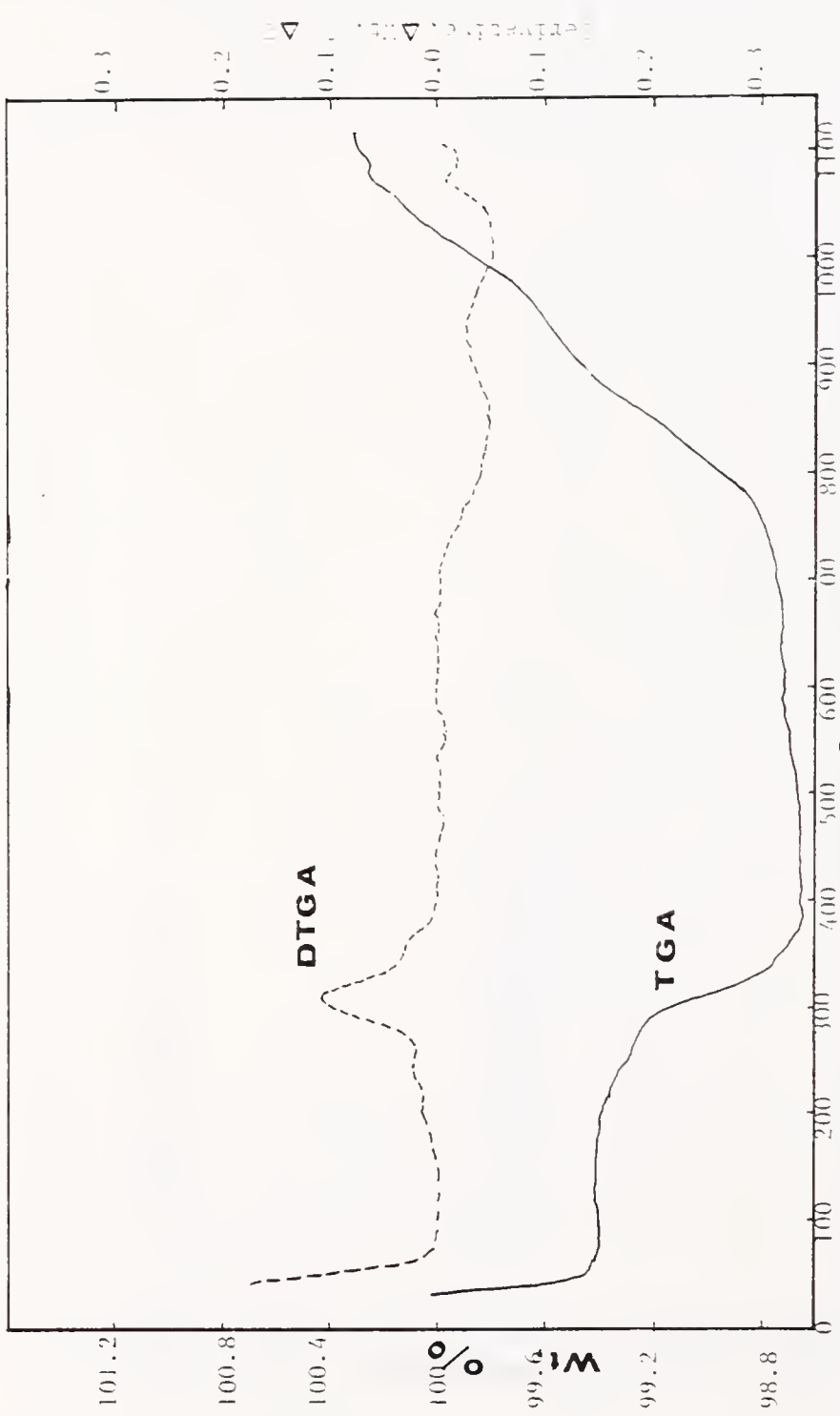

Fig.IV-6. TGA and DTGA Thermograms of as-received Nicalon® Fiber Showing a Loss of Weight by the Oxidation of the Polyvinylacetate Sizing at ~320°C, Significant Weight gain by Oxidation of the SiC Fiber Above ~800°C is Shown.

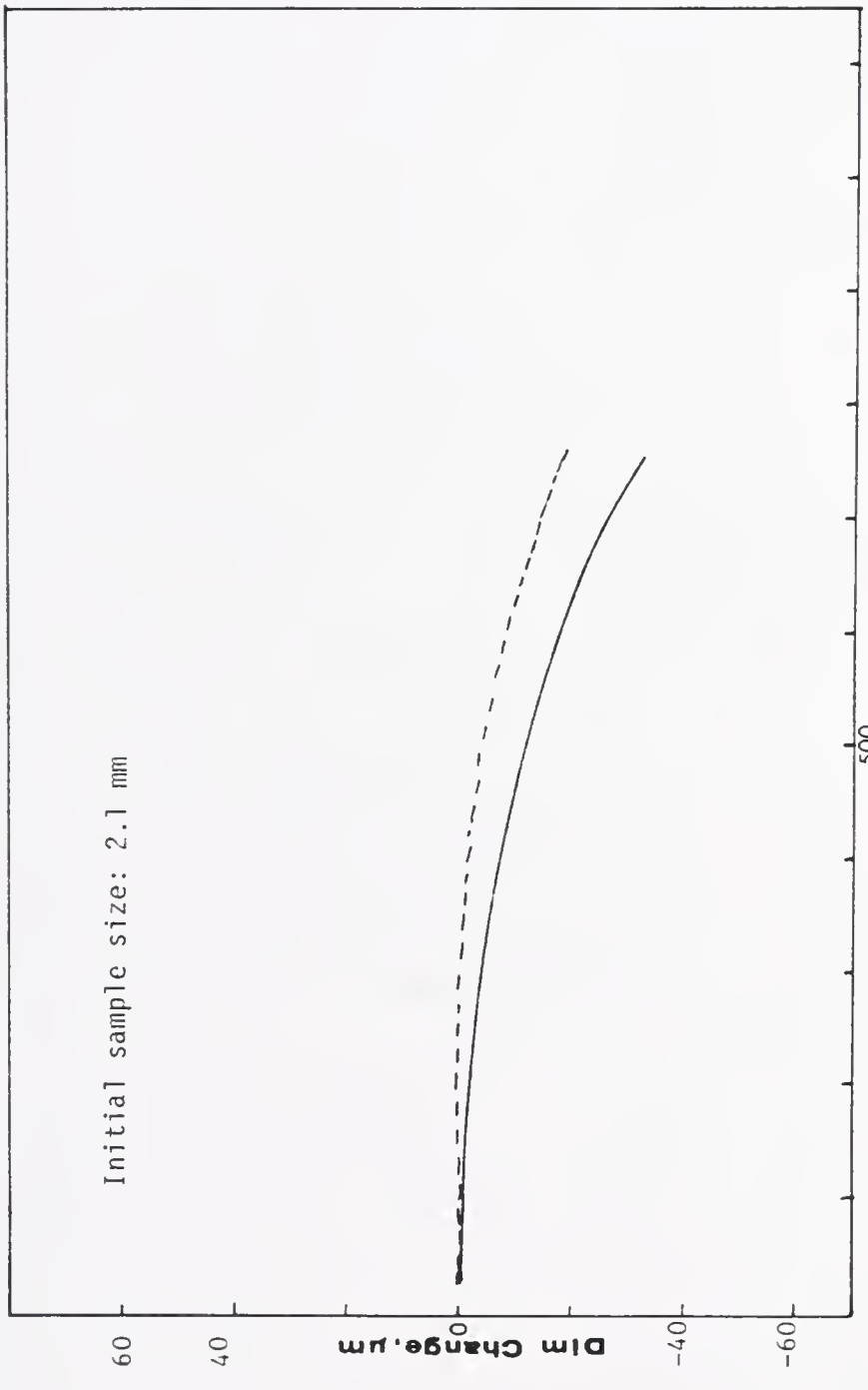

Fig.IV-7. TMA Thermograms of Cast Nicalon®/SiO_2 Gel Composite After 80°C Drying(solid line) and After Heating at 900°C for 1 hr(dotted line)

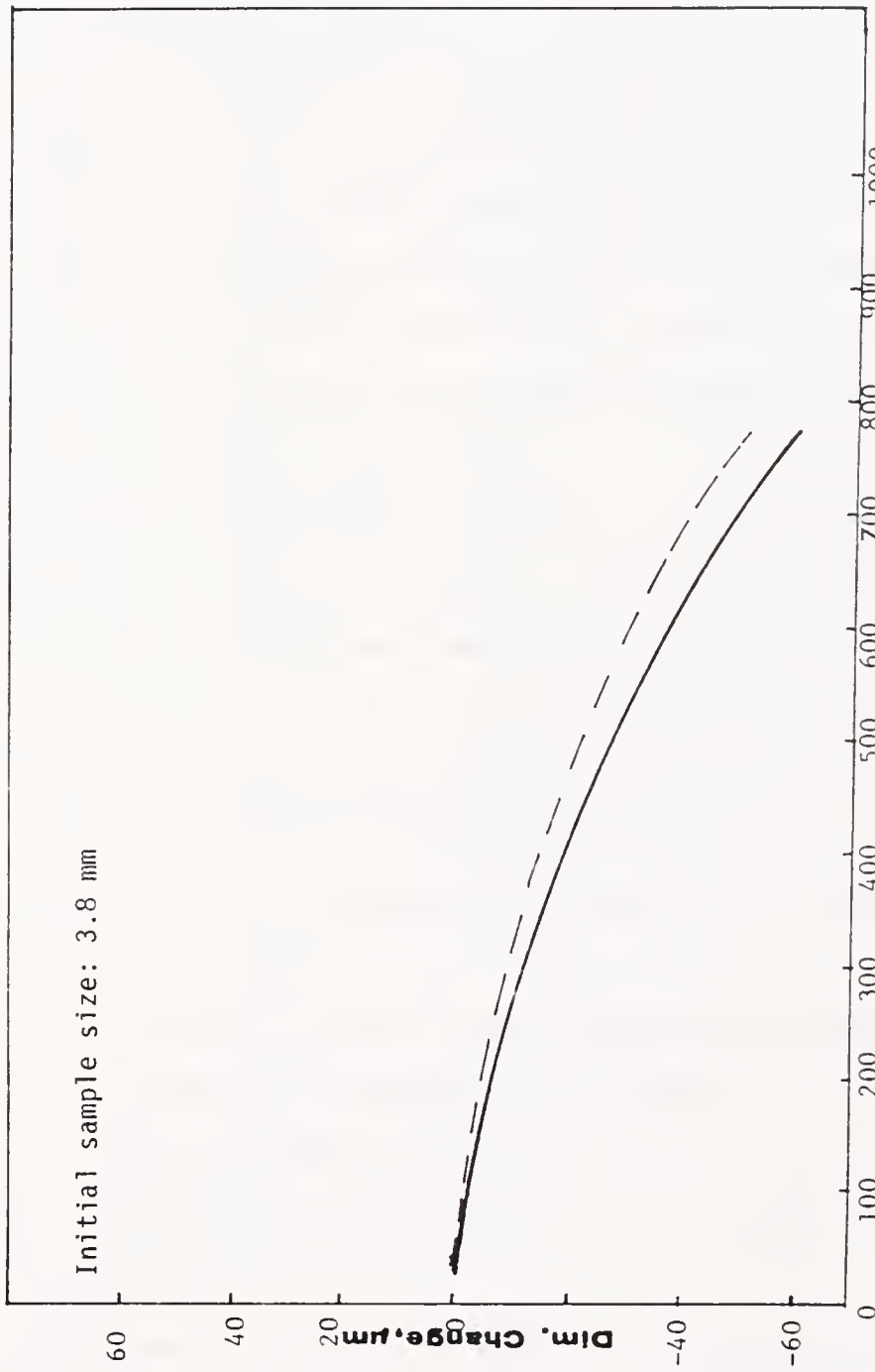

Fig.IV-8. TMA Thermograms of Cast Silar™/SiO_2 Gel Composite After Drying at 80°C(---) and After Heating at 900°C for 1 hr. (—)

The compressive modulus of cast NC after a 1,000°C heat treatment, yielding a density of 1.79 g/cc, is 571 MPa. Flexural strengths (σ_{flex}), densities, and microhardnesses of the composites are given in Table IV-1. Table IV-2 lists the BET surface areas, pore sizes, and the total pore volume of NC and SC. Densities as a function of infiltration cycle and a function of heat treatment temperature are given in Table IV-3.

Density and σ_{flex} as a function of processing temperature for 100% chopped fiber NC is given in Table IV-4. The maximum σ_{flex} of NC with different layouts and processing conditions after 1100°C heat treatments for two hours are given in Table IV-5.

Graphical representations of density vs. firing temperature for cast NC and SC are shown in Fig. IV-9. Microhardness (DPN) vs. density for cold pressed NC and SC are shown in Fig. IV-10. Greater density and DPN are shown for NC than SC. Flexural strength vs. DPN in Fig. IV-11 also show an exponential type of function. σ_{flex} vs. density in Fig. IV-12 shows a straight line function for both NC and SC. The pressed Silar composites (SC) have nearly 2-3x the σ_{flex} of pressed NC at the same density.

A sample specimen for the fracture toughness represented by K_{IC} is shown in Fig. IV-13. The parameters to calculate K_{IC} and the resulting K_{IC} values for cold pressed NC and SC are given in Table IV-6. Typical load vs. crosshead displacement curves are shown in Figs. IV-14, IV-15, and IV-16.

Calculation of flexural strengths was done according to Eqn. IV-5.[108]

Table IV-1. Three-Point Flexural Strengths, Densities, and Microhardness and the Ratio of Strength to Density of NC and SC.

Specimen	σ_{flex}, MPa*	ρ, g/cc	Hardness, DPN	σ_{flex}/ρ
Cast NC				
100% chopped fiber, 800°C	19±2 (2)	1.64±0.1	370±25	11.6
100% chopped fiber, 1400°C	83±3 (2)	1.82±0.2	660±37	45.6
100% chopped fiber, ViSP infilt., 800°C	37.2±3 (2)	1.90±0.1	467±21	19.5
100% chopped fiber, ViSP infilt., 800°C	33±1 (2)	1.23±0.1	520±52	26.8
unidirectional fiber, J-PSS1 infilt., 1000°C	9.3±4 (2)	1.66±0.1	551±48	5.6
unidirectional fiber, 1400°C	53±6 (2) 120±5 (2)	1.82±0.1 1.98±0.1	1051±56	29.1 60.6
Pressed NC				
80°C dried	12±1 (2)	1.73±0.2		6.9
J-PSS1 infilt. 800°C	31±2 (2)	1.85±0.1		16.8
800°C and quenched to RT	115±5 (2) 22±1 (2)	2.07±0.1 1.72±0.1	916±58	55.5
900°C 1100°C 1400°C	19±5 (2) 45±3 (2) 47±4 (2)	 1.92±0.1 2.18±0.1	 958±63	 23.4 21.6
900°C, 4 hrs in N_2	25 (3) 29 40	1.90 2.01 1.97		13 14 20
900°C, 4 hrs in air	23 (3) 22 35	2.00 1.88 1.65		12 12 21

Table IV-1 (continued).

Specimen	σ_{flex}, MPa*	ρ, g/cc	Hardness, DPN	σ_{flex}/ρ
Cast SC				
1000°C	10±2 (3)	1.45±0.2	378±76	6.9
Pressed SC				
80°C dried	18±3 (2)	1.41±0.1		12.8
700°C	31±2 (2)	1.80±0.1		17.2
800°C	42±3 (2)			
900°C	88±6 (2)	1.87±0.1		47
950°C	116±8 (2)	1.88±0.1		62
ViSP infilt.				
820°C	53±3 (2)	1.86±0.1	403	28.5
900°C	89±7 (3)	1.91±0.1	413±42	46.6
950°C	216±11 (2)	1.83±0.1	1284±85	118.0
ViSP infilt.				
950°C	78±6 (2)	1.94±0.1		40.2
1400°C	112±8 (2)	2.08±0.1		53.8
800°C quenched to RT	125±7 (2)	1.82±0.1	805±25	68.7
900°C in N_2	39	1.92±0.1		20
4 hrs	149	1.72±0.1		87
	117	1.76±0.1		66
	88	1.71±0.1		51
	68	1.87±0.1		36
900°C in air	45	1.88±0.1		24
4 hrs	101	1.91±0.1		53
	95	1.75±0.1		54

* The numbers in parentheses denote the number of specimens tested.

Table IV-2. The BET Surface Areas, Mean Pore Sizes, and Total Pore Volumes of NC and SC.

Composite	Heat Treatment Temp., °C	BET Area, m^2/g	Mean Pore Size, Å	Total Pore Vol., cc/g
Cast NC	300 in air	141	16.2	0.114
	800 in N_2	45	16	0.036
	1500 in air	0.86	163	0.0071
ViSP infilt. NC	800 in N_2	99	13	0.063
Pressed NC	300	73	14	0.0517
	900	4.6	68	0.0155
Cast SC	300	184	17	0.16
	850	18	14	0.13
Pressed SC	300	143	18	0.12
	850	5.8	140	0.040
Pressed/ ViSP infilt. SC	800	29	33	0.049

Table IV-3. Density Changes as Function of Processing Temperature and Sol Impregnation Cycles for Cast NC and SC.*

Dipping Cycle After 500°C for 2 Hours	Density, g/cc ±0.1	
	NC	SC
0	1.44	1.11
1	1.56	1.29
2	1.70	1.41
3	1.81	1.52
4	1.86	1.59
5	1.87	1.62

Temperature, °C After 2 Dipping Cycles	Density, g/cc ±0.1	
	NC	SC
500	1.72	1.41
900	1.80	1.49
950	1.88	1.54
1100	1.98	1.62
1400	2.11	1.73

* Two specimens were used for each cycle and each temperature.

Table IV-4. Density and Flexural Strengths of Cast NC 100% Chopped Fiber as Function of Processing Temperature.

Temperature, °C	ρ, g/cc ± 0.1	σ_{flex}, MPa	σ_{flex}/ρ
80	1.62	15±4	9.26
500	1.71	17±3	9.94
900	1.83	20±4	10.9
1100	1.95	27±5	13.8
1400	2.06	83±3	40.3

* Two specimens were tested for each temperature.

Table IV-5. Maximum σ_{flex} of NC of Different Layouts and after Processing at 1100°C or 1400°C.

Composite	σ_{flex}, MPa*
cast 100% chopped fiber	27±5 (3) 83±3 (1400°C) (2)
bidirectional weave/ chopped fiber	15±3 (4)
continuous fiber/ chopped fiber	25±4 (2) 120±5 (1400°C) (2)
cold pressed 100% chopped fiber	115±12 (3)

* The numbers in parentheses denote the numbers of specimens tested.

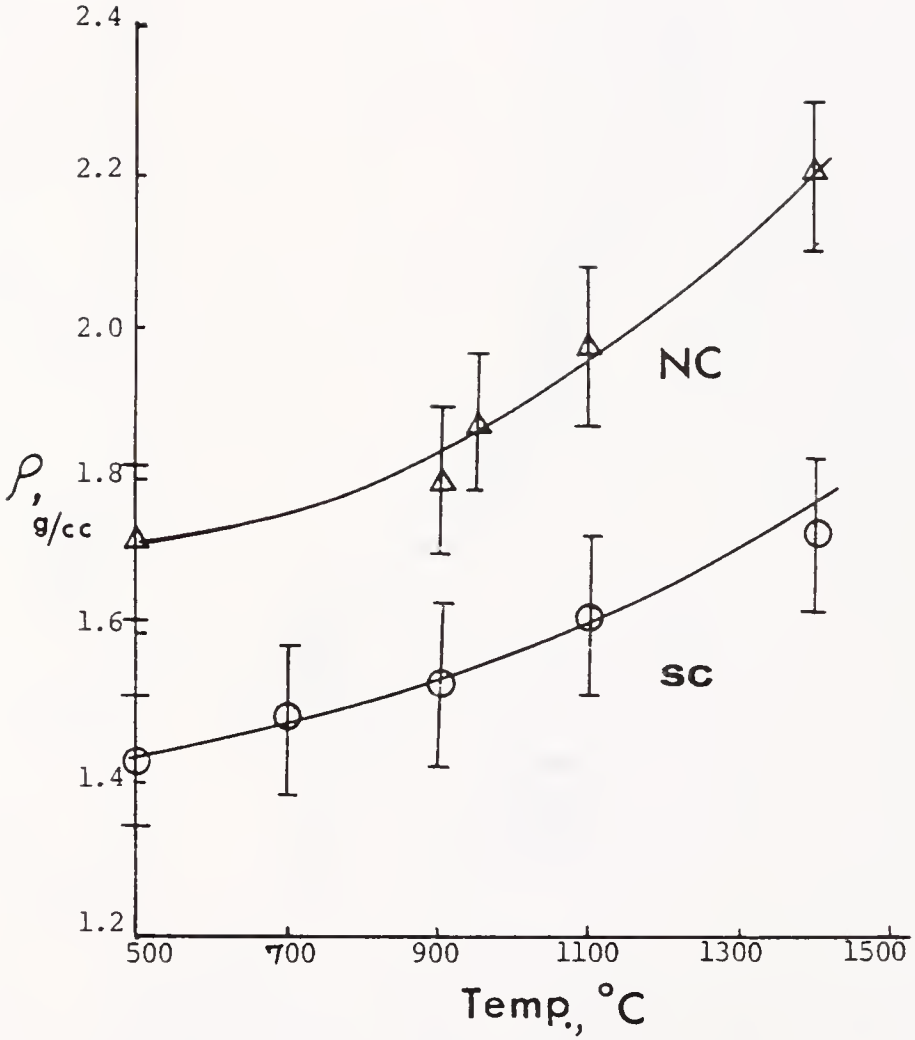

Fig.IV-9. Density as a Function of Firing Temperature of Cast Nicalon®/SiO_2 Gel Composites and Silar™/SiO_2 Gel Composites

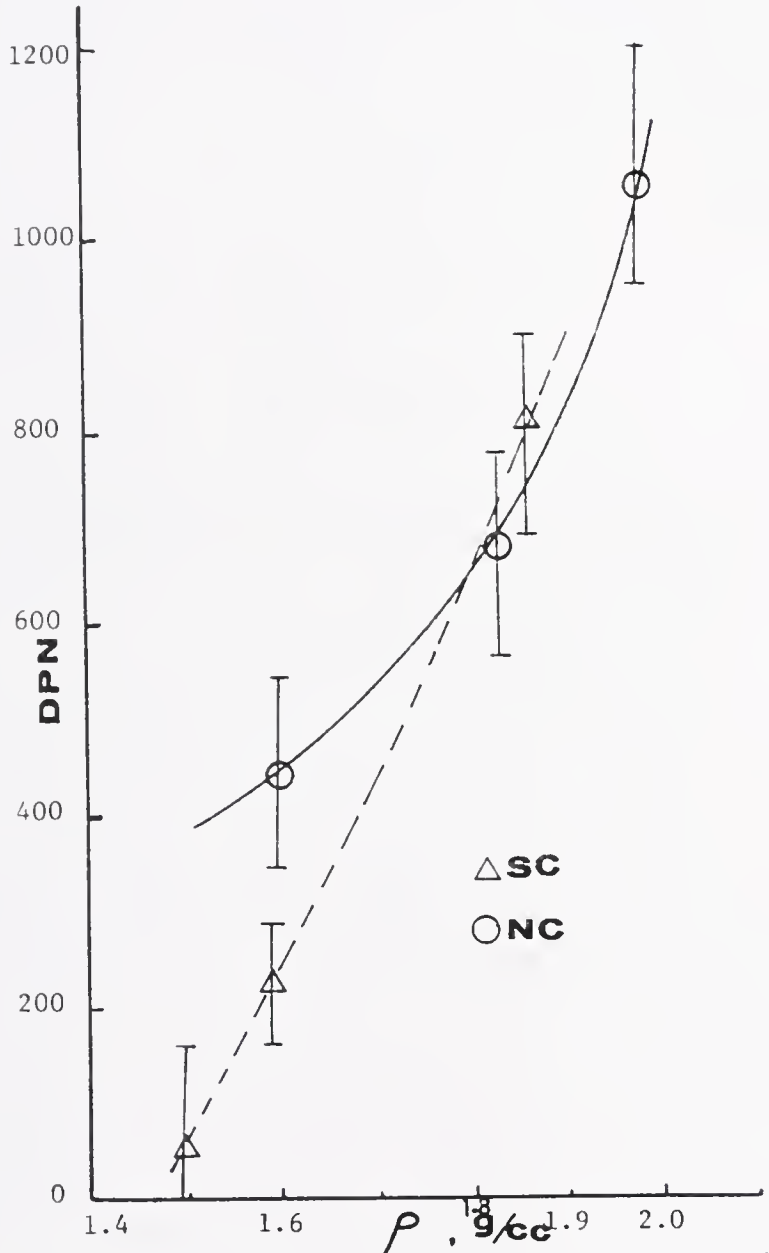

Fig.IV-10. Microhardness as a Function of Density for Cast Nicalon®/ SiO_2 Gel and Silar™/SiO_2 Gel Composites

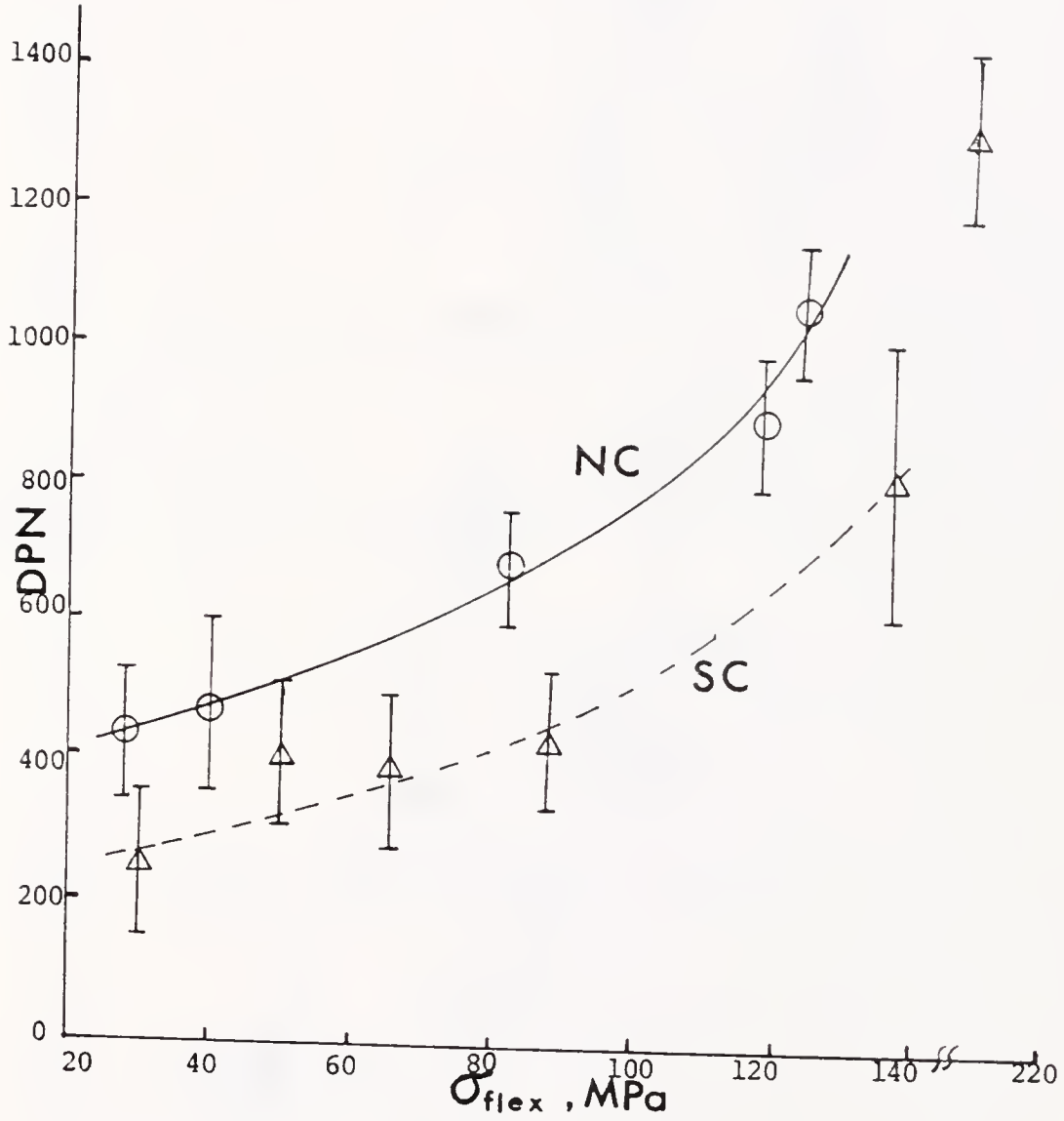

Fig.IV-11. Microhardness vs Flexural Strenth of Cold Pressed NC and SC

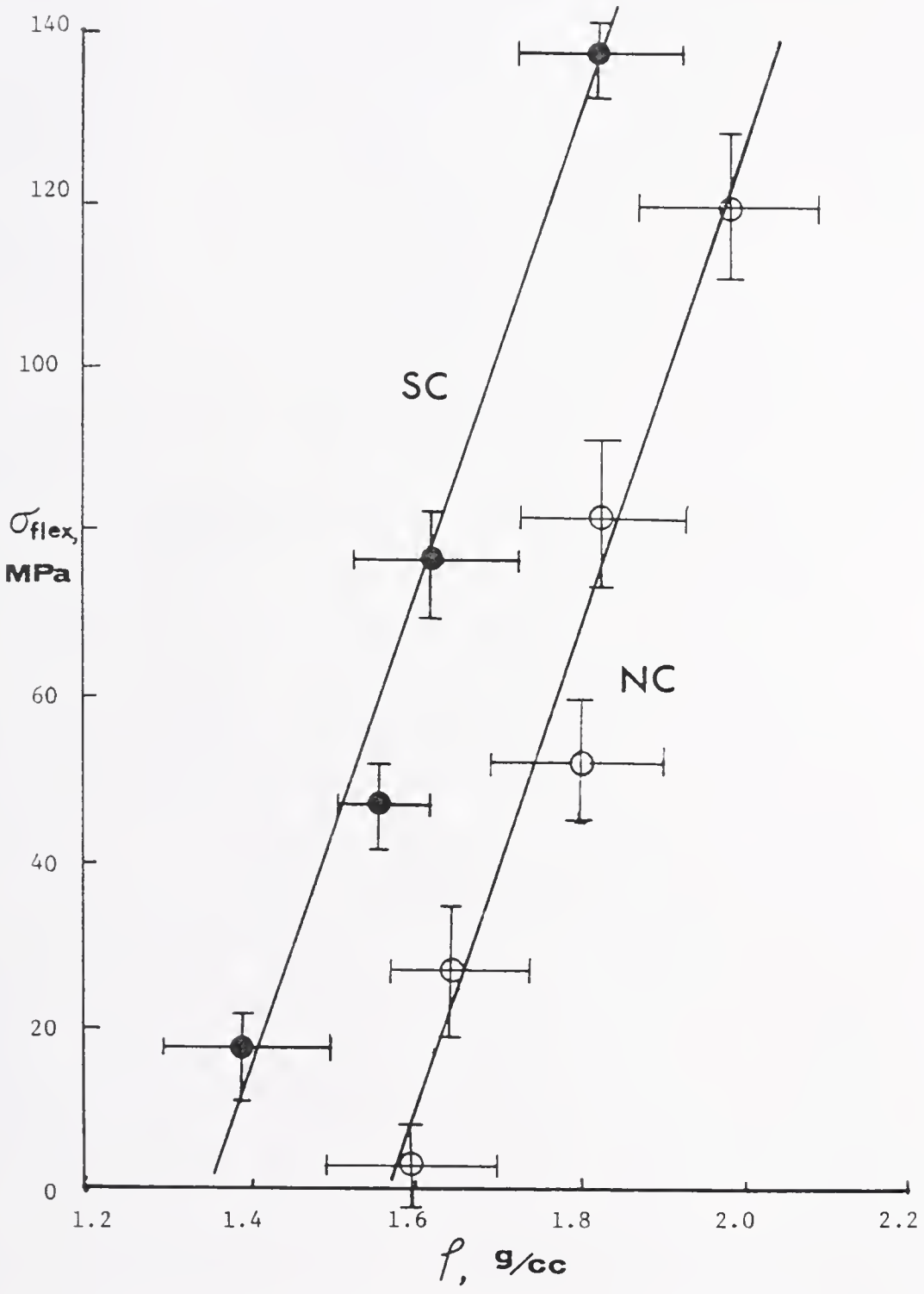

Fig.IV-12. Flexural Strengths of Pressed Nicalon®/SiO_2 Gel and Silar™/SiO_2 Gel Composites As a Function of Density

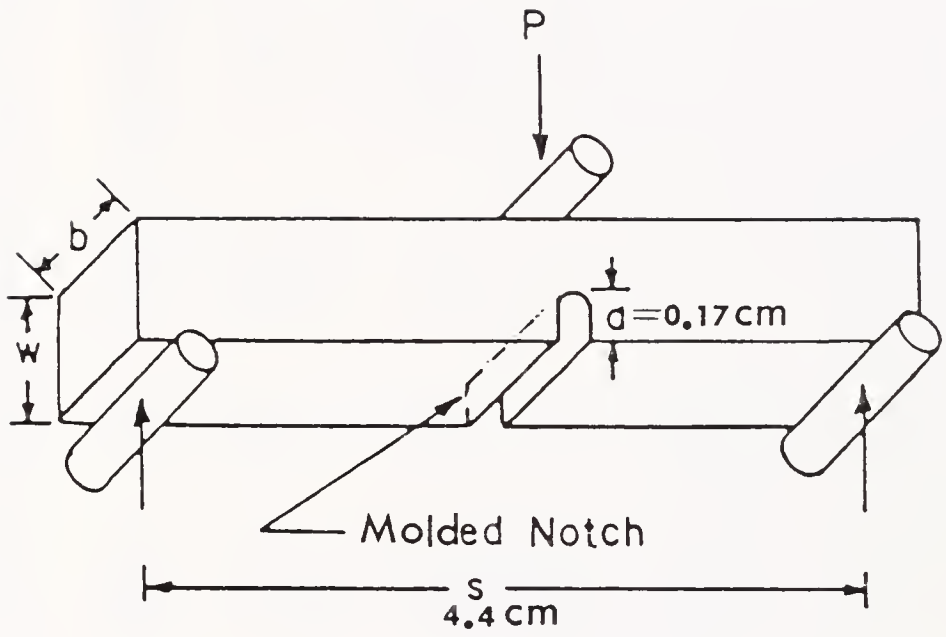

Fig.IV-13. Schematic of Notch-Beam Test in Three-Point Bending for Fracture Toughness of Pressed NC and SC

Table IV-6. Parameters and Dimensions for Three-Point Notched Fracture Toughness of Cold Pressed NC and SC as Shown in Fig. IV-13 and Eq. IV-6.

Composite	ρ, g/cc	a/w	Y	M, Nm	b, cm	W, cm	K_{IC}, MPa•$m^{1/2}$	K_{IC}/ρ
NC, 500°C	1.91±0.05	0.34	2.01	1.82	1.04	0.50	3.48∓0.5	1.82
NC, 1400°C	2.01±0.05	0.36	2.05	2.81	1.04	0.47	6.20∓1.2	3.12
SC, 500°C	1.86±0.06	0.52	2.69	1.25	1.10	0.33	6.93∓1.1	3.73
SC, 1400°C	1.98±0.04	0.43	2.27	2.38	1.06	0.40	7.87∓1.4	3.97

Two specimens for each composite were used in the test.

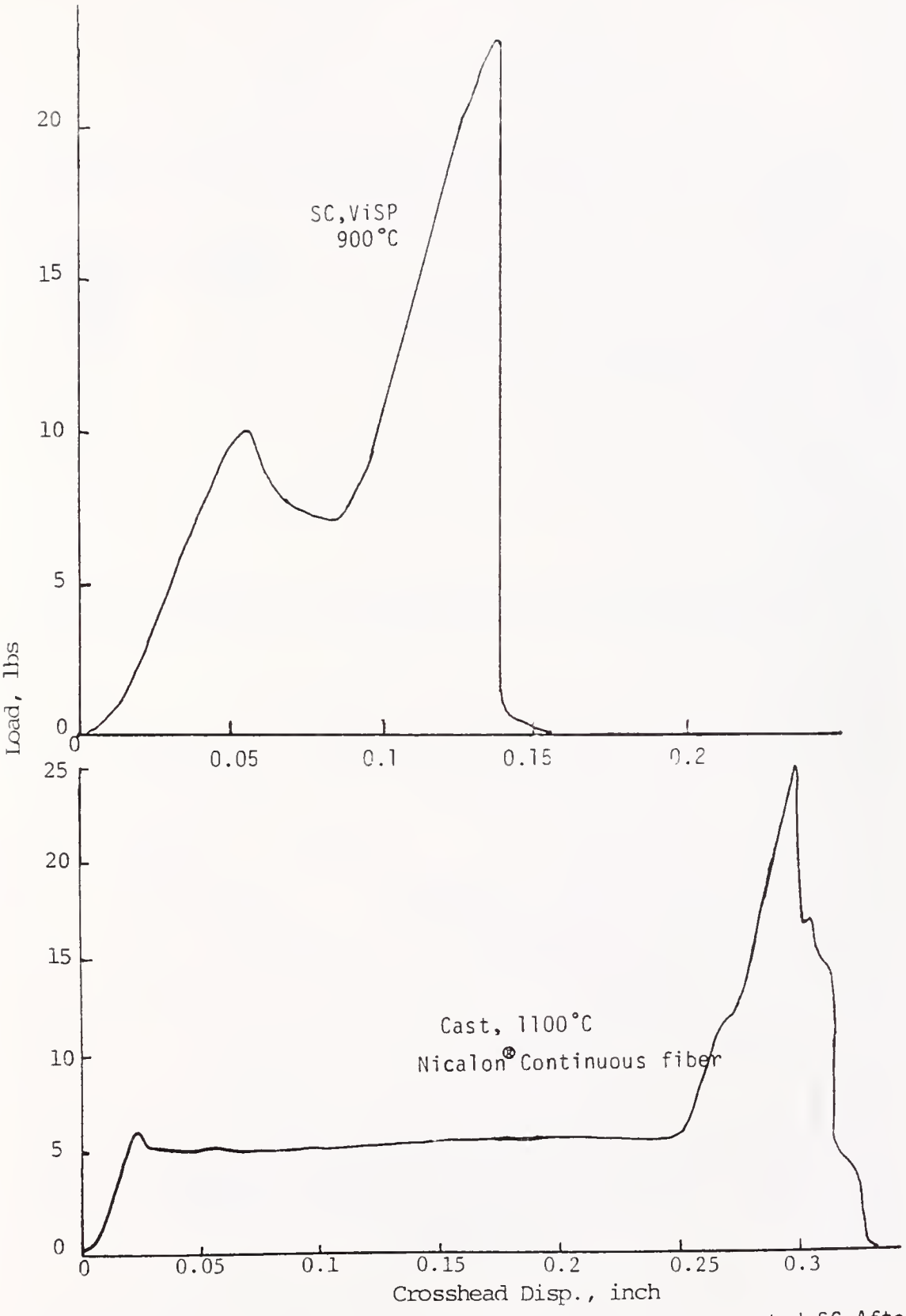

Fig.IV-14. Load vs Crosshead Displacement of ViSP Impregnated SC After Pyrolysis at 900°C(top) and Nicalon® Cont. Fiber/SiO_2 Gel Comp.(bottom)

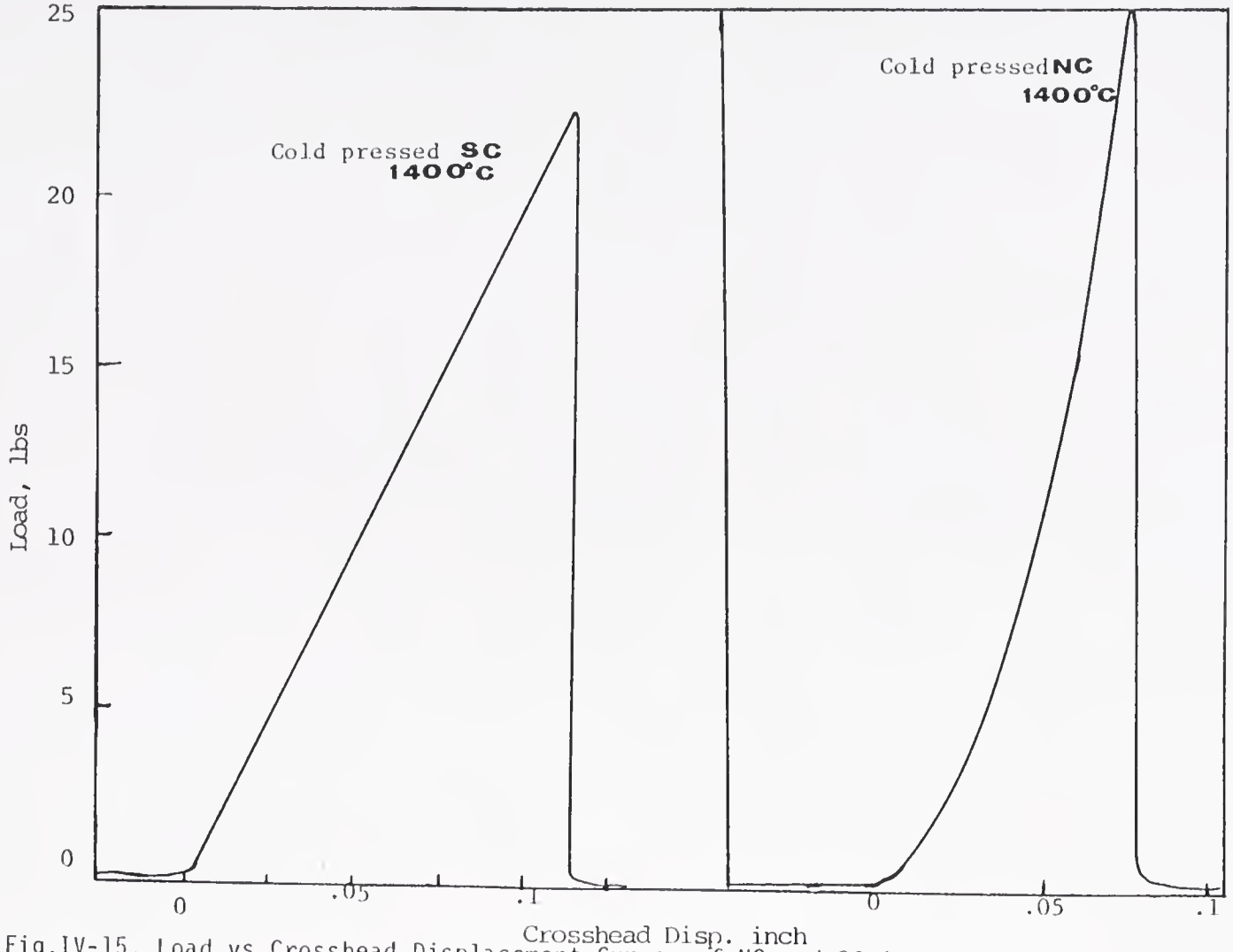

Fig.IV-15. Load vs Crosshead Displacement Curves of NC and SC in 3-point Flexure

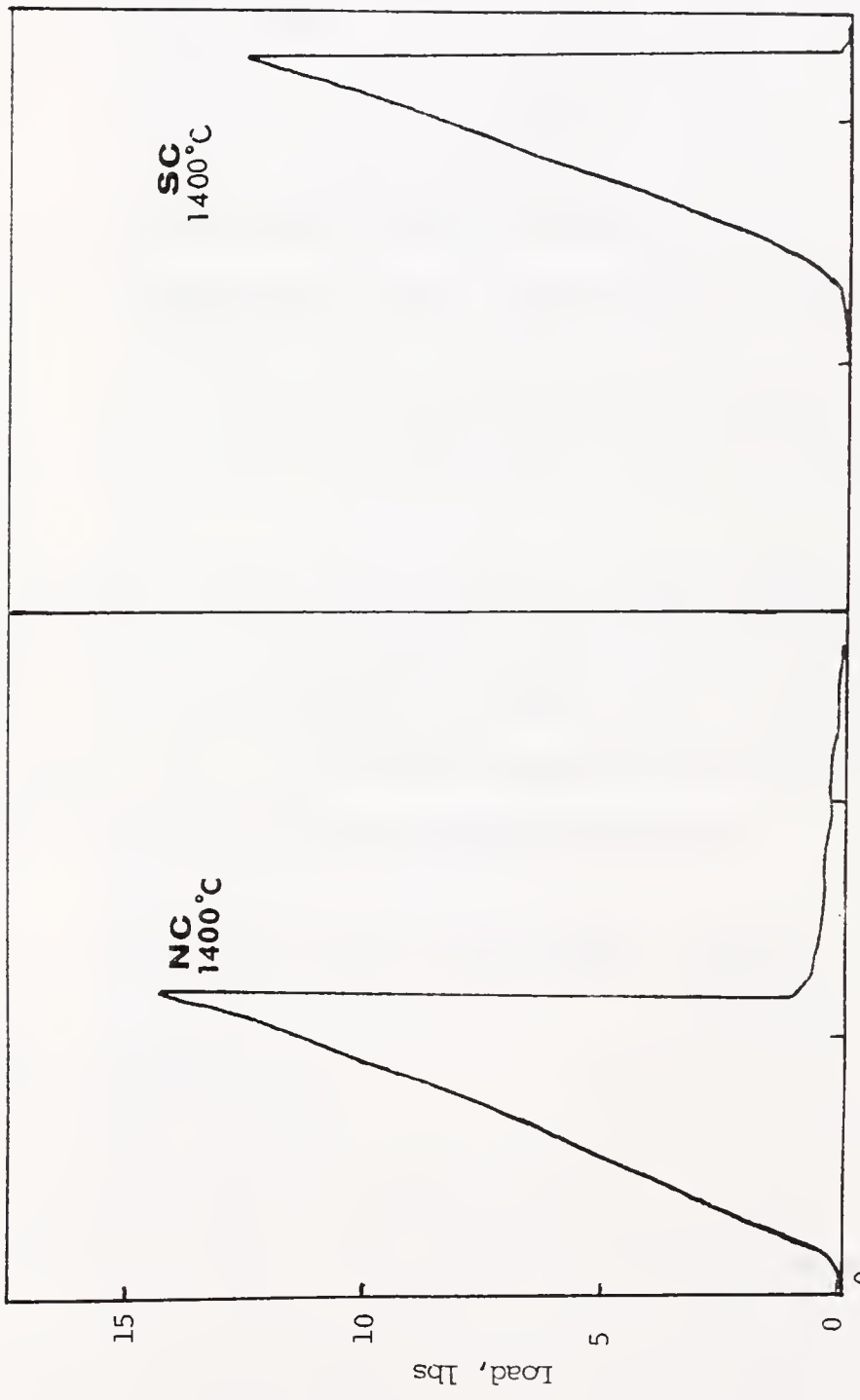

Fig.IV-16. Load vs Crosshead Displacement of Notched NC and SC in 3-point Flexure.

$$\sigma_{flex} = 3/2 \frac{(load)(span)}{(width)(thickness)^2} \qquad (IV\text{-}5)$$

Calculation of K_{IC} is based on Bansal and Duckworth[109] and shown by Equ. IV-6.

$$K_{IC} = \frac{6\ Ma^{1/2}}{b\ W^2}\ Y \qquad (IV\text{-}6)$$

where M = applied bending moment at fracture = P x S

Y = dimensionless parameter which depends on a/w and type of loading

$= A_o + A_1\ (a/w) + A_2(a/w)^2 + A_3(a/w)^3 + A_4(a/w)^4$

for s/w = 8, A_o = 1.96, A_1 = -2.73, A_2 = 13.66, A_3 = -23.98, and A_4 = 25.22.

A fracture toughness measurement by a Vicker indentation method[73] has been described in Chapter III. The results of the crack lengths, hardness, and K_{IC} are summarized in Table IV-7. The relation between crack length and K_{IC} is as follows, although the validity of this metnod has not yet been fully proven for composite materials.

$$H = \frac{P}{2(\bar{a}/2)^2} \text{ and } K_{IC} = 0.016\ (\frac{E}{H})^{1/2} \frac{P}{(\bar{c}/2)^{3/2}} \qquad (IV\text{-}1)$$

where: H = hardness in Pa

P = load in newtons

$\bar{a}$= mean diameter of Vicker indentation

$\bar{c}$= mean diameter of the extended crack due to loading

E = elastic modulus estimated using the rule of mixture

The TEM micrographs of cast NC and SC before and after heat treatment at 900°C are shown in Figs. IV-17, IV-18, IV-19, and IV-20.

Table IV-7. Fracture Toughness of Cold Pressed NC and SC Determined by Indentation Crack Lengths Under 1 kg Load

Sample*	ρ, g/cc	E, GPa	$\bar{a}$, μm	$\bar{c}$, μm	$\bar{H}$, GPa	K_{IC}, MPa·$m^{1/2}$	K_{IC}/ρ
NC, 1400°C	1.96±0.1	242	40±5	48±7	12±2	5.9±1	3.0
NC, 1400°C infilt. with ViSP, 900°C	1.97±0.1	242	39±6	45±7	15±2	6.0±1	3.0
SC, 1400°C	2.01±0.1	242	58±5	75±6	5.8±1	5.1±1.2	2.54
SC, 1400°C infilt. with ViSP, 900°C	2.02±0.1	242	57±5	73±4	6.2±1	6.2±1.2	3.07

* 2-3 specimens and 3-7 measurements for each specimen were used.

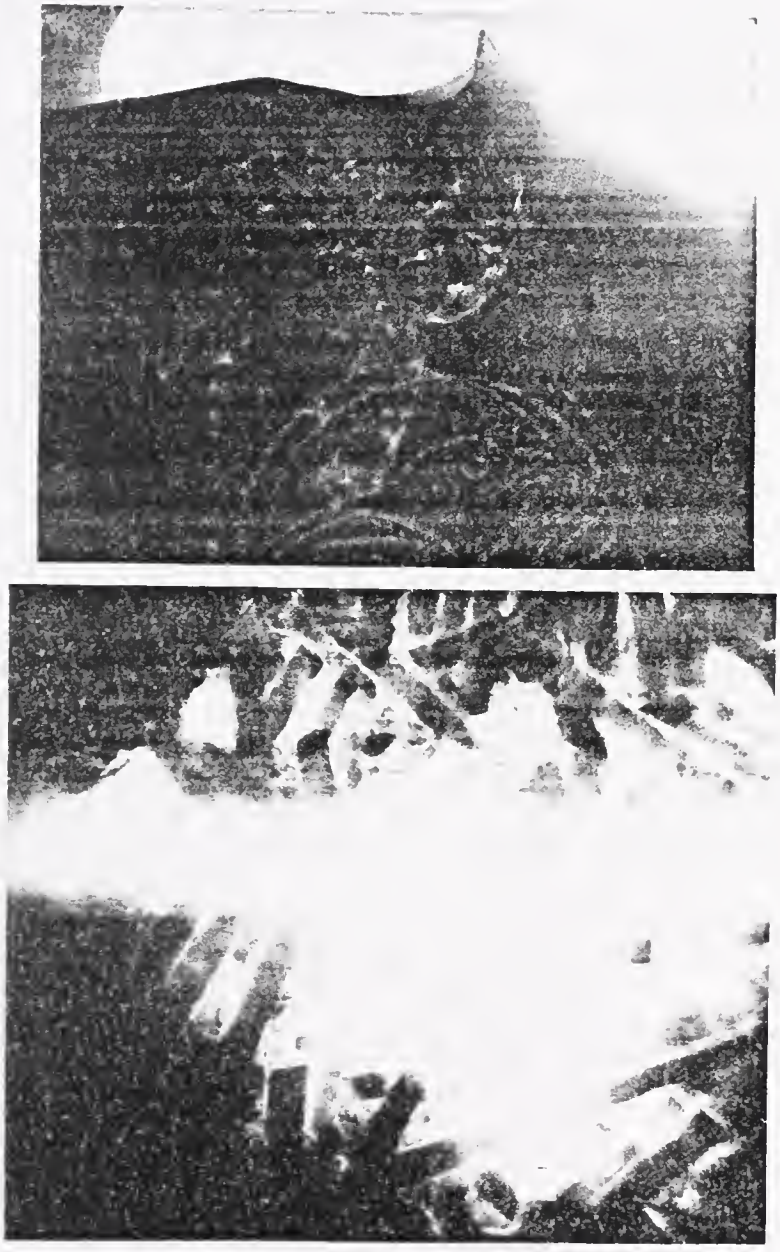

Fig.IV-17. Bright Field TEM Micrograph of NC After 80°C Drying at 59KX Mag. (top) and STEM Micrograph of the Above at 300X Mag. (bottom)

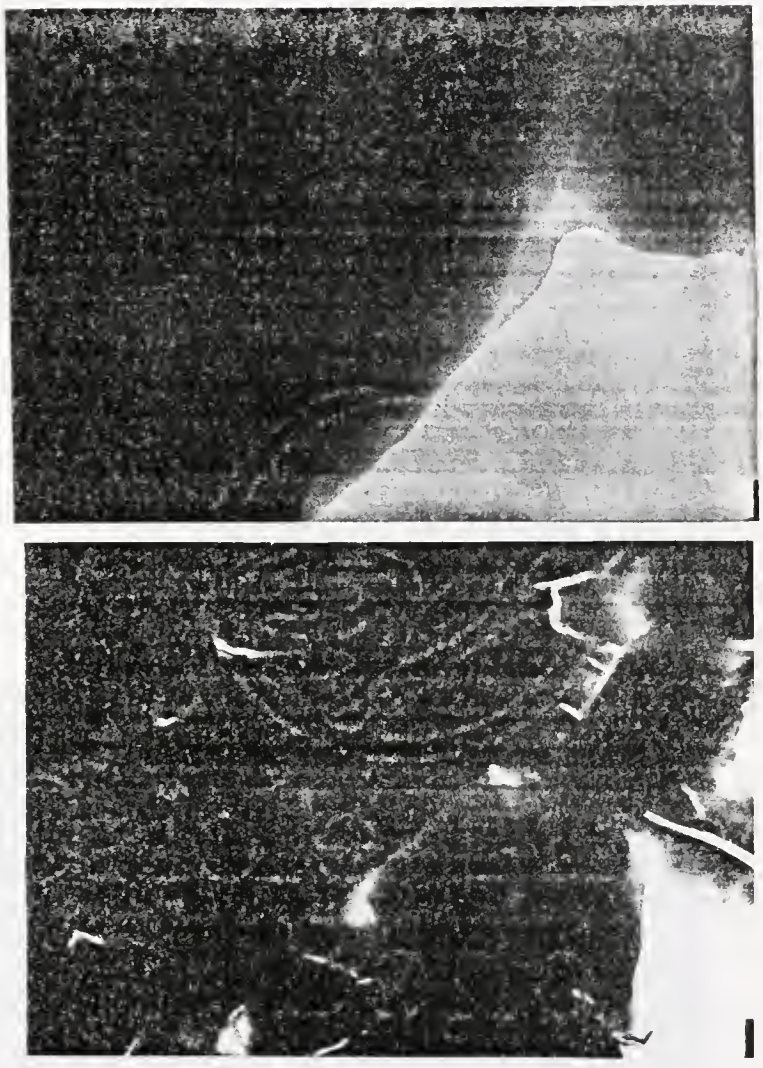

Fig.IV-18. Bright Field TEM Micrographs of Cast NC After 900°C Heat Treatment in N_2, Top: 50KX Mag., Bottom: 1KX Mag., Darker Contrast = fiber and Lighter Cont. = Silica

Fig.IV-19. Bright Field TEM Micrographs of SC After Drying at 80°C, Top: 50KX Mag. and Bottom: 200KX Mag.

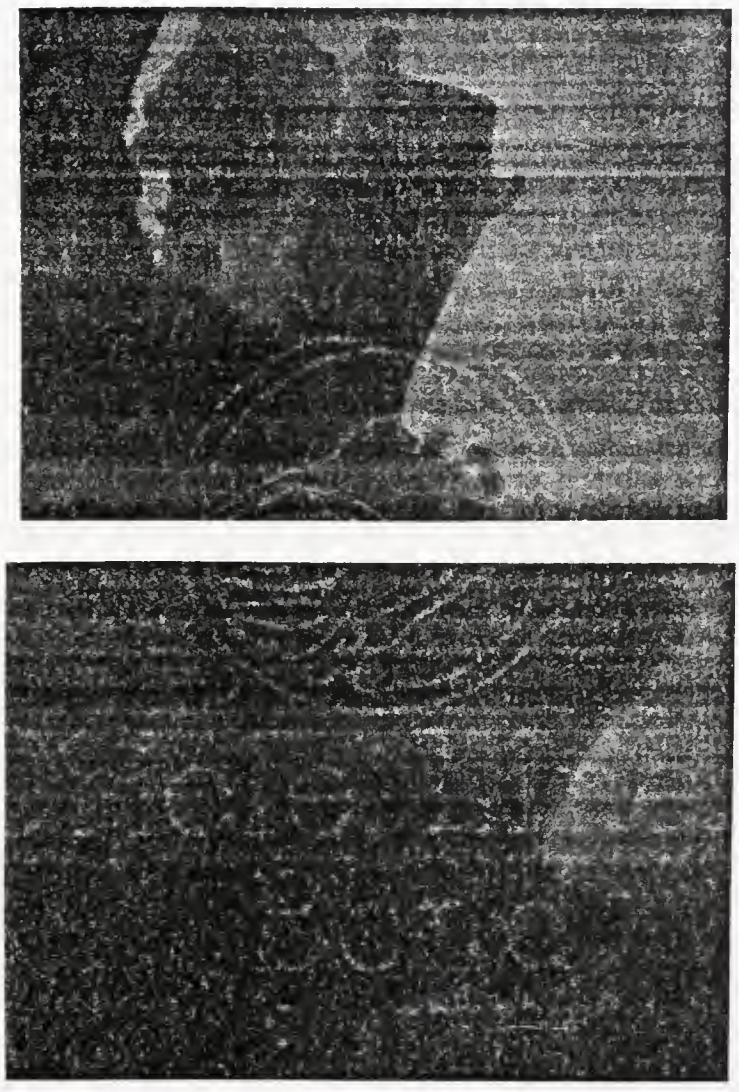

Fig.IV-20. Bright Field TEM Micrographs of SC After Heating at 900°C in N_2, Top: 50KX Mag. and Bottom: 200KX Mag..

Figure IV-21 shows SEM micrographs of a surface of cast NC and SC after drying at 80°C. Figure IV-22 shows a polished surface of NC after 1100°C for two hours in N_2. Figure IV-23 shows fractured surfaces of unidirectional continuous Nicalon® fiber in SiO_2 matrix showing dislodging of the interfaces and of random 100% chopped fiber NC.

The extent of 1100°C dry static air oxidation of SiC in the SiO_2 composite was quantitatively estimated using reflectance values (R) of FT-IR and the base-line method.[110] The base-line method was applied to compensate for the fluctuation in IR response of the instrument. A few typical FT-IR spectra are given in Figs. IV-24, IV-25, IV-26, IV-27, and IV-28. The IR bands to estimate R values of each species are tabulated in Table IV-8. Reflectances at ~789 cm^{-1} (R_c), ~1086 cm^{-1} (R_g), and ~1167 cm^{-1} (R_x) are due to vibrational motions of the Si-C bond, vitreous Si-O bond, and cristobalite Si-O, respectively.[111-113] Plots of time vs. R values were made and are shown in Figs. IV-29, IV-30, IV-31, and IV-32.

In the composites, the total amount of vitreous silica is shown to be relatively constant throughout the oxidative heat treatments. This means that the oxidation of SiC in SiO_2 glass produces predominantly a crystalline SiO_2, namely, cristobalite. This was demonstrated by Figs. IV-24, IV-25, IV-26, IV-27, and IV-28.

Thus the normalization of R's by R_g should compensate R due to sample shapes, sizes, and surface morphology after each heat treatment.

The results of isothermal TGA carried out in dry static oxygen are given in Figs. IV-33, IV-34, IV-35, and IV-36. The weight gains are tabulated and given in Table IV-9.

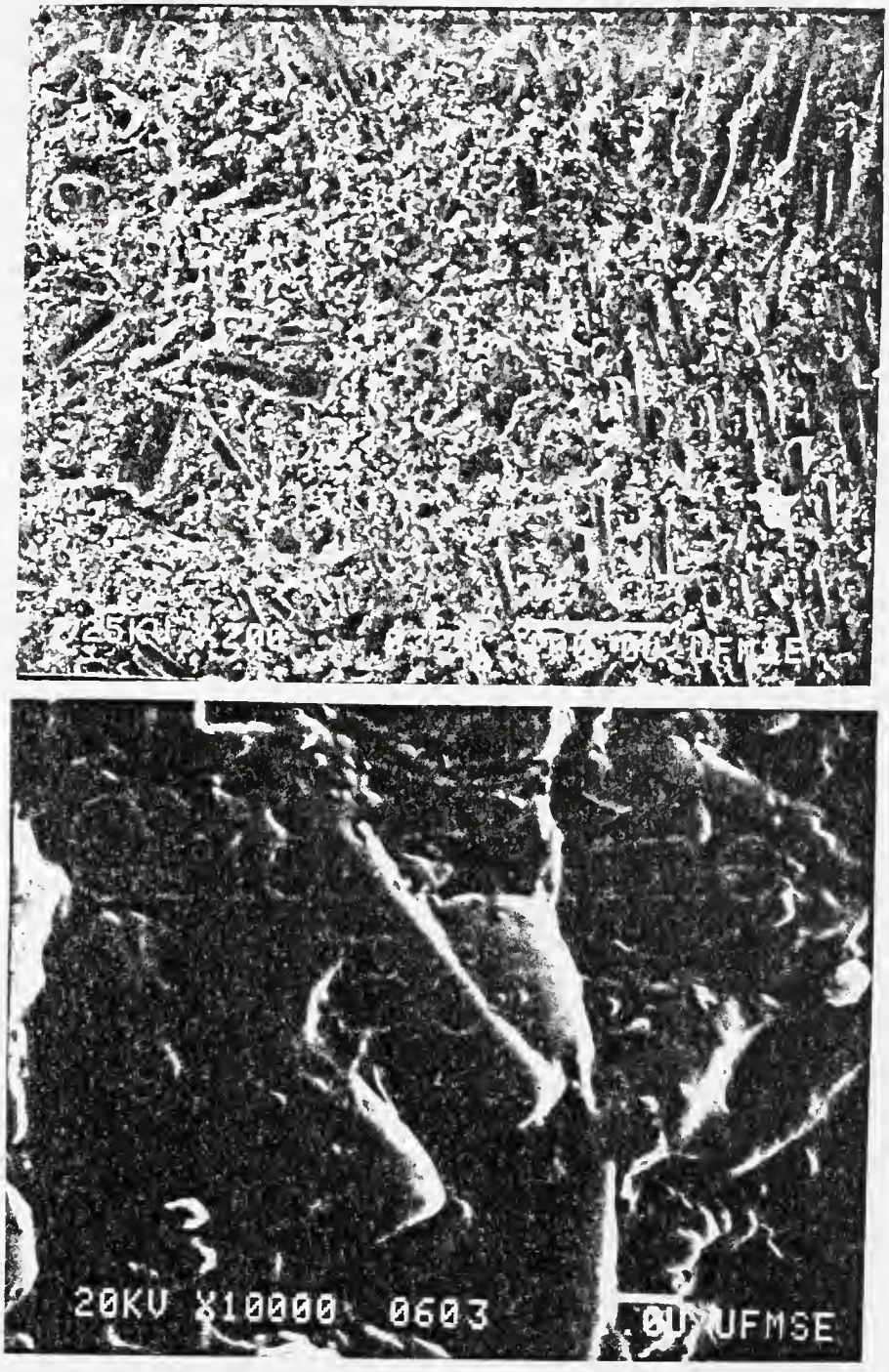

Fig.IV-21. SEM Micrographs of As-Cast NC (top) and As-Cast SC (bottom) After Drying at 80°C.

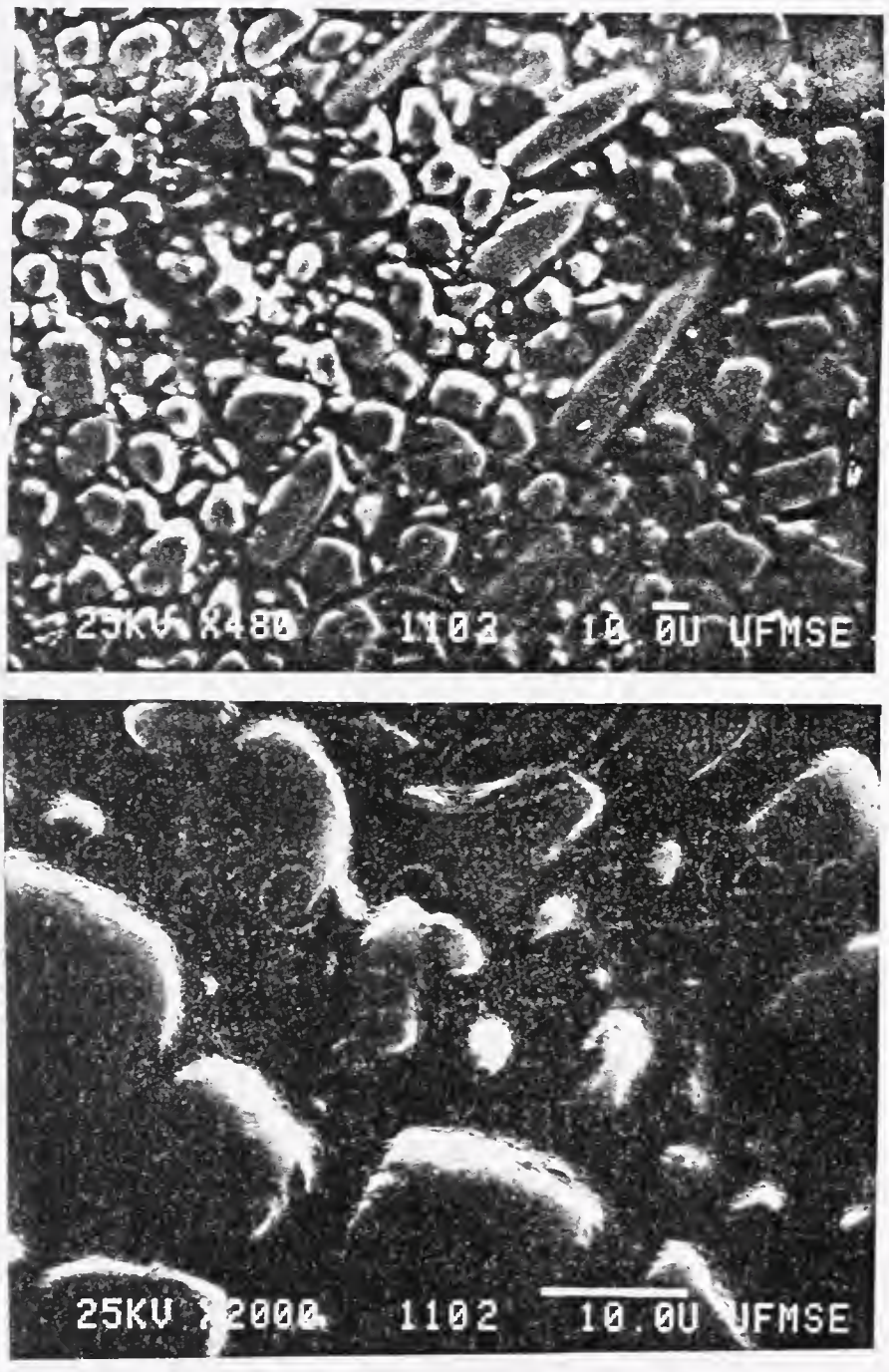

Fig.IV-22. SEM Micrographs of Polished Surface of NC After 1100°C Heating in N_2.

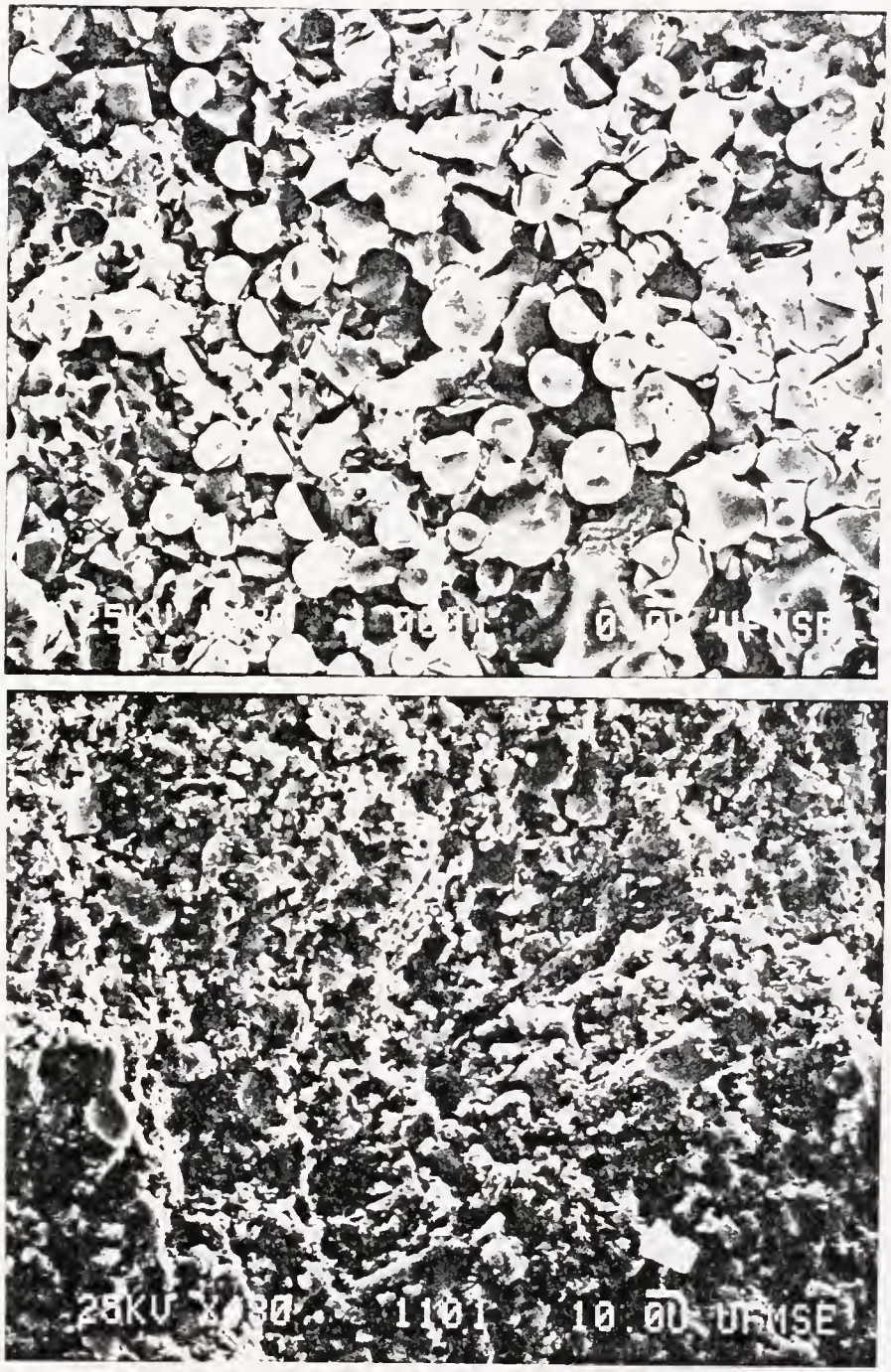

Fig.IV-23. Fractographs of NC, Top: Uniaxial fiber after 1000°C
Bottom: Random chopped fibers after 1100°C

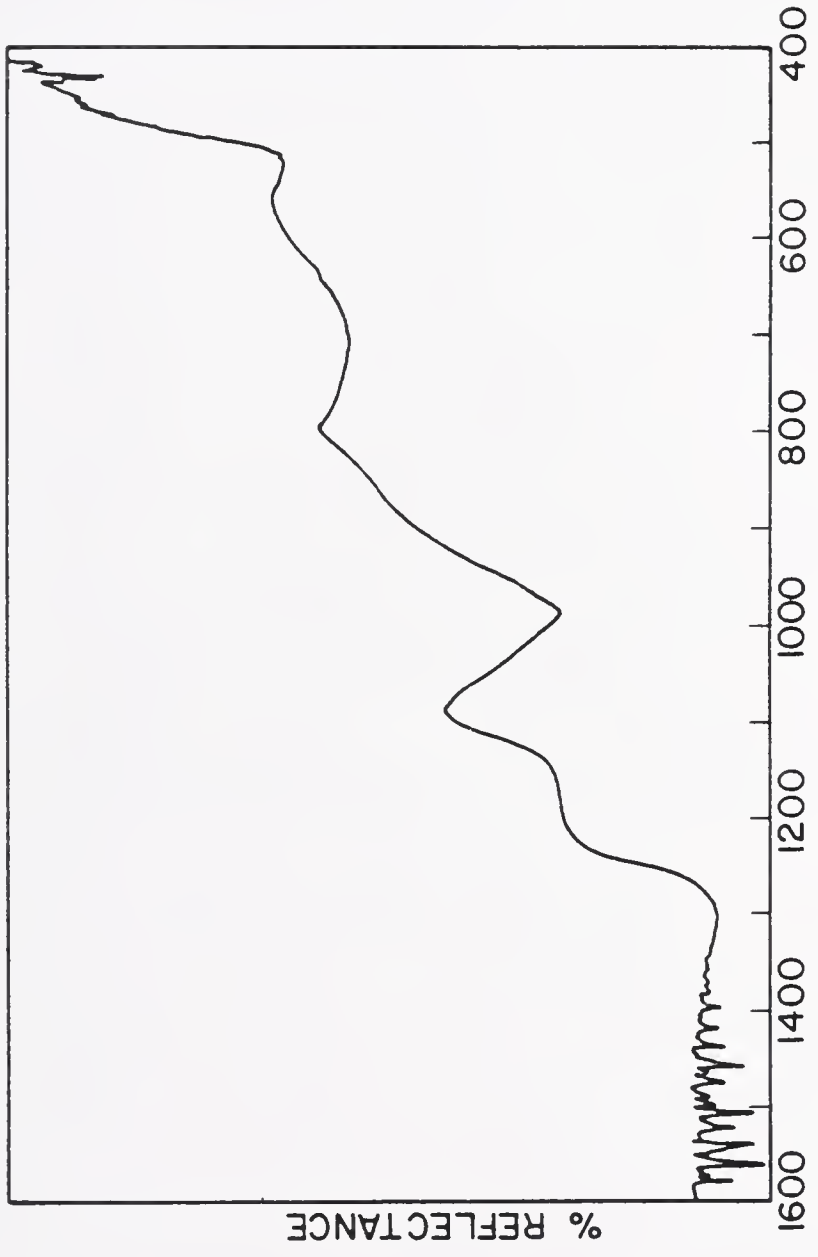

Fig.IV-24. FT-IR Spectrum of Nicalon /SiO_2 Composite After Drying in Air

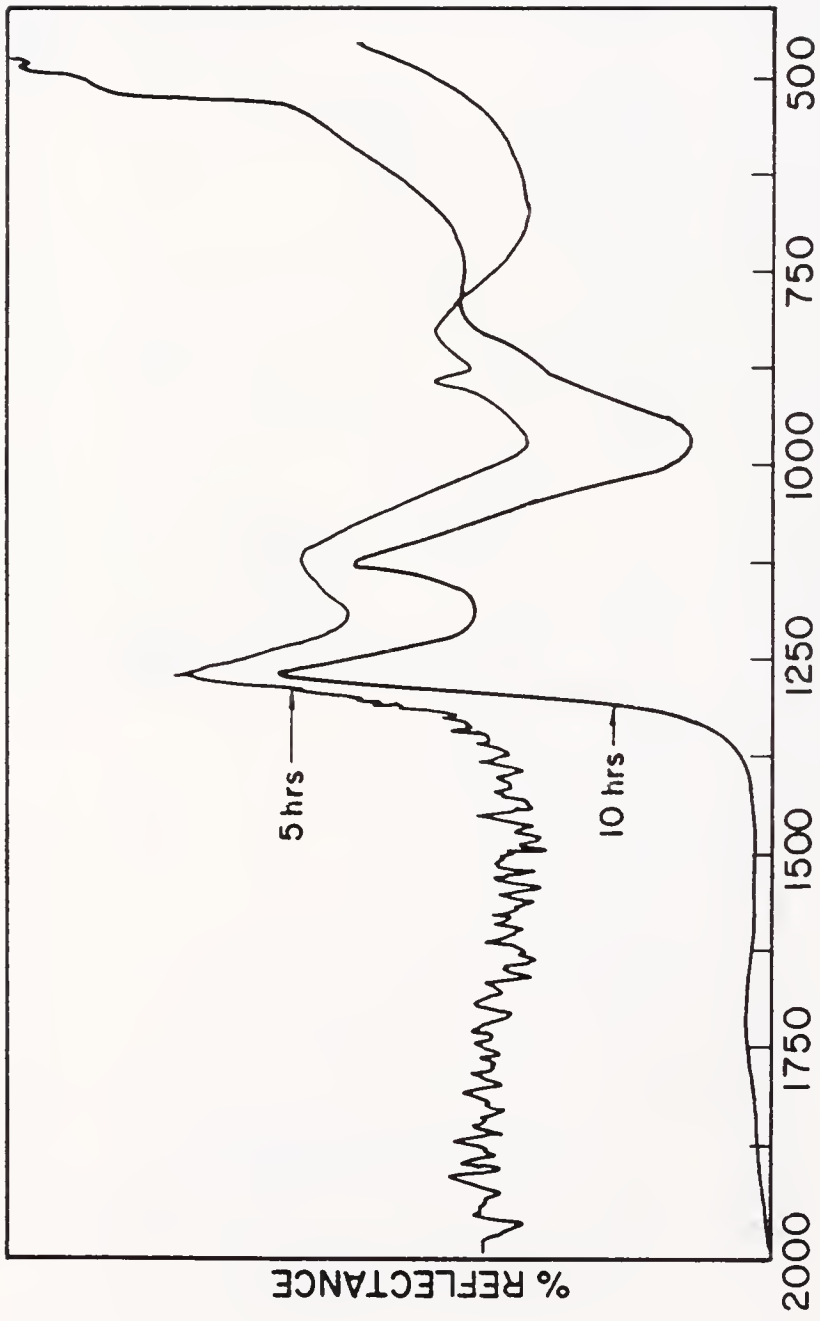

Fig.IV-25. FT-IR Spectrum of NC After Heating at 1100°C in Static Air for 5 and 10 hrs.

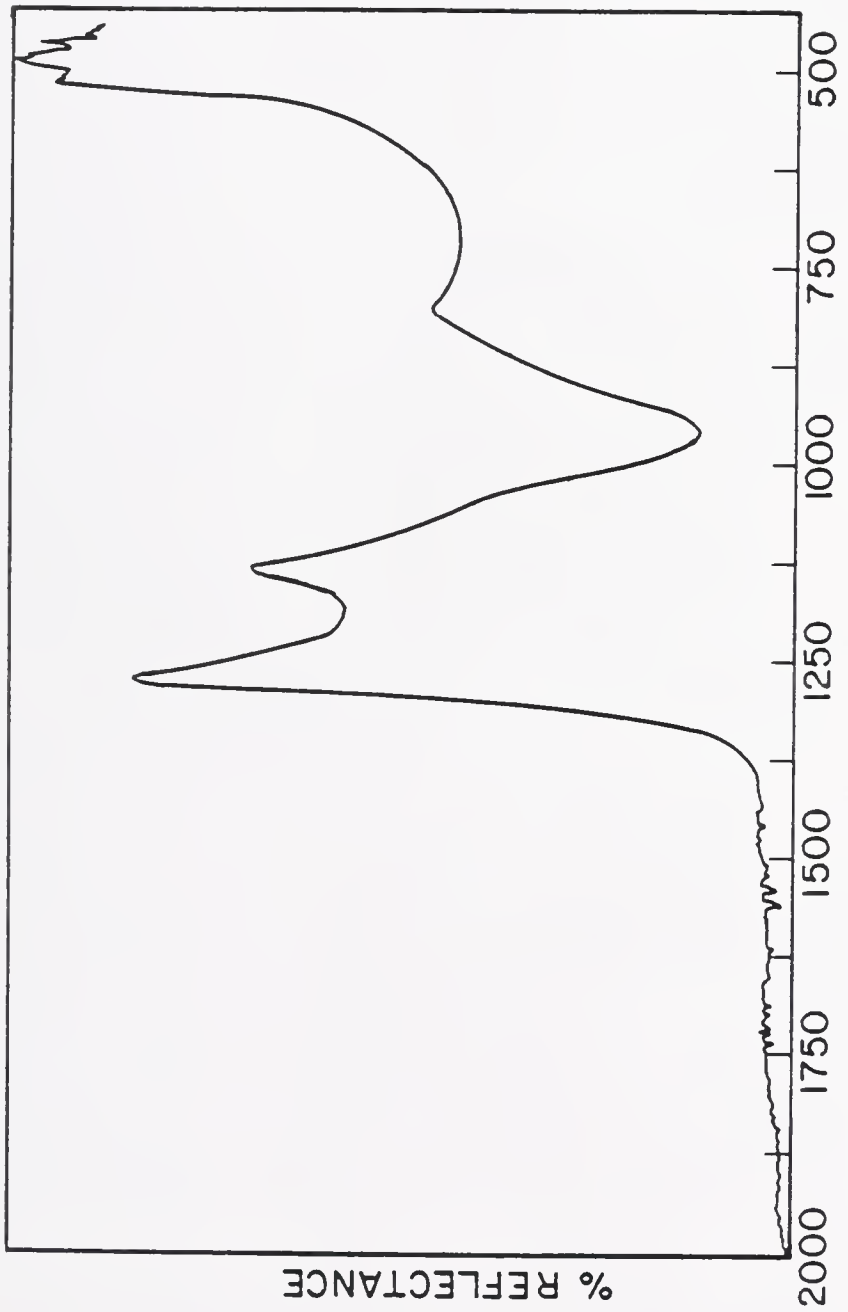

Fig.IV-26. FT-IR Spectrum of NC After 26 hrs. of Exposure in Air at 1100°C

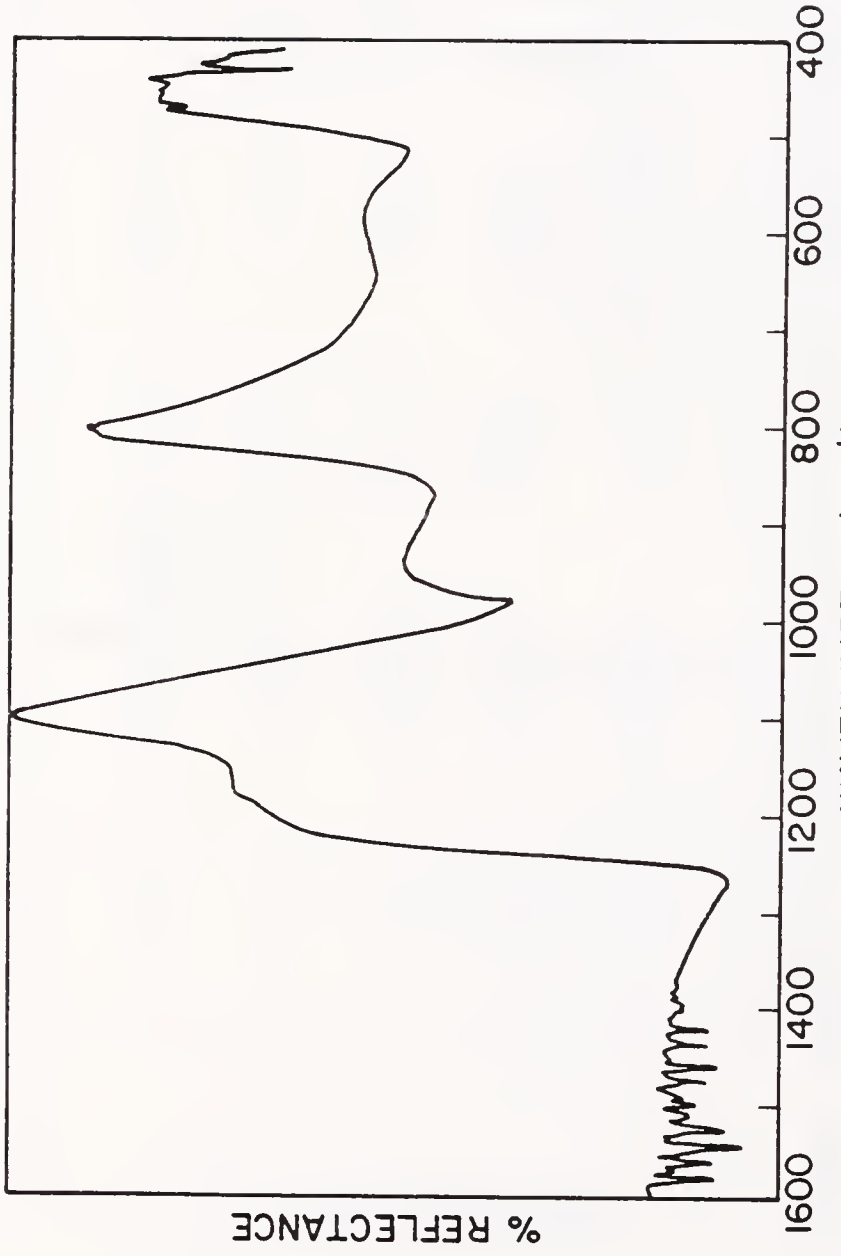

Fig.IV-27. FT-IR Spectrum of SC After Drying at 80°C in Air

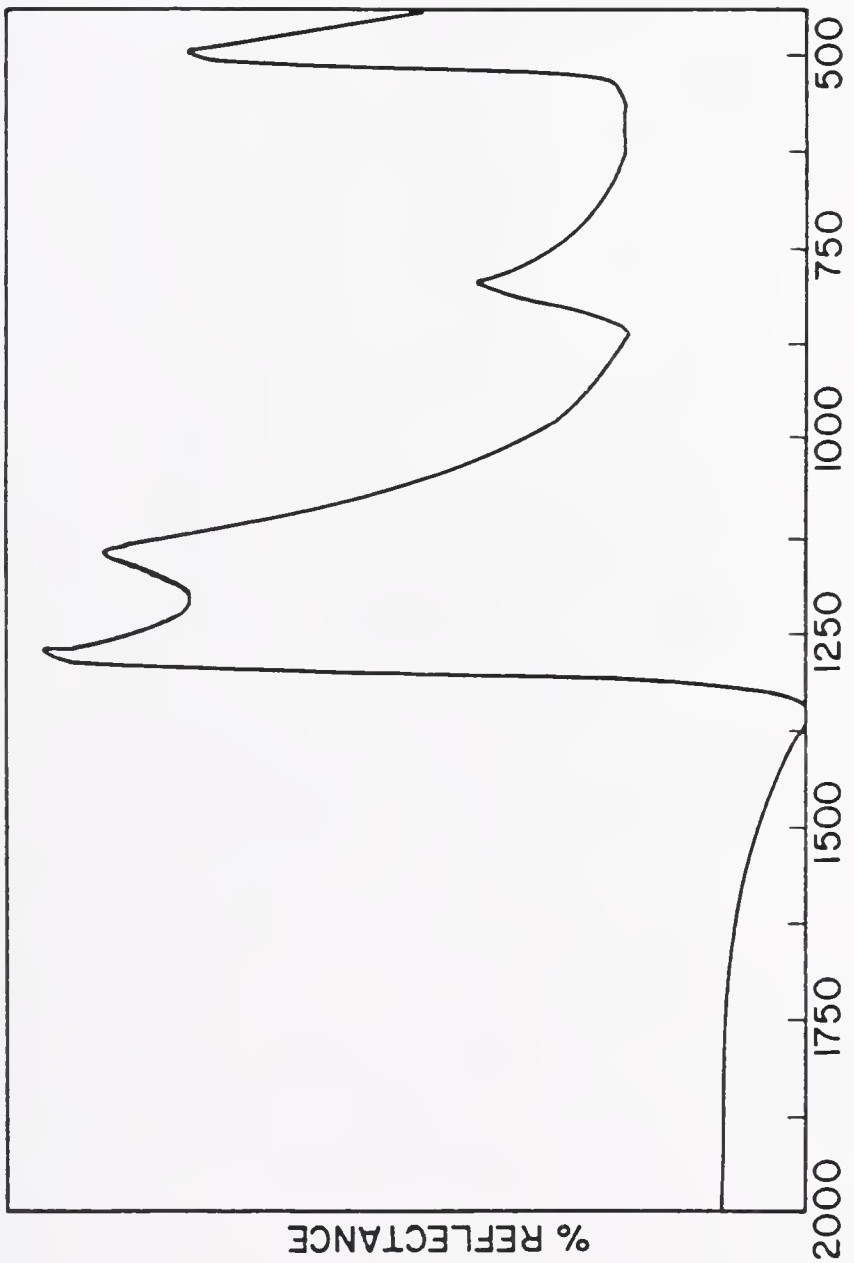

Fig.IV-28. FT-IR Spectrum of SC After 26 hrs. of Heating in Static Air at 1100°C

Table IV-8. Summary of FT-IR Spectra for a Sequential Oxidation of SiC and SiC/Sol-Gel Derived SiO_2 Composite in Dry Static Air at 1100°C, ~55 v/o SiC, ~25 v/o SiO_2.

Exposure Time, hr	$\bar{\nu}_x$, cm^{-1}	R_x	$\bar{\nu}_g$, cm^{-1}	R_g	$\bar{\nu}_c$, cm^{-1}	R_c	R_x/R_g	R_c/R_g
Nicalon® (β-SiC) Composite								
0	1167	0.004	1086	0.10	789	0.072	0.04	0.72
5	1257	0.22	1114	0.15	800	0.14	1.44	1.0
10	1260	0.14	1118	0.30	798	0.14	0.47	0.53
16	1265	0.49	1120	0.31	794	0.10	2.0	0.78
Raw Nicalon® (β-SiC) Particulate								
0	undetectable				790	0.1	0	∞
11	1256	0.075	1104	0.16	798	0.069	0.47	0.43
26	1260	0.15	1112	0.17	816	0.10	0.88	0.59
Silar™ (α-SiC) Composite								
0	1126	0.01	1087	0.13	792	0.15	0.08	1.16
5	1246	0.17	1126	0.15	790	0.20	1.13	1.37
10	1250	0.34	1124	0.22	788	0.38	1.55	1.72
16	1256	0.27	1126	0.14	788	0.21	1.93	1.50
26	1260	0.31	1126	0.11	786	0.17	2.82	1.55
Raw Silar™ (α-SiC) Whisker								
0	1259	0.029	1152	0.038	805	0.293	>0.77	>7.7
11	1282	0.054	1156	0.015	806	0.423	>3.6	28
26	1248	0.142	1144	<0.01	764	0.249	>14	>25

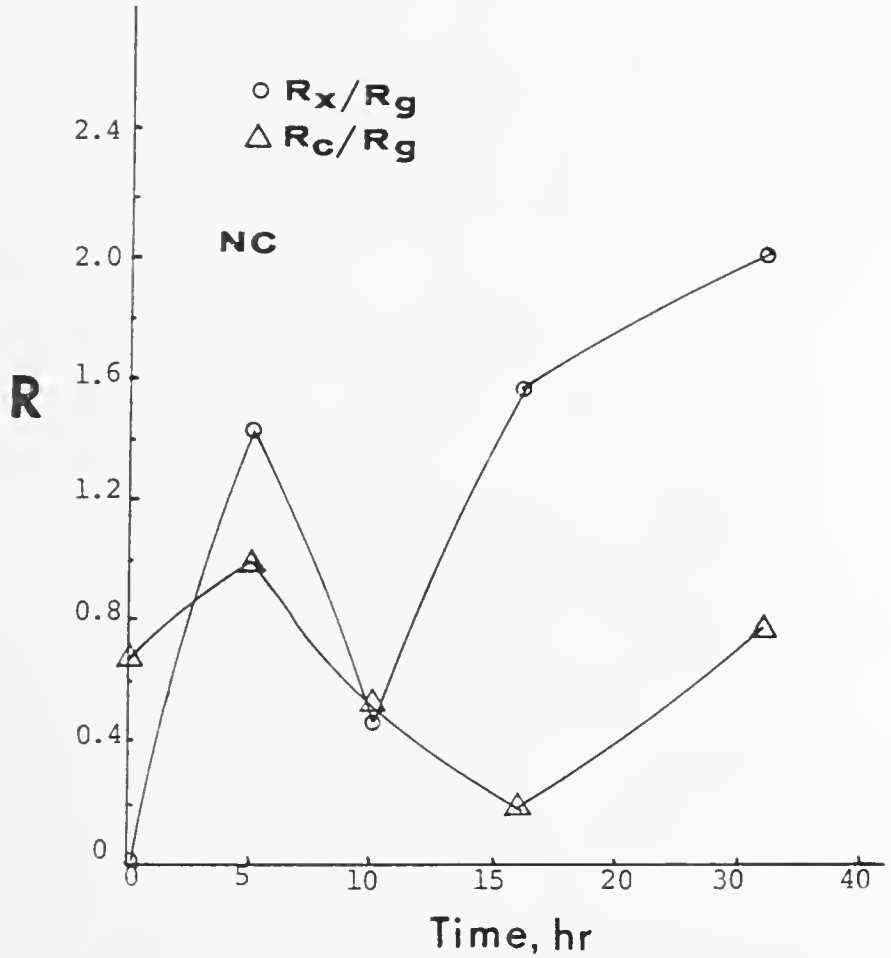

Fig.IV-29. FT-IR Rflectance of NC As a Function of the Exposure Time in Air at 1100°C for a Carbide and a Cristobalite

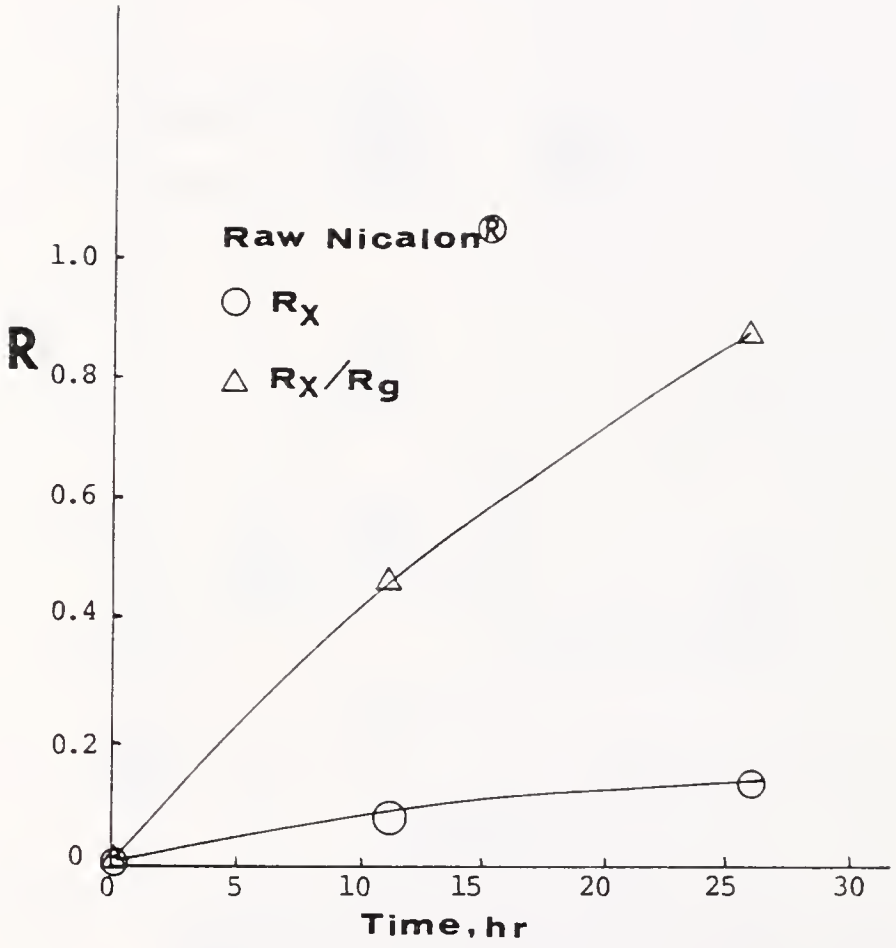

Fig.IV-30. FT-IR Reflectance of Raw Nicalon As a Function of Time Under Oxidative Exposure at 1100°C in Air

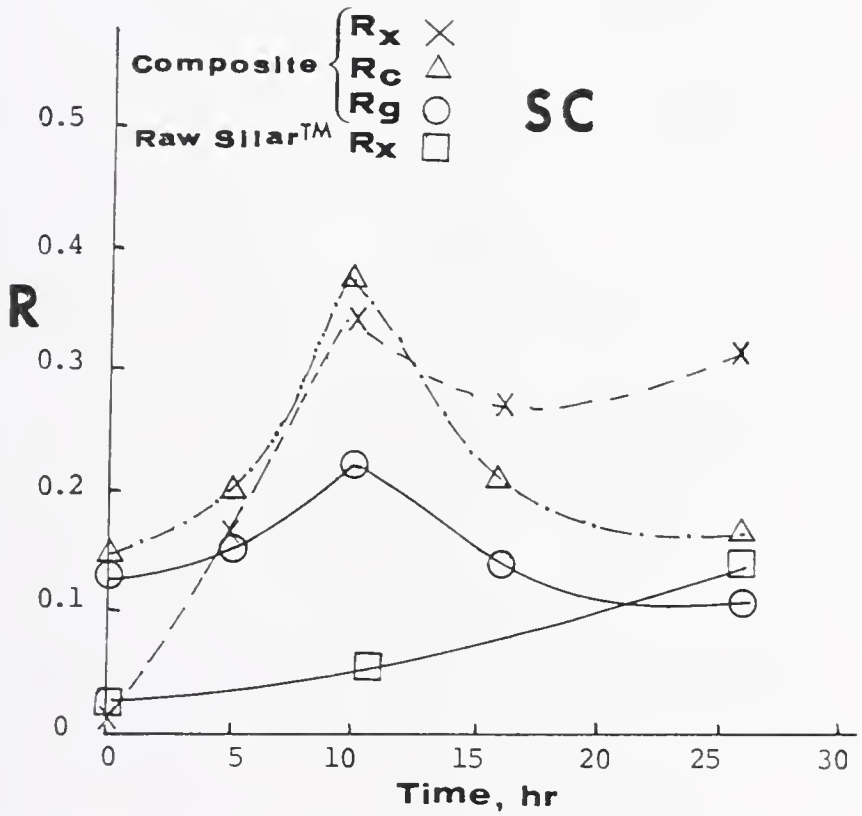

Fig.IV-31. FT-IR Reflectance of Silar™/SiO_2 Composite and Raw Silar™ As a Function of Time Under Oxidative Exposure

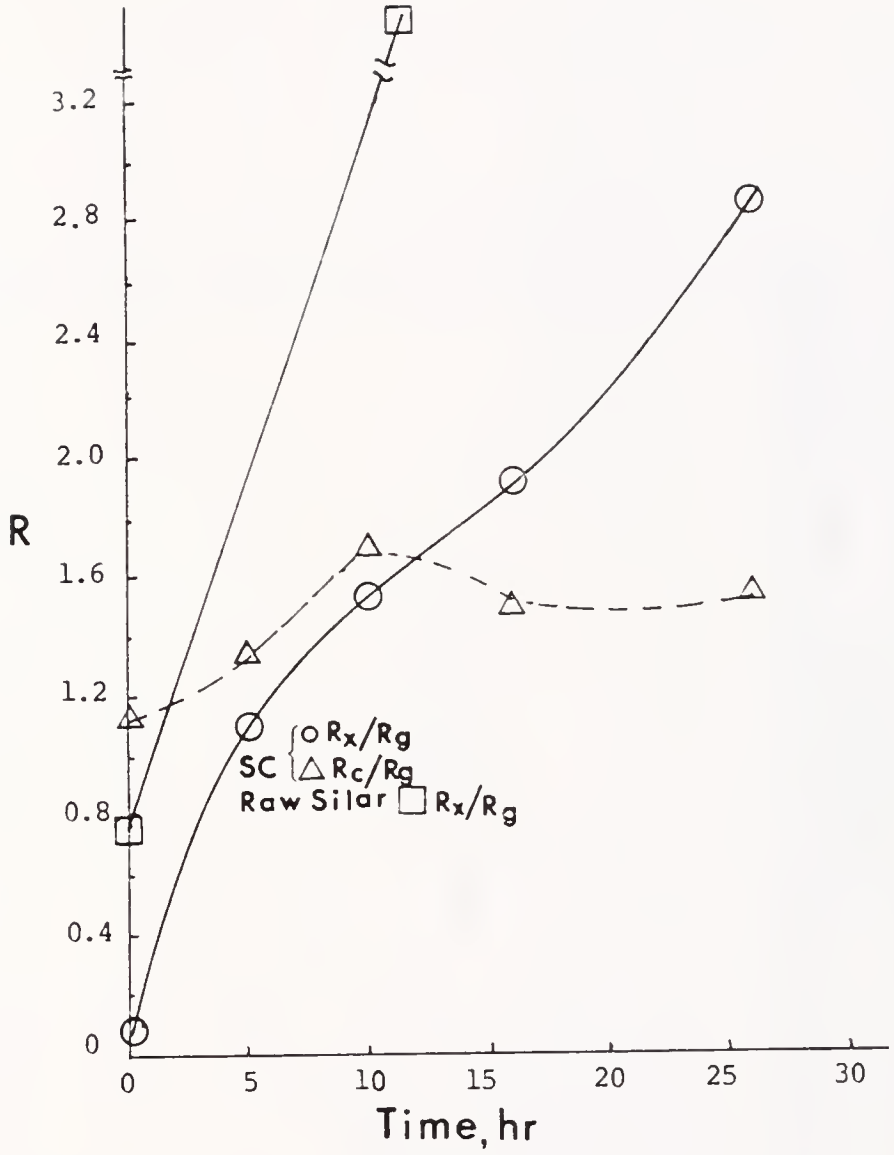

Fig.IV-32. FT-IR Reflectance of Silar™/SiO_2 Composite and Raw Silar™ As a Function of Time Under Oxidative Exposure, After Normalization

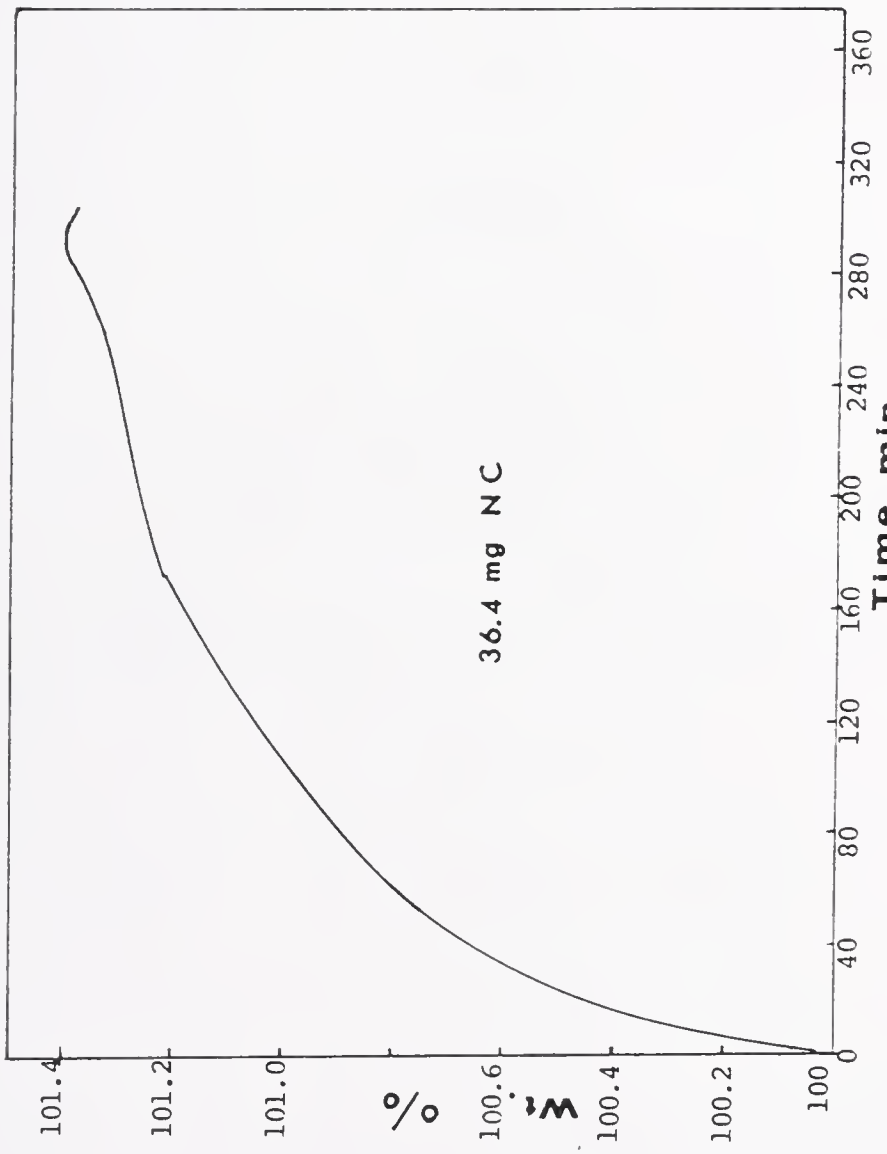

Fig.IV-33. Isothermal TGA for NC Exposed in Dry O_2 at 100°C With ~10 ml/sec Flow Rate

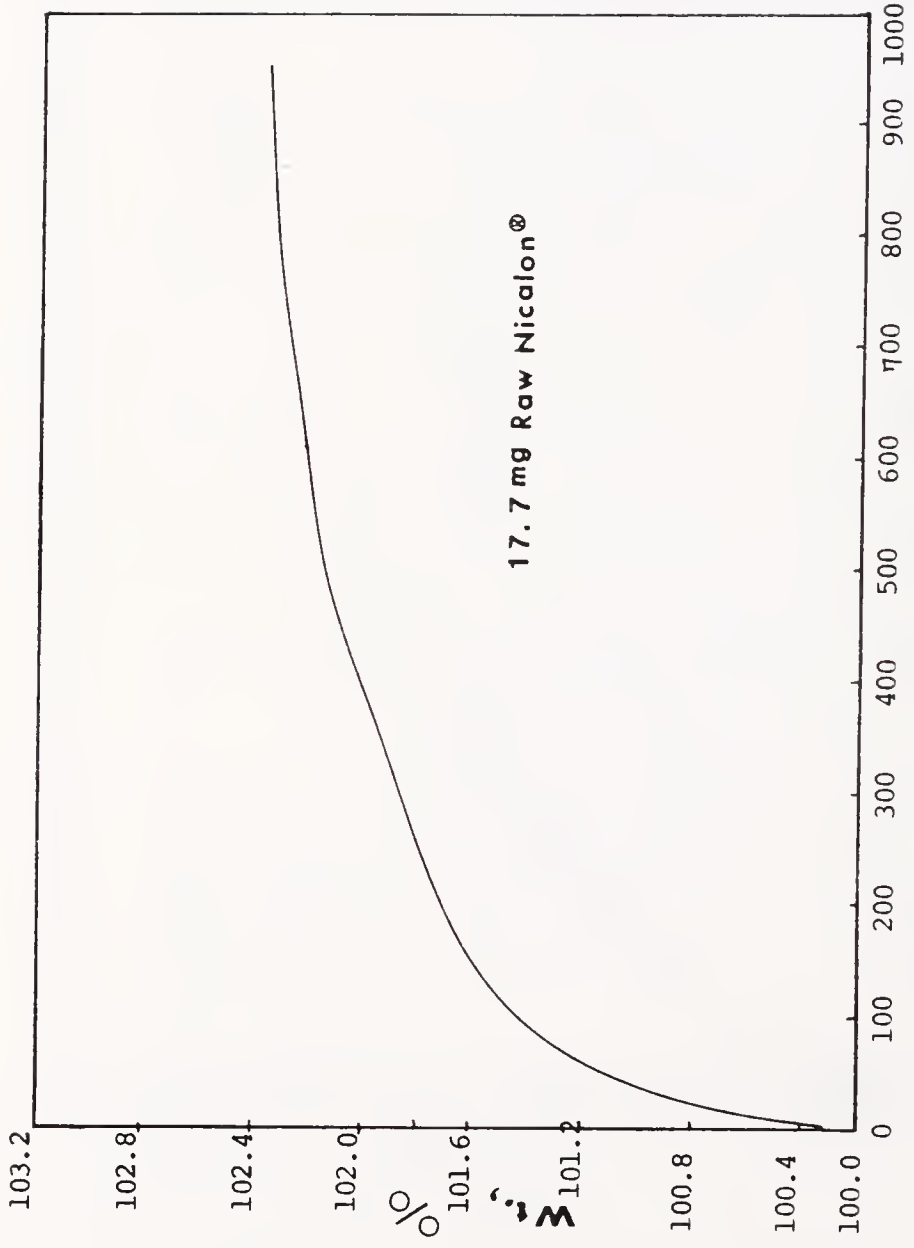

Fig.IV-34. Isothermal TGA for Raw Nicalon® in Dry O_2 at 1000°C With ~10 ml/sec Flow Rate

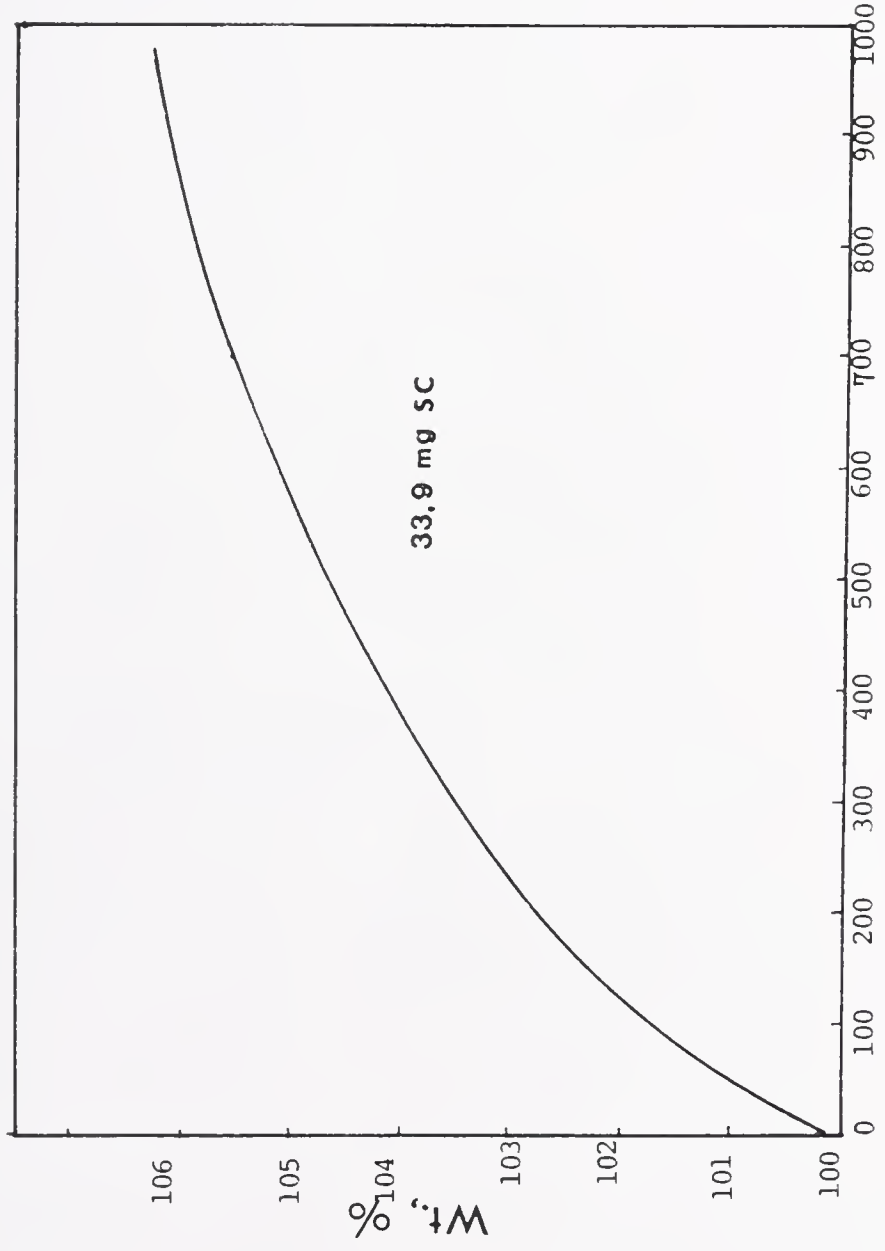

Fig.IV-35. Isothermal TGA for SC in Dry O_2 at 1000°C With ~10 ml/sec Flow Rate

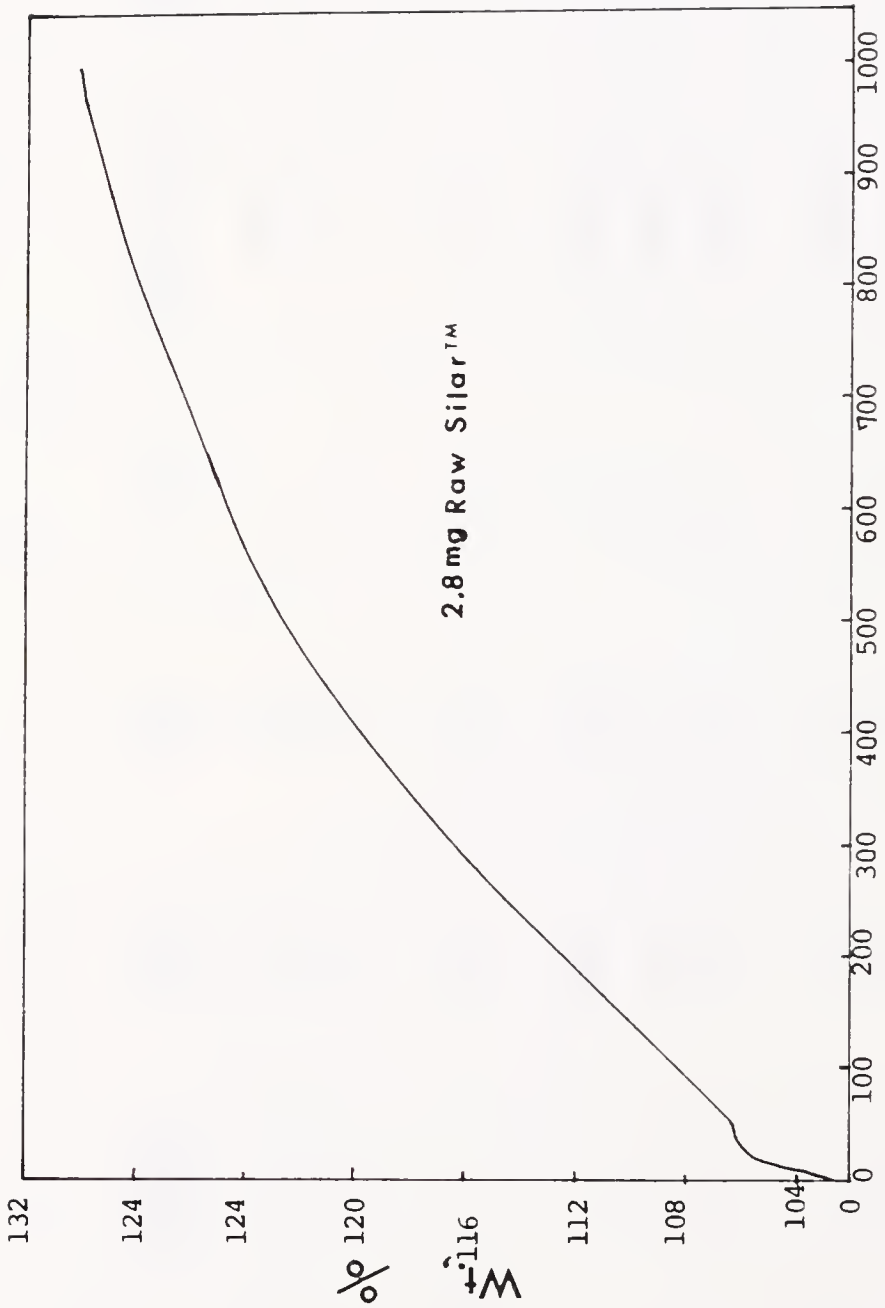

Fig.IV-36. Isothermal TGA of Raw Silar™ in Dry O_2 at 1000°C with ~10 ml/sec Flow Rate

Table IV-9. Isothermal TGA for SiC and SiC/SiO_2 Composite at 1000°C in Dry O_2.

Sample	Exposure Time, Hr	Initial Wt %	Final Wt %	Δ (w/o)	Initial Sample Wt (g)	Δ (w/o) / Sample Wt (g)
Raw Nicalon	5	100.2	102.4	1.7	0.01767	96
	16	100.2	102.4	2.2	0.01767	125
Nicalon/SiO_2	5	93.0	94.4	1.4	0.03641	39
Raw Silar	5	102	93.6	3.5	0.00281	4982
	12	102	127	25	0.00281	8996
	17	102	130	28	0.00281	9964
Silar/SiO_2	5	90.1	93.6	3.5	0.03392	103
	12	90.1	95.7	5.6	0.03392	165

A heat treatment of the composites up to 1500°C in air showed no visible change in shape or physical state. However, heating the composite bodies in vacuum (~10^{-2} torr) at 1400°C resulted in a disintegration of the composite body and an evolved gas resembling H_2S. This must have been caused by some type of chemcial reactions between the two phases which has been noted in Chapter III.

Discussion

Several differences between the fibrous SiC Nicalon® and Silar™ can be listed:

1. phase: Nicalon®; β-SiC
   Silar™; α-SiC
2. dimension: Nicalon® is ~10 times greater in diameter and length
3. crystalline form: Nicalon® is polycrystalline fiber
   Silar™ is single crystal whisker

Extremely large particle sized SiC phases i.e. continuous fibers and weaves as shown in Fig. IV-2 showed much lower density and strength in cast NC. Fracture energy, however, is expected to be higher as shown in Fig. IV-16.

The polyvinyl acetate sizing on Nicalon® could be removed by heating in air at ~350°C as shown in Figs. IV-5 and IV-6. As shown in Fig. IV-6, heating the fiber in air above ~700°C caused weight gain by SiO_2 formation.

Shrinkage due to heating begins at ~200°C and accelerated above ~700°C (Figs. IV-7 and IV-8). At 700°C ~10 μm linear shrinkage is shown

for both NC and SC. Greater slope for SC after drying at 80°C is shown. Considering the initial sample sizes, NC shows a greater densification rate of 0.48% linear shrinkage vs. 0.26% linear shrinkage of SC in ten hours. This must be partly due to the greater initial density of NC indicative of better compaction of Nicalon® and suggests a better compatibility between the silica sol and the Nicalon® fiber phase than that between the Silar whiskers and the matrix. This agrees with the results in Fig. IV-9.

The three-point flexural strengths given in Table IV-1 indicate that there is general agreement among σ_{flex}, ρ, and hardness. However the large variations in σ_{flex} from sample to sample are probably due to the number of variables involved in the sample preparation; 1) particle size and degree of agglomeration, 2) sol concentration and wettability of the sol, and 3) the amount of surface oxide on the starting SiC. Infiltrations of SiC precursor polymers in the porous composite bodies result in a little increase in σ_{flex} (Table IV-2) and K_{IC} (Table IV-7). The density values suggest that very little silane is infiltrated under the conditions used.

A linear type of relationship between σ_{flex} and ρ is shown in Fig. IV-12. This means that one may need only density measurements to predict flexural strengths. Extrapolations based on the Fig. IV-12, assuming a theoretical density of the composites of 60 vol% SiC:2.4 g/cc for NC and 2.8 g/cc for SC, result in a theoretical σ_{flex} of 244 MPa for NC and 425 MPa for SC. These maximum theoretical values are still lower than the experimental σ_{flex} of ~700 MPa obtained by Prewo and Brennan[92]

by hot pressing borosilicate glass and continuous unidirectional Nicalon fibers. This shows the difference between random fiber orientation and uniaxial fiber orientation in σ_{flex}. In the uniaxial fiber composites, the fiber length to diameter ratio, R = ∞. The fact that a SC gives much greater σ_{flex} must be attributed to the R values, R ≈ 3 for NC and R ≈ 10 for SC. This supports the theory[105] that the reinforcement effect of a composite is a function of the "aspect ratio," R. This is consistent with results of Sambell et al.[88,114] for carbon fiber/glass matrices composites.

No attempts, other than incorporating unidirectional continuous fiber, were made to orient the chopped fiber in the SiO_2 matrix. The resulting composites are thus expected to have randomly oriented fibers and are treated as being isotropic. The volume fraction of SiC was kept at a constant level of ~60 v/o for cast composites and ~70 v/o for pressed composites. Variations in SiC loading were limited by the inherent porous matrix of gel derived silica and monolithicity of the composite body. The former limits the SiC volume loading toward a lower level and the latter tends toward higher volume loading. This forces the SiC loading to be at approximately a constant level (~60 v/o) of the saturation to maintain monolithicity.

Based on a small number of specimens used for a testing of thermal shock resistance of the composites, both NC and SC have good thermal shock resistance between 800°C and room temperature.

Figure IV-9 shows that heating the composites at atmospheric pressure up to 1400°C in a reducing atmosphere did not yield the theoretical

density. This imposes a major problem in densifying the composites. Heating the composites in water vapor may hasten the densification process but oxidation of SiC by the water may be a problem. A vacuum heating to 1400°C was shown to be detrimental to these composites by disintegrating the composites. This is thought to be a result of chemical reaction between SiO_2 and SiC according to Eq. IV-7.[67,77]

$$2\ SiO_2(S) + SiC(S) \rightleftarrows 3\ SiO(g) + CO(g) \quad \Delta G = -70\ Kcal/mole \qquad (IV\text{-}7)$$

This is probably the main cause of the "cracker effect" observed for the organosilane/SiO_2 gel composites in Chapter III as well.

Silicon carbide ceramics have modest fracture toughness, expressed by the critical stress-intensity factor, K_{IC} : ~3 $MPa \cdot m^{1/2}$.[115,116] The NC and SC, however, have K_{IC} values as high as ~8 $MPa \cdot m^{1/2}$ for SC and ~6 $MPa \cdot m^{1/2}$ for NC (Table IV-6). These are remarkably high toughness values considering the modest σ_{flex} of these composites. This high toughness must be attributed to the action of yielding fibers which bridged the crack surface. This is evidenced in the load vs. displacement curves in Figs. IV-14.

Among the various mechanical properties, fracture toughness as expressed by K_{IC} is considered as important a parameter in design consideration as the various strengths. This parameter provides a measure of tolerance of the material to presence of discontinuities. In some applications, the fracture toughness is even more important than strength. The fracture toughness relates to fracture strength, impact resistance, and thermal shock and fatigue behavior.[117] This implies that NC and SC are potential candidates for heat-engine materials.

The generally lower mechanical properties of cold pressed NC than those of cold pressed SC are attributed to the lower length to diameter of fiber ratio (R).[112] For Nicalon® R ≈ 3 and R ≈ 10 for Silar™.

Figure IV-14 shows increases of fracture energy represented by the area under the curves by silane impregnation into SC and into uniaxially laminated NC. The initial sharp increase of load must be attributed to the elastic behavior of the composites. Until the crack is propagated to the fiber, no load increase is shown. This is the stage of the weak matrix cracking. Then the sharp increase in load is the stage of fiber controlled crack propagation and finally to failure.

Composites fired at 1400°C show a typical load vs. crosshead displacement of a brittle material. The toughness curves shown in Fig. IV-16 are essentially the same as those for flexural strength (Fig. IV-15).

One of factor listed as important in mechanical properties of fiber reinforced ceramic matrix composites is the interfacial bonding between the fiber and the matrix.[107] As a result of chemical reactions between the fiber and the matrix, the bond strength between the two phases can be increased and this can cause fiber degradation. Rice et al.[107] have shown that this fiber-matrix interaction can be controlled by a third chemical reagent as an additive to the matrix or as fiber coatings. Characterization of fibers, matrix, and fiber-matrix interactions thus requires microanalytical techniques because the scale over the critical processes occur is quite small; 2-3 μm across the interface.

Figure IV-17 shows NC after 80°C drying. The 59,000X TEM micrograph reveals that the particle-like gel matrix has a distinct interface

with Nicalon® fiber. It shows no matrix-fiber interaction at 80°C. The STEM micrograph at 300X, however, shows debondings or cracks in the interfaces. These cracks must have developed during the thinning processes. This means that the bond between fiber and matrix is relatively weak in cast SiC/SiO_2 composites. The composite after heating to 900°C in nitrogen shows the gel matrix is no longer particle-like as shown in Fig. IV-18 at 50KX. The interface is certainly less distinct than the composite at 80°C. This may be an indication of the fiber matrix interaction. At 1KX, cracks in the matrix are still present.

Figure IV-19 shows a SC sample after 80°C drying. The TEM micrographs at 50KX shows a random orientation of Silar™ whiskers bonded by SiO_2 gel matrix with a distinct interfacial boundary. This is also shown by the micrograph at 200KX. After 900°C heating, the extension of the matrix into the whisker is not clear (Fig. IV-20). The whiskers show a distinct columnar subgrain structure representing crytallographic misorientations. This kind of planar stacking disorder is common in SiC, partly because of the very low stacking fault energy {0001} of α planes.[118] Corresponding selected area diffraction patterns exhibit spotty rings for the α-SiC single crystal.

The as cast surface of NC after a 1100°C heat treatment, Fig. IV-21, shows the random orientation and distribution of the fibers in the SiO_2 matrix. Figure IV-22 shows that the fibers and Silar™ whiskers are well bonded by the gel matrix after drying.

Scanning electron micrographs of fractured surfaces of NC with unidirectional and random chopped fibers show fiber-pull-out as indicated

by the rough surfaces. This either disagrees with the work of Bender et al.[119] or an extensive matrix-fiber interaction may not occur at temperatures below ~1200°C. This may be another advantage of forming a SiC/SiO_2 composite via sol-gel process. In the work of Bender et al.,[119] they used hot-pressing to form Nicalon®/SiO_2 composite at temperatures well above 1300°C. At this temperature, the fiber-matrix interaction is expected to be quite extensive resulting in a significant reduction of mechanical properties.[119]

Rather large scattering of data points are seen in Table IV-1, Figs. IV-9, IV-10, IV-11, and IV-12. This is caused by the difficulty of using one identical sample throughout the thermal treatments as well as the characterization steps. Even each composite sample prepared under identical experimental conditions tended to be different after an identical thermal history. This is because there are other variables present such as nonuniform property and distribution of the starting materials, uneven distribution of flaws, impurities, etc. which affect the properties.

As given in Table IV-1 and shown in Fig. IV-37, the mean σ_{flex} after treatment at 900°C in N_2 for four hours is 92 ± 26 MPa for SC and 31 ± 6 MPa for NC. Under same condition but in air, σ_{flex} is 80 ± 23 MPa for SC and 27 ± 5 MPa for NC. Both NC and SC exhibited ~14% and ~13% reduction respectively in the strength by the oxidative exposure. However, within the uncertainty range, this reduction in strength may not be significant. Clark et al.[120] showed a reduction of Nicalon® tensile strength from ~1900 MPa to ~850 MPa after treatment at 1000°C in

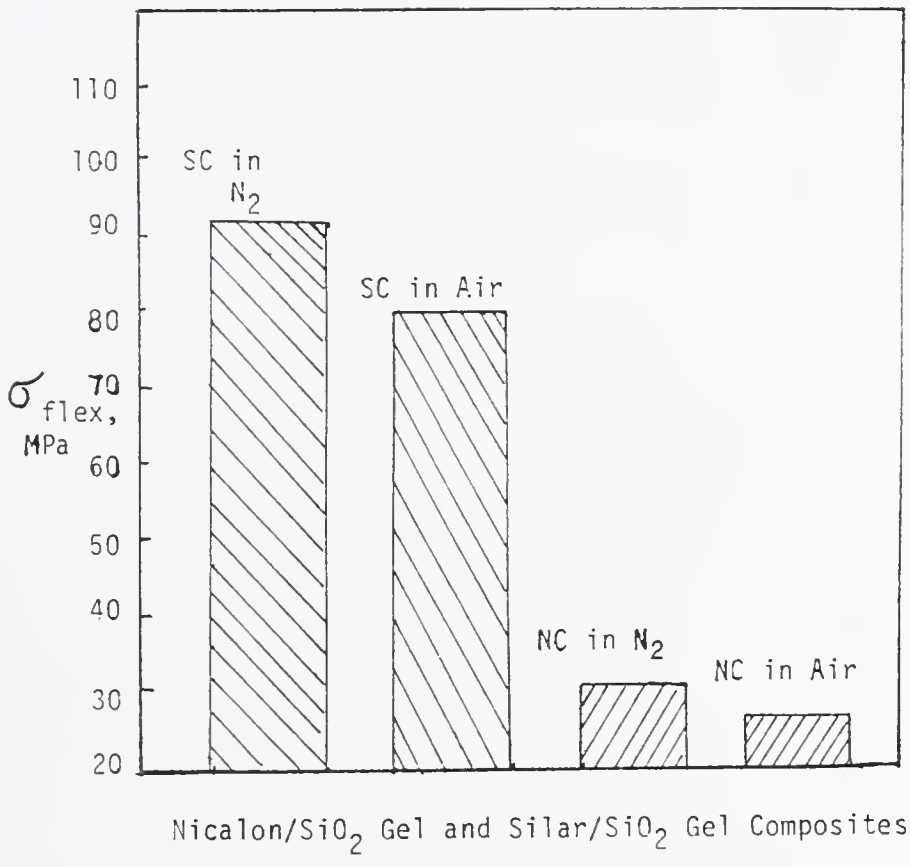

Fig.IV-37. Flexural Strengths of SC and NC After Exposed to Air or Nitrogen at 900°C for 5 hours.

wet air for twelve hours. This ~80% reduction in strength may not be used in direct comparison with NC because of the differences in the experimental conditions and the nature of the sample. NC was heated in dry air at 900°C for four hours while the Nicalon fiber of Clark et al.[120] was heated at 1000°C for twelve hours. Moreover, the testing method is tensile vs. bending. However, it may be inferred that Nicalon fibers in NC are more resistant to oxidation than the naked Nicalon fiber in a similar environment.

Figure IV-38 compares flexural strengths of NC and SC with some other ceramic composites of comparable composition fabricated by other investigators as given by the reference numbers. Comparisons here are based on the most recent literature and not necessarily on the highest values available in all the literature. The purpose of these comparisons is not to show the superiority of the NC and SC of this work over other composites of similar composition but to show that NC and SC are not inferior or, rather, that they are comparable in some cases. These other ceramic composites were mostly fabricated by hot pressing technique. A direct comparison shows that SC and NC are generally inferior to other composites but superior to those of Gac et al.[78] and Wilson and Breit.[121]

The lower values for NC and SC are due to lower densities. When this is taken into account by calculating the σ_{flex}/ρ ratio, the values for NC and SC become comparable with other ceramic composites as shown in Fig. IV-39. Figure IV-39 compares the ratio of flexural strength to density of NC and SC with various other reinforced ceramic composites by

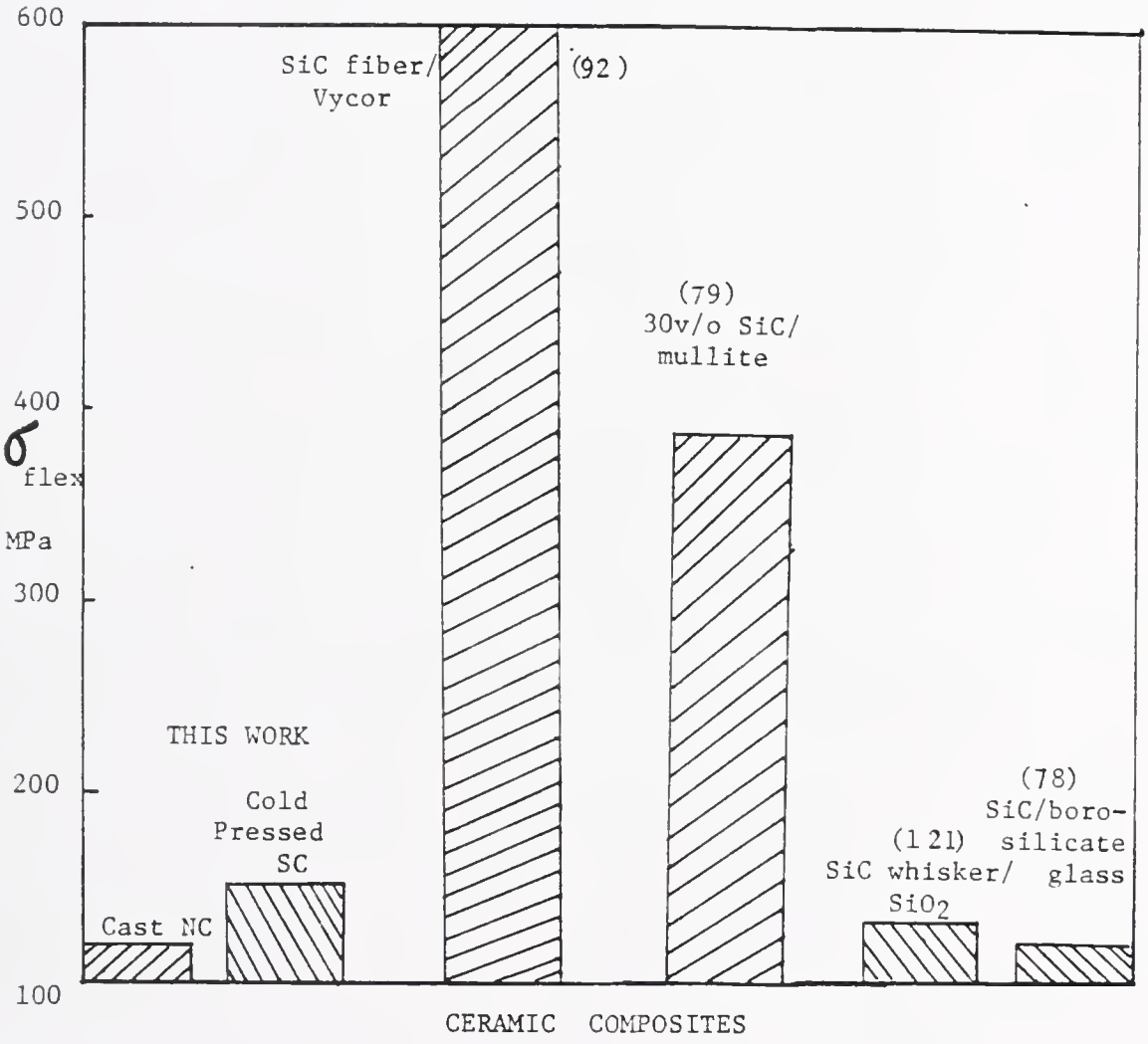

Fig.IV-38. Flexural Strengths of NC and SC as Compared with Some Other Ceramic Matrix Composites

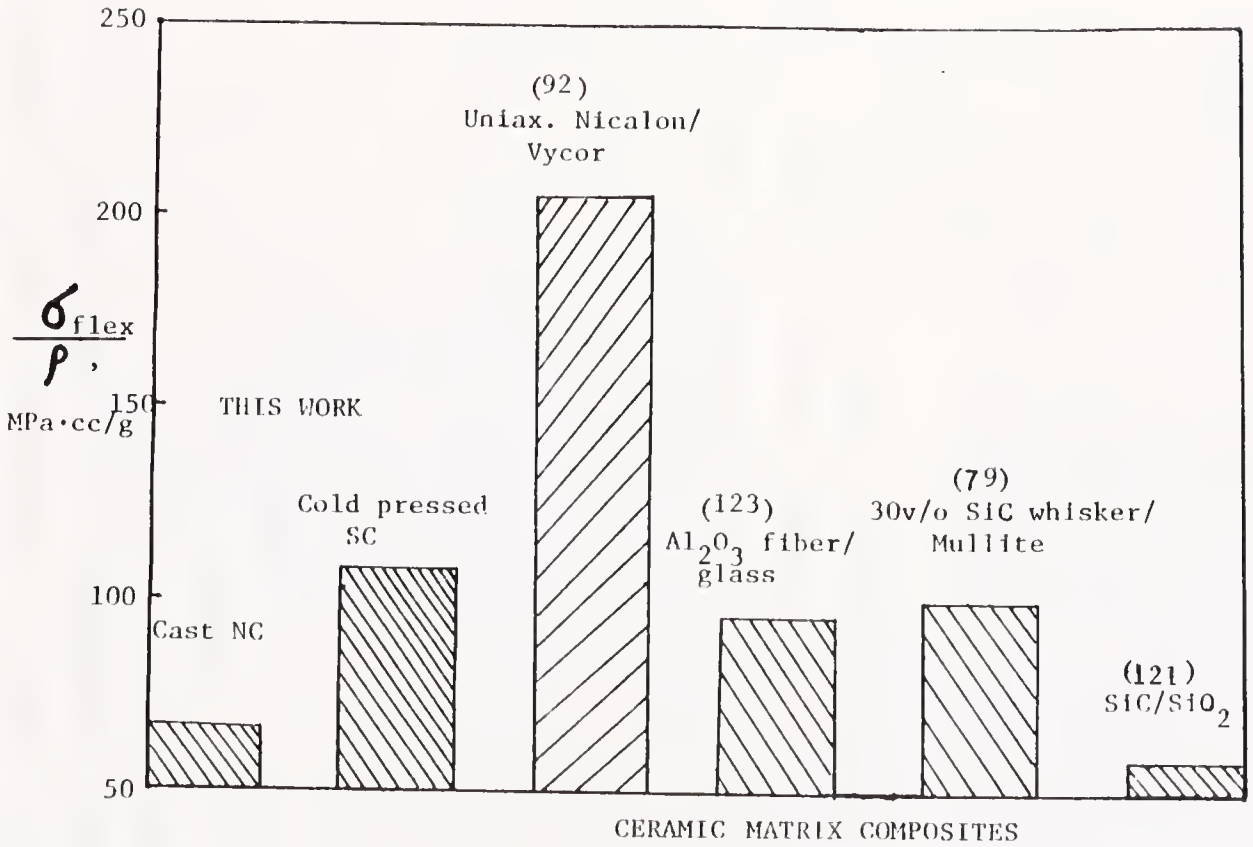

Fig.IV-39. Strength to Density Ratios of NC and SC as Compared With Other Ceramic Composites

other investigators as given by the reference numbers. Cast or cold-pressed NC and SC of this work are comparable with other composites of similar composition fabricated by hot pressing technique. The Nicalon®/Vycor® composites of Prewo and Brennan[92] show exceptionally high σ_{flex}/ρ. This exceptional property is, in part, resulted from the uniaxial orientation of continuous Nicalon fiber and two-step process i.e. preform the composite using wet traditional ceramic processing then hot pressing. Lange et al.[82] showed 1340 MPa in σ_{flex} value for their ZrO_2/Al_2O_3 in a four step process. On the other hand, NC and SC were fabricated in a one step process.

Figure IV-40 compares K_{IC} values of NC and SC (Table IV-6) with other comparable composites. Fracture toughness of values of NC and SC compare well with those of other composites. The K_{IC} of NC and SC are generally superior to the other composites with exception of those of Prewo and Brennan[91] and Rice[123] for SiC fiber/glass matrix composites. The SiC fibers in these exceptional composites were unidirectionally preformed followed by hot pressing procedure while NC and SC are randomly oriented short fibers and whiskers without hot pressing. Even more exciting comparison of NC and SC with other ceramic composites for the ratio of K_{IC} to density is shown in Fig. IV-41.

It has now been shown that mechanical properties of NC and SC are comparable or superior to many other "the state-of-the-art" ceramic composites of similar composition made by more conventional, tedious, and restricted techniques. Moreover, fabrication of SiC using sol-gel technique still has a room for improvements as discussed previously.

The composites NC and SC upon heating at 1100°C in air caused the oxidation of SiC as shown in Figs. IV-24 through IV-28. At 1100°C, both

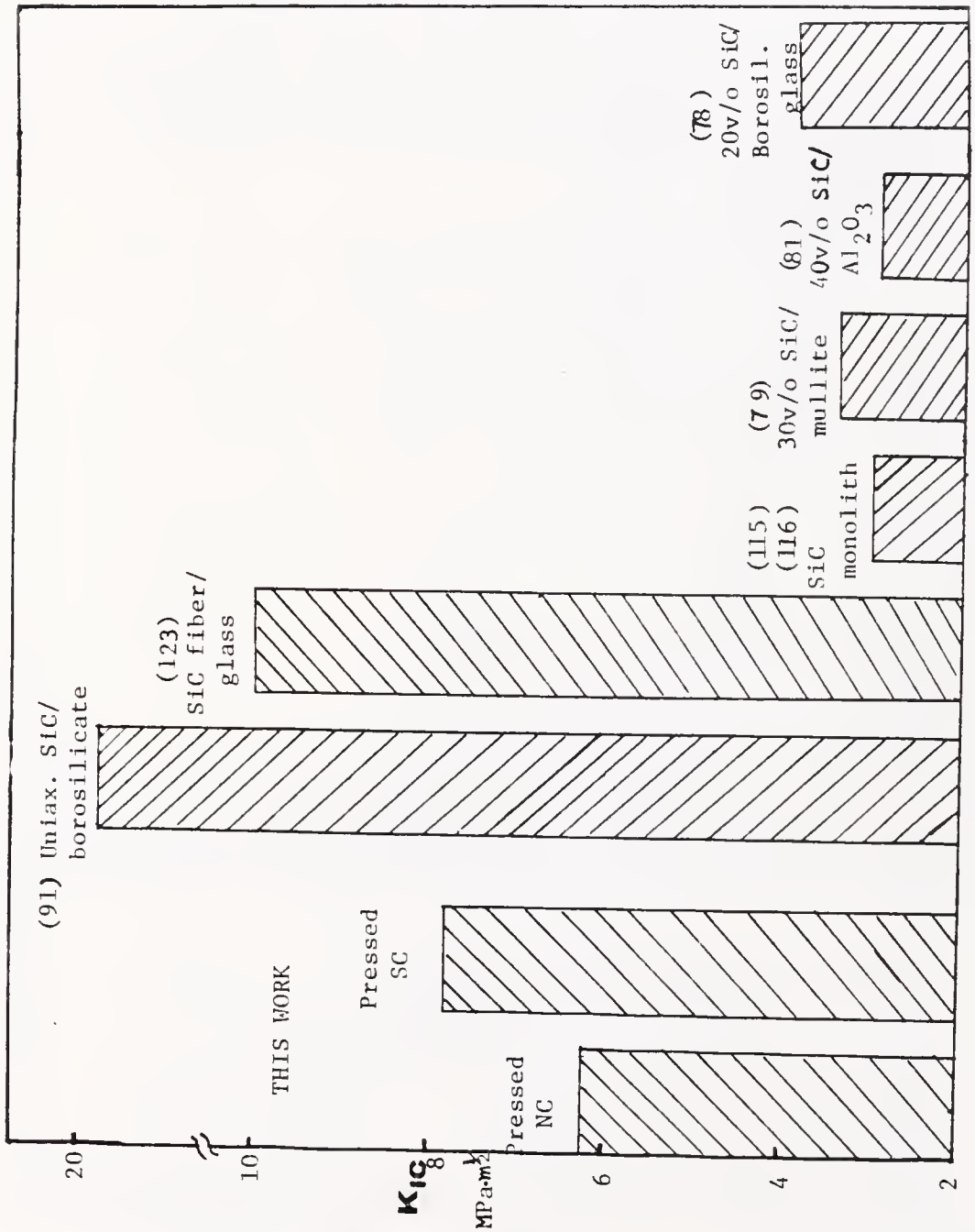

Fig.IV-40. Fracture Toughness of NC and SC as Compared With Other Ceramic Composites

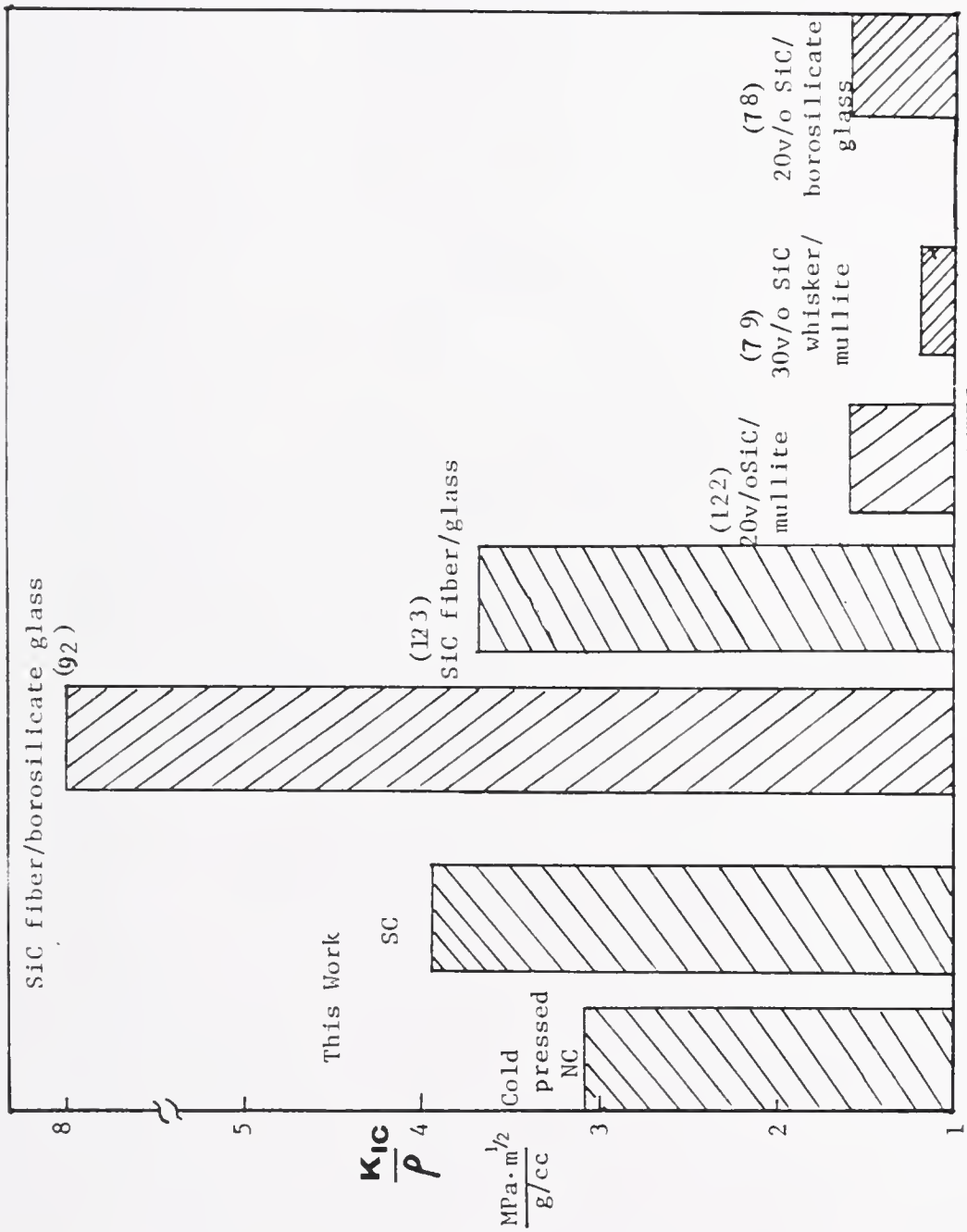

Fig.IV-41. Fracture Toughness to Density Ratios of NC and SC as Compared with Other Ceramic Matrix Composites

the vitreous SiO_2 and cristobalite can be formed as products of SiC oxidation. Cristobalite formation rapidly progressed as indicated by a reflection band at ~1170 cm^{-1} (R_x) for both β-SiC (Nicalon) and α-SiC (Silar). Figures IV-29 through IV-32 illustrate this phenomenon more vividly.

A large amount of vitreous SiO_2 matrix in the composite should suppress the forward reaction of the oxidation, $\alpha\text{-SiC} \xrightarrow[O_2]{1100^0C}$ vitreous SiO_2. As a result, formation of cristobalite over vitreous SiO_2 predominates. This was supported by an XRD analysis of the heat treated composites.

For Nicalon® (β-SiC) in silica matrix, the rate of cristobalite formation, which is a direct result of oxidation of SiC at 1100°C, rapidly increased up to ~5 hours then decreased up to ~10 hours (Fig. IV-29). The rate increased again after ~10 hours and slowed down after ~15 hours. On the other hand, the raw Nicalon (no matrix) showed a continuous increase of the rate of cristobalite formation.

A similar but less dramatic behavior is shown for the Silar™ (α-SiC) composite. Silica crystal formation rate for the raw Silar™ continued to increase, however (Figs. IV-31 and IV-32).

These complex oxidation rates of SiC may be explained by works of Pampuch and coworkers.[124,125] They showed a growth of a ternary intermediate species Si-O-C which could not be etched by HF.

In Nicalon/SiO_2 composite, a rapid increase of R_x/R_g with time up to ~5 hours may be an indicative of the initial oxidation of SiC. As the SiO_2 film from the initial oxidation of SiC passivates or decrease

the oxidation rate, the reaction of SiC + SiO_2 to yield SiOC may take place after ~5 hours of an oxidative heat treatment of Nicalon/SiO_2 composite. In that case, the amount of SiO_2 and SiC would decrease as long as the reaction rate to give SiOC is appreciable. However after ~10 hours of oxidative exposure, the rate of SiO_2 growth increases and slows down after ~15 hours. This may be the period of a reaction

$$SiOC + O_2 \rightarrow SiO_2 + CO, \qquad \text{(IV-8)}$$

thus increasing R_x/R_g and decreasing R_c/R_g. The increase in R_c/R_g after ~15 hours, however, may be due to a development of microcracks in the matrix by evolution of gaseous products, e.g. CO, CO_2. This is also a cause of the continuous oxidation of SiC after ~20 hours, although at a slower rate.

The TGA data of SiC and the composites as given in Table IV-8 indicate that the weight gain due to SiO_2 formation per unit weight of sample is much smaller for SiC in a SiO_2 glass matrix than the raw SiC. In 5 hours, raw Nicalon® (β-SiC) gained more than twice the % wt than did the Nicalon fiber in a glass matrix. The Silar™ (α-SiC) whiskers in a glass matrix are nearly 50X more resistant to oxidation than raw Silar™ within 12 hours of oxidative heat treatment.

The R_x/R_g vs. time plot for Silar™ given in Fig. IV-32 does not show the downward curve as does Nicalon®. However the R_x/R_g values due to oxidation of Silar™ somewhat flattened between 10-15 hours of oxidative exposure. This may mean that the formation of the SiOC intermediate phase in Silar™ is not as extensive as in Nicalon. The period of SiOC also came somewhat later (~10 hours) in Silar™ than in Nicalon® (~5

hours). It appears that a little longer time is needed for Silar™ to be passivated than for Nicalon. This may be due to the greater SiO_2 content in as-received Nicalon® than in as-received Silar™.

Therefore, the ternary intermediate SiOC phase is formed between ~5-10 hours for Nicalon® and ~10-15 hours for Silar™ in porous SiO_2 glass matrix. However this SiOC is formation was not detected for raw SiC samples (Figs. IV-30 and IV-31). This can be explained by the physical properties of the SiC materials. Silar™ is a single crystal α-SiC with greater density (3.2 g/cm^3) of hexagonal crystal and greater purity, while Nicalon® is a microcrystalline β-SiC which has a cubic form with a density of 2.6 g/cm^3 and substantial amount of graphitic carbon, SiO_2, and Si as impurities. These impurities should act as oxygen scavengers hindering oxygen diffusion to reach SiC unlike aluminosilicates, where the aluminosilicate impurity increased the oxidation rate of hot-pressed SiC by enhancing oxygen diffusion.[126]

It appears that the ternary intermediate SiOC exists between SiC and SiO_2 interface[105] and unless the SiO_2 blocks oxygen diffusion completely, the reaction of $SiOC + O_2 \rightleftarrows SiO_2 + CO$ should continue until the SiO_2 film brings complete passivation. It seems more likely then that oxygen diffusion is the rate limiting step rather than CO removal.

The trend of deceleration of the oxidation rate of SiC in the gel derived glass matrix as shown in Figs. IV-29, IV-31, and IV-32 after ~5-10 hours has been explained by the formation of a SiOC ternary intermediate phase. This similar trend was also observed by Suzuki et al.[127] in their study of α-SiC oxidation. They observed a break in the curve

of increasing SiO_2 layer thickness after ~6 hours of oxidative exposure, but no explanation as to what caused the break was given. Lee[128] also has observed the similar trend of a break in the increasing oxidation of SiC with time in oxygen atmosphere, but he treated this anomaly as an artifact despite the repeated observations. Again a similar behavior of SiC oxidation in a gel derived alumina matrix was observed by LaTorre et al.[129] They also gave no explanation for this behavior.

Conclusion

Low density SiC/SiO_2 composites can be prepared easily by a sol-gel method without hot pressing. Complex shapes can be easily cast using SiC particles dispersed in the SiO_2 sol.

The ease of forming and fabrication, stability at high temperature with a moderate flexural strength, high fracture toughness and high hardness have been demonstrated. It was further demonstrated that NC and SC have attractive strength-to-weight ratios and even more attractive toughness-to-weight ratios, good oxidation resistance, and good thermal shock resistance, yielding a potential ability to withstand severe environment. Achieving the full density of the composites will undoubtedly improve the properties. Considering the low density of the composites tested ($\rho \approx 1.9$ g/cc), the toughness observed ($K_{IC} \approx 6$-8 $MPa \cdot m^{1/2}$) is truly remarkable. The K_{IC} of NC and SC is superior to many other ceramic composites and the K_{IC}/ρ values of NC and SC are superior to all but highly oriented hot-pressed samples.

The high porosity of NC and SC is due to the large inherent shrinkage in the silica gel matrix. The flexural strength was shown to be

directly related to the density of the composite body. The lower density and lower strengths of the Silar™ system indicate that the SiO_2 sol is less compatible with α-SiC Silar™ than with β-SiC Nicalon®. This must be because of the amorphous nature of Nicalon and the large amount of SiO_2 and graphite present in Nicalon®.

Although an improvement in density and strength can be achieved by multiple impregnation of SiO_2 sol into the micropores of the composite bodies by dipping, there is a limit on the improvement since the impregnation is confined to a the surface region after ~4 cycles.

Impregnation of the porous NC and SC with polysilanes, SiC precursors, followed by a pyrolysis show a little improvement in the flexural strength after each cycle.

Nicalon® and Silar™ SiC have less oxidation in air at 1100°C when SiC is incorporated in a sol-gel derived SiO_2 glass matrix than when raw SiC is exposed to same condition. The oxidation kinetics of SiC in SiO_2 matrix (ρ = 1.8 g/ml) after heating in air at 1100°C is 3-5 times slower than the pure SiC under same conditions. However due to the residual porosity, complete immunity of SiC oxidation in the matrix in the beginning was not observed.

Both Nicalon® and Silar™ in a SiO_2 porous glass matrix may be oxidized via formation of a ternary intermediate SiOC phase. The oxidation reaction mechanism of SiC in porous SiO_2 glass matrix appears to be complex and requires further work to understand completely. Silar™ (α-SiC) is more prone to oxidation than less pure Nicalon (β-SiC). This may be due to the larger surface area of Silar™ than Nicalon®.

In order to improve the oxidation resistance of SiC further, it is necessary to reduce the porosity of the composite and prevent matrix damage after a prolonged oxidative exposure at high temperatures.

Some immediate applications of this material may be in fusion power reactors. Silicon carbide material because of its low plasma contamination, low induced radioactivity, capability of high operation temperature, and relatively abundant raw material supply, may be a leading candidate in the plasma chamber of a fusion machine. A formed SiC/SiO_2 bulk composite may be used directly or as a metallic part coated with this composite. As mentioned in this chapter, coating of a material is expected to be as simple and easy as casting.

Another area of application may be in high temperature radomes. Requirements for high temperature radomes demand a material with a high toughness, good thermal shock resistance, high resistance to rain and sand erosion, and light weight. The composites described in this chapter should meet these requirements.

The high values of K_{IC}/ρ and/or σ_{flex}/ρ of these materials may be especially significant in space applications such as materials for advanced spacecrafts, space transport systems, and large scale antenna arrays, which require high thermal performance and light weight. The NC and SC should provide significant improvement in thermal stability and mechanical properties and be capable of in-space processing. It should be possible to control the elastic modulus and stiffness of such space structures and their damping capacity by varying the volume fraction of fibers or whiskers in the composites.

CHAPTER V
OTHER CHEMICALLY DERIVED CERAMIC COMPOSITES

Introduction

The advantages of chemically derived ceramics and composites have been presented in the previous chapters. In this chapter, processing of several other chemically derived ceramic composites of mullite fibers and gel derived silica, alumina powder and polysilastyrene, SiC/SiC composites of Nicalon® and Silar™ with polysilastyrene, and molecular composite powders of SiC/TiC and SiC/Al_2O_3 are presented.

The mullite fiber is commercially readily available as Nextel™‡ which is derived from a sol-gel process. A monolithic composite incorporating Nextel™ into a sol-gel derived silica matrix is attempted similar to the processing of the SiC/SiO_2 composite in decribed Chapter IV.

Using the processing techniques of SiC from PSS as described in Chapter II, it is anticipated that a SiC fiber/SiC matrix composite can be made. A successful fabrication of SiC/SiC composite should yield many desired properties.

Wei and Becher[115] were able to increase σ_{flex} from 500 MPa to 680 MPa and K_{IC} from 4 to 6 MPa$\cdot m^{1/2}$ by incorporating fine TiC particles into a SiC matrix followed by hot pressing at 2000°C. Yajima et al.[12] have obtained SiC/TiC powder by mixing their polycarbosilane with a $Ti(OR)_4$ followed by pyrolysis to above 1500°C. Hence, it is hoped to synthesize a SiC/TiC molecular composite powder using polysilastyrene to

‡ Manufactured and provided by 3M Company, St. Paul, MN.

demonstrate that the desired ceramic material can be obtained by chemical processing.

Silicon carbide/Al_2O_3 composites have been made by Wei and Becher[71] and by Cutler et al.[81] by hot pressing mixed powder of SiC and Al_2O_3. In this chapter, a novel way of synthesizing SiC/Al_2O_3 composite powder at the molecular level is demonstrated by mixing the precursors of SiC and Al_2O_3.

Experimental

Nextel™ 312 continuous fiber which has a mullite composition was provided by 3M Co. Nextel™ fibers were cut and stacked unidirectionally with a desired thickness in a rectangular plastic mold. The fiber stack was filled with silica sol as described in Chapter 4. After covering and sealing the mold, it was aged, dried, and infiltrated with the sol 4X as for Nicalon® composites in Chapter 4. After an appropriate heat treatment in air, density and flexural strengths were measured the same way as described for Nicalon® and Silar™ composites in Chapter 4.

Alumina/silicon carbide composites were prepared by mixing 3 g of Baikalox CR6* fine powder with 5 ml of 20 w/v PSS solution in benzene followed by cold pressing in the steel die as shown in Fig. IV-4. The cold pressed green bodies were pyrolyzed to convert PSS to SiC at 800°C.

Silicon carbide/silicon carbide composites were prepared by mixing 3 g of chopped Nicalon® or 3 g of Silar™ with 5 ml of 20 w/v PSS solution in benzene and cold pressing as above.

---

* α-Al_2O_3 with 1 μm particle size by Baikowski International.

A molecular composite of SiC/TiC powder was prepared by mixing 10 g J-PSS2, 0.82 g DCP, and 8.5 ml of titanium isopropoxide in 50 ml of toluene under N_2 at 110°C in an apparatus shown in Fig. II-3 and a gentle reflux condition for 14 hours. The solution had a dark green color at the end of 14 hours. The product was precipitated out by ethanol and washed with ethanol three times before vacuum oven drying. The dried and agglomerated product had a bright orange color. Nearly 100% yield was achieved.

A molecular composite of SiC/Al_2O_3 was prepared in a similar way to SiC/TiC above but 0.75 9 DCP and 9 ml of aluminum sec-butoxide with refluxing for 22 hours under N_2. The product was precipitated out by ethanol and washed twice with methanol followed by vacuum oven drying at 150°C. The dried agglomerate appeared dull white in color and ~70% yield was achieved.

Fourier-transform IR spectra before and after pyrolysis of the composites were taken by a Nicolet MX-1. Hot stage XRD by a Philips Electronic Automated X-ray Powder Diffractometer with HTK10 Hot Stage was used to obtain x-ray diffraction patterns of the molecular composites. The composite powders were introduced on a platinum substrate using a polymeric glue. Resistive heating was applied to the substrate in helium atmosphere.

Results

Mechanical properties of Nextel™ composites and Al_2O_3/SiC composites are given in Table V-1. Char yields of molecular composites powders are given in Table V-2. Energy dispersive spectra of PSS/$Al(OR)_3$

Table V-1. Mechanical Properties and Densities of Nextel™/SiO_2 Composite, SiC/SiC Composites, and Alumina/SiC Composites.

Composites*	σ_{flex}, MPa	K_{IC}, MPa $m^{1/2}$	DPN	ρ, g/cc
Nextel (60)/ SiO_2, 900°C	29±3			1.92±0.1
Silar (70)/ PSS, 800°C	15±2	0.43±1	434±28	1.60±0.1
Nicalon (70)/ PSS, 800°C	30±3	2.41±1	551±32	1.65±0.1
Al_2O_3 (75)/ PSS, 900°C	22±2			1.87±0.1

* Three specimens used for each composite. The numbers in parentheses are vol% in the pyrolyzed composite.

Table V-2. Char Yields of Molecular Composite Powders

Composite	Wt% SiC	% Weight Char Yield at 940°C in N_2 for 14 Hours
PSS/$Ti(OR)_4$	30	25±6
PSS/$Al(OR)_3$	35	55±7

and PSS/$Ti(OR)_4$ before pyrolysis are shown in Figs. V-1 and V-2. They show the constituent elements Si; Al and Si; Ti respectively.

Fourier-transform IR spectra of PSS/$Al(OR)_3$ after drying and after pyrolysis at 900°C are shown in Figs. V-3 and V-4. Figure V-5 shows FT-IR spectra of PSS/$Ti(OR)_4$ composite before and after pyrolyzing at 940°C.

Scanning electron micrographs of PSS/$Al(OR)_3$ and PSS/$Ti(OR)_4$ after pyrolyzing at 940°C in N_2 and hand-grinding are shown in Fig. V-6. They all show agglomerates.

Hot-stage XRD of the pyrolyzed molecular composite powders are shown in Figs. V-7 through V-15.

Discussion

Nextel™ fiber is not a strong fiber. The tensile strength data, provided by the manufacturer, 3M Co. is ~10 MPa. The σ_{flex} of Nextel/SiO_2 composites after multiple sol impregnation and 900°C sintering in Table V-1 is modest after considering the relatively low tensile strength of the fiber. The significance here is that Nextel™ fibers can be formed into monolithic structural composites if necessary. A higher temperature heat treatment should improve density and, thus, mechanical properties.

The SiC/SiC composites made from Silar™/PSS and Nicalon®/PSS after pyrolyzing at 800°C yield a somewhat low σ_{flex} mainly because of the high porosity. Sintering of these composites to full density is expected to be difficult by the reasons given in Chapter 2.

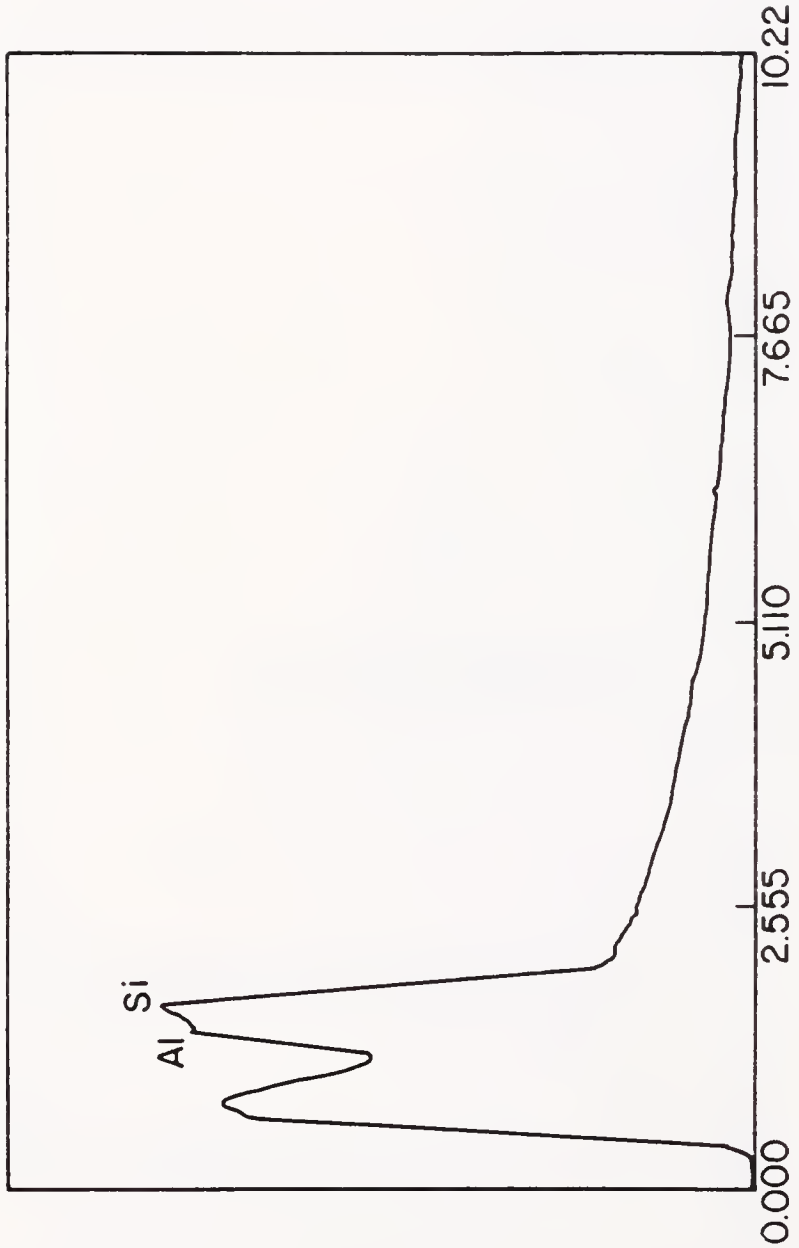

Fig.V-1. EDS Spectrum of PSS/Al(OR)$_3$ Composite

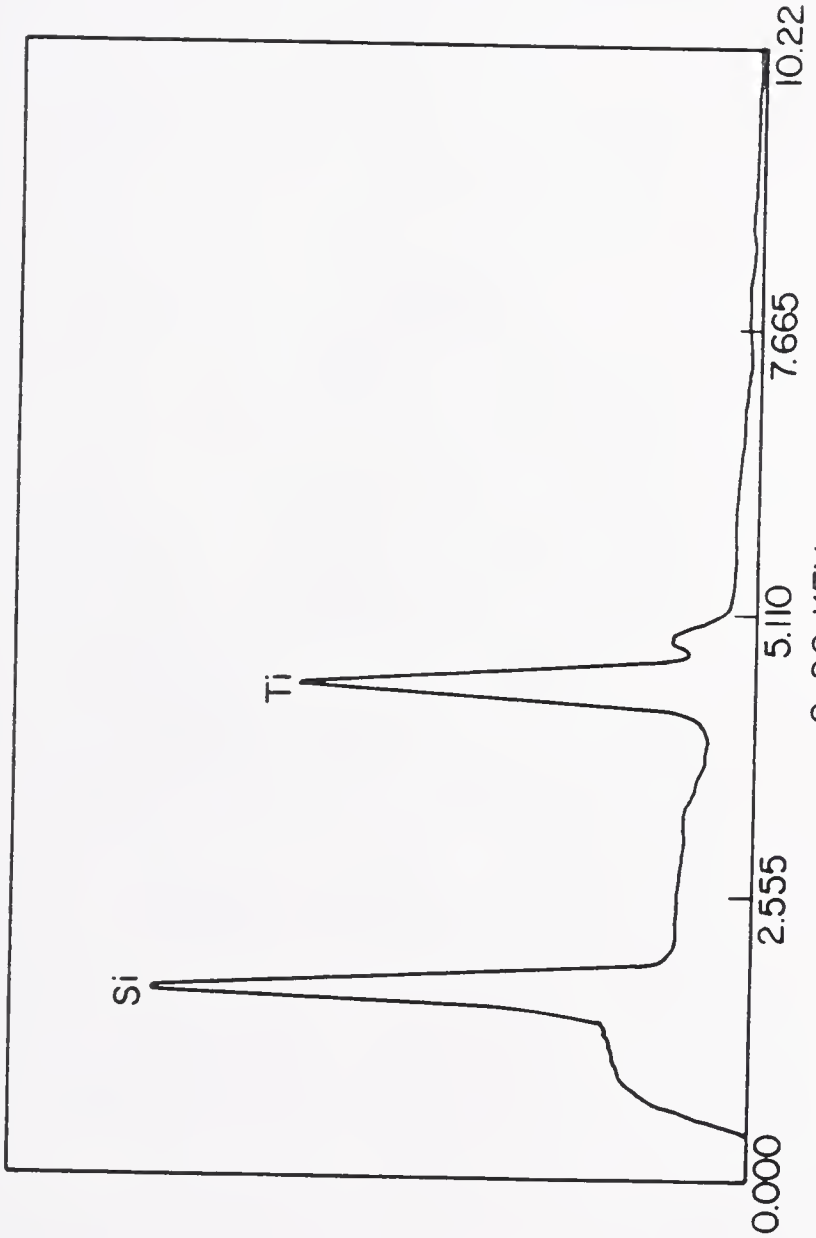

Fig.V-2. EDS Spectrum of PSS/$Ti(OR)_4$ Composite

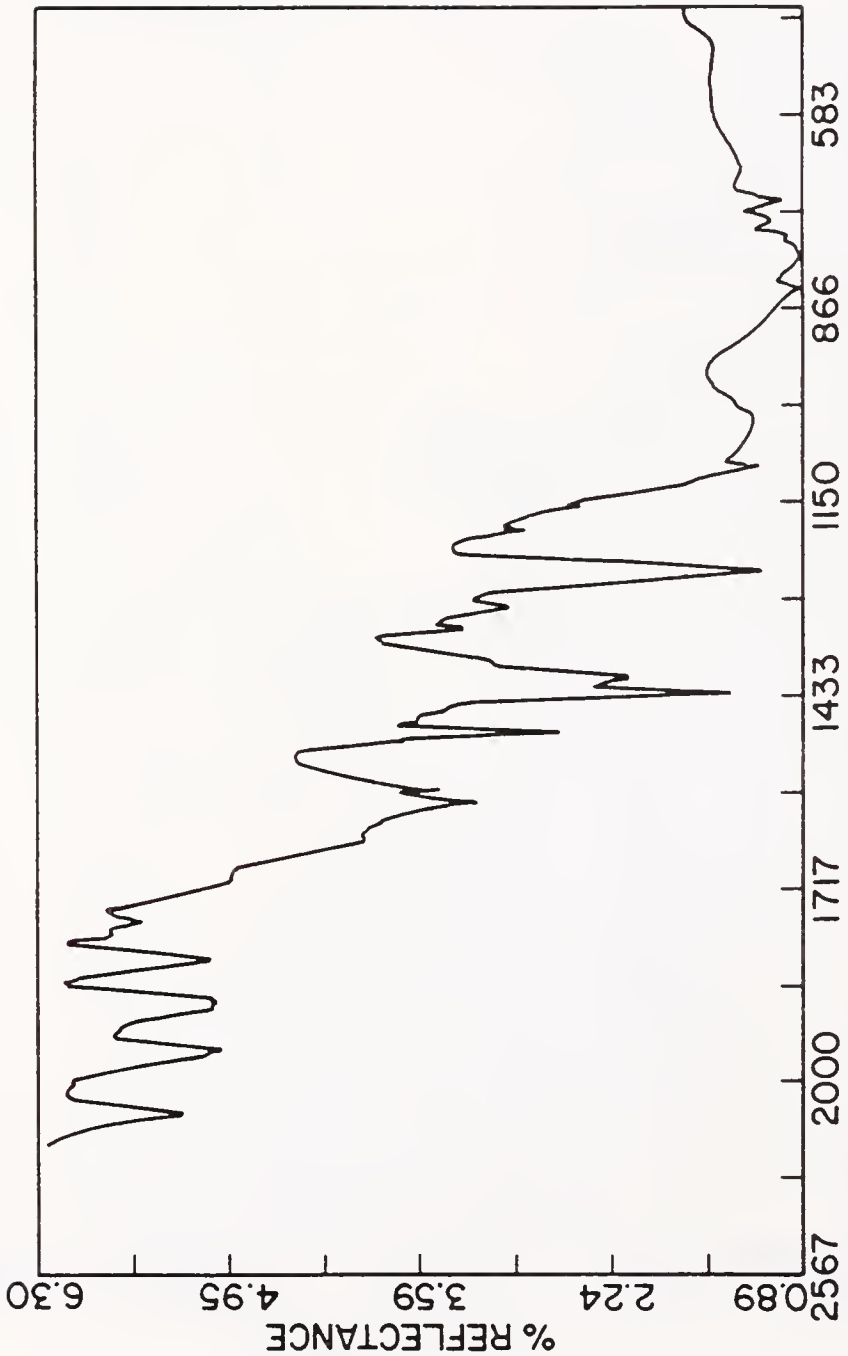

Fig.V-3. FT-IR Spectrum of As-Synthesized PSS/Al(OR)$_3$ Composite

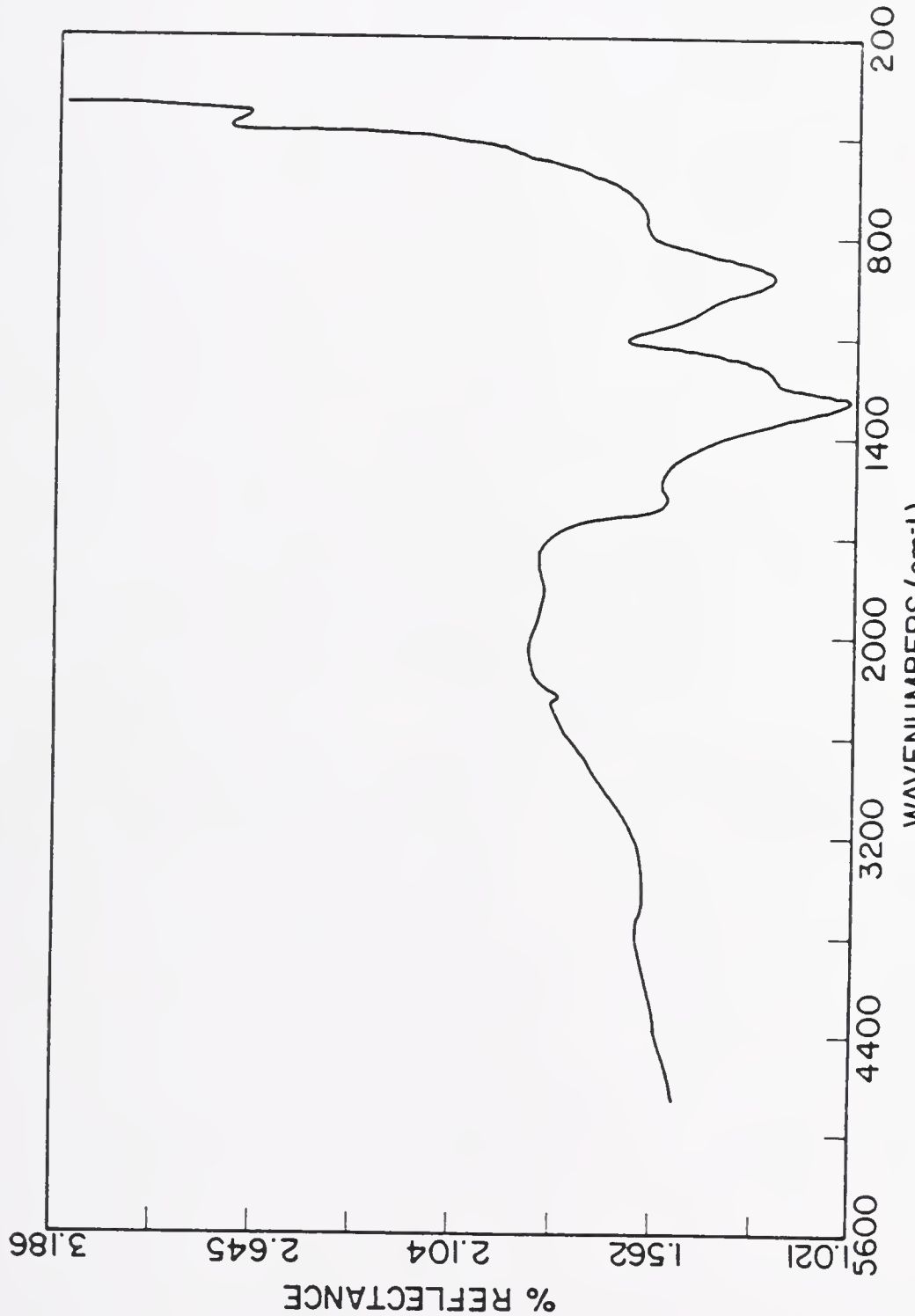

Fig.V-4. FT-IR Spectrum of PSS/$Al(OR)_3$ After Pyrolysis at 900°C in Nitrogen

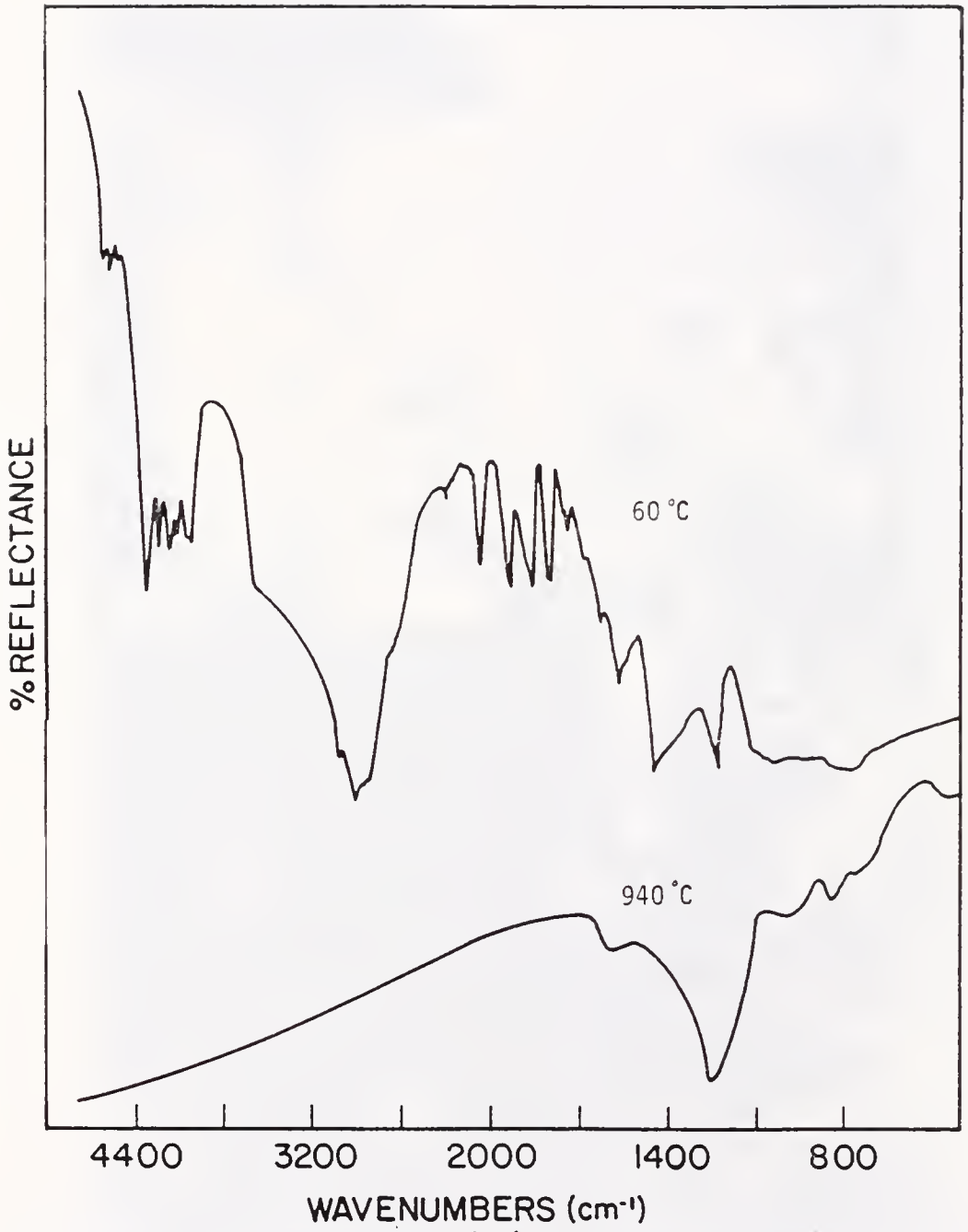

Fig.V-5. FT-IR Spectra of PSS/Ti(OR)$_4$ After Drying at 60°C and Pyrolyzing at 940°C

Fig.V-6. SEM Micrographs of PSS/$Al(OR)_3$ (top) and PSS/$Ti(OR)_4$ (bottom) After Pyrolyzing at 940°C

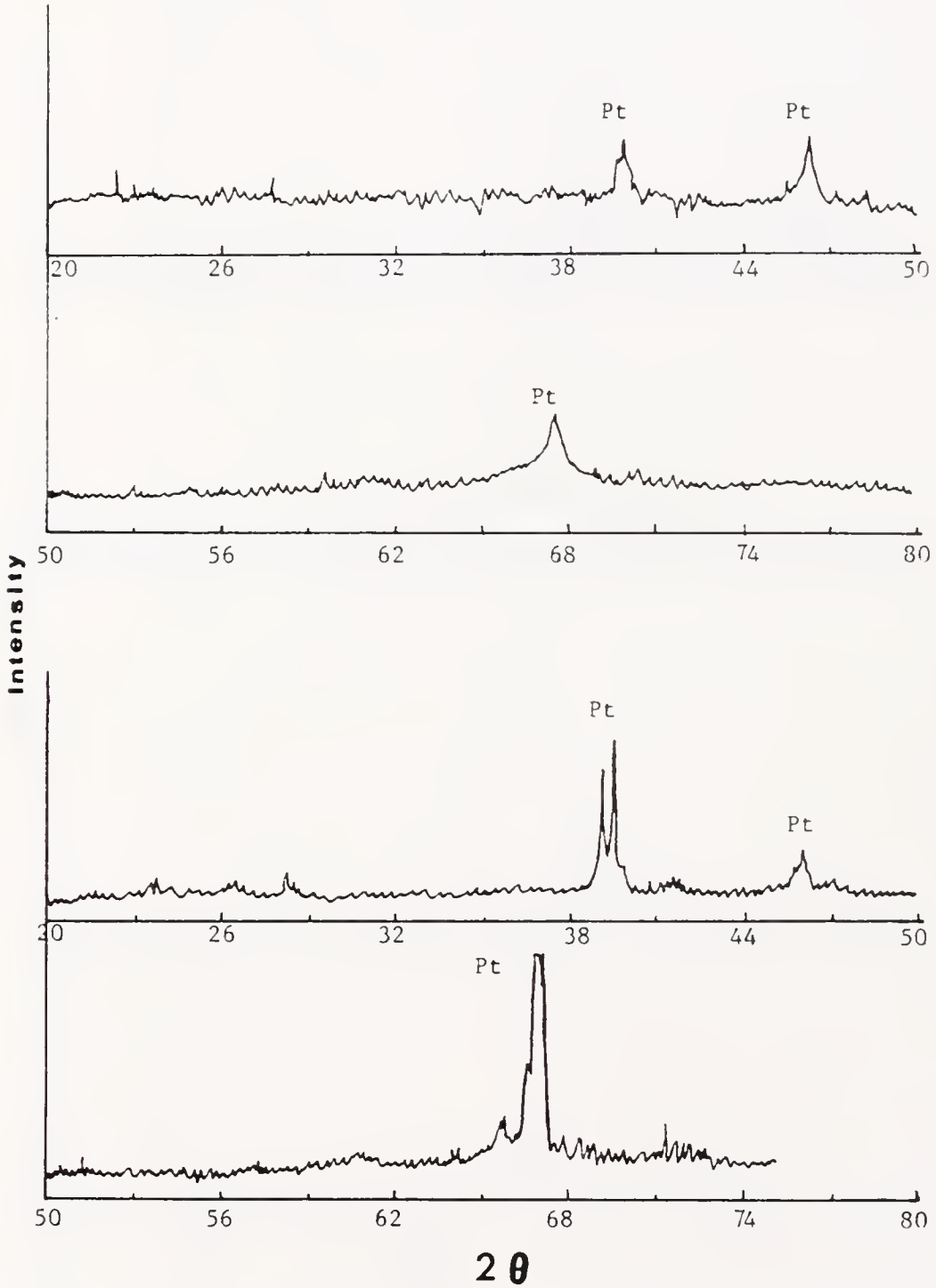

Fig.V-7. Hot Stage XRD Pattern SiC/Al_2O_3 Composite, Top: at RT After Pyrolysis at 940°C in N_2, Bottom: at 1350°C after 10 min.

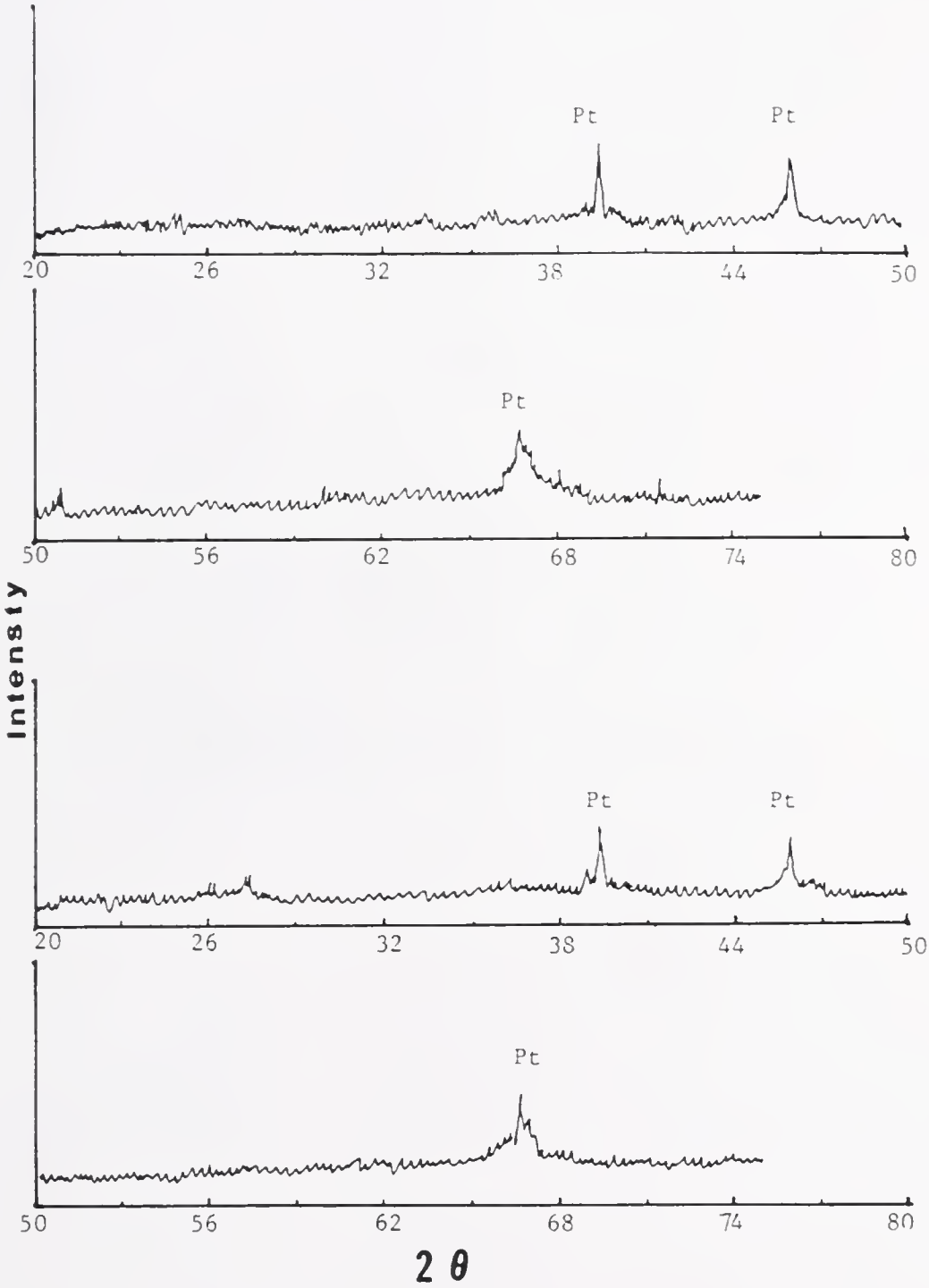

Fig.V-8. Hot-Stage XRD Pattern of SiC/Al_2O_3 Composite,
Top: at 1350°C after 50 min.
Bottom: at 1400°C after 12 min.

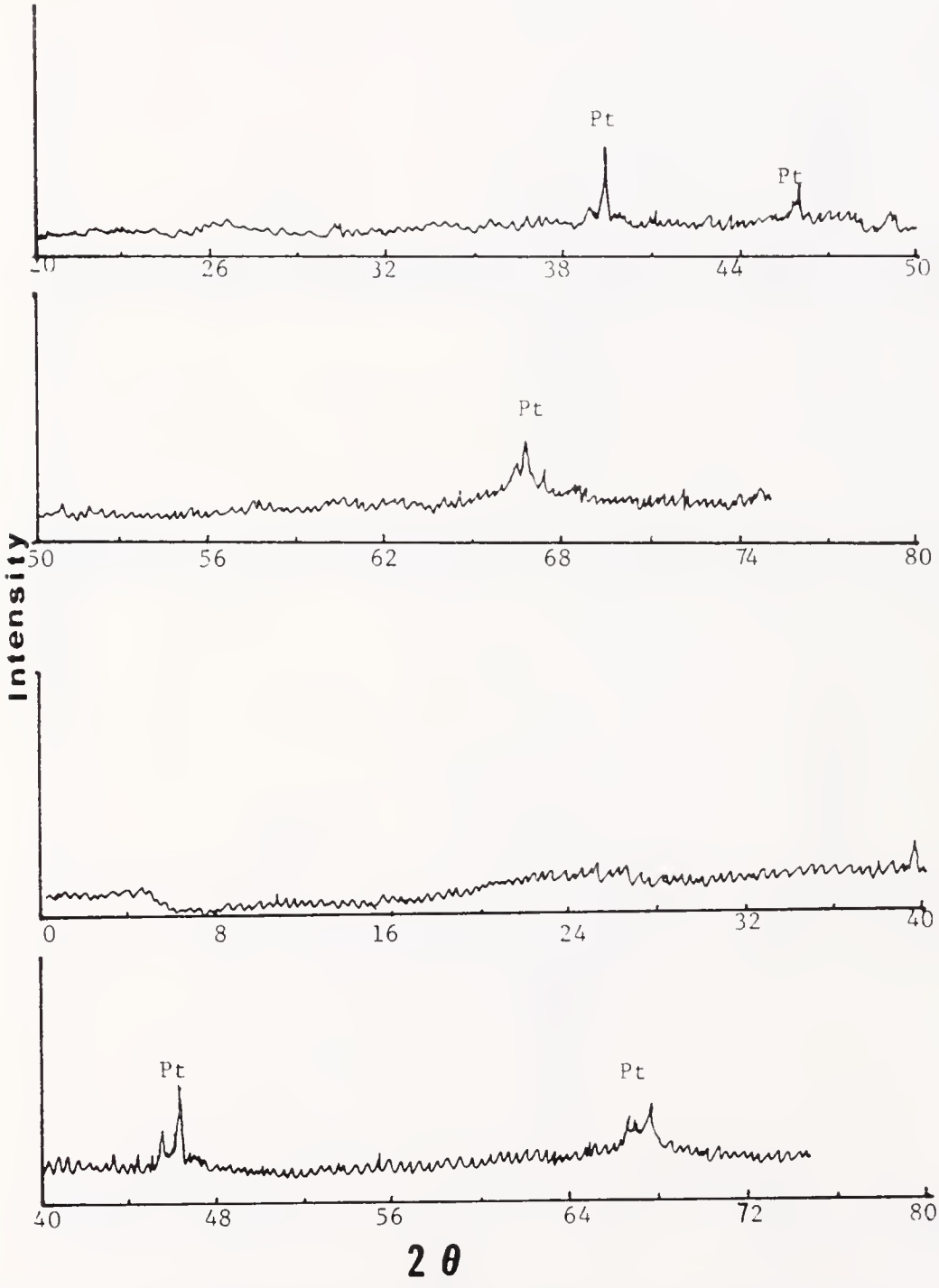

Fig.V-9. Hot-Stage XRD Pattern of SiC/Al_2O_3 Composite, Top: at 1400°C After 30 min., Bottom: at RT After 45 min. at 1400°C

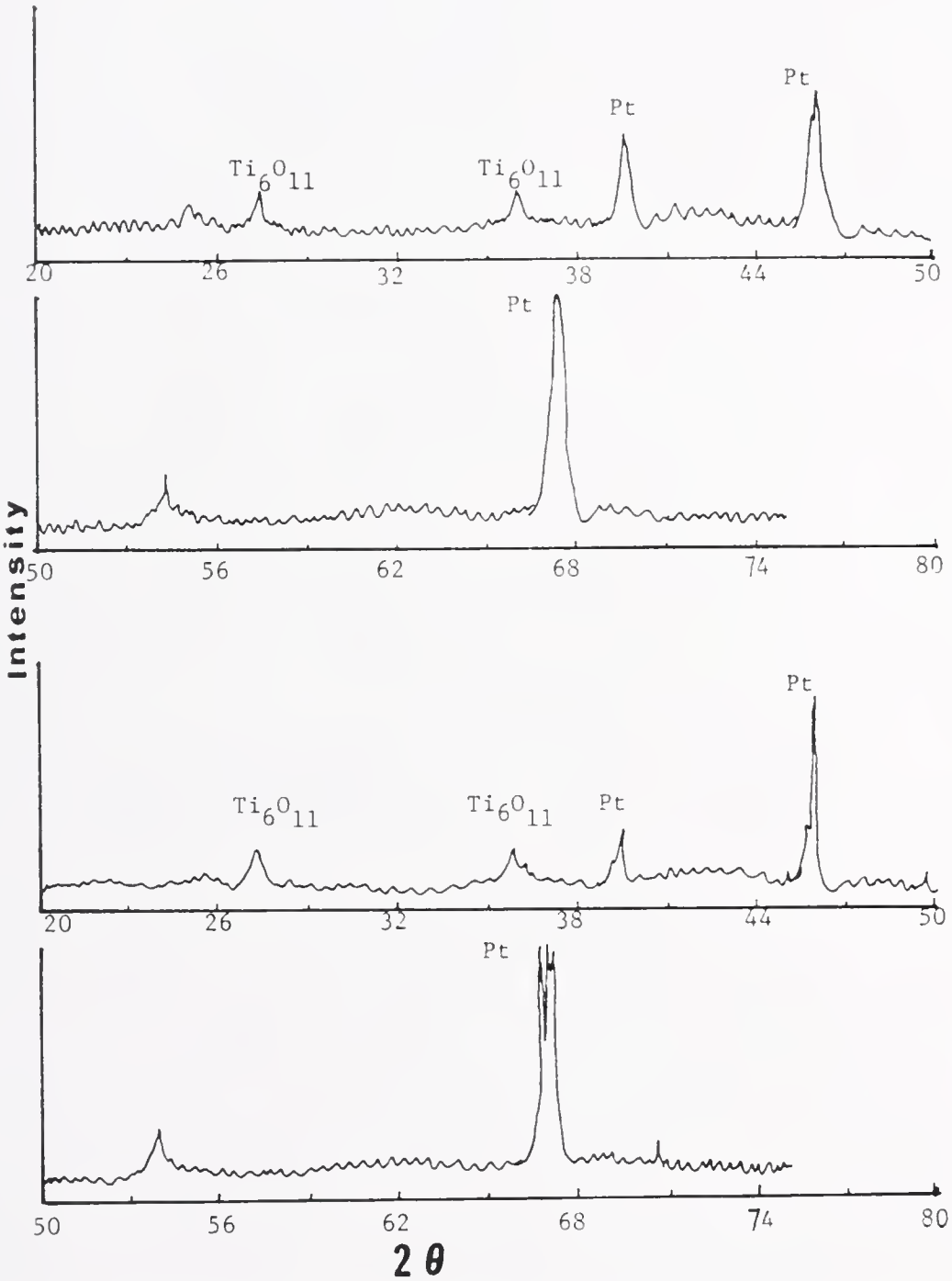

Fig.V-10. Hot-Stage XRD Pattern of PSS/$Ti(OR)_4$ Composite, Top: at RT After Pyrolysis at 940°C, Bottom: at 900°C After 10 min.

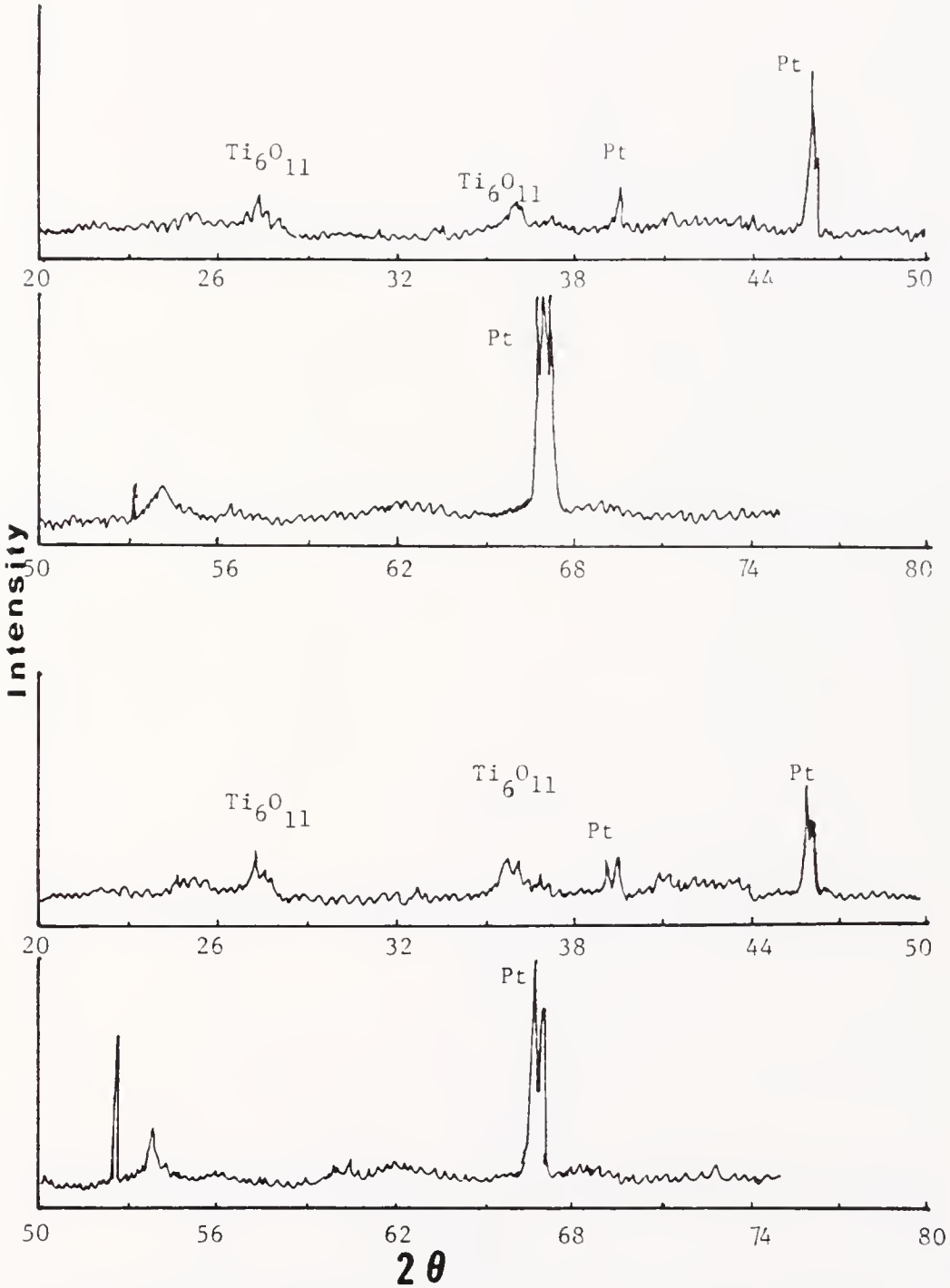

Fig.V-11. Hot-Stage XRD Pattern of PSS/$Ti(OR)_4$ Composite, Top: At 900°C After 40 min., Bottom: At 1100°C After 10 min.

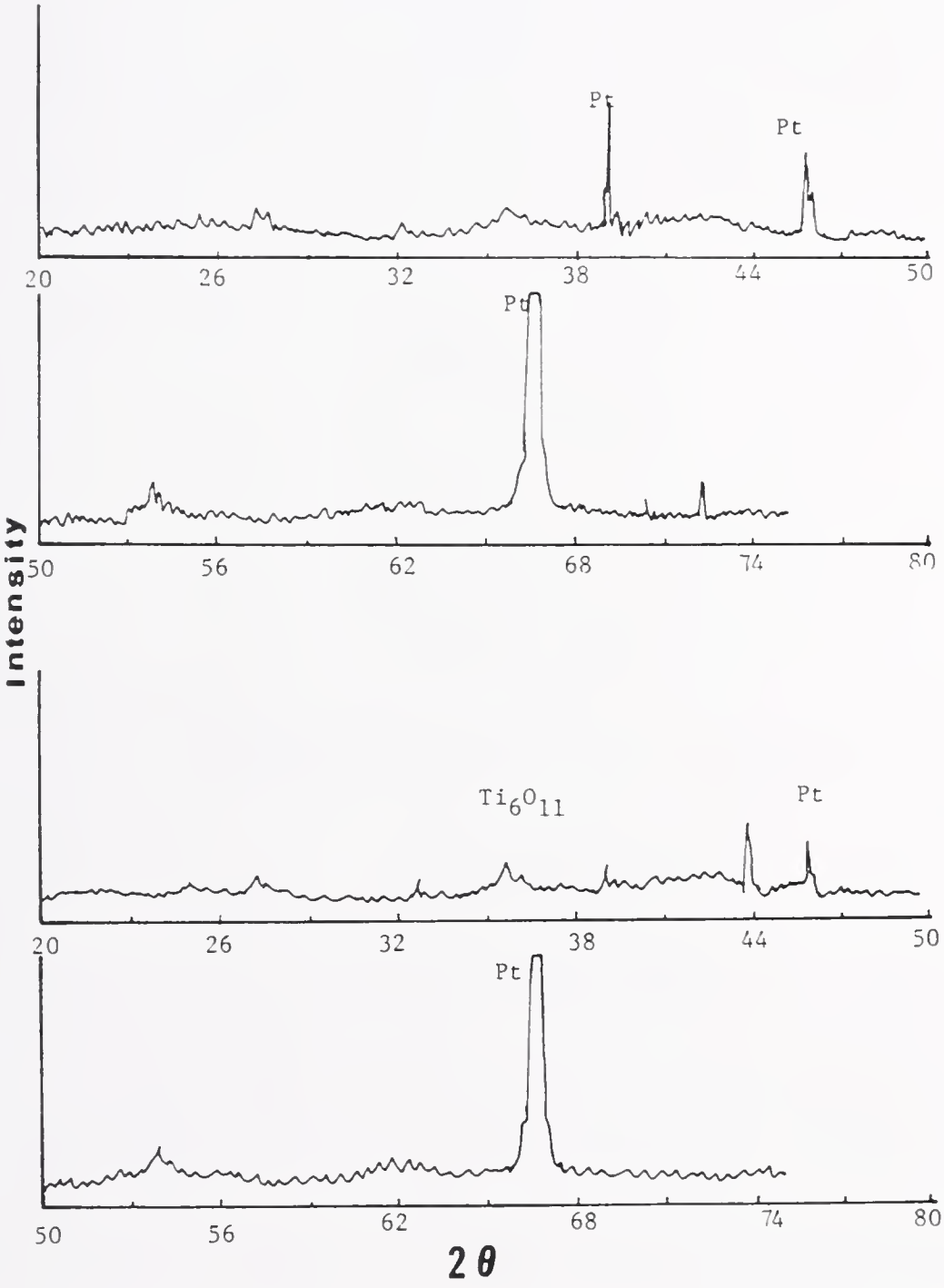

Fig.V-12. Hot-Stage XRD Pattern of PSS/$Ti(OR)_4$ Composite, Top: at 1200°C After 13 min., Bottom: at 1200°C after 30 min.

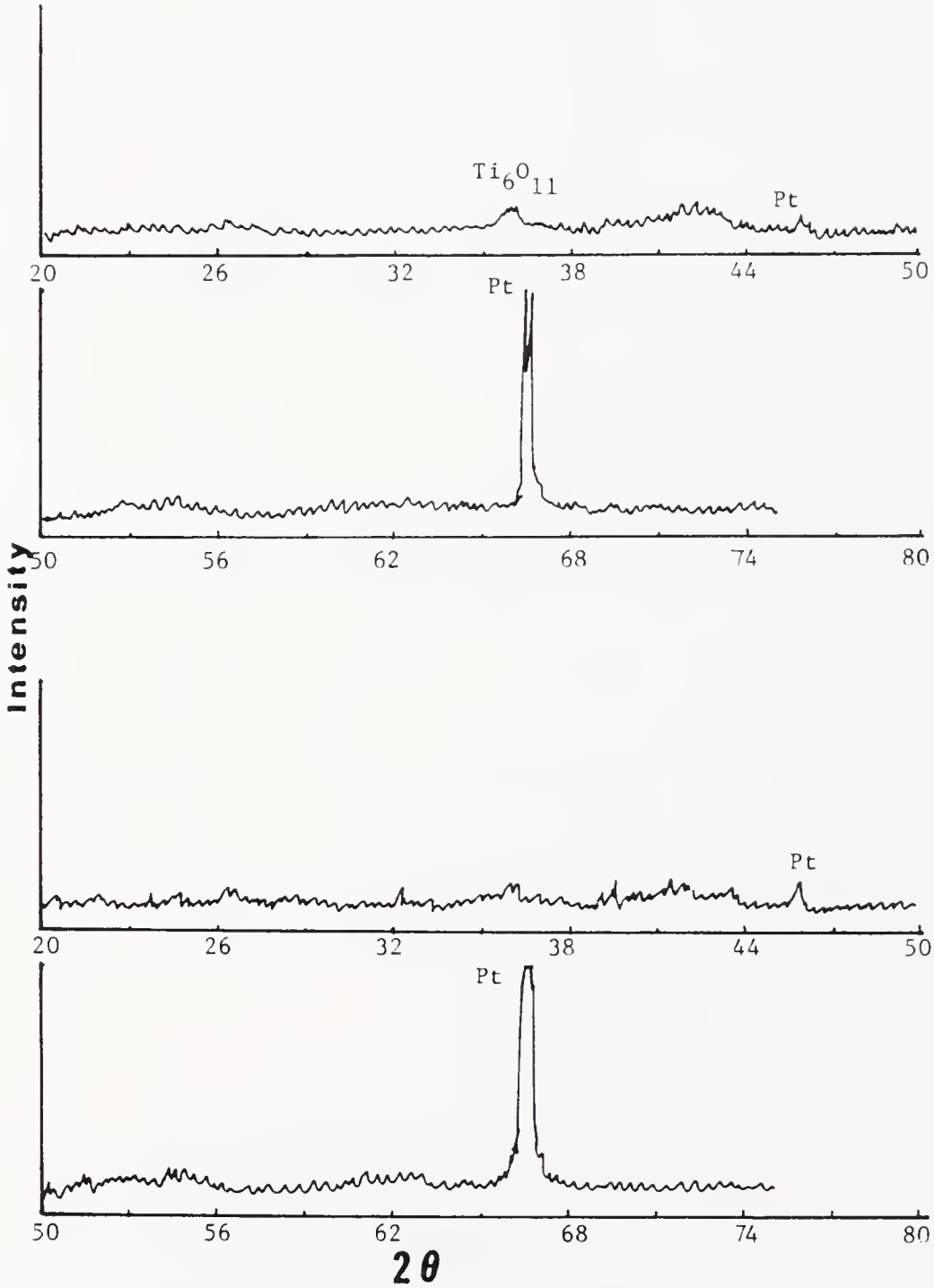

Fig.V-13. Hot-Stage XRD Pattern of PSS/$Ti(OR)_4$ Composite, Top: at 1300°C After 12 min., Bottom: at 1300°C After 30 min.

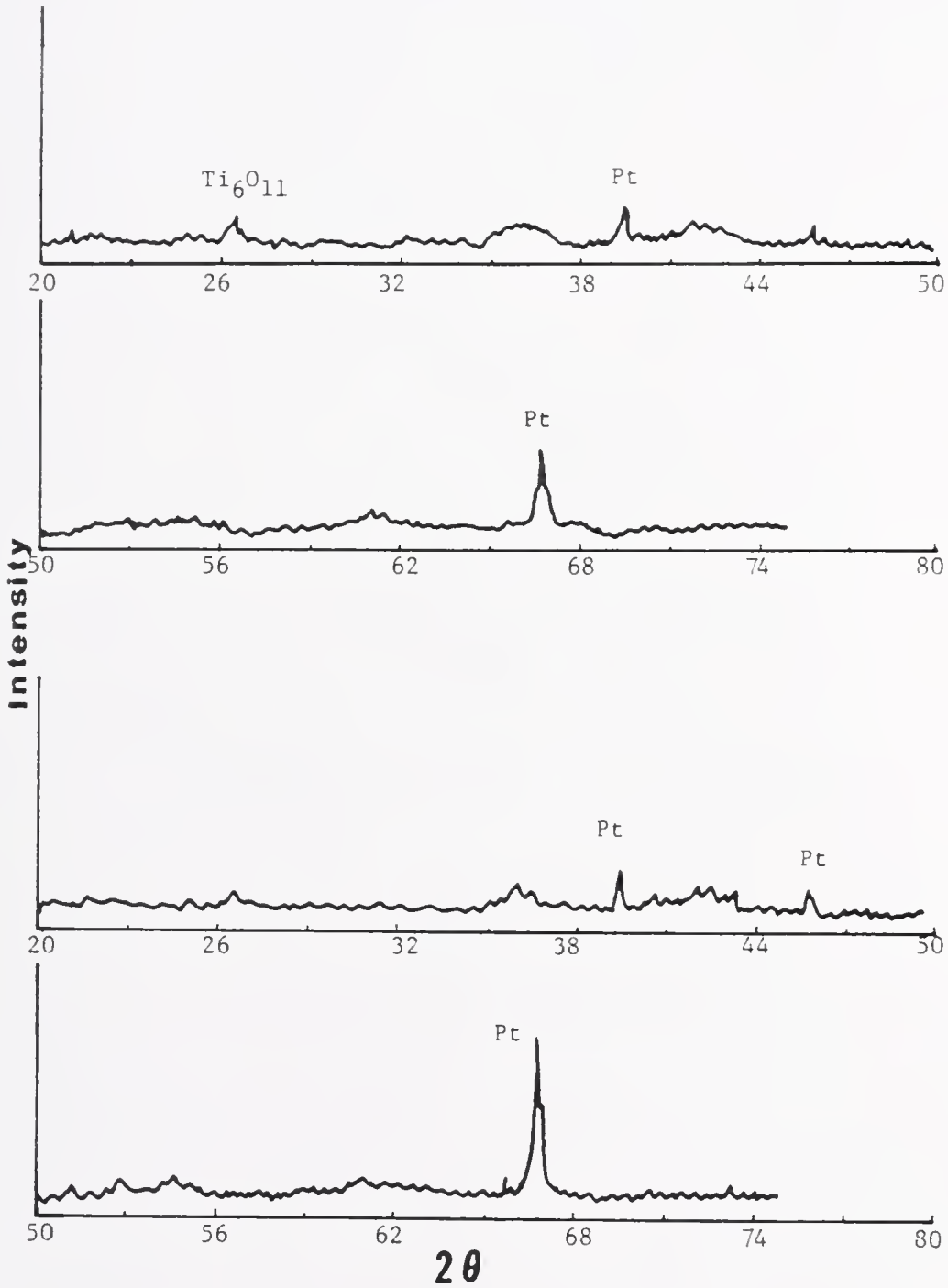

Fig.V-14. Hot-Stage XRD Pattern of PSS/$Ti(OR)_4$ Composite, Top: at 1360°C After 10 min., Bottom: at 1360°C After 30 min.

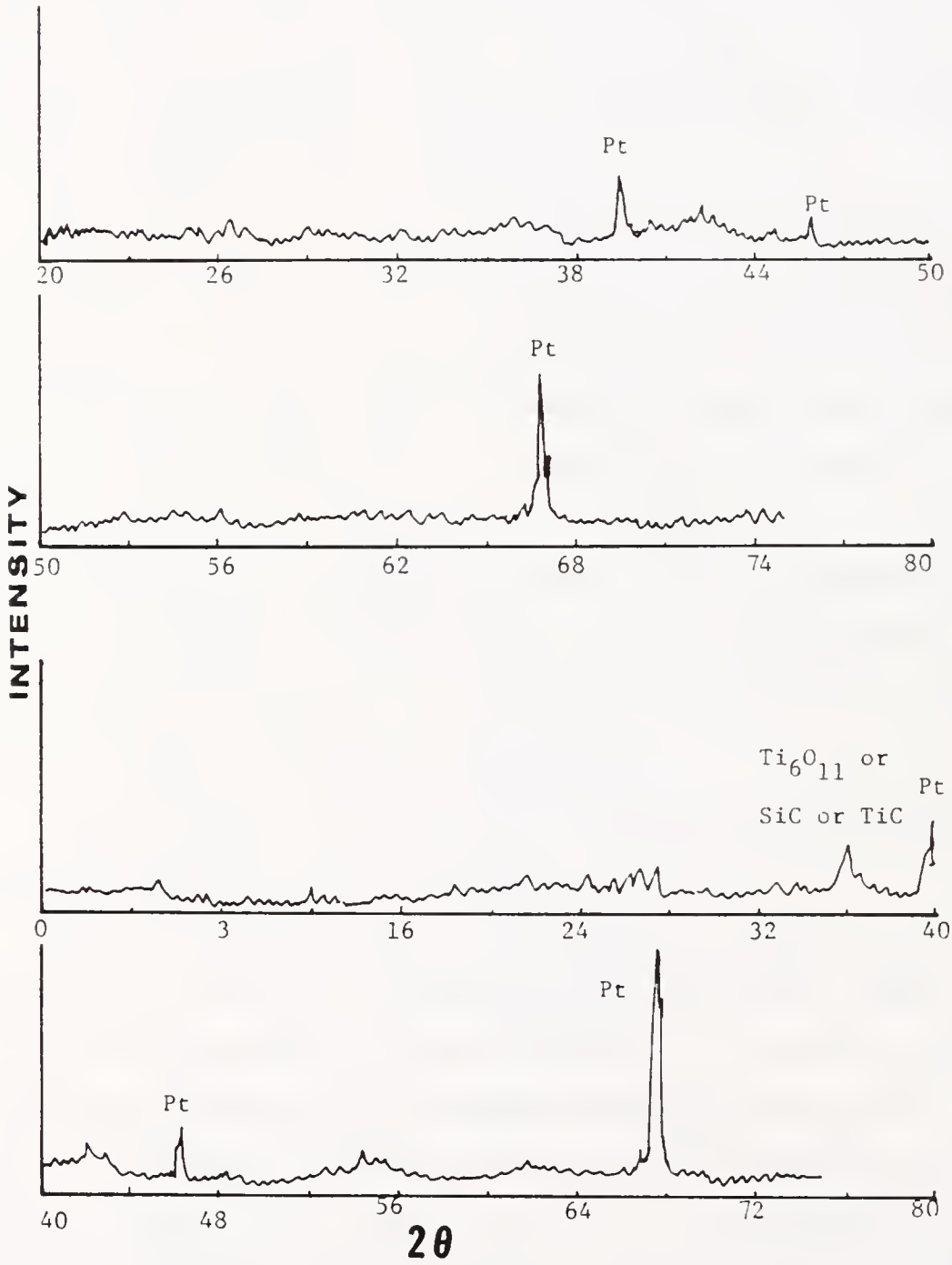

Fig.V-15. Hot-Stage XRD Pattern of PSS/Ti(OR)4 Composite, Top: at 1360°C After 1 hr., Bottom: at RT After 1360°C for 1 hr.

Alumina/SiC composites formed from α-Al_2O_3 fine powder and PSS following pyrolysis at 800°C show similar mechanical properties and densities to SiC/SiC composites above. Since SiC phase is the matrix, the sintering may be difficult. More work is needed to show the strength as a function of heat treatment temperature.

The char yields of PSS/$Ti(OR)_4$ and PSS/$Al(OR)_3$ composites are modest to low. These are crosslinked polymers which are insoluble in common solvents. Yajima et al.[12] postulated that their polycarbosilane is crosslinked via Si-O-Ti. In the PSS system, because of the absence of hydrogen directly bonded to Si, the crosslinking was expected to occur via Si-CH_2-O-Ti and via Si-CH_2-O-Al for PSS/$Al(OR)_3$.

These are only speculations and there is no way to know the precise nature of the chemical reaction between PSS and $Al(OR)_3$ and between PSS and $Ti(OR)_4$ without further studies. Further study varying the reactant ratio and amount of the CFRI should be helpful.

Energy dispersive spectra in Figs. V-1 and V-2 show the constituent metallic elements in the green polymers.

Fourier-transform spectra of PSS/$Al(OR)_3$ in Figs. V-3 and V-16 resemble the spectrum of PSS more than that of $Al(OR)_3$. However, the Al-O-Al vibrational mode is shown at ~1100 cm^{-1}. The band at 1100 cm^{-1} became more prominent after the composite was pyrolyzed to 900°C (Fig. V-4). A reflectance response representing the Si-C stretching mode is shown at ~800 cm^{-1} as a step. In Fig. V-4, it can be seen that the pyrolyzed PSS/$Al(OR)_3$ composite indeed has Al-O-Al and Si-C as expected.

Figure V-5 shows the FT-IR spectra for PSS/$Ti(OR)_4$. Most of Si-CH_3 features in PSS are lost after crosslinking with $Ti(OR)_4$. After

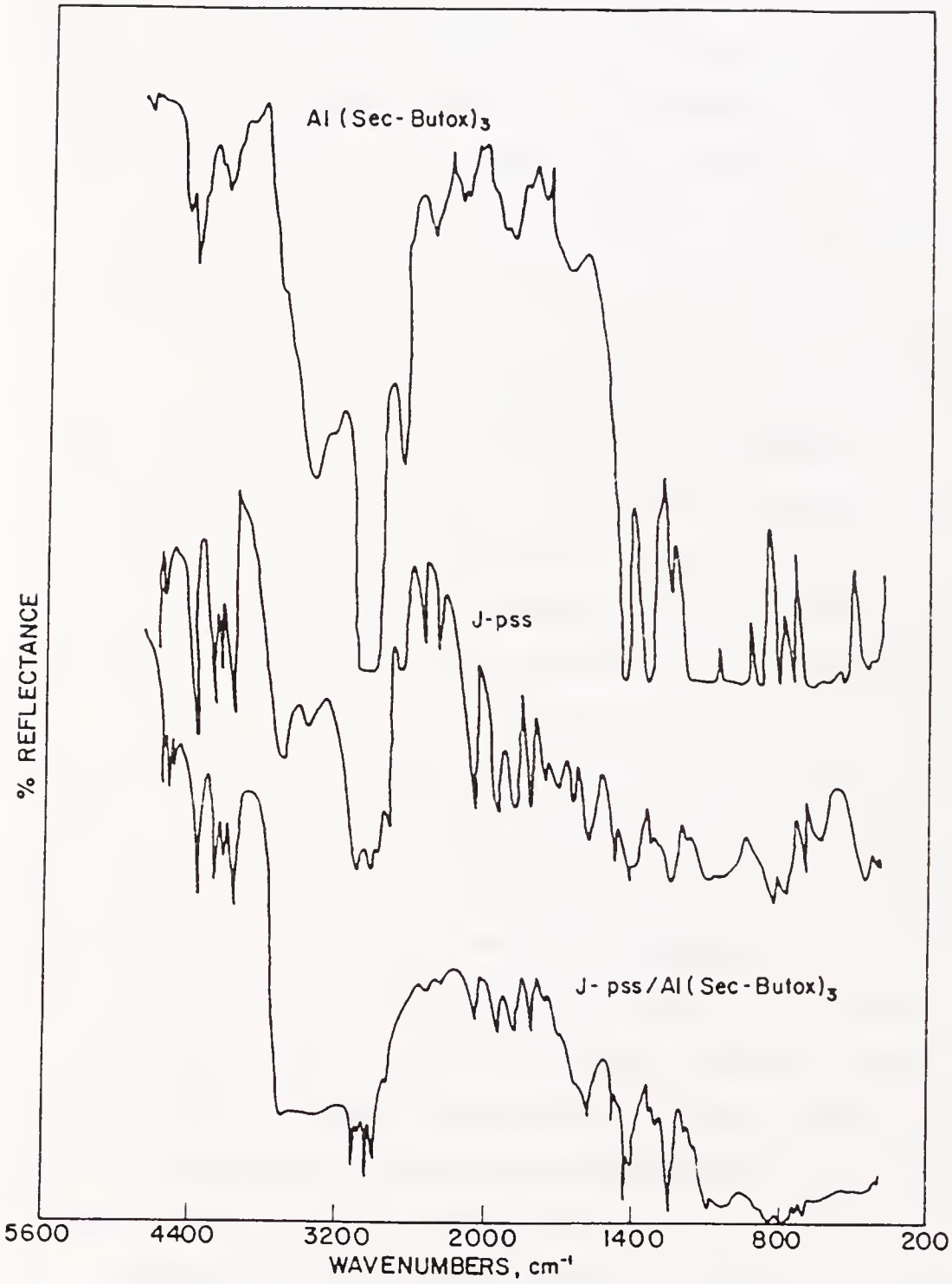

Fig.V-16. FT-IR Spectra of PSS, $Al(OR)_3$, and PSS/$Al(OR)_3$ After Drying

pyrolyzing at 940°C, the bands for TiO_2 (~750 cm^{-1}) and SiC (~800 cm^{-1}) are shown. The conversion of TiO_2 phase to TiC phase is only possible at temperatures above 1400°C. Yajima et al.[12] showed the transformation of TiO_2 to TiC at 1700°C. Thus at 940°C, the composite must consist of SiC and TiO_2 and that is what is shown in Fig. V-5. This is documented by hot-stage XRD as shown in Fig. V-10. A small amount of titanium dioxide, actually Ti_6O_{11}, is formed below at ~950°C. As temperature of the composite in He is increased, the XRD intensity for Ti_6O_{11} did not increase. The peak at 54.3° 2θ (1.69 Å) cannot be identified. It is not SiC, TiC, SiO_2, Al_2O_3, nor TiO_2. As temperature increased to 1100°C (Fig. V-11), a new and sharp peak appeared at 52.5 2θ (1.74 Å). This peak may be an artifact or an intermediate species because it disappeared immediately after raising the temperature. At a temperature of 1200°C, the peaks for Ti_6O_{11} are diminished (Fig. V-12). A further diminishing is observed at 1300°C and after 30 min at 1300°C, they all disappeared. At 1360°C, even platinum peaks are diminished. After one hour at 1360°C and cooling to room temperature, the small peak at 36° 2θ representing Ti_6O_{11} came back. However the position of 36° 2θ is the position for SiC as well as TiC. The true identity of the peak at 36° 2θ is not clear. The reason why the Ti_6O_{11} crystalline phase disappeared at 1300°C is unknown since the m.p. of TiO_2 is ~1840°C. This may be the temperature at where the transformation from TiO_2 to TiC and solid state reactions among the components might begin.

It appears that the crystallization of Ti_6O_{11} is somewhat suppressed as discussed in Chapter 3 for SiO_2/SiC composites. This

phenomenon is even more strongly demonstrated in the PSS/$Al(OR)_3$ composite. Figures V-7 through V-9 show that no crystalline phase is present in the SiC/Al_2O_3 composite at a temperature as high as 1400°C for 40 min except the peaks for the Pt substrate.

Figure V-6 shows that the SiC/Al_2O_3 and SiC/TiO_2 composites powders are agglomerated.

Conclusion

Composites of Nextel™ fiber/SiO_2 gel and Al_2O_3 powder/SiC from PSS can be formed with modest flexural strengths. Silicon carbide/silicon carbide composites can also be formed easily and also have modest mechanical properties. Temperatures higher than ~900°C for sintering should improve the density as well as the mechanical properties of these composites.

The molecular composites of SiC/Al_2O_3 and SiC/TiO_2 are formed from chemicals of metal-organic derivatives. They appear to have a submicron particle size and suppress crystallization of each phase in the composite at temperatures up to ~1400°C. A higher temperature than 1400°C is required to transform SiC/TiO_2 to SiC/TiC.

The primary and common problem associated with the physical and mechanical properties of the composites produced herein is the densification. Use of sintering aids, a controlled atmosphere with higher temperature capability should help the problem.

It has been further demonstrated in this chapter that the potential to produce desired ceramic materials, which are difficult to obtain by

the conventional processing, via chemical process is enormous. However, this enormous potential can only be made useful through a continued understanding of the chemical processes involved and elimination of uncontrolled porosity.

The significance of this chapter should be in the concepts rather than a production of exciting mechanical properties of these composites. The concept of mixing two precursors of a composite at a molecular level can be applied to many other systems. Testings for mechanical properties of these composites must be followed after a successful synthesis of a molecular composite is made.

CHAPTER VI
CONCLUSIONS AND RECOMMENDATIONS

Silicon carbide material can be made from silicon and carbon containing polymers in a relatively easy manner. These precursors can be used to strengthen the brittle materials such as glass by forming composites. These composites show increased strength and fracture toughness even with the low temperature heat treatments and low densities (1.7-2.1 g/cc).

It becomes rather clear that there are variety of functional groups which may be introduced to the polysilane backbone. A systematic study of how these groups are related to char yield of silicon carbide, viscosity, green density, chared density, susceptibility to oxidation in green state and in the pyrolyzed state and crosslinkability is recommended.

Changing the porosity and pore size of silica gel matrices could be used to vary the amount and depth of SiC precursor silanes and thereby improve the control over the physical and mechanical and/or optical properties of silane impregnated silica glass monoliths. To achieve this control, the behavior of pure silica gel monoliths with respect to pore collapse and densification must be better understood.

Use of a nonpolar high vapor pressure solvent should help to increase the loading of the SiC phase in monolithic SiC/SiO_2 molecular bulk components. However, the increasing difficulty of maintaining

monolithicity of the composites with increased loading of the SiC precursor needs to be investigated as well.

The chemical reaction between the SiC precursor and the SiO_2 gel matrix is a serious problem and needs to be understood. A systematic study of the reaction should help to produce better composites and is highly recommended.

Although the Nicalon/SiO_2 and Silar/SiO_2 composites have a remarkable strength-to-density ratio and toughness-to-density ratio, further study to consolidate the bodies is needed. Complete consolidation may be possible using a controlled atmosphere high temperature furnace.

The molecular composite powders of SiC/Al_2O_3, SiC/SiO_2, and SiC/TiO_2 should be hot pressed to determine their mechanical behavior. The SiC/TiO_2 composite may be converted to SiC/TiC composite by heating at temperatures of ~1700°C. A TEM study to examine how the two phases are arranged would be helpful in optimizing the process. This idea of molecular composite may also be applied to other systems such as ZrO_2 and Si_3N_4.

Tinted and tempered glasses may be made by an impregnation of the SiC precursors within the ultraporous SiO_2 gel glass matrix. This glass should produce very high strength and toughness with good IR absorption characteristics which may conserve heat for example in cooking wares. The high temperature limit of these wares may be raised to ~1500°C which is 400-500°C higher than that of pure silica glass ware. Thermal shock resistance of these composites due to the surface compressive stress may be even higher than the pure silica glass.

Although the mechanical properties of these composites derived from chemical processes described in this dissertation are far from the theoretical limit, the possibility of closing the gap has been demonstrated to be real through the continuous understanding of the chemistry in the processes. The results are encouraging for the first attempts and values for σ_{flex}/ρ and K_{IC}/ρ are equal to or surpass all but the uniaxially oriented SiC fiber/glass hot-pressed composites.

As the science of materials has developed it has moved more from giant leaps into the unknown to small steps forward in fairly clear directions. The small steps are many times more sophisticated and represent a new level of scientific achievement.

It is hoped that the small understandings of ceramics and molecular composites presented in this dissertation may accelerate the movements toward clearly defined targets which we know will be achieved.

Some of more notable principles that were learned from this research for Chemically Derived Ceramic Composites may be summarized below.

1) A precursor to SiC, known as polysilastyrene (PSS), had been shown to be potentially useful and superior to the existing precursor (polycarbosilane) if it can be crosslinked without adding oxygen to the polymer chain. First it was learned that PSS can be routinely synthesized in a one-step process with a relatively straight forward manner.

2) Crosslinking of PSS can be achieved by using a chemical free radical initiator. Through the crosslinking process, production of a SiC monolithic body is possible without hot-pressing or high temperature sintering.

3) Increased crosslinkability of an organosilane is achieved through reactive functional groups such as

4) These organosilanes can be used to impregnate porous ceramic bodies such as silica gel followed by in situ crosslinking to yield a SiC/SiO_2 composite. The subsequent pyrolysis leads to hardening effect as well as a toughening and strengthening effect by the dispersed SiC in the surface layer of the matrix.

5) The organosilane precursor can also be mixed with silica sol, followed by a cogellation, by an in situ crosslinking, and by a pyrolysis to yield bulk SiC/SiO_2 composites.

6) There is(are) a chemical reaction(s) between the impregnated silane and the silica matrix which weaken the silica glass network. These chemical reaction(s) must be identified and controlled for improved mechanical properties of silane/SiO_2 gel composites.

7) The sol-gel process to obtain SiO_2 glass can be used to form fibrous SiC/SiO_2 composites by dispersing the whiskers (or fibers) in the silica sol followed by castings, gellating, or cold pressing, and sintering. Characteristics of these composites are: a) low temperature processed (~200-500°C lower than the conventional hot-pressing process) so there is little damage on the fibers, and matrix and fiber interaction is minimal; b) low density materials (~1.7-2.1 g/cc); c) mediocre flexural strengths but good flexural strength to density ratio; d) superior fracture toughness represented by the critical intensity factor, K_{IC}. Even more superior in K_{IC} to density ratio to other ceramic composites of comparable composition. e) This remarkable K_{IC} value comes

from the load transfer from the matrix to the fiber as well as the mechanism of crack wandering and branching by pores. It was learned that the fracture toughness is limited by the diameter to length ratio of the fiber. f) Higher thermal shock resistance and better oxidation resistance than the SiC not in the composite. g) Complex shapes can be formed easily in plastic molds. The shapes and sizes are only limited by the molds.

8) Molecular composite powders of SiO_2/SiC, TiO_2(TiC)/SiC, and Al_2O_3/SiC can be made by mixing the two precursors of the respective phase with in situ crosslinking by a chemical free radical initiator. These composites appear to have a high devitrification temperature as well as high purity.

9) These technques: crosslinking, impregnation, sol-gel processing for monolithic ceramics or glasses, and molecular level mixing of two or more precursors can be applied to many other ceramic composite systems.

10) Silicon carbide incorporated into a porous silica glass matrix is more oxidation resistant than raw SiC. The SiC in the composite appears to be oxidized via an intermediate phase SiOC.

REFERENCES

1. Ultrastructure Processing of Ceramics, Glasses, and Composites, L. L. Hench and D. R. Ulrich, eds., John Wiley and Sons, New York, 1984, pp. 15-557.

2. Better Ceramics Through Chemistry, C. J. Brinker, D. E. Clark, and D. R. Ulrich, eds., Materials Research Society Symposia Proceedings, Vol. 32, North-Holland, New York, 1984, pp. 1-387.

3. C. D. Hendricks, Lawrence Livermore Laboratory Report, UCRL-8145, Rev. 1, 1979.

4. K. J. Wynne and R. W. Rice, "Ceramics Via Polymer Pyrolysis" in Ann. Rev. Mater. Sci., R. A. Huggins, ed., 14, 297 (1984).

5. B. E. Yoldas, J. Mater. Sci., 10, 1856 (1975).

6. B. E. Yoldas, Am. Ceram. Soc. Bull., 3, 2896 (1975).

7. S. R. Gurkovich and J. B. Blum, "Preparation of Monolithic Lead-Titanate by a Sol-Gel Process," in Ultrastructure Processing of Ceramics, Glasses, and Composites," L. L. Hench and D. R. Ulrich, eds., John Wiley and Sons, New York, 1984, p. 152.

8. N. J. Arfsten, R. Kaufman, and H. Dislich, "Sol-Gel Derived Indium-Tin-Oxide Coatings," in Ultrastructure Processing of Ceramics, Glasses, and Composites," L. L. Hench and D. R. Ulrich, eds., John Wiley and Sons, New York, 1984, p. 189.

9. E. Barringer, N. Jubb, B. Fegley, R. L. Pober, and H. K. Bowen, "Processing Monosized Powders," in Ultrastructure Processing of Ceramics, Glasses, and Composites," L. L. Hench and D. R. Ulrich, eds., John Wiley and Sons, New York, 1984, p. 315.

10. K. S. Mazdiyasni, "Chemical Synthesis of Single and Mixed Phase Oxide Ceramics," in Better Ceramics Through Chemistry, C. J. Brinker, D. E. Clark, and D. R. Ulrich, eds., Material Research Society Symposia Proceedings, Vol. 32, North-Holland, New York, 1984, p. 175.

11. R. Rice, Am. Ceram. Soc. Bull, 62, 889 (1983).

12. S. Yajima, T. Iwai, T. Yamamura, K. Okamura, and Y. Hasegawa, J. Mat. Sci., 16, 1349 (1981).

13. R. Roy, presented at the Second International Conf. on Ultrastructure Processing of Ceramics, Glasses, and Composites, Palm Coast, FL, Feb., 1985.

14. J. Persh, Ceramic Eng. and Sci. Proceedings, 5, 443 (1984).

15. "Silicon Carbide-1973," R. C. Marshall, J. Faust, and C. Ryan, eds., University of South Carolina Press, Columbia, South Carolina, 1974.

16. I. B. Cutler, "Production of Silicon Carbide from Rice Hulls," U.S. Patent No. 3,754,676, assigned to the University of Utah, Salt Lake City, Utah (Filed Oct. 30, 1970).

17. G. Jenkins and K. Kawamura, Polymer Carbons-Carbon Fibre, Glass and Char, Cambridge University Press, London, 1976.

18. F. Ainger and J. Herbert, "The Preparation of Phosphorus-Nitrogen Compounds as Non-Porous Solids," in Special Ceramics, P. Popper, ed., Academic Press, New York, 1960, pp. 168-181.

19. P. Chantrell and P. Popper, "Inorganic Polymers and Ceramics," in Special Ceramics, P. Popper, ed., Academic Press, New York, 1964, pp. 87-103.

20. W. Verbeek, U.S. Patent No. 3,853,567 (1974).

21. G. Winter, W. Verbeek, and M. Mansmann, U.S. Patent No. 3,892,583 (1975).

22. S. Yajima, J. Hayashi, and M. Omori, Chem. Lett., 931 (1975).

23. S. Yajima, K. Okamura, and J. Hayashi, Chem. Lett., 1209 (1975).

24. S. Yajima, K. Okamura, J. Hayashi, and M. Omori, J. Am. Ceram. Soc., 59, 324 (1976).

25. S. Yajima, T. Shishido, and H. Kayano, Nature, 264, 237 (1976).

26. S. Yajima, Philos. Trans. Res. Soc. London, A294, 419 (1980).

27. S. Yajima, J. Hayashi, M. Omori, and K. Okamura, Nature, 261, 683 (1976).

28. S. Yajima, J. Hayashi, and K. Okamura, Nature, 266, 521 (1977).

29. S. Yajima, Y. Hasegawa, K. Okamura, and T. Matsuzowa, Nature, 273, 525 (1978).

30. S. Yajima, J. Hayashi, M. Omori, U.S. Patent No. 4,052,430 (1978).

31. I. Taniguchi, K. Harada, and T. Maeda, Chem. Abstr., 85, 96582V (1976).

32. R. Rice, K. Wynne, and W. Fox, U.S. Patent No. 4,097,294 (1978).

33. B. Walker, R. Rice, P. Becker, B. Bender, and W. Coblenz, Am. Ceram. Soc. Bull., 62 916 (1983).

34. J. Wesson and T. Williams, J. Polym. Sci., 17, 2833 (1979).

35. J. Wesson and T. Williams, J. Polym. Sci., 18, 959 (1980).

36. J. Wesson and T. Williams, J. Polym. Sci., 19, 65 (1981).

37. C. Schilling, J. Wesson, and T. Williams, Am. Ceram. Soc. Bull., 62, 912 (1983).

38. C. Schilling, J. Wesson, and T. Williams, U.S. Patent No. 4,414,403 (1983).

39. C. Schilling, T. Williams, ACS Polymer Preprints, 25, 1 (1984).

40. R. West, L. David, P. Djurovich, H. Yu, and R. Sinclair, Am. Ceram. Soc. Bull., 62, 899 (1983).

41. R. Baney and J. Gaul, U.S. Patent No. 4,310,651 (1982).

42. R. Baney and J. Gaul, U.S. Patent No. 4,298,558 (1981).

43. R. Baney and J. Gaul, U.S. Patent No. 4,298,559 (1981).

44. R. Baney, U.S. Patent No. 4,310,481 (1982).

45. R. Baney, U.S. Patent No. 4,310,482 (1982).

46. R. Baney and J. Gaul, U.S. Patent No. 4,310,956 (1982).

47. B. Penn, F. Ledbetter, J. Clemons, and J. Daniels, J. Appl. Polym. Sci., 27, 3751 (1982).

48. D. Seyferth, G. Wiseman, and C. Prud'homme, J. Am. Ceram. Soc., 13 66 (1983).

49. D. Seyferth and G. Wiseman, "Silazane Precursors to Silicon Nitride," in Ultrastructure Processing of Ceramics, Glasses, and Composites, L. L. Hench and D. R. Ulrich, eds., John Wiley and Sons, New York, 1984, pp. 265-271.

50. F. S. Kipping, J. Chem. Soc, 125, 2291 (1924).

51. E. G. Rochow, An Introduction to the Chemistry of the Silicons, John Wiley and Sons, New York, 1946, p. 46.

52. E. Carberry and R. West, J. Am. Chem. Soc., 91, 5449 (1969).

53. S. Yajima, J. Hayashi, and M. Omori, U.S. Patent No. 4,100,233 (1978).

54. S. Yajima, Y. Hasegawa, J. Hayashi, and M. Iimura, J. Mat. Sci., 13, 2569 (1978).

55. Y. Hasegawa, M. Iimura, and S. Yajima, J. Mat. Sci., 15, 720 (1980).

56. L. David, "New Polysilane Polymers: Polysilastyrene and Polyphenylmethylsilylene," Ph.D. Dissertation, University of Wisconsin, 1981, p. 61.

57. B. Arkles, President of Petrarch Systems, Inc., private communication.

58. A. Miller, "Polysiloxanes," in Radiation Chemistry of Polymers, M. Dole and R. Salovey, eds., Academic Press, New York, 1973, p. 179.

59. Y. Okada, "Irradiation of Polymers," in Advances in Chemistry Series, R. F. Gould, ed., Am. Chem. Soc., Washington, DC, 1969, p. 44.

60. J. Speier, J. Webster, and G. Barnes, J. Am. Chem. Soc., 79, 974 (1957).

61. C. Schilling, Union Carbide, private communication, 1985.

62. C. Morterra and M. J. D. Low, Chem. Commun., 23, 203 (1968).

63. J. Roberts and M. Caserio, Basic Principles of Organic Chemistry, 2nd edition, W. A. Benzamin, Inc., Menlo Park, California, 1977, p. 92.

64. M. Kumada and K. Shiina, J. Org. Chem., 23, 139 (1958).

65. CRC Handbook of Chemistry and Physics, 52nd ed., Chemical Rubber Co., Cleveland, OH, p. F-186.

66. R. A. Sinclair, "Pyrolysis of Polysilanes," in Ultrastructure Processing of Ceramics, Glasses, and Composites, L. L. Hench and D. R. Ulrich, eds., John Wiley and Sons, New York, 1984, p. 258.

67. N. A. Toropov and V. P. Barzakovskii, High-Temperature Chemistry of Silicates and Other Oxide Systems, Consultants Bureau, New York, 1966, p. 126.

68. H. P. Kirchner, "Strengthening of Ceramics," Marcel Dekker, Inc., New York, 1979.

69. I. W. Donald and P. W. McMillan, J. Mat. Sci., 11, 949 (1976).

70. A. Kelly and R. B. Robinson, Prog. Mat. Sci., 10, 1 (1963).

71. D. P. H. Hasselman and R. M. Fulrath, J. Am. Ceram. Soc., 49, 68 (1966).

72. F. F. Lange, J. Am. Ceram. Soc., 54, 614 (1971).

73. G. R. Antis, P. Chantikul, B. R. Lawn, and D. B. Marshall, J. Am. Ceram. Soc., 64, 532 (1981).

74. J. K. MacKenzie, Proc. Physic. Soc. (London), B63, 2 (1950).

75. W. D. Kingery, H. K. Bowen, and D. R. Uhlmann, Introduction to Ceramics, 2nd edition, John Wiley and Sons, New York, 1976, p. 595.

76. W. D. Kingery, H. K. Bowen, and D. R. Uhlman, Introduction to Ceramics, 2nd edition, John Wiley and Sons, New York, 1976, pp. 830-844.

77. E. Fitzer and R. Ebi, "Kinetic Studies on the Oxidation of Silicon Carbide," in Silicon Carbide-1973, R. C. Marshall, J. Faust, and C. F. Ryan, eds., University of South Carolina Press, Columbia, SC, 1973, p. 320.

78. F. Gac, J. W. Milewski, J. J. Petrovic, and P. D. Schalek, "Silicon Carbide Whisker Reinforced Glass and Ceramics," in Metal Matrix, Carbon, and Ceramic Matrix Composites 1985, NASA Conference Publication 2406, Hampton, VA, J. D. Buckley, ed., p. 53.

79. S. C. Samanta and S. Musikant, "SiC Whiskers-Reinforced Ceramic Matrix Composites," in Ceramic Eng. & Sci., Proc., Am. Ceramic Soc., Columbus, OH, July-Aug. 1985, p. 663.

80. F. P. Meyer, G. D. Quinn, and J. C. Walk, "Reinforcing Fused Silica with High Purity Fibers" in Ceramic Eng. & Sci., Am. Ceramic Soc., Columbus, OH, July-Aug. 1985, p. 646.

81. R. A. Cutler, A. V. Virkar, and J. Holt, "Synthesis and Densification of Oxide-Carbide Composites," in Ceramic Eng. & Sci., Am. Ceramic Soc., Columbus, OH, July-Aug. 1985, p. 715.

82. F. F. Lange, B. I. Davis, and E. Wright, J. Am. Ceram. Soc., 69, 66 (1986).

83. J. Zarzycki, M. Parassas, and J. Phalippou, J. Mat. Sci., 17, 3371 (1982).

84. P. Yu, H. Liu, and Y. Wang, J. Non-Cryst. Solids, 52, 511 (1982).

85. A. V. Kiselev and V. I. Lygin, Infrared Spectra of Surface Compounds, Halsted Press, New York, 1975, p. 117.

86. K. Hashimoto, K. Asami, and K. Teramoto, Corrosion Sci., 19, 3 (1978).

87. S. Wallace and L. L. Hench, "The Processing and Characterization of DCCA Modified Gel-Derived Silica" in Better Ceramics Through Chemistry, C. J. Brinker, D. E. Clark, and D. R. Ulrich, eds., Material Research Society Symposium Proceeding, Vol. 32, North-Holland Pub. Co., New York, NY, 1984, p. 47.

88. R. A. J. Sambell, A. Briggs, D. C. Phillips, and D. H. Bowen, J. Mater. Sci., 7, 676 (1972).

89. D. C. Phillips, J. Mater. Sci., 7, 1175 (1972).

90. D. C. Phillips, J. Mater. Sci., 9, 1847 (1974).

91. K. M. Prewo and J. J. Brennan, J. Mater. Sci. 15, 463 (1980).

92. K. M. Prewo and J. J. Brennan, J. Mater. Sci. 17, 1201 (1982).

93. K. M. Prewo and J. J. Brennan, J. Mater. Sci. 17, 2371 (1982).

94. K. M. Prewo, J. Mater. Sci. 17, 3549 (1982).

95. W. W. Pultz, J. Am. Ceramic Soc., 50, 419 (1966).

96. P. J. Jorgensen, M. E. Wadsworth, and I. B. Cutler, J. Am. Ceramic Soc., 44, 258 (1961).

97. G. E. Ervin, Jr., J. Am. Ceramic Soc., 41, 347 (1958).

98. J. A. Costello and R. E. Tressler, J. Am. Ceramic Soc., 64, 327 (1981).

99. S. C. Singhal, J. Materials Sci., 11, 1246 (1976).

100. E. A. Gulbransen and S. A. Jansson, Oxid. Met., 4, 181 (1981).

101. E. A. Gulbransen, K. R. Andrew, and F. A. Brassart, J. Electrochem. Soc., 113, 1311 (1966).

102. J. Bialoskorski and K. Konsztowicz, Szklo Ceram., 28, 207 (1977).

103. F. E. Wang and K. A. Sutula, J. Appl. Phys., 49, 944 (1978).

104. J. J. Lannutti and D. E. Clark, "Sol-Gel Derived Coatings on SiC and Silicate Fibers" in Ceramic Proceedings, 8th Annual Conference on Composites and Advanced Ceramic Material, Am. Ceram. Soc., Columbus, Ohio, 1984, p. 574.

105. J. J. Lannutti and D. E. Clark, "Sol-Gel Derived Ceramic-Ceramic Composites" in Better Ceramics Through Chemistry. C. J. Brinker, D. E. Clark, and D. R. Ulrich, eds., Materials Research Society Symposia Proceedings, Vol. 32, North-Holland, New York, 1984, p. 369.

106. J. J. Lannutti and D. E. Clark, "Long Fiber Reinforced Sol-Gel Derived Al_2O_3 in Better Ceramics Through Chemistry. C. J. Brinker, D. E. Clark, and D. R. Ulrich, eds., Materials Research Society Symposia Proceedings, Vol. 32, North-Holland, New York, 1984, p. 375.

107. R. W. Rice, J. R. Span, D. Lewis, and W. Coblenz, "Effect of Ceramic Fiber Coatings on the Room-Temperature Mechanical Behavior of Ceramic-Fiber Composites" in Ceramic Proceedings, 8th Annual Conference on Composites and Advanced Ceramic Materials, Am. Ceram. Soc., Columbus, Ohio, 1984, p. 614.

108. Annual Book of ASTM Standards, "Flexural Testing of Glass," section 15, Am. Soc. of Testing Mater., Philadelphia, PA, 1983, p. 25.

109. G. K. Bansal and W. H. Duckworth, "Fracture Surface Energy Measurements by the Notch-Beam Technique," in Fracture Mechanics Applied to Brittle Materials, S. W. Freiman, ed., ASTM STP 678, Am. Soc. for Testing and Materials, Philadelphia, PA, 1978, p. 38.

110. H. H. Willard, L. L. Merritt, J. A. Dean, and F. A. Settle, Instrumental Methods of Analysis, 6th ed., D. Van Nostrand Co., New York, 1981, p. 209.

111. A. K. Ramdas, Indian Academy of Sci., proceedings, 37AA, 571 (1953).

112. M. Haccuria, Bull. Soc. Chim., Belgium, 62, 428 (1953).

113. I. Simm and H. O. McMahon, J. of Chem. Phys., 21 23 (1953).

114. R. A. J. Sambell, D. H. Bowen, and D. C. Phillips, J. Mater. Sci., 7, 663 (1972).

115. J. L. Henshall, D. J. Rowcliffe, and J. W. Eddington, J. Am. Ceram. Soc., 60, 373 (1977).

116. J. L. Henshall and C. A. Brookes, J. Mater. Sci. Letters, 4, 783 (1985).

117. G. C. Wei and P. F. Becher, J. Am. Cer. Soc., 67, 571 (1984).

118. S. R. Nutt and F. E. Wawner, J. Mater. Sci., 20, 1953 (1985).

119. B. A. Bender, D. Lewis, W. S. Coblenz, and R. W. Rice, "Electron Microscopy of Ceramic Fiber-Ceramic Matrix Composites - Comparison with Processing and Behavior," in NASA Conference Pub. 2357, Hampton, VA, J. D. Buckley, ed., 1984, p. 171.

120. T. J. Clark, R. M. Arons, J. B. Stamatoff, and J. Rabe, "Thermal Degradation of Nicalon™ SiC Fibers," in Ceramic Eng. & Sci. Proc., Vol. 6, Am. Ceramic Soc., Columbus, Ohio, 1985, p. 576.

121. R. E. Wilson and D. M Breit, "Near Net Shape SiC Whisker Reinforced SiC Oxidation Resistant Structural Composites Made by the TEOSiC Process," in Metal Matrix, Carbon, and Ceramic Matrix Composites 1985, J. D. Buckley, ed., p. 229.

122. R. Rice, "Ceramic Composites," in Ceramic Eng. & Sci. Proc., Vol. 2, Am. Ceramic. Soc., Columbus, Ohio, 1981, p. 493.

123. G. C. Wei and P. F. Becher, Am. Ceram. Bull., 64, 298 (1985).

124. R. Pampuch, W. S. Ptak, S. Jonas, and S. Stoch, Proc. 4th CIMTES, St. Vincent, Amy, 1974, P. Vincenzini, ed., Elsevier Pub. Co., Amsterdam, 1980.

125. V. A. Lavenko, S. Jones, and R. Pampuch, Ceramic International, 7, 75 (1981).

126. S. C. Singhal and F. F. Lange, J. Am. Ceram. Soc., 58, 433 (1975).

127. A. Suzuki, H. Ashido, N. Fruii, K. Mameno, and H. Matsunami, Japan, J. Appl. Phys., 21, 579 (1982).

128. S. Y. Lee, "Low Temperature Oxidation of SiC," Third Annual Report to Air Force Office of Scientific Research, L. L. Hench and D. E. Clark, eds., Gainesville, Florida, March 1982-Feb. 1983, p. 158.

129. G. P. LaTorre, R. A. Stokell, R. H. Krabill, and D. E. Clark, Air Force Report from University of Florida, April 1983-March 1985. To be presented at the Engineering Ceramic Conf., Cocoa Beach, FL, Jan. 1986.

BIOGRAPHICAL SKETCH

Burtrand Insung Lee attended and graduated from Montgomery Blair High School in Silver Spring, Maryland and Southern College in Collegedale, Tennessee, in 1971 and 1975, respectively. Upon graduation from Southern College as Chemistry major, he was employed by Biospherics Inc., in Rockville, Maryland, as a chemist. At Biospherics he was indirectly engaged in the Viking Project search of life on Mars.

After the decision to pursue full-time graduate work, he enrolled and graduated from Western Michigan University majoring in analytical chemistry in 1979. After some experiences in teaching and research in chemistry at State University of New York, he entered the University of Florida as a doctoral student.

I certify that I have read this study and that in my opinion it conforms to acceptable standards of scholarly presentation and is fully adequate in scope and quality, as a dissertation for the degree of Doctor of Philosophy.

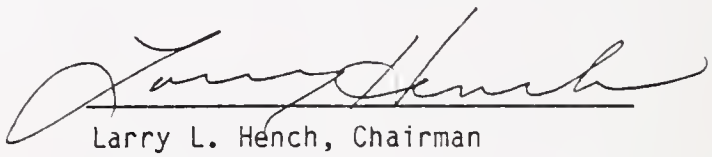

Larry L. Hench, Chairman
Professor of Materials Science and Engineering

I certify that I have read this study and that in my opinion it conforms to acceptable standards of scholarly presentation and is fully adequate in scope and quality, as a dissertation for the degree of Doctor of Philosophy.

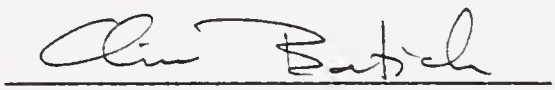

Christopher D. Batich
Associate Professor of Materials Science and Engineering

I certify that I have read this study and that in my opinion it conforms to acceptable standards of scholarly presentation and is fully adequate in scope and quality, as a dissertation for the degree of Doctor of Philosophy.

Michael D. Sacks
Associate Professor of Materials Science and Engineering

I certify that I have read this study and that in my opinion it conforms to acceptable standards of scholarly presentation and is fully adequate in scope and quality, as a dissertation for the degree of Doctor of Philosophy.

Lawrence E. Malvern
Professor of Engineering Science

I certify that I have read this study and that in my opinion it conforms to acceptable standards of scholarly presentation and is fully adequate in scope and quality, as a dissertation for the degree of Doctor of Philosophy.

David E. Clark
Associate Professor of Materials Science and Engineering

This dissertation was submitted to the Graduate Faculty of the College of Engineering and to the Graduate School, and was accepted as partial fulfillment of the requirements for the degree of Doctor of Philosophy.

May 1986

Dean, College of Engineering

Dean, Graduate School